MULTIWAVELENGTH BRILLOUIN FIBER LASERS

MOHAMMADREZA REZAZADEH SHIRAZI

DEPARTMENT OF PHYSICS

FACULTY OF SCIENCE

UNIVERSITY OF MALAYA

2009

MULTIWAVELENGTH BRILLOUIN FIBER LASERS

BY

MOHAMMADREZA REZAZADEH SHIRAZI

DEPARTMENT OF PHYSICS

FACULTY OF SCIENCE

UNIVERSITY OF MALAYA

THIS THESIS SUBMITTED IN FULFILLEMENT

OF THE REQUIREMENT FOR THE DEGREE OF

DOCTOR OF PHILOSOPY

UNIVERSITY OF MALAYA

KUALA LUMPUR

MALAYSIA

2009

UNIVERSITI MALAYA

ORIGINAL LITERARY WORK DECLARTION

Name of Candidate: Mohammadreza Rezazadeh Shirazi (I.C/Passport No: I2164800)

Registration/Matric No: SHC060014

Name of Degree: Doctor of Philosophy

Title of Project Paper/Research Report/Dissertation/Thesis ("This Work"):

Multiwavelength Brillouin Fiber Lasers

Field of Study: Physics, Lasers/Photonics

I do solemnly and sincerely declare that:

(1) I am the sole author/writer of this work;
(2) This work is original;
(3) Any use of any work in which copyright exists was done by way of fair dealing and for permitted purposes and any excerpt or extract form, or reference to or reproduction of any copyright work has been disclosed expressly and sufficiently and the title of the Work and its authorship have been acknowledged in this Work;
(4) I do not have any actual knowledge nor do I ought reasonably to know that making of this work constitutes an infringement of any copyright work;
(5) I hereby assign all and every rights in the copy right to this Work to the University of Malaya ("UM"), who henceforth shall be owner of the copyright in this Work and that any reproduction or use in any form or by any means whatsoever is prohibited without the written consent of UM having been first had and obtained;
(6) I am fully aware that if in the course of making this Work I have infringed any copyright whether intentionally or otherwise, I may be subjected to legal action or any other action as may be determined by UM.

Candidate's Signature 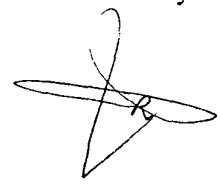 Date Feb 6, 2010

Subscribed and solemnly declared before,

Witness's Signature  Date 6/2/2010

Name: Dr. Sulaiman Wadi Harun

Designation: Associate Professor
Dept. of Electrical Engineering
University of Malaya
50603 Kuala Lumpur

Abstract

This thesis describes to solve the problem of higher power generation of Brillouin fiber lasers (BFLs), to measure their linewidth as a challenging issue and to generate multiwavelength Brillouin fiber laser (MBFL) sources as an application of BFL generation in the both linear and ring cavities. By using the proposed ring cavity with the same components used in the conventional ring cavities, a new Brillouin fiber ring laser (BFRL) with higher output power has been generated. The proposed BFRL configuration shows an output peak power of -0.5 dBm, which is 5.7 dB higher compared to the conventional configuration. In the proposed linear cavity, BFL configuration has been demonstrated by incorporating a 3-dB coupler, a 95/5 coupler, two optical circulators, and a 25 km SMF that allows very high conversation efficiency from the Brillouin pump (BP) to the BFL compared with the conventional linear cavity BFL. Stable BFL operation was obtained at an up-shifted wavelength of 0.086 nm from the pump wavelength with the BFL peak power at -1 dBm, which is 12.3 dB higher than the conventional BFL with the same BP power 13 dBm, due to the reduced cavity loss in the proposed configuration.

In the MBFL generation, more than 14 and 9 BFL lines are demonstrated in the ring and linear cavities, respectively. In the ring cavity, the both wavelength spacing 0.08 nm (~10 GHz) and 0.16 nm (~20 GHz) are obtained with the bi-directional multi-wavelength generation whereas in the linear cavity only the wavelength spacing 0.08 nm (~10 GHz) is obtained. The used BP powers are about 14 dBm and 11.7 dBm in respectively the ring and linear MBFL generation. By using a Bismuth Erbium doped fiber amplifier (Bi-EDFA) in the linear BFL cavity, multiwavelength Brillouin Erbium fiber laser (MBEFL) has been

demonstrated in the L band wavelength region (1565-1625 nm). The generated MBEFL has more number of lines (~50 lines) in comparision with the MBFL by using the Bi-EDFA pumped bidirectionaly with two EDFA pump power 125 mW and Brillouin pump power 5 dBm. The MBEFL generation is limited to the Bi-EDFA operational wavelength region (1525-1625 nm) although it is extended to L band region by using Bi-EDFA in comparison with the traditional MBEFL which can be generated only in the C band wavelength region (1525-1565 nm). In addition, multiwavelength Brillouin Raman fiber laser (MBRFL) is also generated by using a Raman amplifier in a BFL cavity with a 25 km single-mode fiber as the nonlinear gain medium. The second and the third Brillouin stoke waves are obtained by using the Raman pump power 150 mW and Brillouin pump 5.5 dBm at the BP wavelength 1568 nm. The anti-Stokes line is also produced due to four-wave mixing phenomenon. The number of MBRFL lines can be increased by using higher Raman pump power in addition to an optical fiber with the higher Raman gain such as dispersion compensating fiber (DCF).

As a high coherent light source with ultranarrow linewidth, Brillouin fiber lasers have been used in many applications especially in microwave generation, gyroscopes. BFL linewidth measurement has also been a challenging research due to the ultranarrow BFL linewidth. In this work, the BFL linewidth has been measured 8 Hz and 24 Hz by using BP linewidth 15 MHz and 124 MHz, respectively. This measurement has been done by the heterodyne method between two independent BFLs. The measured BFL linewidth values are in the range a few hertz as expected from the most of the last reports.

Abstrak

Tesis ini menerangkan tentang penyelesaian masalah mengenai kuasa tinggi dalam pembentukan Laser Gentian Optik Brillouin (BFL), untuk mengukur lebar garis dan juga untuk membentuk (MBFL) adalah aplikasi dari pembentukan BFL di dalam semua rongga iaitu rongga linear dan rongga membulat. Dengan mencadangkan rongga membulat yang menggunakan komponen yang sama seperti konvesional rongga membulat, satu Laser Gentian Optik Brillouin Berongga Membulat (BFRL) yang baru dengan kuasa keluaran yang tinggi telah terhasil. Konfigurasi cadangan BFRL menunjukkan kuasa puncak keluaran berjumlah -0.5dBm, dengan berbezaan 5.7dB lebih tinggi dari konventional konfigurasi. Di dalam candangan rongga linear, BFL telah ditunjukan dengan menggabungkan satu 3-dB penyatu, satu 95/5 penyatu, dua pemusing cahaya dan 25km Gentian Optic Mode Tunggal (SMF) yang membenarkan kecekapan penukaran yang tinggi daripada Pengepam Brillouin (BP) kepada BFL berbanding dengan konventional BFL berongga linear. BFL dengan operasi yang stabil telah dicapai pada satu perpindahan atas panjang gelombang 0.086nm dari pengepam panjang gelombang dengan BFL kuasa puncak pada -1dBm, iaitu 12.3dB lebih tinggi dari konventional BFL dengan kuasa BP yang sama iaitu 13dBm, disebabkan oleh pengurangan penghilang rongga dalam konfigurasi yang dicadangkan.

Di dalam pembentukan MBFL, lebih daripada 14 dan 9 BFL telah ditunjukkan di dalam ronga membulat dan rongga linear masing-masing. Di dalam rongga membulat kedua-dua jarak panjang gelombang 0.08nm (~10Ghz) and 0.16nm (~20GHz) telah diperolehi dengan pembentukan pelbagai panjang gelombang dwi-arah sementara di dalam rongga linear hanya jarak panjang gelombang 0.08nm (~10GHz) terhasil. Penggunaan BP adalah kira-kira 14dBm

and 11.7dBm masing-masing di dalam rongga membulat dan rongga linear MBFL. Dengan menggunakan Penguat Gentian Optik berdop Bismuth (Bi-EDFA) di dalam BFL berongga linear, Laser Gentian Optik dengan Pelbagai Panjang Gelombang Erbium-Brillouin (MBEFL) telah ditunjukkan dalam kawasan panjang gelombang rantau L (1565-1625nm). Pembentukan MBEFL mempunyai bilangan garis (~50 lines) jika dibandingkan dengan MBFL yang menggunakan Bi-EDFA yang telah dipam secara dwi-hala dengan dua kuasa pengepam EDFA iaitu 125mW dan kuasa pump Brillouin 5dBm. Pembentukan MBFL di hadkan oleh kawasan operasi panjang gelombang Bi-EDFA (1525-1625nm) walaupun ianya dipanjangkan kepada kawasan ratau L dengan menggunakan Bi-EDFA dalam membezakan dengan tradisional MBEFL yang mana boleh menghasilkan hanya pada panjang gelombang rantau C (1525-1565nm). Sebagai tambahan, Laser Gentian Optik pelbagai gelombang Raman Brillouin (MBRFL) juga terhasil dengan menggunakan penguat Raman di dalam rongga BFL dengan 25km SMF digunakan sebagai medium tak linear. Gelombang Brillouin Stokes kedua dan ketiga telah terhasil dengan menggunakan kuasa pengepam raman 150mW dan pengepam Brillouin 5.5dBm pada panjang gelombang BP 1568nm. Garis anti Stokes juga terhasil disebabkan oleh fenomena campuran empat gelombang. Bilangan garis MBRFL boleh ditingkatkan dengan menggunkan pengepam Raman berkuasa tinggi dan tambahan gentian optik dengan gandaan Raman yang tinggi seperti gentian optik penggantian penyelerakkan (DCF)

Sebagai sumber cahaya koheran dengan lebar garis ultra sempit, BFL telah digunakan di dalam banyak aplikasi terutamanya di dalam pembentukan gelombang mikro, gyroscopes dan MBFL. Pengukuran lebar garis BFL juga amat mencabar disebabkan oleh lebar garis BFL yang ultra sempit. Di dalam kerja ini,

lebar garis BFL telah diukur iaitu 8Hz dan 24Hz dengan menggunakan 15MHz dan 124MHz BP lebar garis. Pengukuran telah dibuat dengan menggunakan kaedah heterodyne di antara dua BFLS bebas.Nilai pengukuran lebar garis BFL adalah di dalam julat hertz seperti di dalam laporan yang lepas.

Acknowledgment

I would like to thank my supervisor Professor Dr. Harith Ahmad for allowing me to work in his Photonics Research center, for encouraging independent thinking, and for his guidance throughout this work.

I am also particularly grateful to my co-supervisor, Associate Prof. Dr. Sulaiman Wadi Harun who presented consistent concern and helpful advice regarding my research. Their valuable advice was crucial in my research work. They also reviewed my whole thesis and provided invaluable comments and suggestions.

My special thanks should go with the member of Photonics Research Center, Nizam Tamcheck, Mohd Zamani Zulkifili, Sharifeh Shahi, Nurul Shahrizan, T. Kavintheran, Mohammadreza Moghadam and all the Photonics Research members for their assistance during the experiments as well as the living in Malaysia.

My full-hearted thanks should go to my family members specially my wife, Mozhgun Biglary and my son, Behnia whose love and support throughout the good times and the bad have been both needed and cherished. Without their help and patient, I was not able to do my researches in Malaysia.

Acronyms

Throughout this work, some jargons are used to avoid the repeated unnecessary some group of words. Although, each acronym is usually defined the first time it appears in a chapter, here a list of acronyms are presented to help the readers.

A_{eff}	Effective Area
AOM	Acousto Optical Modulator
BEFL(s)	Brillouin Erbium Fiber Laser(s)
BFL(s)	Brillouin Fiber Laser(s)
Bi-EDF	Bismuth-Based Erbium Doped Fiber
Bi-EDFA	Bismuth-Based Erbium Doped Fiber Amplifier
BP	Brillouin Pump
BPRS	Brillouin Pump Rayleigh Scattering
BRFL(s)	Brillouin Raman Fiber Laser(s)
BS	Brillouin Stokes
CPM	Cross-Phase Modulation
CW	Continuous Wave
DCF	Dispersion Compensating Fiber
DFBL(s)	Distributed Feedback Laser(s)
DSF	Dispersion Shifted Fiber
DWDM	Dense Wavelength Division Multiplexing
EDF(s)	Erbium Doped Fiber(s)
EDFA(s)	Erbium Doped Fiber Amplifier(s)
FBG	Fiber Bragg Grating

FSR	Free Spectral Range
FWHM	Full Width At Half Maximum
FWM	Four-Wave Mixing
L_{eff}	Effective Length
LO	Local Oscillator
LS	Laser Source
MBEFL(s)	Multiwavelength BEFL(s)
MBFL(s)	Multiwavelength BFL(s)
MBRFL(s)	Multiwavelength BRFL(s)
MCVD	Modified Chemical Vapor Deposition
MFR	Mode Field Radius
OC	Optical Circulator
OSA	Optical Spectrum Analyzer
PD	Photodiode
P_{th}	Threshold Power
RF	Radio Frequency
RFSA	Radio Frequency Spectrum Analyzer
RS	Raman Stokes
RP	Raman Pump
SBS	Stimulated Brillouin Scattering
SBSTR	Stimulated Brillouin Scattering Threshold Reduction
SMF	Single-Mode Fiber
SMSR	Side-Mode Supprestion Ratio
SNR	Signal to Noise Ratio
SOA	Semiconductor Optical Amplifier

SPM	Self-Phase Modulation
SVEA	Slowly Varying Envelope Approximation
TDM	Time-Division Multiplexing
TLS	Tunable Laser Source

LIST OF CONTENTS

Chapter 1:

Introduction

1.1 Introduction

The interaction of light with matter can be observed in almost every aspect of life, ranging from scattering in optical communications to data processing, laser eye surgery and so on and so forth. Therefore, the interaction of light has many advantages and disadvantages to a system, depending on the nature of the interaction. In some cases, the interaction leads to a loss in performance, such as signal loss and signal disruptions (especially in telecommunications systems), while at the same time, the interaction may be beneficial, such as in the case of Stimulated Brillouin Scattering (SBS) or Stimulated Raman Scattering (SRS) for multiwavelength sources.

The terms interaction of light has many meanings. In fiber optics, the interaction of light refers to the interaction of the photons in the travelling beam with the atoms and molecules that make up the optical fiber (be they part of the optical fiber composition or merely impurities). In a simple description, light will interact with the atoms and molecules, setting the electrons or even the whole atom into oscillations at relatively low amplitudes as simple harmonic oscillators. At this point, the interaction between the light photons and the constituent atoms of the fiber material is linear and can thus be easily predicted. However, if these oscillations are pushed further (in a sense the oscillations are overdriven) the physical oscillating system will now exhibit a nonlinear response and no longer be predictable.

Initially, studies of the interaction of light with other materials were limited to fairly linear reactions due to the availability of only low intensity light fields. This issue was soon resolved with the introduction of lasers and subsequently laser diode systems, thus making it possible to obtain a beam with high field intensity. With the restriction of the low field intensity now removed a number of interesting effects, which had previously been negligible due to the low intensity fields, were quickly observed. These effects, known as nonlinear optical phenomenon, exhibit a nonlinear dependence on the incident field strength. Nonlinear optical phenomenon is especially evident in optical fibers, where the intensities are high due to the small cross-sectional area involved (as compared to the more modest intensity levels in other materials). As a result of this, nonlinear optical phenomenon occurs effectively in optical fibers even though they often do not possess a large nonlinear coefficient. Despite this fact, long interaction distances of light propagation are often needed to achieve nonlinear mixing of any significance so that nonlinear processes can be phase matched or nearly so to allow the signal ,generated by the nonlinear effects, grow to appreciable levels. In 1979, the progress in fiber fabrication technology resulted in producing low loss fibers in which the loss level limited effectively by the fundamentals loss of Rayleigh scattering of about 0.2 dB/km in the 1550 nm region [1]. This caused a revolution in optical fiber communication and nonlinear fiber optics which was started before by the study of stimulated Raman scattering (SRS) and stimulated Brillouin scattering (SBS) [2], [3], [4]. Then, SRS and SBS were used for generating Raman and Brillouin amplifiers, as well as Raman and Brillouin fiber lasers [5],[6],[7],[8]. In 1990s, a new aspect in the field of nonlinear fiber optics was obtained when optical fibers were doped with rare-earth elements. As a result,

these fibers have improved the performance of optical fiber amplifiers and fiber lasers [9],[10],[11]. Erbium doped fiber amplifiers (EDFAs) attractted most of attention due to their operational wavelength region near 1550 nm which is suitable for fiber-optics communication systems [12]. The use of EDFAs led to a revolution in the design of multiwavelength optical systems [13],[14],[15]. At the same time, fiber gratings were developed so that they became an important part of lightwave technology systems [16],[17]. New fibers such as photonic crystal fibers, holey fibers, highly nonlinear fibers, and dispersion compensating fibers were studied and developed. In these fibers, dispersion and nonlinear properties are changed. That is, zero dispersion wavelength shifts toward the visible region and the nonlinear effects are enhanced due to their relatively small core size [18],[19],[20],[21]. Raman amplifiers based on stimulated Raman scattering has progressively become a quite common area in modern optical fiber communication systems [22]. In addition, fiber optic parametric amplifiers based on four-wave mixing (FWM) also been attractive due to their potential for ultrafast signal processing [23]. Even though EDFAs working only near 1550 nm region, Raman and parametric amplifiers can operate in any special region without using any doped fiber when the appropriate pump are provided. All in all, nonlinear fiber optics has grown considerably and it is expected to continue as an effective research area in the future.

In this thesis, after discussing about Brillouin fiber laser (BFL) and its performance, we pay our attention to multiwavelength BFLs (MBFLs) generation. Then, multiwavelength Brillouin Erbium fiber lasers (MBEFLs) will be investigated by using Bismuth based EDFA. Finally, we will consider the generation of multiwavelength Brillouin Raman fiber lasers (MBRFLs).

Therefore, here, after presenting an introduction about stimulated Brillouin scattering (SBS) and BFLs, we review the generation of MBFLs, MBEFLs, and MBRFLs which are useful in WDM and DWDM systems in optical communications.

1.2 Stimulate Brillouin Scattering (SBS) and its Applications

Material absorption and Rayleigh scattering are the main loss factors in optical fibers. The latter factor contributes most of the loss in optical fibers and arises from local density fluctuations of silica frozen into the fused silica during a silica fiber manufacturing process. The density fluctuations results in local fluctuations of the refractive index on a scale smaller than the optical wavelength. In Rayleigh scattering which is an elastic scattering, the frequency of scattered light is the same as the frequency of the incident light [24],[25]. On the other hand, there are inelastic scatterings such as Brillouin scattering, and Raman scattering in which the frequency of the scattered light is shifted downward [26]. Both can be understood in a simple quantum picture as the conversion of an incident photon belonging to pump wave to a lower-frequency scattered photon related to the Stokes wave such that the energy difference appears in the form of a phonon to conserve the energy and the momentum. When the phonon of right energy and momentum is available, a higher-energy photon at the so-called anti-Stokes frequency wave can also be observed. The main difference between Brillouin and Raman scattering is that acoustic phonons relating to moving grating participate in Brillouin scattering whereas optical phonons relating to vibrations of silica molecules participate in Raman scattering. The difference in the type of phonons causes a fundamental difference; Brillouin scattering occurs in the backward

direction in optical fibers whereas Raman scattering can occur in the both directions. Although theses nonlinear inelastic scattering processes result in a loss of power at the incident frequency, their loss are negligible at low incident power levels due to their small cross sections. However, they become stimulated at high power levels for incident light and the nonlinear phenomena of stimulated Brillouin scattering (SBS) and stimulated Raman scattering (SRS) will be resulted.

Historically, in 1918, the first theoretical study of the Brillouin light scattering was done by Mandelstam by supposing thermal phonons related to vibrations of the medium molecules by the acoustic waves, however, Mandelstam's paper was published only in 1926 [27], [28], [29]. Independently, L. Brillouin predicted light scattering from thermally excited acoustic waves in 1922 [30]. Later Brillouin's prediction is confirmed experimentally by E. Gross in liquids and crystals in 1930 [31], [32]. When the interference between pump light and the back scattered downshifted light (Stokes wave) reinforces the acoustic waves another phenomenon known as SBS occurs. However, this was observed after the invention of lasers in 1964 [33]. On the other hand, in 1928, the Indian physicist C. V. Raman reported that a small fraction of power can be transferred from one optical field to another field whose frequency is downshifted by an exact amount determined by the vibrational mode of the medium [34]. For this discovery of the effect that bears his name and for his work on scattering, C. V. Raman was awarded the Nobel prize in 1930. In 1962, it is showed that for the intense fields as the Raman pump, the Raman scattered wave, or Raman Stoks, grows rapidly inside the medium such that most of the Raman pump energy is transferred to the Raman Stokes; this phenomenon is called SRS [35]. Then, SRS has been studied extensively in a variety of molecular media [26].

SBS and SRS can be detrimental in lightwave systems and can considerably affect the performance of the systems. They can generate Brillouin and Raman Stokes wave in the expense of depleting a light pump. They can cause Brillouin and Raman induced crosstalk effects in a multiwavelength communication systems. The reason is that a short-wavelength channel can act as a Brillouin or Raman pump and thus transfer part of its power to the neighboring longer wavelength channel depending on the appropriate wavelength difference between the channels (about 11 GHz for Brillouin and about 13 THz for Raman crosstalk in the 1550 nm region in silica fibers). In addition, the nonlinear Brillouin gain bandwidth is about 20 MHz extremely narrow compared with the Raman gain bandwidth of about 5 THz. In other words, the channel spacing must match almost exactly the Brillouin shift of about 11 GHz in the 1550 nm region in silica fiber and the two channels must be counterpropagating for Brillouin-induced crosstalk to occur. Thus, Brillouin crosstalk in contrast with the case of Raman crosstalk can be easily avoided with the proper design of multiwavelength communication systems [36], [37]. Although SBS in the form of Brillouin-induced crosstalk cannot affect channels propagating in the same direction, SBS limits the channel transmitted powers. This is due to the fact that SBS threshold power is very low in comparison with SRS threshold power. This condition is independent of the presence and the number of other channels. Therefore no more power can be transmitted through an optical fiber once the power of each channel reaches the Brillouin threshold power which is a few milliwatts in practice. Several schemes have been applied for raising the Brillouin threshold power relying on the increasing of the Brillouin gain bandwidth or the spectral width of the optical carrier wave [38], [39].

On the other hand, both SBS and SRS can be used to advantage. For example, they can be used to amplify an optical signal by transferring energy to it from a pump beam, whose wavelength is suitably chosen [22], [40]. Indeed SRS is especially useful for amplification because the Raman gain has an extremely large bandwidth. After year 2000, Raman amplifiers are used routinely in modern optical fiber systems [41-45]. SBS can also be used to make fiber sensors for measuring temperature and strain changes over a relatively long distance. The basic idea behind this usage is the dependence of the Brillouin shift to the effective index of the fiber mode which changes whenever the refractive index changes in response to the local environment variations such as temperature and pressure [46],[47],[48]. One of the most interesting applications of SBS is Billouin fiber lasers which have been an active topic of study and research since it was proposed as early as 1976 [8] ,[11],[49],[50],[51]. In these lasers, the nonlinear Brillouin gain in an optical fiber is used by placing the fiber as a gain medium inside a cavity. Although fiber lasers can also be obtained by any optical fibers doped with rare-earth elements as erbium [52], and ytterbium [53], fiber lasers generated in this method are operated only in a special wavelength region governed by optical doped fiber characteristics. For example, erbium-doped fiber lasers can work near 1550 nm region and this makes such lasers suitable in commercial band at wavelength 1550 nm for some applications as optical communication, ultrafast phenomena, and fiber-based sensors. In addition, due to some interesting aspects as the low intensity noise, low frequency noise and movable focusing, fiber lasers have been used in a variety of applications such as microwave photonics, spectroscopy, coherent optical communications, coherent lidar detection, interferometric sensing material processing, and medicine [54-58]. However, due

to the fact that BFLs can be generated in any wavelength by using the nonlinear Brillouin gain, and due to their extremely narrow linewidth which could be a few Hz [51], [59], [60], BFLs have attracted additional interests for a number of other applications such as optical communication, ultrafast phenomena, and fiber-based optical sensors and gyroscopes [61]. The key aspects of BFLs for most applications are their very high coherency, low threshold, and high efficiency in addition to the directional sensitivity of the Brillouin gain. Among all the applications, the generation of multiple lasing wavelengths by cascading SBS process is becoming very important especially in wavelength-division-multiplexing transmission and sensor applications.

1.3 Brillouin Fiber Lasers (BFLs)

Fiber lasers are usually lasers which uses optical fibers as the gain media in optical resonators. Fiber Lasers have their specific features making them different from standard lasers with inverted population media. First of all, a fiber laser is pumped by another laser known as a pump with a spectral selection of radiation. As mentioned before, the gain medium can be a fiber doped with rare-earth ions such as Erbium (Er^{3+}), Neodymium (Nd^{3+}), Praseodymium (Pr^{3+}) Thulium (Tm^{3+}), and Yetterbium (Yb^{3+}) pumped by some laser diodes to generate linear gain media in these fibers. In this method, different types of dopants in different host materials such as silica and fluoride give different physical characteristic in the laser systems. However, we can use the nonlinear Brillouin and Raman gain to produce Brillouin and Raman fiber lasers, respectively, which can be generated at any wavelength depending on the availability of the Brillouin and Raman pump. In BFL generation, for example, the quantity of major importance is called the

Brillouin shift, which is the difference in the BFL and Brillouin pump (BP) frequencies, rather than the BFL and the BP frequencies.

For BFL oscillation, closed –loop gain must exceed unity so that Brillouin amplification must over-compensate the cavity loss. By adding a proper feedback to a SBS system in the form of a Fabry-Perot (linear) cavity or a ring cavity, the BFL oscillation happens in the condition that the BP power exceeds a certain power called the SBS threshold power. The BFL will operate at a frequency which is separated from the BP frequency by the Brillouin shift due to the Doppler effect in the backward BP inelastic scattering through moving grating generated in electrostriction phenomenon. In this thesis, we use a 25 km single mode fiber as the nonlinear gain medium, in addition to optical circulators and optical couplers to produce the Fabry-Perot (linear) cavity and the ring cavity configurations [51],[62-65]. By using linear cavities, it is easier to generate multiple lasing wavelengths due to the feature of the standing wave generation in them. Higher order Stokes waves are generated through cascaded SBS which is a process in which each successive Stokes line is a pump to generate the next-order Stokes line after its power reaches the next-order Stokes threshold power. At the same time, anti-Stokes lines are generated through another process called FWM between the copropagating BP and the Stokes waves. The collection of the transmitted BP, the Stokes and the anti-Stokes waves all together generate the multiple lasing wavelengths in a linear cavity [51], [66]. On the other hand, in a ring cavity, even-order Stokes and anti-Stokes lines are observed with the transmitted BP in the forward direction in which they copropagate with the BP whereas odd-order Stokes and anti-Stokes line appears in the backward direction in comparison to BP due to the counterpropagating feature of SBS process and the unidirectional aspect

of the ring cavity [63]. The generated multiple lasing wavelengths have been advantageously utilized in the past few years in optical fiber sensors, optical component testing, and spectroscopy applications [67],[68]. Perhaps the largest interest has arisen from the use of multiple lasing wavelengths in wavelength division multiplexing (WDM) and dense WDM (DWDM) optical transmission systems.

1.4 The Generation of Multiple Lasing Wavelengths

Instead of transmitting data at lower rates over multiple fibers, we can transmit them at higher rates over a single fiber using channel multiplexing technique which increases the transmission capacity. One of the primary concerns in optical transmission systems is the ultimate transmission capacity which is critically depended on the temporal and spectral characteristics of light. This dependence can result basically in time-division multiplexing (TDM) and wavelength-division multiplexing (WDM) techniques. The simultaneous use of TDM and WDM is always critically affected by the uncertainty principle in the fundamental physics. In addition, there are some inherent physical limitations in using TDM and WDM techniques. For example, it is known that the effects of the chromatic and the polarization-mode dispersion are the primary limiting factors in the TDM optical transmission systems whereas ,in the WDM systems, nonlinear effects such as self-phase modulation, cross-phase modulation, SBS, SRS, FWM, parametric generation, and photorefractive effects can be degenerative factors [69]. In the TDM system, the maximum bit rate is theoretically limited to below 10 Gb/s for long distance transmission of 100 km by the chromatic dispersion effect although this limitation is reported to increase up to 1 Tb/s by using dispersion compensating fibers and management technology [70]. In WDM systems,

however, the maximum capacity could be readily obtained with low channel bit rates but with dense WDM (DWDM) rather than high bit rates per channel in a less dense scheme. Although each of N channels is a laser line carrying data at lower rates, the aggregate multiwavelength laser of N lines is transmitting data at N times the individual laser line so that there is an enhancement in the transmitting capacity; the lower data rate of each channel also reduces not only the dispersion but also other degrading effects in an optical transmission system [71]. Early WDM, known as wideband WDM, began using the two widely spaced wavelengths in the 1310 nm and 1550 nm. Then, In the early 1990s, the second generation of WDM, called narrow-band WDM, was introduced by using two to eight wavelengths spaced at an interval of about 400 GHz in the commercial band 1550 nm region [72]. In the middle of 1990s, DWDM systems with 16 to 40 wavelength spaced from 100 to 200 GHz were generated. Currently, 160 and 357 parallel channels densely packed at 10 GHz spacing are generated by using uniform Brillouin Stokes line with EDFA and Raman amplification, respectively [73],[74]. Nowadays, by using some multimedia applications such as interactive TV, video conferencing and by using internet, the need for having higher carrying capacity is unprecedented. In fact, this is a reason for introducing higher capacity DWDM systems in which a transmitter and a DWDM filter module must provide some requirements such as the number of wavelengths with precise wavelength spacing between them, very narrow bandwidth for each of the wavelengths, and extremely little drift due to environmental condition tolerance during the multiwavelength operation [75].

In general, several laser sources as transmitters are needed due to transmission of different wavelengths along a single fiber in an optical

transmission system. One choice is a combination of several similar functional devices such as distributed feedback lasers (DFBLs) to form laser arrays. Besides, a modulator is usually external to the DFBLs especially when modulation rates are high. In this way, multiwavelength DFBLs arrays have been demonstrated in the 1550 nm region [76],[77],[78]. Despite of using DFBLs in optical transmission systems due to their excellent side-mode suppression, and their compactness, as a kind of semiconductor lasers, DFBLs are sensitive to back reflections and temperature which cause fluctuation in their output power and their operational wavelength [79]. In comparison with semiconductor lasers, fiber lasers have many benefits such as a wide range of operation wavelength, broad tunability, high quantum efficiency, large output power and stability with fiber optics devices [80],[81]. In addition, since fiber lasers can be generated by all fiber components, they are flexible in design without using special requirements such as a clean room, gas systems, and optical tables which are important for laser diode fabrications and main frame lasers.

Several researches have been done by using Erbium doped fiber lasers (EDFLs) to produce multiple wavelengths with constant wavelength spacings. In an approach, EDF were cooled by liquid nitrogen to reduce the homogenous linewidth, to minimize cross-gain saturation effects, to narrow the line spacing between consecutive lines, and to prevent mode competition between the adjacent laser lines [82]. Inhomogeneous broadening has also been achieved by the use of twin-core EDF to produce triple frequency EDFs [83]. Single mode operation of a compact multiwavelength Erbium-Yetterbium fiber lasers have generated up to 29 wavelengths in a simple Fabry-Perot design [84]. A high birefringence fiber loop mirror has also been used to adjust the operation wavelength and channel spacing

[85]. As another method, a multiple-quantum-well waveguide as an equivalent reflector has been employed to enhance the polarization hole burning of laser and to achieve Eleven wavelength with the spacing 0.08 nm using EDFs [86]. On the other hand, a group of laser lines, known as MBFLs, can be generated from Brillouin Stokes as a seed signal by using nonlinear Brillouin gain in an optical fiber. All Stokes waves are generated through cascaded SBS, which is a process in which each successive Stokes wave pumps the next-order Stokes wave after its power becomes large enough to satisfy the Brillouin threshold condition. At the same time, anti-Stokes waves are generated through FWM between copropagating pump and Stokes waves. After the oscillation of each Stokes, there will be the group of BFLs that generate MBFLs. The number of BFL lines depends on the Brillouin pump power. Another fiber laser is the hybrid of Brillouin Erbium fiber laser (BEFL) which manipulates narrow bandwidth of nonlinear Brillouin gain in an optical fiber with the linear gain from EDF to yield laser sources with the properties of BFL and the large output power from EDFA [87]. BEFLs are capable of generating optical combs, which is also known as MBEFLs, with line spacing 10 GHz at room temperature due to the Brillouin Stokes-shifted frequency from the injected Brillouin pump. Such combs with higher number of lines in comparison with MBFLs have been used as sources for DWDM systems [88], [89],[90],[91]. Bidirectional MBEFL was also demonstrated by using two identical EDFA and a single-mode fiber [92],[93]. Bismuth-based erbium doped fiber (Bi-EDF) was firstly used in compact optical amplifiers with short gain medium lengths and it is showed that Bi-EDF can extend the operational wavelength region of EDFA from 1600 nm region to 1610 nm region and its gain is higher than EDF [94]. In this work, it is showed that we can also generate MBEFLs by using Bi-

EDF and a 55 line MBEFL has been demonstrated by using bidirectional EDFA with two EDFA pump each of about 21 dBm (130 mW) and the Brillouin pump 3.5 dBm [95]. By using a semiconductor optical amplifier (SOA) instead of EDFA, multiwavelength operation of a hybrid Brillouin-semiconductor fiber laser (BSFL) has also been demonstrated. Firstly, the advantage of using a SOA instead of an EDFA is the possibility of multiwavelength generation in any wavelength band where SOA is available and EDFA cannot work, for example 1300 nm or 1650 nm. Secondly, SOA can work over a wide wavelength range using the same amplifying medium as well as the entire used components [96]. However, the number of lines is a few in multiwavelength BSFLs.

The other approach in the generation of multiple lasing wavelengths is multiwavelength Brillouin Raman fiber lasers (MBRFLs) in which a Raman amplifier is used to increase the number of Brillouin Stokes. Since the Raman amplification has a wide gain bandwidth, the number of lines is higher in MBRFLs compared to its counterpart MBEFLs. However, the optical pump power required in Raman amplification is significantly higher than that in EDFA. This was the reason that MBRFLs were not used in the early optical systems. Now, with the improvement of pump laser technology, Raman amplification is an important tool of expanding span transmission range and transmission capacity in optical systems. MBRFLs require a relatively long nonlinear fiber owing to the nature of Raman amplification. Compared with hybrid MBEFLs, MBRFls have more remarkable advantages such as room-temperature stable operation and extremely broad band operational wavelengths as long as Raman pump lasers at the corresponding wavelength are available [97],[98],[99],[100]. Although MBRFLs have some advantages in comparison with MBEFLs, the stability of

MBRFL outputs are unsatisfactory due to unstable mode hopping observed from the given spectra in some experiments [100],[101]. Moreover, the output peak power of MBRFL lines is less than -15 dBm even though Raman pump power is more than 300 mW in somewhat complicated configuration [100]. This problem has also observed in the MBEFL generation. Considering these problems and the limitation in the workable wavelength region of MBEFL due to EDFA wavelength limitation, MBFL generation has been considered in this thesis since MBFLs manipulate only nonlinear Brillouin gain in optical fibers. As soon as the Brillouin pump source is provided, MBFLs can be generated in a simpler configuration in comparison to the configurations used in the generation of MBEFLs and MBRFLs.

In this thesis, after discussing about Brillouin fiber laser (BFL) and its performance, we pay our attention to multiwavelength BFLs (MBFLs) generation. Then, multiwavelength Brillouin Erbium fiber lasers (MBEFLs) will be investigated by using Bismuth based EDFA. Finally, we will consider the generation of multiwavelength Brillouin Raman fiber lasers (MBRFLs).

1.5 Objective of This Thesis

The objective of this research is to investigate the characteristics of MBFLs, MBEFLs, and MBRFLs which have numerous applications such DWDM systems in optical communications. Although, there are a lot of reported researches about MBEFLs and MBRFLs in which some EDFA pumps and high power Raman pumps are used, the number of lines in some of the reported works is a few and the generated comb is not flat [91], [102] ,[101]. Therefore, this work is firstly focused on improving energy conversion in BFL generation. It will be

shown that the generation of BFL peak power higher than the transmitted Brillouin laser pump is possible by using only a 25 km single-mode fiber in a Fabry-Perot cavity [51]. In fact, this possibility provides higher Brillouin pump energy conversion that has not been observed before in the BFL systems. In addition, this work also aims to determine the BFL linewidth which has been a challenge. Although different values have been reported for BFL linewidth by using different Brillouin laser pumps, most of them are in the range of a few hertz and some measurement have been failed due to the resolution limitations of the radio frequency spectrum analyzer as it has been mentioned in the reports [51], [59]. In this thesis, BFL linewidth is measured at 8 Hz and 24 Hz by using the BP linewidth 15 MHz and 124 MHz, respectively [60]. As an application of the BFL generation, the generation of MBFLs will be demonstrated by using simple linear and ring cavities. In this work, we will be demonstrated 14 and 8 lines of MBFLs by using 14 dBm and 11.7 dBm BP power in the ring and linear cavities, respectively [63], [66]. As long as a suitable BP is used, MBFLs can be generated at any wavelength using a simple configuration. The generated MBFL has more number of lines and better flatness compared to some reported MBEFLs previously mentioned. In order to increase number of lines, a Bismuth based EDFA (Bi-EDFA) and a Raman amplifier will be also used separately to generate MBEFLs and MBRFLs, respectively. More than 50 lines of MBEFLs will be generated by using the compact Bi-EDFA [98]. The generated MBEFLs can be generated in only C band (1525-1565 nm) and L band (1565-1625 nm) wavelength regions which is the operational wavelength region of the Bi-EDFA. Finally, MBRFLs will be presented to generate multiwavelength laser source at any wavelength. In the generated MBRFL, the first, the second and the third Brillouin

Stokes will be generated by using a 25 km single-mode fiber as the Raman and Brillouin gain medium and a Raman pump power 150 mW [103]. The number of lines in the MBRFLs can be more when a fiber with higher Raman gain such as DCF and a Raman pump with higher power will be available. Under different Raman pumping schemes, the reduction of the SBS threshold power is highest for the bi-directional Raman amplification and is the lowest for the backward Raman pumping scheme. In addition, the reduction of the SBS threshold with the increase of Raman gain will be studied. It will be observed that this decrease is much faster for bi-directional and forward pumping than backward pumping. However, the amount of reduction depends strongly and solely on the Raman gain, independent of Raman pumping scheme [104].

1.6 The Research Methodology

In this thesis, the generation of BFLs and MBFLs in both ring and linear cavities will be studied after a literature review about BFL generation. Then, by changing cavity parameters such as coupler ratios, component locations, and by using available components, new BFL cavity configuration will be demonstrated to generate higher power BFLs. As a challenging issue, the linewidth of BFLs will be measured and it will be compared with the measured BP linewidth.Then, by using optical amplifiers such as Bi-EDFA and Raman amplifiers, the behavior of MBFLs will be studied.

1.7 Thesis Overview

This thesis consists of 6 main chapters. After reviewing the overall topics in the chapter 1, the theory of nonlinear optics will be discussed in the chapter 2 which leads to the theory of stimulated Brillouin scattering and the

description of BFL generation as effects in nonlinear optics. In the chapter 3, after an experimental review on SBS, the theory of MBFL generation and the experimental results of BFLs and MBFLs will be demonstrated in both ring and linear cavities. This chapter also contains the coherent detection and the linewidth measurement by homodyne and heterodyne methods. Then the experimental results on the linewidth measurement of a tunable laser source and a BFL will be mentioned by using another independent BFL in a heterodyne method. In the chapter 4, by using a Bi-EDF, MBEFLs will be generated in a linear cavity. The discussion and results of the MBEFLs will also be presented in the chapter 4. MBRFLs will be introduced in the chapter 5 by using only a single-mode fiber as the Raman and Brillouin gain medium. The thesis will be ended by the chapter 6 as the conclusion chapter which summarizes all the researches done in this thesis.

References

[1] T. Miya, Y. Terunuma, T. Hosaka, and T. Miyashita, **"***Ultimate. low-loss single- mode fibers at 1.55 pm,*" Electron**.** Lett**.,** Vol**.** 15, 1979**,** pp**.** 106-108.

[2] R. G. Smith, "*Optical power handling capacity of low loss optical fibers as determined by stimulated Raman and Brillouin scattering*," Appl. Opt. Vol. 11, 1972, pp. 2489- 2494.

[3] R. H. Stolen, E. P. Ippen, and A. R. Tynes, "*Raman oscillation in glass optical waveguide*," Appl. Phys. Lett., Vol. 20, 1972, pp. 62-64.

[4] E. P. Ippen and R. H. Stolen, "*Stimulated Brillouin scattering in optical fibers*," Appl. Phys. Lett., Vol. 21, 1972, pp. 539-541.

[5] C. Lin and R. H. Stolen, "*Backward Raman amplification and pulse steepening in silica fibers*," Appl. Phys. Lett., Vol. 29, 1976, pp. 428-431.

[6] N. A. Olsson, and J. P. van der Ziel, "*Cancellation of fiber loss by semiconductor laser pumped Brillouin amplification at 1.5 μm*," Appl. Phys. Lett. , Vol. 48, 1986, pp. 1329-1330.

[7] K. O. Hill, B. S. Kawasaki, and D. C. Johnson, "*Cw Brillouin laser* ,"Appl. Phys. Lett., Vol. 28, 1976, pp. 608-609.

[8] K. O. Hill, , D. C. Johnson, and B. S. Kawasaki, "*Low-threshold CW Raman laser*," Appl. Phys. Lett. Vol. 29, 1976, pp. 181-183.

[9] C. J. Koester and E. Snitzer, "*Amplification in a fiber laser*," Appl. Opt., Vol. 3, 1964, pp. 1182-1186.

[10] E. Desuvire, J. R. Simpson, and P.C. Becker, "*High-gain erbium-doped traveling -wave fiber amplifier*," Opt. Lett., Vol. 12, 1987, pp. 888-889.

[11] P. Bayvel and I. P. Giles, "*Evaluation of performance parameters of single-mode all-fiber Brillouin ring lasers*", Opt. Lett., Vol. 14, 1989, pp. 581-583.

[12] E. Desuvire, D. Bayart, B. Desthieux, and S. Bigo, "*Erbium-Doped Fiber Amplifiers: Device and System Development*," Wiley, New York, 2002.

[13] G. P. Agrawal, "*Ligthwave Technology: Telecommunication systems*," Wiley, Hoboken, NJ, 2005.

[14] I. P. Kaminow and T. Li, Eds., "*Optical Fiber Telecommunications*," Vols. 4A and 4B, Academic Press, Boston, 2002.

[15] R. Ramaswami and K. Sivarjan, "*Optical Networks: A Practical Prospective*," 2 nd. Ed., Morgan Kaufmann Publishers, San Francisco, 2002.

[16] K. O. Hill, Y. Fujii, D. C. Johnson, and B. S. Kawasaki, "*Photosensitivity in optical fiber waveguides: Application to reflection filter fabrication*," Appl. Phys. Lett., Vol. 32, 1978, pp. 647-649.

[17] R. Kashyap, "*Fiber Bragg Gratings*," Academic Press, Boston, 1999.

[18] J. C. Knight, T. A. Birks, P. St. J. Russell, and D. M. Atkin, "*All-silica single-mode optical fiber with photonic crystal cladding*," Opt. Lett., Vol. 21, 1996, pp. 1547-1549.

[19] J. Broeng, D. Mogilevstev, S. B. Barkou, and A. Bjarklev, "*Photonic crystal fibers: A new class of optical waveguides,*" Opt. Fiber Technol., Vol. 5, 1999, pp. 305-330.

[20] T. M. Monro, D. J. Richardson, N. G. R. Broderick, and P. J. Bennett, "*Holey optical fibers: An efficient modal model*," J. Lightwave Technol., Vol. 17, 1999, pp. 1093-1102.

[21] Y. Koyamada, S. Sato, S. Nakamura, H. Sotobayashi, and W. Chujo, "*Simulating and Designing Brillouin Gain Spectrum in Single-Mode Fibers*," J. Lightwave Technol., Vol. 22, 2004, pp. 631-639.

[22] C. Headly and G. P. Agrawal, Eds., "*Raman Amplification in Fiber Optical Communication Systems," Academic Press*, Boston, 2005.

[23] F. Yaman, Q. Lin, and G. P. Agrawal, in "*Guided Wave Optical Components and Devices*," B. P. Pal, ed., Academic Press, Boston, ch.7, 2006.

[24] M. Born, and E. Wolf, "*Principles of Optics*," 7$^{th.}$ ed., Cambridge University Press, New York, 1999.

[25] F. A. Jenkins, H. E. White, "*Fundamentals of Optics*," 4th Ed., Mc Graw-Hill, New York, 2001.

[26] R. W. Boyd, "*Nonlinear Optics*," Academic Press, San Diego, 2008.

[27] I. L. Fabelinskii, "*Molecular scattering of light*," New York, Plenum, 1968.

[28] L. D. Landau, E. M. Lifshits and L. P. Pitaevskii, "*Electrodynamics of continuous media*," Pergamon, Oxford, 1984.

[29] L. I. Mandelstam, "*Light scattering by inhomogeneous media*," Zh. Russ. Fiz-Khim. Ova., Vol. 58, 1926, p. 381 (In Russian).

[30] L. Brillouin, "*Diffusion dela lumiere et des rayonnes X par un corps transparent homogene; influence del`agitation thermique*," Ann. Phys. (Paris), Vol. 17, 1922, p. 88.

[31] E. Gross, "*Change of wavelength of light due to elastic heat waves at scattering in liquids*," Nature, Vol. 126 (201), 1930, p. 400.

[32] E. Gross, "Über Änderun der Wellenlänge *bei Lichtzerstreuung in Kriztallen*," Z. Phys., Vol. 63, 1930, p. 685.

[33] R. Y. Chiao, C. H. Townes, and B. P. Stoicheff, "*Stimulated Brillouin Scattering and Coherent Generation of Intense Hypersonic Waves*," Phys. Rev. Lett., Vol. 12, 1964, pp. 592-595.

[34] C. V. Raman, "*A new radiation*," Indian J. Phys. Vol. 2, 1928, p. 387.

[35] E. J. Woodbury, and W. K. Ng, "*Ruby laser operation in the near IR*," Proc. IRE Vol. 50, 1962, p. 2367.

[36] D. N. Christodoulides, and R. B. Jander, "*Evolution of stimulated Raman. crosstalk in wavelength division multiplexed systems*," IEEE Photon. Technol. Lett., Vol. 8, 1996, pp. 1722-1724.

[37] K. P. Ho, "*Statistical properties of stimulated Raman crosstalk in WDM systems*," J Lightwave Technol., Vol. 18, 2000, pp. 915- 921.

[38] Y. Horiuchi, S. Yamamoto, and S. Akiba, "*Stimulated Brillouin scattering suppression effects induced by cross-phase modulation in high power WDM repeaterless transmission*," Electron. Lett., Vol. 34, 1998, pp. 390-391.

[39] S. S. Lee, H. J. Lee, W. Seo, and S. G. Lee, "*Stimulated Brillouin scattering suppression using cross-phase modulation induced by an optical supervisory channel in WDM links* ," Photon. Technol. Lett., Vol. 13, 2001, pp.741-743.

[40] S. J. Strutz, K. J. Williams, and R. D. Esman, "*Polarization-maintaining hybrid erbium-Brillouin amplifier for high-power low-noise sources*," Photon. Technol. Lett., Vol. 13, 2001, pp. 936-938.

[41] H. Suzuki, J. Kani, H. Masuda, N. Takachio, K. Iwatsuki, Y. Tada, and M. Sumida, "*1–Tb/s (100 10 Gb/s) Super-Dense WDM Transmission with 25–GHz Channel Spacing in the Zero-Dispersion Region Employing Distributed Raman Amplification Technology*," Photon. Technol. Lett., Vol. 12, 2000, pp. 903-905.

[42] S. Namiki and Y. Emori, "*Ultrabroad-band Raman amplifiers pumped and gain equalized by wavelength-division-multiplexed high-power laser diodes*," J. Sel. Topics Quantum Electron., Vol. 7, 2001, pp. 3- 16.

[43] M. N. Islam, Ed., "*Raman Amplifiers for Telecommunications*," Springer, New York, 2004.

[44] J. Bromage, "*Raman Amplification for Fiber Communications Systems*," J. Lightwave Technol., Vol. 22, 2004, pp. 79-93.

[45] D. F. Grosz, A. Agarwal, S. Banerjee, D. N. Maywar, and A. P. K̈ung , "*All-Raman Ultralong-Haul Single-Wideband DWDM Transmission Systems With OADM Capability*," J. Lightwave Technol., Vol. 22, 2004, pp. 423-432.

[46] C. Culverhouse, F. Farahi, C. N. Pannel, and D. A. Johnson, "*Potential of stimulated Brillouin scattering as sensing mechanism for distributed temperature sensors* ," Electron. Lett., Vol. 25, 1989, pp. 913-914.

[47] T. R. Parker, M. Farhadiroushan, R. Feced, V. A. Handerek, and A. J. Rogers, "*Simultaneous distributed measurement of strain and temperature from noise*

initiated Brillouin scattering in optical fibers," J. Quantum Electron. Vol. 34, 1998, pp. 645-659.

[48] Y. T. Cho, M. N. Alahbabi, G. Brambilla, and T. P. Newson, "*Distributed raman amplification combined with a remotely pumped EDFA utilized to enhance the performance of spontaneous brillouin-based distributed temperature sensors*," Photon. Technol. Lett., Vol. 17, 2005, pp. 1256-1258.

[49] S. P. Smith, F. Zarinetchi, and S. Ezekiel, "*Narrow-linewidth stimulated Brillouin fiber laser and applications*," Opt. Lett., Vol. 16, 1991, pp. 393-395.

[50] J. Geng, S. Staines, and S. Jiang, "*Dual-frequency Brillouin fiber laser for optical generation of tunable low-noise radio frequency/microwave frequency*," Opt. Lett., Vol. 33, 2008, pp. 16-18.

[51] M. R. Shirazi, S. W. Harun, M. Biglary, and H. Ahmad "*Linear cavity Brillouin fiber laser with improved characteristics*," Opt. Lett., Vol. 33, 2008, pp. 770-772.

[52] A.V. Tausenev , E. D. Obraztsova, A. S. Lobach, A. I. Chernov, V. I. Konov, P. G. Kryukov, A. V. Konyashchenko, E. M. Dianov**,** "*177 fs erbium-doped fiber laser mode locked with a cellulose polymer film containing single-wall carbon nanotubes*," Appl. Phys. Lett., Vol. 92, 2008, 171113-171116.

[53] D. Y. Shen, J. K. Sahu, and W. A. Clakson, "*Highly efficient Er,Yb-doped fiber laser with 188W free-running and > 100W tunable output power*,"Opt. Express, Vol. 12, 2004, pp. 6230-6239.

[54] B. M. Walsh and N. P. Barnes, "*Comparison of Tm: ZBLAN and Tm: silica fiber lasers, spectroscopy and tunable pulsed laser operation around 1.9 μm*," Appl. Phys. B, Vol. 78, 2004, pp. 325-333.

[55] P. Polynkin, R. Roussev, M. Fejer, N. Peyghambarian, J. Moloney, "*Laser transmitter for undersea communications using third-harmonic generation of fiber-laser system at 1.5 μm*," Photon. Technol. Lett., 2007 pp. 1328-1330.

[56] J. E. Koroshetz*,"Fiber Lasers for lider*," in IEEE OFC conference, Optical Fiber Communication Conference, Vol. 5, 2005 , pp. 202-205.

[57] R. Hack, "*Material processing with fiber lasers*," Industrial Laser Solutions for Manufacturing, Vol. 18, 2003, Issue 2.

[58] K. Kincade, "*Optoelectronic Application: Biophotonics fiber lasers find opportunities in medical applications*," Laser Focus World, Vol. 41, 2005, Issue 9.

[59] J. Geng, S. Staines, Z. Wang, J. Zong, M. Blake, and S. Jiang."*Highly stable low-noise Brillouin fiber laser with ultra narrow spectral line width*," Photon. Technol. Lett., Vol. 18, 2006, pp. 1813-1815.

[60] M. R. Shirazi, S. W. Harun, M. Biglary, K. Thambiratnam, and H. Ahmad, "*Effect of Brillouin pump linewidth on the performance of Brillouin Fiber Lasers*," ISAST Transactions on Electronics and Signal Processing, No. 1, Vol. 1, 2007, pp. 30-32.

[61] F. Zarinetchi, S.P. Smith, and S. Ezekiel, "*Stimulated Brillouin fiber optic laser gyroscope*," Opt. Lett., Vol.16, 1991, pp. 229-231.

[62] M. R. Shirazi, S. W. Harun , K. Thambiratnam M. Biglary and H. Ahmad "*New Brillouin Fiber Laser Configuration with High Output Power*," Microwave Opt. Technol. Lett., Vol. 49, 2007, pp. 2656-2658.

[63] M R Shirazi, M Biglary, S W Harun, K Thambiratnam and H Ahmad, "*Bidirectional multiwavelength Brillouin fiber laser generation in a ring cavity*,"IOP, J. Opt. A: Pure Appl. Opt. Vol. 10, 2008, 055101, 3pp.

[64] V. Lecoeuche, P. Niay, M. Douay, P. Bernage, S. Randoux and J. Zemmouri, " *Bragg grating based Brillouin fiber laser*," Opt. Commun., Vol. 177, 2000, pp. 303-306.

[65] H. Ahmad, M. R. Shirazi, M. Biglary, and S. W. Harun, "*Linear Cavity Brillouin Fiber Laser Using a Fiber Bragg Grating*," Microwave Opt. Technol. Lett., Vol. 50, 2008, pp. 265-266.

[66] M. R. Shirazi, N. S. Shahabuddin, S. N. Aziz, K. Thambiratnam, S. W. Harun, and H. Ahmad, "*A linear cavity Brillouin fiber laser with multiple wavelength output*," Laser Phys. Lett., Vol.5, 2008, pp. 361-363.

[67] Y. Han, T. V. A. Tran, S. Kim, and S. B. Lee, "*Multiwavelength Raman-fiber-laser-based long-distance remote sensor for simultaneous measurement of strain and temperature*," Opt. Lett., Vol. 30, 2005, pp. 1282-1284.

[68] A. During, C. Fossati, and M. Commandré, "*Multiwavelength Imaging of Defects in Ultraviolet Optical Materials*," Appl. Opt., Vol. 41, 2002, pp. 3118-3126.

[69] E. - H. Lee, K. H. Kim and H. K. Lee, "*Nonlinear effects in optical fiber: Advantages and disadvantages for high capacity all-optical communication application*," Springer, Optical and Quantum Electronics, Vol. 34, 2002, pp.1167–1174.

[70] M. Nakazawa, T. Yamamoto, and K. R. Tamura, "*1.28 Tbit/s - 70 km OTDM transmission using third- and fourth-order simultaneous dispersion compensation with a phase modulator*," ECOC'OO, Munich, Germany, 2000, Post Deadline paper, PD 2.6.

[71] A. Shtainhart, R. Segal, A. Tsherniak, "*Wavelength division multiplexing*,"Networks, Rada Communication, 1999.

[72] D. Derickson, *Fiber Optic Test and Measurement*, Prentice-Hall Inc., 1998.

[73] L. Zhan, J. H. Ji, J. Xia, S. Y. Luo, and Y. X. Xia, "*160-line multiwavelength generation of linear cavity self-seed Brillouin-Erbium fiber laser*," Opt. Express, Vol. 14, 2006, pp. 10233-10238.

[74] A. K. Zamzuri, M. A. Mahdi, A. Ahmad, M. I. Md Ali, and M. H. Al-Mansoori, "*Flat amplitude multiwavelength Brillouin-Raman comb fiber laser in Rayliegh-scattering-enhanced linear cavity*," Opt. Express, Vol. 15, 2007, pp. 3000-3005.

[75] S. Mysore, R. Villa and G. Beveridge, "*Performance of Broadband DWDM Networks*,"IEEE Digest of the LEOS Summer Topical Meetings, July 2000, Page(s):IV23 - IV24.

[76] C. E. Zah, P. S. D. Lin, F. Favire, B. Pathak, R. Bhat, C. Caneau, A. S. Gozdz, N. C. Andreadakis, M. A. Koza, T. P. Lee, T. C. Wu and K. Y. Lau, "*1.5 pm compressive-strained multiple quantum-well 20 wavelength distributed-feedback laser arrays*," Electron. Lett., Vol. 28, 1992, pp. 824-826.

[77] C. E. Zah, J. Gamelin, B. Pathak, F. Favire, P. S. D. Lin, N. C. Andreadakis, "*Multiwavelength light source with integrated DFB laser array and star coupler for WDM lightwave communications*," Int. J. of High Speed Electronics and Systems, Vol. 5, 1994, pp. 91-109.

[78] C. E. Zah, B. Pathak, R. Bhat, W. C. Young, and T. P. Lee, "*Monolithic integrated multiwavelength laser arrays for WDM lightwave systems*," J. of Optoelectronics Devices and Technologies, Vol. 9, 1994, pp. 153-166.

[79] Hewlett Packard "*Backreflection and return loss consideration for optical transmission systems*," 8156 A Solution Brief, Germany, 1993.

[80] M. S. O'Sullivan, J Chrostowski, E Desurvire, J. R. Simpson, "*High power narrow linewidth* Er^{+3} *doped fiber laser*," Opt. Lett., Vol. 14,1989, pp. 438-440.

[81] P. W. France, "*Optical fiber lasers and amplifiers*," CRC Press Inc., Florida, 2000.

[82] E. Desurvive, J. L. Zyskind, and J. R. Simpson, "*Spectral gain hole-burning at* $1.53\mu m$ *in erbium-doped fiber amplifiers*," Photon. Technol. Lett., Vol. 2, 1990, pp. 246-248.

[83] O. Graydon, W. H. Loh, R. L. Laming, and L. Dong, "*Triple frequency operation of an Er-doped twin core fiber loop laser*," Vol. 8, 1996, pp. 63-65.

[84] Shinji Yamashita, "*Miniature Erbium:Yetterbium fiber Fabry-Perot multiwavelength lasers*," J. Selected Topics in Quantum Electron., Vol. 3, 1997, pp. 1058-1064.

[85] X. P. Dong, S. Li, K. S. Chiang, M. N. Ng, B. C. B. Chu, "*Multiwavelength erbium-doped fiber laser with a high –birefringence fiber loop mirror*," Electron. Lett., Vol. 36, 2000 , pp. 1609-1610.

[86] J. Sun, J. Qiu, D. Huang, "*Multiwavelength erbium-doped fiber laser exploiting polarization hole burning*," Opt Commun., Vol. 182, 2000, pp. 193-197.

[87] G. J. Cowle, and D. Yu. Stephanov, "*Hybrid brillouin/erbium fiber laser*," Opt. Lett., Vol. 21, 1996, pp. 1250-1252.

[88] G. J. Cowle, and D. Yu. Stephanov, "*Multiple wavelength generation with Brillouin/Erbium fiber lasers*," Photon. Technol. Lett., Vol. 8, 1996, pp. 1465-1467.

[89] L. Zhan, J. H. Ji, J. Xia, S. Y. Luo, and Y. X. Xia, "*160-line multiwavelength generation of linear cavity self-seeded Brillouin-Erbium fiber laser*," Opt. Express Vol. 14, 2005, pp. 10233-10238.

[90] H. Ahmad, X. S. Cheng and S. W. Harun, "*An efficient S-band brillouin erbium fiber laser with additional EDFA*," Opt. Laser Technol., Vol. 39, 2007, pp. 616-618.

[91] G. J. Cowle, W. H. Loh, R. I. Laming and D. Yu. Stephanov, "*Multiwavelength operation of Brillouin/erbium fiber lasers with injection-locked seeding*," IEEE Optical Fiber Communication (OFC), Conference on, 1997, pp. 34-35.

[92] M. Kamil, A. Rahman , M. Khazani Abdullah, H. Ahmad, "*Multiwavelength bidirectional operation of twin-cavity Brillouin/Erbium fiber laser*," Opt. Comm., Vol. 181, 2000, pp. 135-139.

[93] W. H. Oh, J. S. Ko, D. S. Lim, W. Seo, "*10 and 20 GHz optical comb generation in Brillouin/Erbium fiber laser with shared cavity of Sagnac reflector*," Opt. Comm., Vol. 181, 2002, pp. 399-403.

[94] N. Sugimoto, K. Ochiai, T. Hirose, S. Ohara, Y. Fukasawa, "*Ultracompact gain block with Bi_2O_3-based erbium-doped fiber*," Jpn. J. Appl. Phys., Vol. 43, 2004, pp. 2551-2552.

[95] S. Shahi, S. W. Harun, N. S. Shahabuddin, M. R. Shirazi, and H. Ahmad, "*Multiwavelength generation using a bismuth-based EDF and Brillouin effect in a linear cavity configuration*," Opt. Laser Technol., Vol. 41, 2009, pp. 198-201.

[96] Alaa Hayder, and L. R. Chen, "*Multiwavelength generation in a Brillouin semiconductor fiber laser*," Proc. IEEE-LEOS. Annual Meeting, 2006, pp. 398-399.

[97] B. Min, P. Kim, and N. Park, "*Flat amplitude equal spacing 798-channel Rayleigh-assisted Brillouin/Raman multiwavelength comb generation in*

dispersion compensating fiber," Photon. Technol. Lett., Vol. 13, 2001, pp. 1352-1354.

[98] K. D. Park, B. Min, P. Kim, N. Park, J. H. Lee, and J. S. Chang, "*Dynamics of cascaded Brillouin-Rayleigh scattering in a distributed fiber Raman amplifier*," Opt. Lett., Vol. 27, 2002, pp. 155-157.

[99] A. K. Zamzuri, M. I. Md Ali, A. Ahmad, R. Mohamad, and M. A. Mahdi, "*Brillouin-Raman comb fiber laser with cooperative Rayleigh scattering in a linear cavity*," Opt. Lett., Vol. 31, 2006, pp. 918-920.

[100] A. K. Zamzuri, M. A. Mahdi, A. Ahmad, M. I. Md Ali, and M. H. Al-Mansoori, "*Flat amplitude multiwavelength Brillouin-Raman comb fiber laser in Rayliegh-scattering-enhanced linear cavity*," Opt. Express, Vol. 15, 2007, pp. 2000-2005,.

[101] Y. Liu and D. Wang, "*Wavelength tunable and amplitude equilibrium dual-wavelength lasing source with dual-pass Raman/ Brillouin amplification configuration*," Opt. Express, Vol. 16, 2008, pp. 3583-3588.

[102] S.W. Harun, X.S. Cheng, N.K. Saat and H. Ahmad, "*S-band Brillouin erbium fibre laser*," Electron. Lett., Vol. 41, 2005, pp. 174- 176.

[103] S. W. Harun, M. R. Shirazi and H. Ahmad, "*Multiple wavelength Brillouin fiber laser from injection of intense signal light*," Laser Phys. Lett., Vol. 4, 2007, pp. 678-680.

[104] M. R. Shirazi, M. Biglary, S. W. Harun, K. Thambiratnam, and H. Ahmad, "*Effects of different Raman pumping schemes on stimulated Brillouin scattering in a linear cavity*," Appl. Opt., Vol. 47, 2008, pp.3088-3091.

Chapter 2:

The Theory of Brillouin Fiber Laser Generation

2.1 Inrtoduction

In this chapter, after introducing principles of nonlinear optics, a short review of cubic nonlinear processes will be discussed. Then the theory of stimulated Brillouin scattering, and Brillouin fiber laser generation will be presented. The subjects and the equations in this chapter are based on the usage of some books and papers mentioned in the references especially Fundamentals of Optical Fibers [1], Nonlinear Optics [2], Nonlinear Optics: Basic Concepts [3], Nonlinear Optics [4], and Lasers [7].

2.2 The Propagation of Light in both linear and nonlinear media

The nonlinear phenomena in optical fiber waveguides can be understood by considering the electromagnetic wave theory in dispersive nonlinear media. By using Maxwell's equations and the constitutive relations, the wave equation describing the light propagation in optical fibers can be obtained. The fundamental equation for the propagation of electric field in both linear and nonlinear medium can be obtained as [1],[2]

$$\nabla\times(\nabla\times\mathbf{E}) - \frac{1}{c^2}\frac{\partial^2\mathbf{E}}{\partial t^2} = \frac{1}{\varepsilon_0 c^2}\frac{\partial^2\mathbf{P}}{\partial t^2} \tag{2.1}$$

where c is the speed of light in vacuum and ε_0 is the vacuum permittivity. This equation is the main equation for describing the propagation of the electric field in linear and nonlinear media. A relation between the induced electric polarization **P** and the electric field **E** must be specified somehow. This cannot be done only within the Maxwell equations since **P** is a property of the material medium where the field **E** propagates in. In order to proceed, we need to know how a dipole moment density **P** is produced in the medium. In other words, we require information on the relationship between **P** and **E** which will be discussed later. In linear media, **P** and **E** are related linearly by

$$\mathbf{P} = \varepsilon_0 \chi \mathbf{E} \tag{2.2}$$

where χ is the electric susceptibility function which is a constant. Therefore, the electric and magnetic fields propagating in a lossless linear medium can also be shown in the real instantaneous form as uniform plane waves

$$\mathbf{E} = \frac{1}{2}\mathbf{E}_0 \{ \exp\left(i(\omega t \pm \beta z + \Phi)\right) + \text{c.c.} \} \tag{2.3}$$

$$\mathbf{H} = \frac{1}{2}\mathbf{H}_0 \{ \exp\left(i(\omega t \pm \beta z + \Phi)\right) + \text{c.c.} \} \tag{2.4}$$

where $\mathbf{E_0}$ and $\mathbf{H_0}$ are the amplitude vectors of the electric and magnetic fields, respectively. ω is the radian frequency and β is known as the wave propagation constant is the phase shift per unit distance of the wave measured along the z axis. Φ represents an overall phase, and c.c. denotes the complex conjugate of the preceding term.

2.3 The Origin of Nonlinear Optical Phenomena

When the optical power within an optical fiber is small, the fiber can be treated as a linear medium; that is, the loss and refractive index of the fiber are independent of the signal power. However, when power reaches enough high levels in an optical system, nonlinear effects arise since refractive index and loss (or gain) depends on optical power.

As soon as high intensity light passes through optical fibers various nonlinear effects may be observed [2]. Nonlinearities can be classified into two main categories. The first category of the nonlinearities occurs due to scattering effect since the photons of the incident light wave interact with phonons in the medium. The two main nonlinear effects in this category are stimulated Brillouin scattering (SBS) and stimulated Raman scattering (SRS). In the second group, however, the dependence of the refractive index on the incident light power is the main factor for the generation. Some nonlinear effects in the second group are four wave mixing (FWM), self-phase modulation (SPM), and cross-phase modulation (CPM). All of these effects except SPM and CPM provide gain for other wavelengths at the expense of depleting power of the incident light known as pump. SPM and CPM change only the phase of the light and cause spectral broadening which leads to an increase in chromatic dispersion.

Nonlinear effects are related to anharmonic motion of the bound electrons under the influence of an applied electromagnetic field. With intense electromagnetic field, nonlinear response of the refractive index in an optical fiber is more obvious. In practice, the largest electric fields obtained in matter fall into the range of 10^6 v/cm in which most forms of matter exhibit electrical breakdown. In addition, an electron bound to an atom or molecule or moving through a solid or

dense liquid, experiences electric fields in the range of 10^9 v/cm because over distance which is the order of an angstrom around the electron, the change in electrostatic potential can be several electron volts. Therefore, the external laboratory fields are very small compared to the electric fields naturally experienced by the electrons in the atom and molecule structures from which dense matter is constructed. In this condition, one can expand the dipole electric moment per unit volume, P(r,t), in a Taylor series in powers of the macroscopic field E(r,t) at the same point and at the same time [2],[3]:

$$P_\alpha(\mathbf{r},t) = P_\alpha(E=0,\mathbf{r},t) + \sum_\beta \left(\frac{\partial P_\alpha}{\partial E_\beta}\right) E_\beta + \frac{1}{2!}\sum_\beta\sum_\gamma \left(\frac{\partial^2 P_\alpha}{\partial E_\beta \partial E_\gamma}\right) E_\beta E_\gamma + \frac{1}{3!}\sum_\beta\sum_\gamma\sum_\delta \left(\frac{\partial^3 P_\alpha}{\partial E_\beta \partial E_\gamma \partial E_\delta}\right) E_\beta E_\gamma E_\delta + \ldots \quad (2.5)$$

where α, β, γ, δ range over the Cartesian components x, y, and z. Then the αth Cartesian component of the dipole moment per unit volume, $P_\alpha(r,t)$ is a function of the three Cartesian components of the external electric field. Our situation is a dielectric waveguide, optical fiber, within which the first term, dipole moment in zero external electric field, vanishes; any dipole moment present is then induced by the externally applied electric field, with their origin in incident laser radiation. The second and the subsequent terms describe the influence of a time-dependent, macroscopic external electric field. Then the response of medium to the external field can be written as

$$P_\alpha(\mathbf{r},t,) = \varepsilon_0 \sum_\beta \chi^{(1)}_{\alpha\beta} E_\beta(\mathbf{r},t) + \varepsilon_0 \sum_{\beta\gamma} \chi^{(2)}_{\alpha\beta\gamma} E_\beta(\mathbf{r},t) E_\gamma(\mathbf{r},t) + \varepsilon_0 \sum_{\beta\gamma\delta} \chi^{(3)}_{\alpha\beta\gamma\delta} E_\beta(\mathbf{r},t) E_\gamma(\mathbf{r},t) E_\delta(\mathbf{r},t) + \ldots \quad (2.6)$$

in which $\chi^{(1)}_{\alpha\beta}$ is the susceptibility tensor of ordinary dielectric theory whereas, $\chi^{(2)}_{\alpha\beta\gamma}$ and $\chi^{(3)}_{\alpha\beta\gamma\delta}$ are referred to as the second and third order susceptibilities, respectively. $\chi^{(1)}_{\alpha\beta}$ is a second rank tensor which is diagonal for isotropic material such as gas, liquid, or a cubic crystal. $\chi^{(2)}_{\alpha\beta\gamma}$, a third rank tensor, must vanish in any material that is left invariant in form under inversion because both **P** and **E** are vectors and thus odd under inversion symmetry. Therefore, in this work in which Si fibers are used $\chi^{(2)}_{\alpha\beta\gamma}$ must vanish. Eq. (2.6) assumes that the system responds instantaneously to the applied field, however, the electrons and nuclei in media rearrange themselves in order to response the macroscopic electric fields. In practice, the dipole moment at any time is the consequence of the response of the medium to the electric field over some time interval in the past times. In addition, the dipole moment at any point depends not only on the electric field at precisely the point but also on the electric field at other points in the vicinity of the point. If an electric field is applied to one single molecule of a crystal lattice, the electrons within this molecule will be redistributed, and the position of the positive charges (nuclei) will be shifted. However, it should be noted that since the wavelength of light is very long compared to the underlying microscopic length scales in the medium, the proportional terms of the nonlinear susceptibilities $\chi^{(n)}(\mathbf{k},\omega)$ to the wave vector of light **k** (or the proportionality of $\chi^{(n)}(\mathbf{r},t)$ to **r** in the Fourier transformation) can be ignored. Nevertheless, as discussed in the perturbation theoretic expressions for the nonlinear susceptibilities, the magnitude of the wave vector dependencies can be enhanced substantially by operating at a frequency very close to that of an isolated resonance. Therefore, in the Fourier transformation, Eq. (2.6) can be written as [4]

$$P_{\alpha}(\omega) = \sum_{n=1} P_{\alpha}^{(n)}(\omega) \tag{2.7}$$

where

$$P_{\alpha}^{(n)}(\omega) = \varepsilon_0 \sum_{i_1,...i_n} \int_{-\infty}^{+\infty} ... \int_{-\infty}^{+\infty} \chi_{\alpha\, i_1...i_n}^{(n)}(\omega_1,...,\omega_n) \times E_{i_1}(\omega_1)...E_{i_n}(\omega_n) \prod_{i=1}^{n-1} d\omega_i \tag{2.8}$$

For strong fields, it is common to separate P_α in Eq. (2.7) into the first term which is linear in the electric field and all the other terms which are nonlinear so that

$$P_\alpha = P_{(L)\alpha} + P_{(N)\alpha} \tag{2.9}$$

The last equation is the most general relation between **P** and **E**. On the other hand, in practice, the nonlinear response of the medium occurs on a very narrow time scale much smaller than the time scale of the linear response, therefore, in practice, the nonlinear response can be assumed to be instantaneous for pulse widths greater than 7 ps high speed optical pulses above of 10 Gb/s [5]. Thus, we can consider instantaneous nonlinear response as

$$\mathbf{P} = \varepsilon_0 [\, \chi^{(1)} \mathbf{.}\, \mathbf{E} + \chi^{(2)} \mathbf{:}\, \mathbf{EE} + \chi^{(3)} \vdots\, \mathbf{EEE} + \ldots \,] \tag{2.10}$$

where ε_0 is the vacuum permittivity and $\chi^{(i)}$ (i=1,2,….) is the $(i+1)^{th}$ order tensor susceptibility. The operations denoted by **.,:,⋮** are convolutions which show summation over repeated indexes. The linear susceptibility $\chi^{(1)}$ represents the dominant contribution which relates linearly **E** to **P** , while the second order susceptibility $\chi^{(2)}$ is the lowest nonlinear susceptibility responsible for second-order nonlinear effects such as second harmonic generation and sum-frequency generation. In addition, the ratio of the magnitude terms in successive order of Eqs. (2.7) can be viewed as [6]

$$\left|\frac{P_{\alpha}^{(n+1)}}{P_{\alpha}^{(n)}}\right| = \left|\frac{E}{E_a}\right| \tag{2.11}$$

In practice, the atomic field E_a has an order of magnitude of 10^{10} (v/m) to 10^{11} (v/m) whereas the largest magnitude of electric field E is limited in the range 10^6 (v/m) because most insulating materials suffer dielectric breakdown for external electric fields with magnitude above this limitation. Therefore, the largest values of $\left|\frac{E}{E_a}\right|$ lies in the range of 10^{-4} to 10^{-5}.

Due to decreasing behavior of the magnitude of the higher order susceptibility tensors, the first and the second nonlinearities referred to as *quadratic* and *cubic* nonlinear polarizations are usually considered. However, as said before, the value of $\chi^{(2)}$ must be zero in any centrosymmetric and isotropic material. Therefore, $\chi^{(2)}$ diminishes in silica fiber where there are symmetrical molecules of SiO_2 used in this work in the form of optical fiber waveguides. In other words, the second-order nonlinear effects can not be exhibited in this work. Then the lowest order nonlinear effects originate from the 3rd order susceptibility $\chi^{(3)}$, which is responsible for the phenomena such as third harmonic generation, four-wave mixing and nonlinear refraction. These phenomena mentioned in the 3rd order susceptibility $\chi^{(3)}$ are elastics as there is no energy exchanged between the electromagnetic fields and matter. They are due to the dependence of the refractive index on the input light power.

However, there are also third-order effects occurring because of the inelastic scattering effect. This class of nonlinear effects results from stimulated Brillouin scattering (SBS) and stimulated Raman scattering (SRS) in which the optical field transfer part of its energy to the nonlinear medium. They can be explained quantum-mechanically as scattering of an incident light photon to a lower energy

photon called Stokes photon by generating a phonon (acoustic phonon in SBS and optical phonon in SRS) with energy equal to the energy reduction of the initial photon. The main difference between the two is the type of interval mode involved. SRS involves nonpropagating collective modes as optical phonons in the medium whereas SBS involves low-frequency propagating acoustic wave phonons in the medium. Another fundamental difference is that SBS occurs only in the backward direction which is the opposite direction respect to the incident light. However, SRS is able to occur in both forward and backward directions although SRS dominates in the forward direction where SRS is in the same direction as the incident light. The other difference is that the downshifted scattered light is about 10 GHz for SBS but 13 THz for SRS respect to the incident light frequency in SMF. Finally, the Brillouin-gain spectrum is less than 100 MHz bandwidth which is very narrow in comparing with Raman-gain spectrum bandwidth which is more than 20 to 30 THz. SBS has been shown to provide harmful effects in optical fiber telecommunication system due to its low threshold power, however it has also been indicated that SBS is useful for applications in Brillouin amplifiers, Brillouin erbium fiber laser (BEFL), and Brillouin fiber laser (BFL) which are of particular interest in this thesis. Principles of SBS generation will be considered later; it describes the implication of Brillouin Stokes in the BFL generation.

2.3.1 Cubic Nonlinear Processes

Nonlinear optical processes usually happen when high intensity stationary fields having very small bandwidth enter a medium. Therefore, we can consider these fields as approximately monochromatic fields. Cubic nonlinear optical processes, also called the third-order nonlinear optical processes, occur as a consequence of the second term in equations (2.7) and (2.10), i.e., $P_{\alpha}^{(3)}$ processes

whose strength is expressed by $\chi^{(3)}_{\alpha\beta\gamma}$. At the most, three different fields contribute in cubic nonlinear processes. In order to describe these processes, suppose we have three plane waves propagating in a medium so that the resulting electric field is given by

$$E_\alpha(t) = \frac{1}{2}\sum_{r=\pm1}^{3} \mathrm{E}_{r\alpha} e^{i\omega_r t} \tag{2.12}$$

By using the Fourier transformation and Dirac-delta function which are

$$\mathrm{F}(\omega) = \int_{-\infty}^{\infty} \mathrm{F(t)e}^{-i\omega t}\, dt \quad , \quad \delta(\omega_1 - \omega_2) = \frac{1}{2\pi}\int_{-\infty}^{+\infty} \mathrm{e}^{-i(\omega_1-\omega_2)t}\, dt \tag{2.13}$$

Eq. (2.12) can be rewritten as

$$\mathrm{E}_\alpha(\omega) = \frac{1}{4\pi}\sum_{r=\pm1}^{3} \mathrm{E}_\alpha(\omega_r)\delta(\omega-\omega_r) \tag{2.14}$$

In the last two equations, we use the following definitions:

$$\omega_{-r} = -\omega_r \,, \mathrm{E}_{r\alpha} = \mathrm{E}_\alpha(\omega_\mathrm{r}) \,, \mathrm{E}(\text{-}\omega_\mathrm{r}) = \mathrm{E}^*(\omega_r) \tag{2.15}$$

In the classical electro-dynamic treatment, cubic nonlinear processes can be found by using Eqs. (2.8) and (2.14). These contain many terms of the cubic processes which have different frequency combination. However, all the terms can be written as [5]

$$\mathrm{P}^{(3)}_\alpha(\omega_4) = A\varepsilon_0 \sum \chi_{\alpha\beta\gamma\delta}(\omega_1,\omega_2,\omega_3)\mathrm{E}_\beta(\omega_1)\mathrm{E}_\gamma(\omega_2)\mathrm{E}_\delta(\omega_3) \tag{2.16}$$

where $\omega_4 = \omega_1 + \omega_2 + \omega_3$, and A is a constant for each term. For example, in Raman effect used in the chapter 5, $\omega_1 = -\omega_2 = \omega_{\mathrm{RP}}$ that is the intensity of the light with the angular frequency which is the same as the frequency of Raman Stokes wave ($\omega_3 = \omega_{\mathrm{RS}}$) is amplified at the expense of the intensity of Raman pump (RP). In third harmonic generation, $\omega_1 = \omega_2 = \omega_3$ so that $\omega_4 = 3\omega_1$ in which ω_1 is the fundamental frequency. Eq. (2.16) can also represent the four-wave

mixing process in which a wave with angular frequency ω_4 is generated when three optical waves at the frequencies ω_1, ω_2, and ω_3 are propagating together.

2.4 Stimulated Brillouin Scattering (SBS)

As mentioned before, the physical process of SBS can be described by a nonlinear interaction among three waves: a pump wave which is the incident light, Stokes wave or scattered light, and an acoustic wave generated through a process known as electrostriction. Once the Brillouin scattered wave at the frequency ω_{BS} is spontaneously generated, it beats with the Brillouin pump wave at the frequency ω_{BP} and produces a beat frequency $(\omega_{BP} - \omega_{BS})$ which is exactly equal to the acoustic wave frequency ω_A. Consequently, this beat acts as a source to amplify the amplitude of the acoustic wave, which in turn amplifies the amplitude of the Brillouin scattered wave as a positive feedback. SBS can transfer ultimately all Brillouin pump power to the Brillouin scattered wave power which is detrimental in optical transmission communication system. The electrostriction phenomenon causes all electrical non-conductors or dielectrics change their shapes under the application of an electric field. Brillouin scattering may be understood via scattering of a Brillouin pump photon by an acoustic phonon which is a unit of energy and momentum for the acoustic or sound wave produced through the electrostriction. The conservation of energy and linear momentum during Brillouin scattering demands following equations for the frequencies and wave vectors [2],[5],[7]

$$\omega_{\mathrm{BP}} = \omega_{\mathrm{BS}} + \omega_{\mathrm{A}} \tag{2.17}$$

$$\mathbf{k}_{\mathrm{BP}} = \mathbf{k}_{\mathrm{BS}} + \mathbf{k}_{\mathrm{A}} \tag{2.18}$$

where the indexes BP, S, and A refer to Brillouin pump, scattered, and acoustic waves, respectively. The acoustic frequency is very small compared to the light frequency, that is $\omega_{\mathrm{A}} << \omega_{\mathrm{P}}, \omega_{\mathrm{BS}}$; therefore, $\omega_{\mathrm{BP}} \approx \omega_{\mathrm{BS}}$, and $\mathrm{k}_{\mathrm{BP}} = \mathrm{k}_{\mathrm{BS}}$. In addition, it can be deduced that

$$\mathrm{k}_{\mathrm{A}}^2 = 4\mathrm{k}_{\mathrm{BP}}^2 \sin^2 \frac{\gamma}{2} \tag{2.19}$$

where γ indicates the angle between the Brillouin pump and Brillouin Stokes wave vectors, k_{BP} and k_{BS}, respectively. By considering $\mathrm{k}_{\mathrm{A}} = \frac{\omega_{\mathrm{A}}}{\mathrm{v}_{\mathrm{A}}}$, and $\mathrm{k}_{\mathrm{BP}} = \frac{\omega_{\mathrm{BP}}}{\mathrm{v}_{\mathrm{BP}}}$, it can be deduced

$$\omega_{\mathrm{BS}} = \omega_{\mathrm{BP}}(1 - 2\frac{\mathrm{v}_{\mathrm{A}}}{\mathrm{v}_{\mathrm{BP}}} \sin\frac{\gamma}{2}) \tag{2.20}$$

which can also be described classically via scattering of the pump light by a moving grating with the sound velocity v_{A} in Doppler effect. It is clear that the Brillouin frequency shift, which is equal to ω_{A}, is zero when the pump and scattered fields propagate in the same direction and has its maximum value $2\frac{\mathrm{v}_{\mathrm{A}}}{\mathrm{v}_{\mathrm{BP}}}\omega_{\mathrm{BP}}$ when the scattered light, Brillouin Stocks, propagates in the opposite direction $(\gamma = \pi)$ which is our case happening in optical fibers.

The propagation of elastic wave in a dissipative medium can be described by a material density function ρ [kg/m^3] satisfying the wave equation driven through electrostriction phenomenon as

$$\mathrm{v}_{\mathrm{A}}^2 \nabla^2 \rho - \frac{\partial^2 \rho}{\partial t^2} + \Gamma \nabla^2 \frac{\partial \rho}{\partial t} = \nabla \bullet \mathbf{f} \tag{2.21}$$

where $\mathrm{f} = \frac{1}{2}\gamma_e \nabla \mathrm{E}^2$, the force per unit volume of the medium, produces the

density fluctuation due to light propagation in the medium [8]. $v_A = \sqrt{Y/\rho}$ is the speed of acoustic wave or longitudinal sound velocity in the medium and $\Gamma = \eta_{11}/\rho_0$ (m^2/s) is known as sound damping factor in the region. Y (Pa) is the Young's modulus, η_{11} (Pa s) is the bulk viscosity coefficient of the optical fiber, and ρ_0 is the unperturbed density. The parameter γ_e called electrostriction coefficient is the strength of the electrostriction effect. The nonlinear polarization for SBS can be obtained by the constitutive relation for the electric displacement vector **D** and Taylor's expansion of the permittivity coefficient as:

$$\mathbf{D} = \varepsilon\ \mathbf{E} = \varepsilon_0 \mathbf{E} + (\rho - \rho_0)\left[\frac{\partial \varepsilon}{\partial \rho}\right]_{\rho=\rho_0} \mathbf{E} \tag{2.22}$$

where ε is the permittivity of the medium. In comparison to the relation $\mathbf{D} = \varepsilon_0 \mathbf{E} + \mathbf{P_L} + \mathbf{P_{NL}}$ which can be deduced by the constitutive relation and Eq. (2.9), the nonlinear polarization for Brillouin scattering is obtained from Eq. (2.22) as the following

$$\mathbf{P}_{\mathrm{NL}} = \frac{\gamma_e}{\rho_0}\rho\mathbf{E} \tag{2.23}$$

where the definition $\gamma_e = \rho_0[\partial\varepsilon/\partial z]_{\rho=\rho_0}$ has been used.

Thus, the electric field in SBS can be evaluated by Eq. (2.1) and the above nonlinear polarization as the following

$$\nabla^2 \mathrm{E} - \frac{1}{v^2}\frac{\partial^2 \mathrm{E}}{\partial t^2} = \frac{\mu_0 \gamma_e}{\rho_0}\frac{\partial^2 \rho \mathrm{E}}{\partial t^2} \tag{2.24}$$

In order to solve the coupled Eqs. (2.21) and (2.24), it is common to suppose that the Brillouin pump, Brillouin Stocks, and acoustic wave are plane waves propagating in z direction assumed to be the axis of the fiber [9]. Hence, the supposed linearly co-polarized pump and Stocks fields and the sound wave with

the propagation vectors $\mathbf{k}_{BP}=k_{BP}\,\mathbf{z}$, $\mathbf{k}_{BS}=k_{BS}\,(-\mathbf{z})$, and $\mathbf{k}_{A}=k_{A}\,\mathbf{z}$, respectively, have the forms

$$E_{BP}(z,t)=\frac{1}{2}E_{0BP}(z)e^{i(\omega_{BP}t-k_{BP}z)}+c.c. \tag{2.25}$$

$$E_{BS}(z,t)=\frac{1}{2}E_{0BS}(z)e^{i(\omega_{BS}t+k_{BS}z)}+c.c. \tag{2.26}$$

$$\rho(z,t)=\rho_0+\frac{1}{2}Ae^{i(\omega_{A}t-k_{A}z)}+c.c. \tag{2.27}$$

in which c.c. denotes the complex conjugate of the first term with the assumption that the amplitudes E_{0BP}, E_{0BS}, and A are not functions of time regarding steady-state regime. With the assumption that the electric field E is obtained by the superposition of the electric fields E_{BP} and $E_{BS,}$ the right hand of Eq. (2.21) will be

∇•f=

$$\frac{\gamma_e}{4}\nabla^2E^2=\frac{-\gamma_e(k_{BP}+k_{BS})^2}{4}[E_{0BP}E_{0BS}^{*}e^{i[(\omega_{BP}-\omega_{BS})-(k_{BP}+k_{BS})z]}+c.c.] \tag{2.28}$$

where the rapidly oscillating terms contributing at frequencies $2\omega_1$, $2\omega_2$, and $(\omega_1+\omega_2)$ are neglected by regarding time averaging. Using Eqs. (2.21), (2.27), and (2.28), it can be obtained

$$A=\frac{(k_{BP}+k_{BS})^2\gamma_eE_{0BP}E_{0BS}/2}{v_A^2k_A^2-i\Gamma k_A^2(\omega_{BP}-\omega_{BS})-(\omega_{BP}-\omega_{BS})^2} \tag{2.29}$$

Now, in order to find the electric fields, it is common to use an assumption known as slowly varying envelope approximation (SVEA), that is the electric fields E_{BP} and E_{BS} exhibit slow variation over the medium length such that their second derivates with respect to z are negligible, in other words [1]

$$\left|k_{BP,BS}\frac{\partial E_{0BP,BS}}{\partial z}\right|>>\left|\frac{\partial^2E_{0BP,BS}}{\partial z^2}\right| \tag{2.30}$$

in which $E_{0BP,BS}$ shows the amplitude E_{0BP} or $E_{0BS,}$ respectively. For a plane wave $k_{BP,BS} = \frac{2\pi}{\lambda_{BP,BS}}$, so that SVEA condition will be as

$$\left|\frac{\partial E_{0BP,BS}}{\partial z}\right| >> \left|\lambda_{BP,BS}\frac{\partial}{\partial z}\left(\frac{\partial E_{0BP,BS}}{\partial z}\right)\right| \tag{2.31}$$

Physically speaking, over a distance of one wavelength, the magnitude of the slope of the electric field is much more than the change in the slope of the field. Thus, in this approximation, the first term of Eq. (2.24) can be written as

$$\nabla^2 E_{BP,BS} = \frac{\partial^2 E_{BP,BS}}{\partial z^2} \approx \frac{1}{2}\left(\mp i2k_{BP,BS}\frac{dE_{0BP,BS}}{dz} - k_{BP,BS}^2 E_{0BP,BS}\right)e^{i(\omega_{BP,BS} \mp k_{BP,BS})} + c.c. \tag{2.32}$$

where minus and plus signs apply with E_{0BP} and $E_{0BS,}$ respectively. Using Eqs. (2.24), (2.25), and (2.32), the wave equation (2.24) is separated into two equations at the frequencies ω_{BP} and ω_{BS} as the following [1]:

$$-ik_{BP}\frac{dE_{0BP}}{dz}e^{i(\omega_{BP}t - k_{BP})} + c.c. = \mu_0\frac{\partial^2 P_{NL}^{\omega BP}}{\partial t^2} \tag{2.33}$$

$$ik_{BS}\frac{dE_{0BS}}{dz}e^{i(\omega_{BS}+k_{BS}z)} + c.c. = \mu_0\frac{\partial^2 P_{NL}^{\omega BS}}{\partial t^2} \tag{2.34}$$

where $P_{NL}^{\omega BP}$ and $P_{NL}^{\omega BS}$, the nonlinear polarizations oscillating at ω_{BP} and ω_{BS}, are given by

$$P_{NL}^{\omega BP} = \frac{\gamma_e}{\rho_0}\rho E_{BS} = \frac{\gamma_e}{4\rho_0}[AE_{0BS}e^{i(\omega_{BP}t - k_{BP}z)} + c.c.] \tag{2.35}$$

$$P_{NL}^{\omega BS} = \frac{\gamma_e}{\rho_0}\rho E_{P} = \frac{\gamma_e}{4\rho_0}[AE_{0P}^{*}e^{-i(\omega_{BS}+k_{BS}z)} + c.c.] \tag{2.36}$$

By substituting Eqs. (2.35) and (2.36) into Eqs. (2.33) and (2.34) respectively, the following equations will be resulted

$$\frac{\mathrm{dE}_{0\mathrm{BP}}}{\mathrm{dz}} = -K\left|E_{0\mathrm{BS}}\right|^2 \mathrm{E}_{0\mathrm{BP}} \tag{2.37}$$

$$\frac{\mathrm{dE}_{0s}}{\mathrm{dz}} = -K\left|E_{0\mathrm{BP}}\right|^2 \mathrm{E}_{0\mathrm{BS}} \tag{2.38}$$

in which K is given by

$$K = \frac{-i\mu_0\omega_{\mathrm{BP}}\gamma_e^2/8\rho_0\mathrm{v}_{\mathrm{A}}}{(\omega_{\mathrm{BP}}-\omega_{\mathrm{BS}})-\omega_{\mathrm{A}}+i\Gamma_{\mathrm{B}}} \tag{2.39}$$

with the assumption $\mathrm{v}_{\mathrm{BP}} \approx \mathrm{v}_{\mathrm{BS}} \approx c/n$, $k_{\mathrm{A}} = 2k_{\mathrm{BP}}$ obtained from Eq. (2.19) in backward scattering ($\gamma = \pi$), $\Gamma_B = \Gamma k_{\mathrm{a}}^2/2$ and $\omega_{\mathrm{PB}} - \omega_{\mathrm{BS}} \approx \omega_{\mathrm{A}} = k_{\mathrm{A}}\mathrm{v}_{\mathrm{A}} = 2\omega_{\mathrm{BP}}n\mathrm{v}_{\mathrm{A}}/c$. By adding the effect of absorption using the absorption coefficients of the Brillouin pump and the Brillouin Stokes waves, α_{BP} and α_{BS}, respectively, the following equations can be obtained

$$\frac{\mathrm{dI}_{\mathrm{BP}}}{\mathrm{dz}} = -g_B\mathrm{I}_{\mathrm{BP}}\mathrm{I}_{\mathrm{BS}} - \alpha_{\mathrm{BP}}\mathrm{I}_{\mathrm{BP}} \tag{2.40}$$

$$\frac{\mathrm{dI}_{\mathrm{BS}}}{\mathrm{dz}} = -g_B\mathrm{I}_{\mathrm{BP}}\mathrm{I}_{\mathrm{BS}} + \alpha_{\mathrm{BS}}\mathrm{I}_{\mathrm{BS}} \tag{2.41}$$

where g_B known as Brillouin gain factor is

$$g_B = g_B^{(0)}\left(\frac{\Gamma_B^2}{(\omega_{\mathrm{A}}-(\omega_{\mathrm{BP}}-\omega_{\mathrm{BS}}))^2+\Gamma_B^2}\right) \tag{2.42}$$

The maximum Brillouin gain factor given by $g_B^{(0)} = \dfrac{\omega_{\mathrm{p}}^2\gamma_e^2}{4\rho_0\varepsilon_0\mathrm{v}_{\mathrm{a}}c^2\Gamma_B}$ at resonance $(\Delta\omega = \omega_{\mathrm{A}} - (\omega_{\mathrm{BP}} - \omega_{BS}) = 0)$ is independent of the incident light frequency ω_{BP}. However, ω_{A} the frequency of acoustic wave and Γ_B the linewidth of the Brillouin gain depend on the light frequency ω_{BP} since we can deduce from Eq. (2.19) that

$$\omega_{\mathrm{A}} = k_{\mathrm{A}}\mathrm{v}_{\mathrm{A}} = \frac{2n\mathrm{v}_{\mathrm{A}}\omega_{\mathrm{BP}}}{\mathrm{c}}\sin\gamma/2 \tag{2.43}$$

$$\Gamma_B = k_A^2 \Gamma / 2 = \frac{2\Gamma n^2 \omega_{BP}^2}{c^2} \sin^2 \gamma / 2 \tag{2.44}$$

As mentioned before, Brillouin scattering can not propagates in the same direction as the Brilouin pump because according to Eq. (2.44) the damping coefficient $\Gamma_B = 0$ when $\gamma = 0$, i.e. $\mathbf{k}_{BP}$ and $\mathbf{k}_{BS}$ are parallel. In addition, the density function ρ induced by the field can not be in the form of Eq. (2.27) when $\Gamma_B = 0$. In addition, Eq. (2.31) also suggests that Γ_B has its largest possible value as $\gamma = \pi$ or $\mathbf{k}_{BP} = -\mathbf{k}_{BS}$ so that the medium of Brillouin cell forms a scattering grating derived by Eq. (2.27) as the respond to the electric fields. It is evident that g_B will be reduced to one-half of its peak value $g_B^{(0)}$ when $\Delta\omega = \pm\Gamma_B$ so that the Brillouin gain spectrum width $\Delta\omega_B$ is defined as the full width at half maximum (FWHM) of the Brillouin gain function g_B and it is equal to $2\Gamma_B$ ($\Delta\omega_B = 2\Gamma_B$). The Brillouin gain linewidth is generally different for various optical fibers since inhomogeneities in the fiber core cross sections along the fiber length is various for fibers. In optical fibers, $\Delta\nu_B = \Delta\omega_B / 2\pi$ is typically between 10 and 100 MHz in the 1550 nm spectral region whereas the measured Brillouin shift, $\Omega_B = \omega_B / 2\pi$, is about 11GHz [3].

In Eqs. (2.40) and (2.41), it is assumed that the counterpropagating Brillouin pump and Brillouin Stokes waves are linearly polarized and maintain their polarization along the fiber. In practice, this assumption is true when the fiber is a polarization-maintaining fiber and the pump and Stokes waves are polarized along its principal axis. In a conventional optical fiber such as SMF, however, the relative polarization angle between the pump and Stokes wave varies randomly as discussed before. This is the case that the Brillouin gain factor g_B will be reduced

by a prefactor of 1.5 [10]. Analytical solutions of the coupled intensity Eqs. (2.27) and (2.28) can be derived as the following.

In order to solve the coupled steady state Eqs. (2.40) and (2.41) describing the SBS dynamics in a SMF, the following transformation can be introduced by these definitions [11]

$$\Sigma = I_{BP} - I_{BS} \quad , \quad \Delta = I_{BP} + I_{BS} \tag{2.45}$$

so that

$$I_{BP} I_{BS} = \frac{1}{4}(\Delta^2 - \Sigma^2) \tag{2.46}$$

Subtracting Eq. (2.37) from Eq. (2.38) results in

$$\frac{d\Sigma}{dz} = -\alpha\ \Delta \tag{2.47}$$

On the other hand, adding Eqs. (2.37) and (2.38) with using Eq. (2.46) gives

$$\frac{d\Delta}{dz} = -\alpha\ \Sigma - \frac{g_B}{2}(\Delta^2 - \Sigma^2) \tag{2.48}$$

If Δ is multiplied on both sides of the last equation, by using Eq. (2.47) it is obtained

$$\frac{d}{dz}(\Delta^2 - \Sigma^2) = \frac{g_B}{\alpha}(\Delta^2 - \Sigma^2)\frac{d\Sigma}{dz} \tag{2.49}$$

By integrating the last equation over the fiber length from $z = 0$ to a given point, a conversion relation will be obtained as

$$\mathrm{Ln}(\Delta^2 - \Sigma^2) - \frac{g_B}{\alpha}\Sigma = \left\{\mathrm{Ln}(\Delta^2 - \Sigma^2) - \frac{g_B}{\alpha}\Sigma\right\}_{z=0} = \text{constant} \tag{2.50}$$

Therefore, Δ can be obtained in terms of Σ by getting the exponential function from Eq. (2.50) as

$$\Delta = \sqrt{(\Delta_0^2 - \Sigma_0^2)\exp[\frac{g_B}{\alpha}(\Sigma - \Sigma_0)] + \Sigma^2} \tag{2.51}$$

where $\Sigma_0 = \Sigma(z=0)$ and $\Delta_0 = \Delta(z=0)$. From Eqs. (2.47) and (2.50), it is revealed that Σ can be solved exactly by using the following integration

$$\int_{\Sigma_0}^{\Sigma(z)} \frac{\mathrm{dx}}{\sqrt{(\Delta_0^2 - \Sigma_0^2)\exp[\frac{g_B}{\alpha}(x-\Sigma_0)] + x^2}} = -\alpha z \tag{2.52}$$

However, no closed form solution has been found for this integral. The last two equations are applicable for all values of g_B and α except for the case of zero attenuation (α=0). For this case, the following result can be obtained readily by integrating Eq. (2.47) as

$$\mathrm{I_{BP0}} - \mathrm{I_{BS0}} = \mathrm{I_{BP0}} - \mathrm{I_{BS0}} = k' = \text{constant} \tag{2.53}$$

which is a conservation law for energy with the assumption $\mathrm{I_{BP0}} = \mathrm{I_{BP}}(z=0)$ and $\mathrm{I_{BS0}} = \mathrm{I_{BS}}(z=0)$. This solution shows that the difference of intensity of the pump and Stokes waves remains constant through the medium at least for the lossless fiber approximation. In addition, Eqs. (2.40) and (2.41) for this case can be solved exactly to yield

$$\mathrm{I_{BP}}(z) = \frac{\frac{\mathrm{I_{BP0}}}{\mathrm{I_{BS0}}} - 1}{\frac{\mathrm{I_{BP0}}}{\mathrm{I_{BS0}}} - \exp(-g_B k' z)} \mathrm{I_{BP0}} \tag{2.54}$$

$$\mathrm{I_{BS}}(z) = \frac{1 - \frac{\mathrm{I_{BS0}}}{\mathrm{I_{BP0}}}}{\exp(\mathrm{g_B} k' z) - \frac{\mathrm{I_{BS0}}}{\mathrm{I_{BP0}}}} \mathrm{I_{BS0}} \tag{2.55}$$

where k' is a constant according to Eq. (2.50). Therefore, it can be deduced from the last two equations that in lossless fiber approximation pump and Stokes intensity are related together with

$$\mathrm{I_{BS}}(z) = \mathrm{I_{BP}}(z)\frac{\mathrm{I_{BS0}}}{\mathrm{I_{BP0}}}\exp(-g_B k' z) \tag{2.56}$$

In the other approximation called no depletion pump, the pump intensity I_p is constant. Due to the relatively small values of the acoustic wave frequency ω_A, we have $\omega_{BP} \approx \omega_{BS}$ and so $\alpha_{BP} \approx \alpha_{BS} \equiv \alpha$. When there is weak nonlinear coupling, so that $I_{BS} << I_{BP}$, the solutions of the coupled Eqs. (2.40) and (2.41)

$$I_{BP}(z) = I_{BP}(0)\exp(-\alpha\ z) \tag{2.57}$$

$$I_{BS}(z) = I_{BS}(L)\exp(\alpha(z-L))\exp(g_B I_{BP}(0)[\exp(-\alpha z) - \exp(-\alpha L)]/\alpha) \tag{2.58}$$

where the integration in Eq. (2.58) is done from the whole fiber length L to the given point z due to the backward propagation nature of Stokes wave. In practice, a given Stokes input at $z = L$ will grow to produce output intensity at $z = 0$ as

$$I_{BS}(0) = I_{BS}(L)\exp[(g_B P_0 L_{eff.}/A_{eff.}) - \alpha L)] \tag{2.59}$$

with the assumption $P_0 = I_{BP}(0)A_{eff.}$ is the input pump power, $A_{eff.}$ is the effective core area of the Stokes wave in an optical fiber where w is the spot size of the beam, and $L_{eff.}$ is the effective interaction length obtained by

$$L_{eff.} = \frac{1}{\alpha}[1 - \exp(-\alpha L)] \tag{2.60}$$

The effective interaction length, L_{eff}, is smaller than the actual fiber length L due to fiber loss. For a long fiber, such as our case in which we use a 25 km SMF, $\exp(-\alpha L) << 1$, so that

$$L_{eff} \approx 1/\alpha \approx 22.86\ \text{(km)} \tag{2.61}$$

Since the fiber attenuation is $\alpha = 0.19$ (dB/km) $= 0.0437$ $(\text{km})^{-1}$. In the both approximation, Eqs. (2.55) and (2.58) describe an increase in Stokes intensity I_s when it propagates because the Brillouin-scattered Stokes field is supposed to

propagate in the –z direction. Therefore, the discussed phenomenon is a stimulated Brillouin scattering (SBS) process in which the Backward Brillouin scattering originates usually from noise or spontaneous Brillouin scattering occurring through the fiber. However, in a Brillouin fiber laser, a Stokes wave incident at $z = L$ is generally fed as a positive feedback which will be discussed later. It is clear that the approximation of undepleted pump breaks when I_{BS} becomes comparable in magnitude to the pump intensity I_{BP}.

One of the important features of Brillouin scattering process is SBS threshold defined theoretically as the input pump intensity at which the resonant gain for Brillouin Stokes wave, $g_B(\Delta\omega = 0)$, is equal to its loss over the same given distance. By setting $\frac{dI_{BS}}{dz} = 0$ in Eq. (2.41), the pump intensity at threshold is found to be

$$I_{BPth} = \frac{\alpha}{g_B^{(0)}} = \frac{4\alpha\rho_0\varepsilon_0 v_a \Gamma_B}{\omega_{BP}^2 \gamma_e^2} \tag{2.62}$$

For a free end optical fiber in which Brillouin Stokes wave grows only from spontaneous Brillouin scattering throughout the fiber, the Brillouin threshold is found analytically to occur at a threshold Brillouin pump power P_{th} at which the backscattered Stokes power is equal to the input pump power [12]:

$$\mathbf{P_{th} \approx 21 \frac{A_{eff}}{g_B^{(0)} L_{eff}}} \tag{2.63}$$

In optical communication systems at 1550nm, the typical values for optical fibers are $A_{eff} = 50\mu m^2$, $L_{eff} \approx 21km$, and $g_B^{(0)} = 5\times10^{-11} m/W$, Eq. (2.59) results in $P_{th} \approx 1mW$. However, the backscattered Stokes power is always less than the input power due to pump depletion in practice. In the other study, it is shown that the threshold power defined by Eq. (2.63) is the pump power required to produce an

SBS output power at the level of Rayleigh back scattering power [13]. Again, it is revealed that $g_B^{(0)}$ is nearly independent of the pump frequency ω_p since $\Gamma_B \propto \omega_p^2$ according to Eq. (2.44). Besides, the Brillouin gain in Eq. (2.42) is obtained under steady state conditions for a continuous pump wave whose spectral width $\Delta\nu_{BP}$ is much smaller than the Brillouin gain $\Delta\nu_B$. However, the Brillouin gain will be reduced considerably if the spectral width of the pump wave exceeds the Brillouin gain spectral width ($\Delta\nu_{BP} > \Delta\nu_B$). If Brillouin pump laser has a Lorentzian spectral profile, it can be shown that the Brillouin gain spectrum $g_B(\omega)$ is still given by Eq. (2.42) but the gain peak $g_B^{(0)}$ is reduced by a factor $[1+(\Delta\nu_{BP}/\Delta\nu_B)]$ [14]. Therefore, in this case, the SBS threshold increases by the factor $1+(\Delta\nu_{BP}/\Delta\nu_B)$ so that

$$\mathbf{P_{th}} \approx \mathbf{21}\frac{\mathbf{A_{eff}}}{\mathbf{g_B^{(0)}L_{eff}}}\left(\mathbf{1}+\frac{\Delta\upsilon_{\mathbf{BP}}}{\Delta\upsilon_{\mathbf{B}}}\right) \tag{2.64}$$

2.5 Brillouin Fiber Laser (BFL) Generation

If an optical fiber is placed inside a cavity, Brillouin fiber lasers (BFLs) can be generated by using the Brillouin gain function g_B in the fiber. BFLs have been an active topic of research since 1976 [15],[16],[17]. Using optical circulators and optical couplers, there is no need to use mirrors for BFL generation in fiber optics. The SBS threshold power can be considerably reduced by placing an optical fiber in a cavity to generate BFL oscillations. In addition, the Brillouin Stokes linewidth becomes significantly narrower than the Brillouin pump linewidth with reductions of up to a few Hertz [18], [19].

2.5.1 Generation of Brillouin Fiber Ring Lasers (BFRLs)

For a conventional ring cavity as shown in Fig. 2.1, the boundary condition for Brillouin Stokes intensity is

$$\mathrm{I}_{\mathrm{BS}}(L) = R \times \mathrm{I}_{\mathrm{BS}}\ (0) \tag{2.65}$$

where L is the ring-cavity length and R is equal to the fraction of the Brillouin Stokes intensity injected into the ring cavity after each round trip.

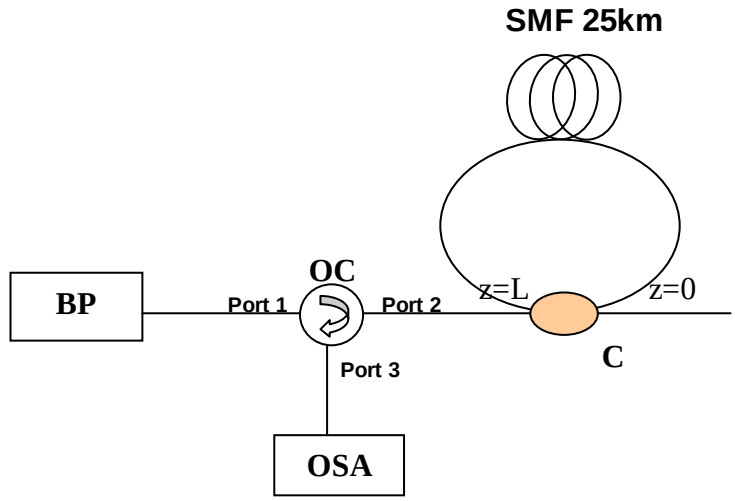

Fig. 2.1: A conventional ring cavity for BFL generation

It is evident that Brillouin Stokes wave is generated in the backward direction due to spontaneous Brillouin scattering at the beginning, however, after generating BFL oscillations, we can ignore spontaneous Brillouin Stokes intensity in comparison to the feedback Stokes. Therefore, the coupled intensity equations for the BFRL generation have the forms

$$\frac{dI_{BP}}{dz} = -g_B I_{BP} I_{BS} - \alpha_{BP} I_{BP} \tag{2.66}$$

$$\frac{dI_{BS}}{dz} = -g_B I_{BP} I_{BS} + \alpha_s I_{BS} \tag{2.67}$$

where the parameters are the same as in Eqs. (2.40) and (2.41). In addition to Eq. (2.65), there is another boundary condition for intensity pump power in the fiber as

$$I_{BP}(z=0) = I_0 \mu + R \times I_{BP}(z=L) \tag{2.68}$$

I_0 is Brillouin pump intensity injected into the optical system and μ plays the role of a dimensionless pump factor.

In this case, using boundary condition in Eq. (2.65), the SBS threshold condition for the undepleted pump approximation will be

$$R \times \exp(g_B P_{th} L_{eff} / A_{eff} - \alpha L) = 1 \tag{2.69}$$

2.5.2 Generation of Brillouin Fiber Lasers in Linear Cavities

Fabry-Perot Brillouin fiber lasers have some aspects qualitatively different from those making the usage of a ring cavity. This difference is due to the simultaneous attending of the forward and backward propagating components of the Brillouin pump and Stokes in the cavity as shown in Fig. 2.2. Therefore, higher order Stokes waves generated through cascading SBS are readily performed in the linear cavity than in the ring one at the same conditions.

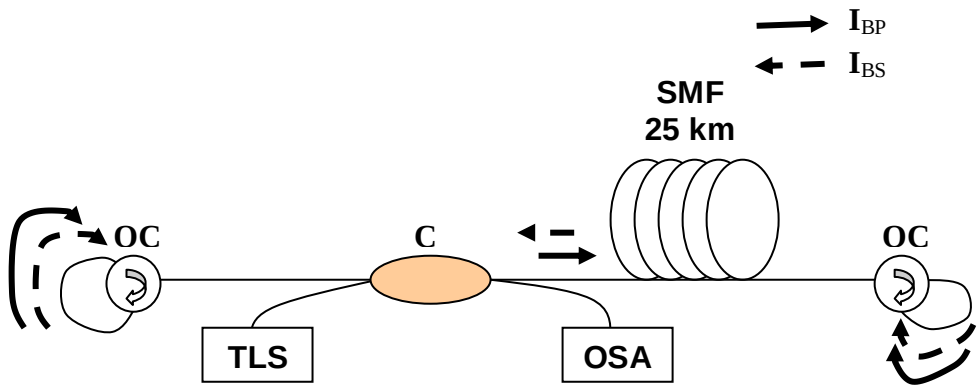

Fig. 2.2: Conventional linear cavity configuration

The BP is injected into the SMF via the coupler (C) in a forward direction as indicated in Fig. 2.2. The generated backward-propagating SBS oscillates inside the resonator to subsequently generate the BFL, which is coupled out via the coupler. The output laser is characterized by using an OSA. The coupled intensity equations in BFRL generation which are Eqs. (2.66) and (2.67) can also be used in this situation; however, the boundary conditions should be modified to simulate the linear cavity. In addition, in some reports, fiber Bragg gratings have been used instead of the optical circulators (OCs) to create a linear cavity [20],[21].

In the process of cascading SBS, each Stokes components pumps the next order Stokes component after its power becomes large enough to satisfy the condition of Brillouin threshold power. At the same time, anti-Stokes waves are also generated through other physical process called four-wave mixing between copropagating pump and Stokes waves. The result is a multiwavelength BFL which is the subject for the next chapter.

References

[1] J. A. Buck, "*Fundamentals of Optical Fibers*," 2nd ed. Wiley Series in Pure and Applied Optics, 2004.

[2] A. C. Newell, J. V. Moloney, "*Nonlinear Optics*," Westview Press, 2004.

[3] D. L. Mills, "*Nonlinear Optics: Basic Concepts*," 2nd Eng. ed., Springer Verlag, New York, 1998.

[4] S. G. Sauter, *"Nonlinear Optics*," Wiley Series in Microwave and Optical Engineering, 1996.

[5] S. Suda, F. Koyama, N. Nishiyama, C. Caneau, and C. Zah, "*High speed response of optical nonlinear phase shifter based on 1.55 μm VCSEL*," OSA, Conference on Lasers and Electro-Optics (CLEO), 2007,paper CMP6.

[6] N. Bloembergen, "*Nonlinear Optics*," 4th ed., World Scientific, Singapore, 1996.

[7] P. W. Millonni and J. H. Eberly, "*Lasers*," New York: John Wiley & Sons, Inc. 1998.

[8] I. L. Fabelinskii, "*Molecular Scattering of Light*," Plenum Press, New York, 1968, p. 506.

[9] R. W. Boyd, "*Nonlinear Optics*," Academic Press, San Diego, CA, 1992.

[10] M. O. van Deventer and A. J. Boot, "*Polarization properties of stimulated Brillouin scattering in single-mode fibers*," J. Lightwave Technol., Vol. 12, 1994, pp. 585-590.

[11] L. Chen and X. Bao, "*Analytical and numerical solutions for steady state stimulated Brillouin scattering in a single-mode fiber*," Opt. Commun., Vol. 152, 1998, pp. 65-70.

[12] R. G. Smith, "*Optical power handling capacity of low loss optical fibers as determined by stimulated Raman and Brillouin scattering*," Appl. Opt., Vol. 11, 1972, pp. 2489- 2494.

[13] X. P. Mao, R. W. Tkach, A. R. Chraplyvy, R. M. Jopson, and R. M. Derosier, "*Stimulated Brillouin threshold dependence on fiber type and uniformity*," Photon. Technol. Lett., Vol. 4, 1992, pp. 66-68.

[14] E. Lichtman, A. A. Friesem, R. G. Waarts, and H. H. Yaffe, "*Stimulated Brillouin scattering excited by two pump waves in single-mode fibers*," J. Opt. Soc. Am. B, Vol. 4, pp. 1397-1403, 1987.

[15] K. O. Hill**,** B. S. Kawasaki**,** and D. C. Johnson, "*cw Brillouin laser*," Appl. Phys. Lett., Vol. 28, 1976, pp. 608-609**.**

[16] C. Montes, D. Bahloul, I. Bongrand, J. Botineau, G. Cheval, A. Mahmhoud, E. Picholle, and A. Picozzi, "*Self-pulsing and dynamic bistability in cw-pumped Brillouin fiber ring lasers*," J. Opt. Soc. Am. B, Vol. 16, 1999, pp. 932-951.

[17] M. R. Shirazi, S. W. Harun, M. Biglari, H. Ahmad, "*Linear cavity Brillouin fiber laser with improved characteristics*," Opt. Lett., Vol. 33, 2008, pp. 770-772.

[18] S. P. Smith, F. Zarinetchi, and S. Ezekiel, "*Narrow-linewidth stimulated Brillouin fiber laser and applications*," Opt. Lett., Vol. 16, 1991, pp. 393–395.

[19] M. R. Shirazi, S. W. Harun, M. Biglary, K. Thambiratnam, and H. Ahmad, "*Effect of Brillouin pump linewidth on the performance of Brillouin Fiber Lasers*," ISAST Transactions on Electronics and Signal Processing, No. 1, Vol. 1, 2007, pp. 30-32.

[20] V. Lecoeuche, P. Niay, M. Douay, P. Bernage, S. Randoux and J. Zemmouri, " *Bragg grating based Brillouin fiber laser*," Optics Commun. Vol. 177, 2000, pp. 303-306.

[21] H. Ahmad, M. R. Shirazi, M. Biglary, and S. W. Harun, "*Linear Cavity Brillouin Fiber Laser Using A Fiber Bragg Grating*," Microwave and Optic. Technol. Lett., Vol. 50, 2008, pp. 265-266.

Chapter 3:

Generation of Brillouin Fiber Lasers (BFLs) and Multiwavelength BFLs (MBFLs) and Their Performance

3.1 Introduction

In this chapter, the generation of BFLs and MBFLs as well as their performance will be reviewed. The first part of this chapter will analyze experimental results obtained for various BFL and MBFL factors such as Brillouin scattering, stimulated Brilluoin scattering (SBS) and SBS threshold power as well as the effect of the Brillouin pump (BP) linewidth and the effective length of single-mode optical fibers used in this work. Subsequently, the design and generation of the BFL in the ring and linear cavities will be discussed and demonstrated. The proposed BFLS are designed to yield high performance efficiency in comparison to the previous works done by researches in this field. In the final part of the chapter the generation of MBFLs as a further application of BFLs will be presented by using the same ring and linear cavities. Also in this work, BFL linewidth measurement will be done by using the heterodyne method between two uncorrelated BFLs generated in the same conditions. This is because BFL linewidth measurement has been a challenging research issue since BFLs as a high coherent source have an ultranarrow linewidth and although some values have been reported for BFL linewidth, most of them are in the range a few hertz

and a few researches failed due to the resolution limitation of radio-frequency spectrum analyzers

3.2 Investigation of Stimulated Brillouin Scattering in Optical Fibers

As described in the Chapter 2, the phonons involved in the Brillouin scattering interaction are acoustic phonons, and the interaction occurs over a very narrow Brillouin gain linewidth which is typically in the order of tens of MHz (for example 35 MHz for fused silica), at the downshifted frequency about 10 GHz from the Brillouin pump in the wavelength 1550 nm [1-4]. This shift is determined by the velocity of the acoustic grating along the fiber and is therefore dependent on the mechanical properties of the fiber such as the elasto-optic coefficient, applied strain and ambient temperature [5, 6]. In doped fibers, such as EDFs the frequency shift has also been demonstrated to be dependent on the dopant concentrations in the core and cladding of the fiber [7, 8].

The Brillouin Stokes (BS) propagates in the opposite direction of a pump signal, thus creating significant distortion within the single. In other terms, SBS produces gain in a direction opposite to that of the Brillouin pump laser source. This is detrimental as it will deplete the pump and generates a potentially strong Brillouin Stokes wave propagating backward to the pump. Therefore, the Brillouin Stokes wave must be shielded by an isolator. The simplest suitable configuration for generating SBS is demonstrated in Fig. 3.1 where BS wave can be obtained in the backward direction in the free end single-mode fiber (SMF). The SMF is G.652.D with ID No. F6285 A0001 produced by The Furukawa Electric Co., LTD as mentioned at the end of this work. At the same time, not only the Brillouin

pump laser source is protected by the optical circulator from any backward reflected power but also the reflected power is readily detected by the optical spectrum analyzer (OSA) at the port 3 of the optical circulator.

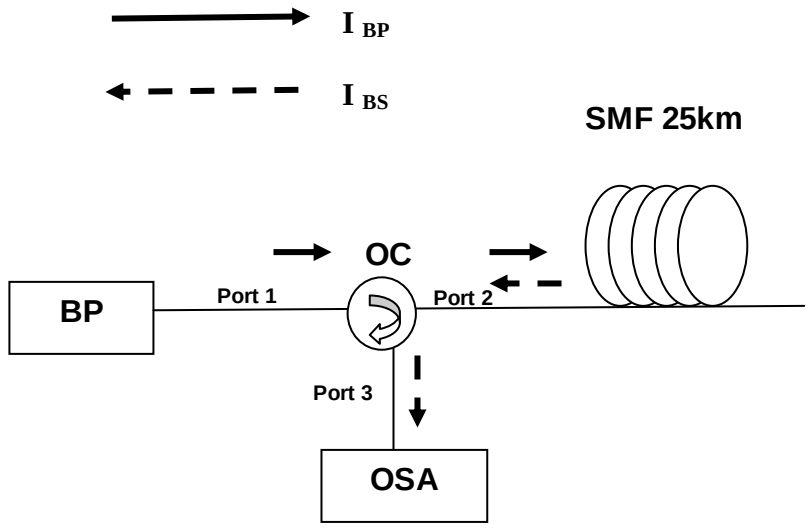

Fig. 3.1: Experimental setup for generating Brillouin scattering (BS).

In this setup as shown in Fig. 3.1, a tunable laser source (TLS) is used as the Brillouin pump (BP) with maximum peak power approximately 5 dBm at the wavelength 1550 nm and the BP wide linewidth 124 MHz. The maximum BP power is launched into the free end single-mode fiber (SMF) through the ports 1 and 2 of the optical circulator (OC). The reflection is detected through the port 3 of the OC by using the optical spectrum analyzer (OSA) with the resolution of 0.01 nm. In Fig. 3.2, the reflection and the injected Brillouin pump intensity spectra are demonstrated for the comparison. The anti-Stokes, the BP Rayleigh reflection and the Brillouin Stokes in the reflection spectrum have the peak power of about -51 dBm, -31 dBm, and -46.5 dBm, respectively. The Brillouin Stokes light wavelength is shifted upward by 0.088 nm from the BP wavelength whereas the

anti-Stokes wavelength is the same shifted but downward due to the degenerate four-wave mixing between the Brillouin pump and Brillouin Stokes waves.

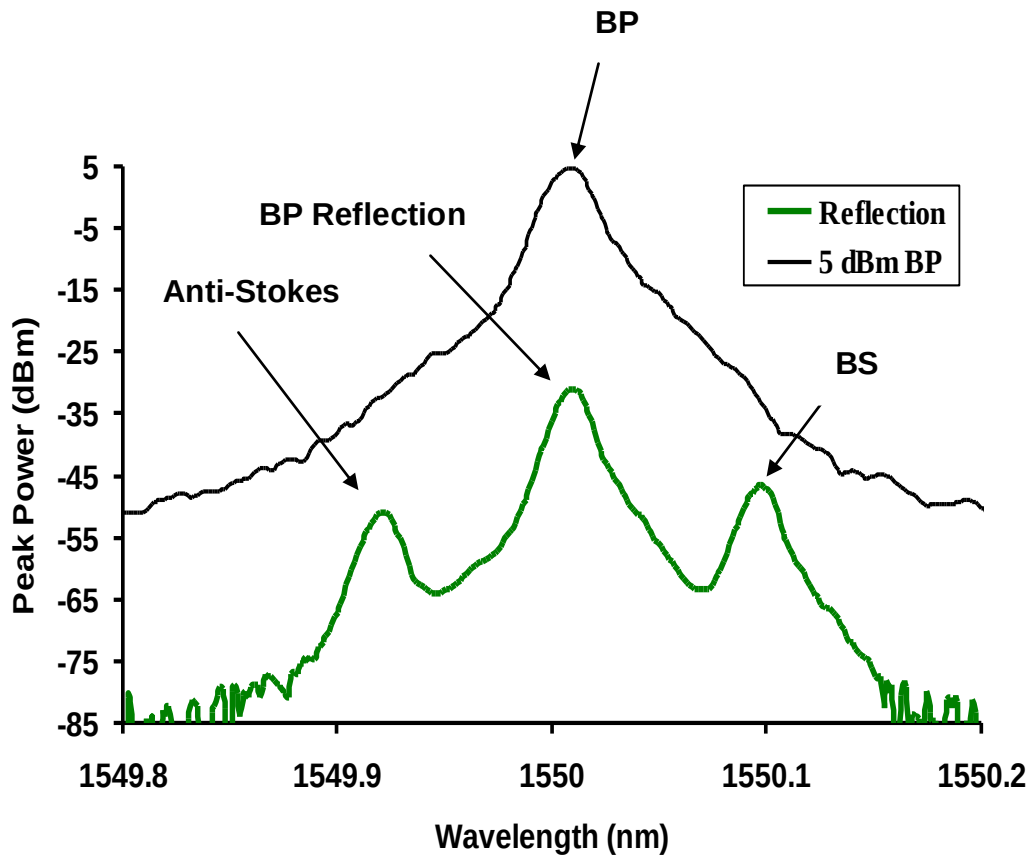

Fig. 3.2: The injected Brillouin pump (BP) spectrum and the reflection spectrum are demonstrated for the comparison. BP reflection is due to BP Rayleigh scattering whereas the Brillouin Stokes (BS) and anti-Stokes waves are generated by Brillouin scattering and degenerate four-wave mixing process, respectively.

Although an optical fiber is used as Brillouin cell to observe Brillouin scattering, it can be a gas, a liquid, or any solid with applications in high-power solid-state master oscillator power amplifier (MOPA) systems which provide average output powers up to kilowatt range with diffraction-limited beam quality [9]. According to the SBS theory, the beat frequency between the Brillouin

scattered wave and the incident BP light is equal to the frequency of the acoustic wave. As soon as the interference of the Brillouin laser pump and the Brillouin Stokes wave reinforces the acoustic wave, it, in turn, causes the amplification of the scattered Brillouin Stokes wave so that the SBS happens. In fact, the interaction between the incident wave and the Brillouin scattered wave in the Brillouin cell can become nonlinear if the interference between the two optical fields can coherently drive the acoustic wave generated by either through electrostriction or through local density fluctuations resulting from the absorption of light and the consequent temperature changes. The Brillouin threshold power is defined as the Brillouin pump power at which Brillouin Stokes power suddenly increases. The nonlinear Brillouin process is a nonlinear function of the incident light intensity. Nevertheless, in using any gas, liquid or solids, stronger focusing does not decrease the SBS thresholds. The reason for this behavior is the reduced active volume when stronger focusing is applied. One way to reduce the Brillouin threshold power is the use of waveguide structures which have been used in optical fibers [10],[11],[12] and in capillaries [13] where a high intensity is obtained along the full length of fiber in contrast to the bulk geometry. However, if very narrow waveguide diameters are used, damage of the incident surface and volume damage inside the capillary are the limiting factors for the maximum power.

In order to study the SBS effect, a higher BP power is needed. Thus, in this work, an Erbium doped fiber (EDF) amplifier (EDFA) is used to boost the TLS output power. As a result, the combination of the TLS and EDFA is the Brillouin pump (BP) which has the maximum output power about 14 dBm. The 14 m EDF

used in the experiment has an Er^{+3} ion concentration of 440 ppm, a numerical aperture of 0.21, and a cutoff wavelength 920 nm. The EDF is pumped by a laser diode at the pump wavelength of 980 nm with the maximum output power of 103 mW. By changing the BP power, we can observe the evolution of the anti-Stokes, the BP reflection, and the Brillouin Stokes peak power. The results are shown in Fig. 3.3 in which the reflection spectra including the peak power of the anti-Stokes, the BP Rayleigh reflection, and the Brillouin Stokes are demonstrated for various BP powers from 1 dBm to the maximum pump power of 14 dBm. By increasing 13 dB BP power, the Brillouin Stokes power is boosted by 45 dB due to the SBS effect, whereas the peak power of the anti-Stokes and the BP Rayleigh reflection are increased by only about 7 dB and 12 dB respectively, as shown in Fig.3.3.

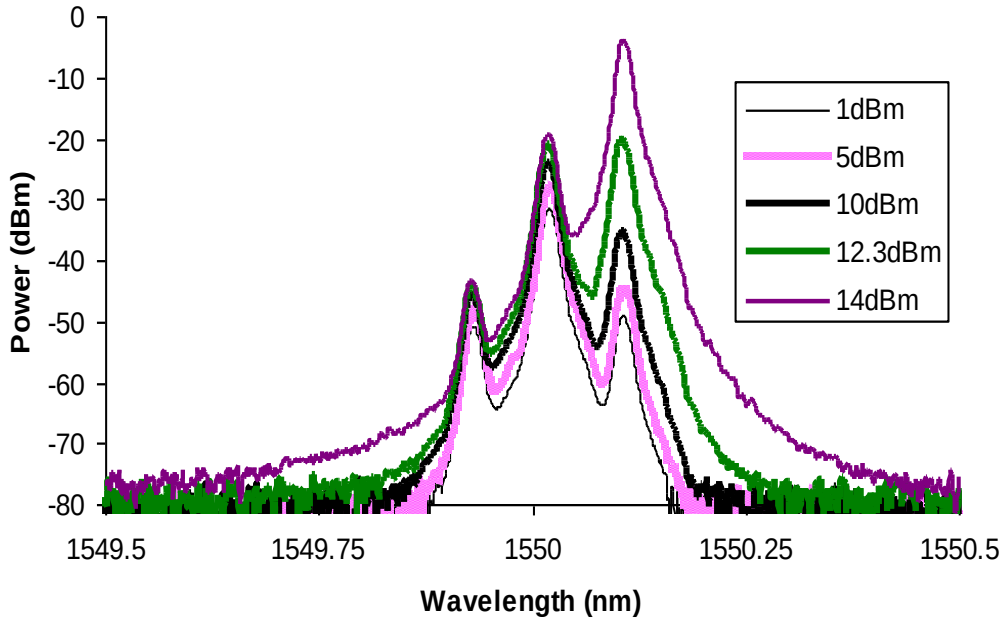

Fig. 3.3: The evolution of the reflection spectrum is demonstrated by changing the Brillouin pump (BP) power. Although the peak power of the anti-Stokes and the BP reflection is not changed by much (about 7 dB and 12 dB, respectively), the Brillouin Stokes peak power is increased a about 45 dB due to the SBS effect.

3.2.1 The BP Linewidth Effect on the SBS

According to Eq. (2.64) mentioned in the SBS theory of the pervious chapter, the SBS threshold power increases by the factor $[1+(\Delta\nu_{\mathrm{P}}/\Delta\nu_{B})]$ where $\Delta\nu_{\mathrm{p}}$ and $\Delta\nu_{\mathrm{B}}$ are the BP bandwidth and the Brillouin gain bandwidth or FWHM of the Brillouin gain curve, respectively [14],[15]. Indeed, the SBS threshold power is dependent on the BP spectral width as [14]

$$P_{th} \propto \frac{\Delta\nu_{P} \otimes \Delta\nu_{B}}{\Delta\nu_{B}} \tag{3.1}$$

where the symbol $\otimes$ represents the convolution of the pump and Brillouin linewidths. For Gaussian profiles, the convolution equates to

$$\Delta\nu_{P} \otimes \Delta\nu_{B} = (\Delta\nu_{P}^{2} + \Delta\nu_{B}^{2})^{\frac{1}{2}} \tag{3.2}$$

whereas for the more common assumption of Lorentzian profiles, it is

$$\Delta\nu_{P} \otimes \Delta\nu_{B} = \Delta\nu_{P} + \Delta\nu_{B} \tag{3.3}$$

In addition, the Lorentzian Brillouin gain curve in Eq. (2.42) has been found experimentally to be valid only for low input pump powers, i.e. up to the SBS threshold. However, it is known to be narrow and evolve into a Gaussian curve as the continuous wave (CW) pump power is increased further [16].

Thus, the Brillouin threshold power is reduced when a narrower BP linewidth is used. Using the narrow BP linewidth 15 MHz, we repeat the procedure leading to Fig. 3.3 and the results are shown in Fig 3.4.

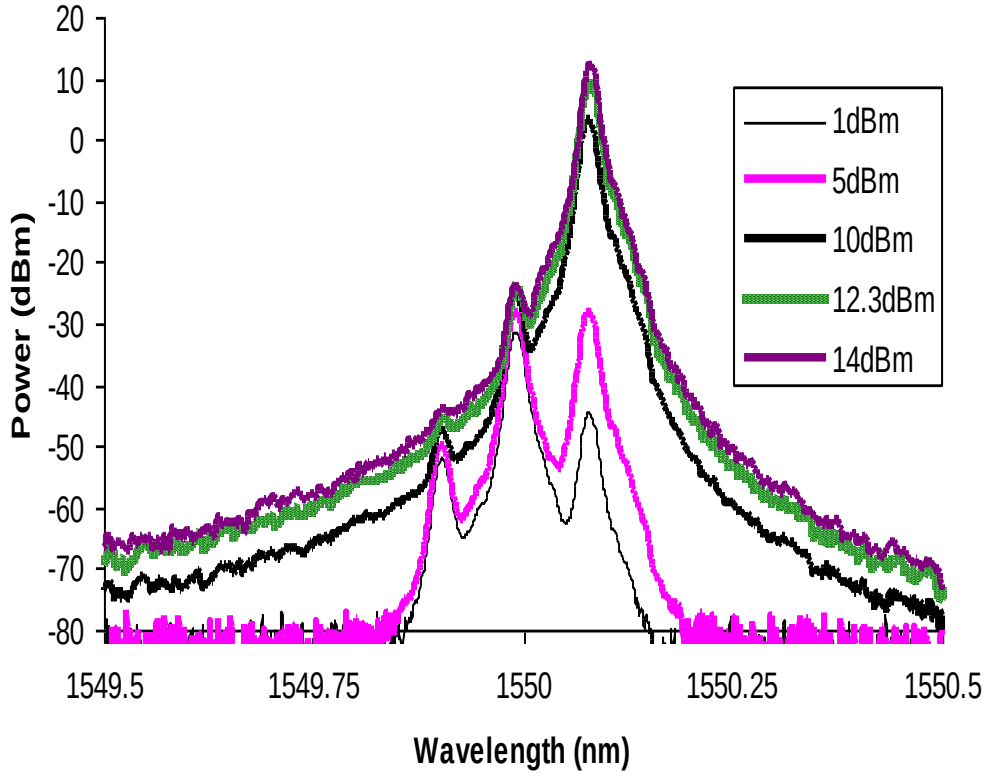

Fig. 3.4: The evolution of anti-Stokes, Brillouin Pump (BP) Rayleigh back scattered BP, and Brillouin Stokes at various BP power obtained by using the BP narrow linewidth 15MHz.

As shown in Fig. 3.4, the Stokes peak power for BP power 10 dBm and above is much higher compared with the pervious Stokes peak power in Fig. 3.3. This is due to the usage of narrower BP linewidth which reduces the SBS threshold power. By using the BP linewidth of 15 MHz and by 13 dB increasing the BP peak power, the Brillouin Stokes power is boosted by 57 dB whereas the peak power of the anti-Stokes and the BP Rayleigh reflection are increased only about 8 dB and 7 dB, respectively.

The evolution of the Brillouin Stokes (BS) power is shown in Fig. 3.5. The Brillouin Stokes peak power measured against the BP power at the wide and narrow BP linewidths of about 15 MHz and 124 MHz, respectively. As shown in Fig. 3.5, the narrow linewidth contributes to a higher output power of the BS and a lower BS threshold power. In the low–BP power range, the BS peak power for both the BP linewidths of 15 MHz and 124 MHz increase linearly as the BP power increases. However, as the BP power exceeds a critical power level, the BS power increases rapidly. The slope of the graph is also measured to be about to be approximately between 1.21 and 1.24 both before and after the critical power levels for the BP linewidths of 15 MHz and 124 MHz, respectively. Defining the SBS threshold power as the BP power at the critical power level, we can obtain the SBS threshold Power which is at approximately 4 dBm and 12 dBm at the BP linewidths of about 15 MHz and 124 MHz respectively.

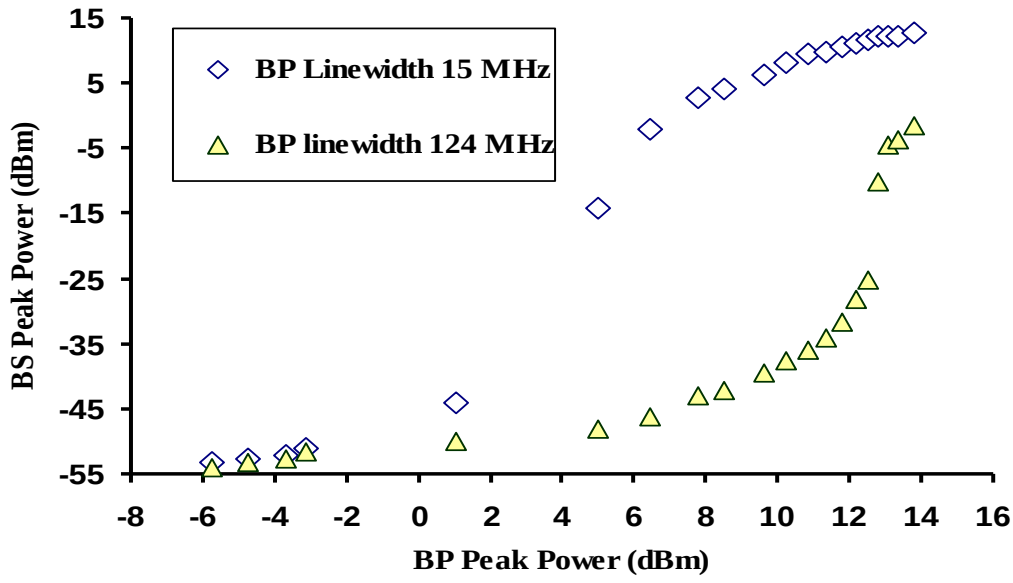

Fig. 3.5: Brillouin Stokes (BS) peak power against Brillouin pump (BP) peak power in using the different BP linewidths 15 MHz and 124 MHz.

3.2.2 Effective Length and Effective area for SBS

The nonlinear interaction depends on the interaction length and the cross-sectional area of the fiber. By using a longer interaction length, more interactions and a stronger effect of the SBS will be obtained as a kind of nonlinear phenomena. However, as the signal propagates along the fiber length, its power decreases due to fiber attenuation. Thus, most of the nonlinear effects occur at the input part of the fiber span and diminishes as the signal propagates. The SBS threshold power also decreases by a factor $(1/L_{\text{eff}})$, in which L_{eff} known as the effective length is proportional to the length of the fiber as mentioned in Eq. (2.60). In fact, modeling this effect can be quite complicated, but in a simple model called undepleted pump approximation [15], [17], it is assumed that the pump power transmitted at some distance z along the link is $P(z) = P_0 \exp(-\alpha z)$ where *Po* denotes the power injected into the fiber and α is the fiber attenuation. If L denotes the actual link length, the effective length (see Fig. 3.6), L_{eff} defined by:

$$P_0 L_{eff} = \int_{z=0}^{z=L} P(z)dz \tag{3.4}$$

which yields exactly Eq. (2.60). This length L_{eff} is chosen in a manner that the area under the curve $P(z) = P_0 \exp(-\alpha z)$ plotted in Fig. 3.6 (a) is equal to the area of the rectangle in 3.6 (b).

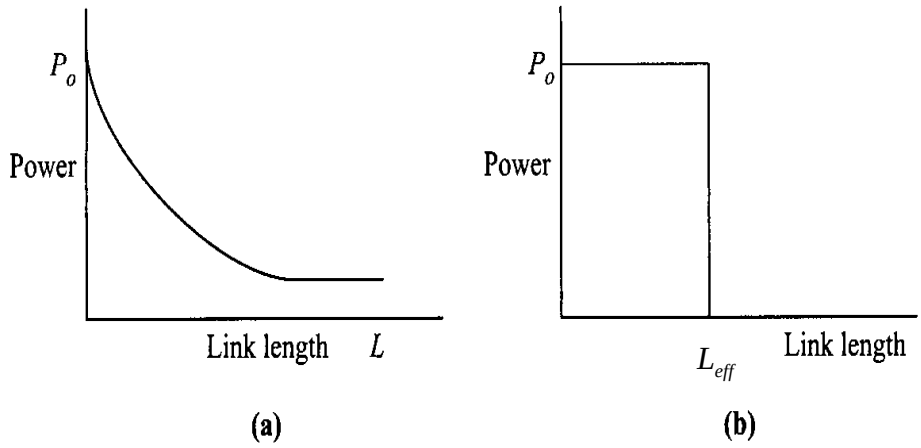

Fig. 3.6: (a) A typical distribution of the power along the length L of a link according to $P(z) = P_0 \exp(-\alpha z)$. (b) A hypothetical uniform distribution of the power along a link up to define the effective length L_{eff} . This length is chosen in a manner that the area under the curve in (a) is equal to the area of the rectangle in (b).

On the other hand, the SBS threshold saturates when the fiber length is longer than a certain value $(1/\alpha)$ where α, the attenuation constant is a measure of total fiber loss from all sources. In our case, $\alpha \cong 0.192$ (dB/km) $= 0.0437$ (km)$^{-1}$. Therefore, regarding Eqs. (2.60) and (2.61), $L_{eff} \cong 22.87\ km$ only if the attenuation coefficient of the used single-mode fiber (SMF) is considered. As a result, an available 25 km SMF is applied in this work.

In addition to the fiber length, the effect of nonlinearities also increases with the intensity in the fiber. For a given power, the intensity is inversely proportional to the area of the core as demonstrated by Eq. (2.64) for SBS threshold power. Since the power is not uniformly distributed within the cross

section of the fiber. It is convenient in fiber optics literature that one uses a mode effective cross-sectional area A_{eff} as shown in Fig.3.7 [15].

In the case that a fiber is operated at closeto cut-off of the fundamental mode, this becomes almost the same as the geometrical area. It is related to the cross-sectional distribution of the fundamental mode $F(r,\theta)$ by:

$$A_{eff} = \frac{[\int |F(r,\theta)|^2 r dr d\theta]^2}{[\int |F(r,\theta)|^4 r dr d\theta]} \tag{3.5}$$

where (r,θ) denotes polar coordinates. The effective area, as defined above, is a very important parameter which most nonlinear effects such as SBS can be expressed in terms of the effective area for the fundamental mode propagating in the given optical fiber. As shown in Fig. 3.7 (b), the intensity distribution in a fiber is nonzero only for an area A_{eff} around the center of the fiber.

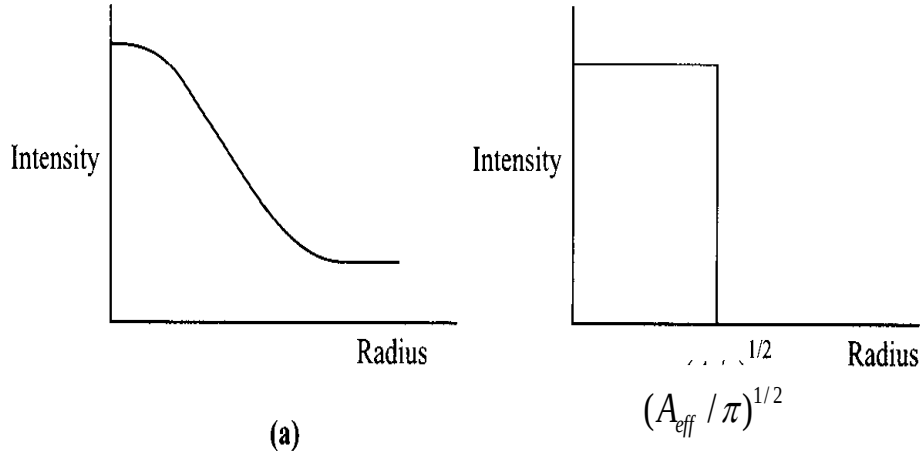

Fig. 3.7: (a) A typical distribution of the signal intensity along the radius of the fiber is demonstrated. (b) A hypothetical intensity distribution, equivalent to that in (a) for many purposes, shows an intensity distribution that is constant and constant and nonzero only for an area A_{eff} around the center of the fiber.

The evaluation of the effective mode area requires the use of modal field distribution F(r,θ). The effective mode area clearly depends on fiber parameters such as a core radius, core refractive index, and core-cladding index difference. For step-index fibers, the effective mode area of the fundamental mode can be defined by the Mode Field Radius (MFR) with Gaussian beam approximation, which is slightly larger than the core radius due to the cladding mode contribution. The effective mode area of πw^2 where w is the MFR is nearly the same to the core area which is defined by πa^2 where a is the core radius, when the normalized frequency V is the single-mode cutoff frequency of 2.4048. Typically, the effective mode area for single-mode silica fibers can vary in the range of 20~100 μm^2 in the 1550 nm region depending on fiber design.

Some nonlinear effects such as self phase modulation, cross phase modulation and four-wave mixing that originate from nonlinear refractive index

$$n = n_0 + \partial n = n_0 + NI_{eff} = n_0 + N\frac{P}{A_{eff}} \tag{3.6}$$

where N the nonlinear-index coefficient, I_{eff} the effective intensity of a propagating laser beam, P the power of the laser beam, n_0 the linear refractive index, and ∂n is the nonlinear refractive index induced by the third-order susceptibility $\chi(3)$. As a result, these nonlinearities in optical fibers are highly dependent on the nonlinear-index coefficient, the optical power, and the effective mode area A_{eff}. The mode effective area of SMFs and DSFs is typically about $85\ \mu m^2$ and $50\ \mu m^2$, respectively, whereas for DCFs so that they generate large negative dispersion coefficient and hence they are more susceptible to exhibit higher nonlinearities.

In this work, the effect of the fiber length on the peak power of the anti-Stokes, BP Rayleigh scattering, and Brillouin Stokes is investigated by observing the spectra in the same manner that obtained in the Figs. 3.3 and 3.4 and by using different lengths of the SMF. The result is shown in Fig. 3.8 (a) and (b). In this experiment, the BP power is fixed at 14 dBm.

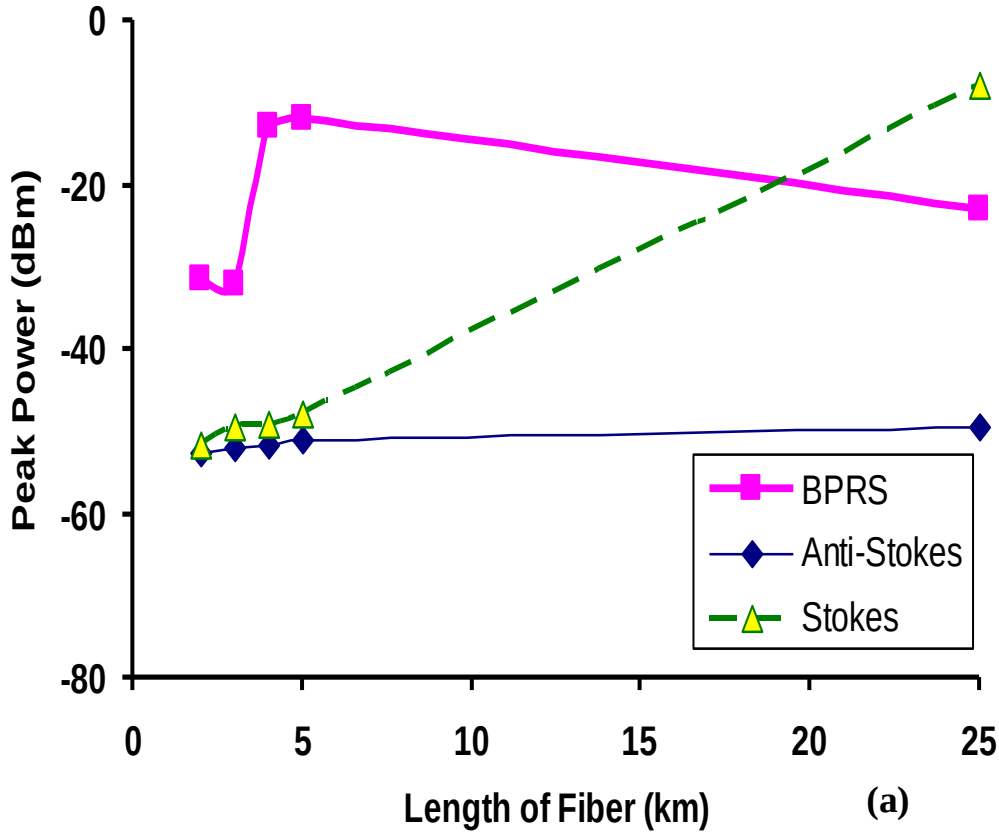

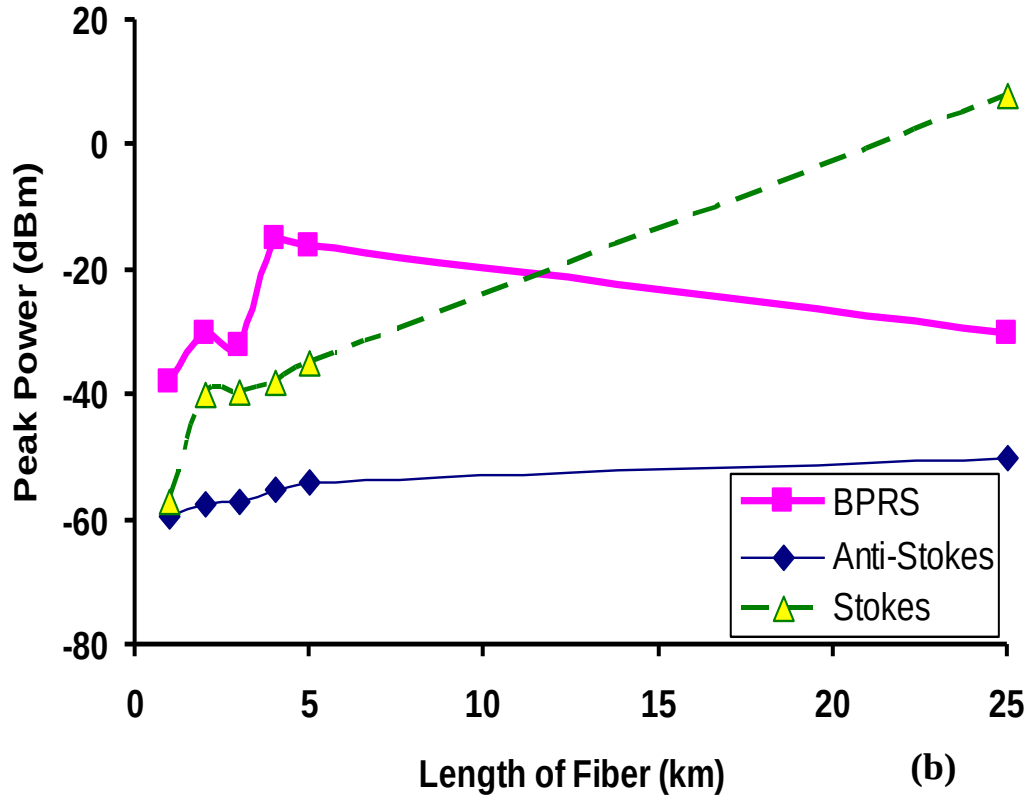

Fig 3.8: The effect of the fiber length on the peak power of Brillouin pump (BP) Rayliegh scattering (BPRS), anti-Stokes, and Brillouin Stokes. The applied BP peak power is fixed approximately 14 dBm with (a) the wide linewidth 124 MHz and (b) the narrow linewidth 15 MHz.

As shown in Fig. 3.8 (a) and (b), the Brillouin Stokes power increases as the length of SMF approaches to L_{eff} due to the increased interaction length in the fiber. The used fiber lengths 1 km, 2 km, 3 km, 4 km, 5 km, and 25 km are according to the available fiber lengths in our laboratory. In addition, by using narrower BP linewidth with the same fiber length, Brillouin Stokes power is higher due to the dependence of Brillouin threshold power on the BP linewidth which was mentioned before in Eq. (2.64). The reduction of the BP Rayleigh scattering power

in the usage of the 25 km fiber length is due to BP depletion occurring during SBS process.

3.2.3 Evaluation Methods for the SBS Threshold Power

According to Eq. (2.64) for the theoretical determination of the SBS threshold power, we have to know the Brillouin gain peak $g_B^{(0)}$ which is an intrinsic parameter related to the material. The typical $g_B^{(0)}$ value of fused silica glass is about $g_B^{(0)} = 5\times10^{-11}\text{m/W}$ [17]. However, it was reported that the effective $g_B^{(0)}$ value in a single-mode fiber is closely related to the refractive index profile [18]. Hence, exact measurement of the Brillouin gain is needed to evaluate theoretically the SBS threshold power in an optical fiber [19].

In practice, the SBS threshold power can be derived by considering the nonlinear characteristics in the transmitted and (or) reflected power. Various definitions for determining the SBS threshold power in optical fibers have been proposed. Some of the SBS threshold definitions are as the following:

(1) The input BP power at which the emerging backscattered power equals the input BP power [1], [20]. However, in practice, the backscattered power will always be less than the input power due to pump depletion. Nevertheless, this definition can be used as a benchmark to determine the pump power level at which SBS becomes excessive [21]. It was shown that definition (1) corresponds to the input BP power at which the Stokes power equals approximately 10% of the input power at the near end of the optical fiber [22].

(2) It has been reported that the transmission characteristic power are degraded when the Stokes conversion power becomes 1% of the input power shown in

Fig.3.9 [22]. Thus, the SBS threshold is defined as the input BP power at which the Brillouin Stokes power at the fiber input is equal to 1% of the input BP power at this point. It is also reported that the factor of 21 must be replaced with 18 in the theoretical SBS threshold definition cited in Eq. (2.116) [22], [23].

(3) Traditionally, the SBS threshold is obtained as the input BP power at which the Brillouin Stokes power equals the transmitted BP power [1], [24], [25], see Fig.3.9.

(4) The input BP power level at which the reflected BP power becomes 4% of the input power [26].

(5) The transmitted power increases in proportional to the input power at the lower BP power level. At the higher input BP power, however, the transmitted power becomes almost independent of the input BP power. Then, SBS can be considered the input BP power at which the two fitting lines cross each other as shown in Fig. 3.9 [26].

(6) The input BP power at which the second derivative of the Stokes power (mW) reaches its maximum value [26].

(7) The input BP power at which the Brillouin Stokes power begins to increase rapidly or equivalently, the transmitted BP power begins to be saturated [27], [28].

(8) The input BP power needed to generate the Brillouin Stokes power at the level of BP Rayleigh back scattering power [28], [29].

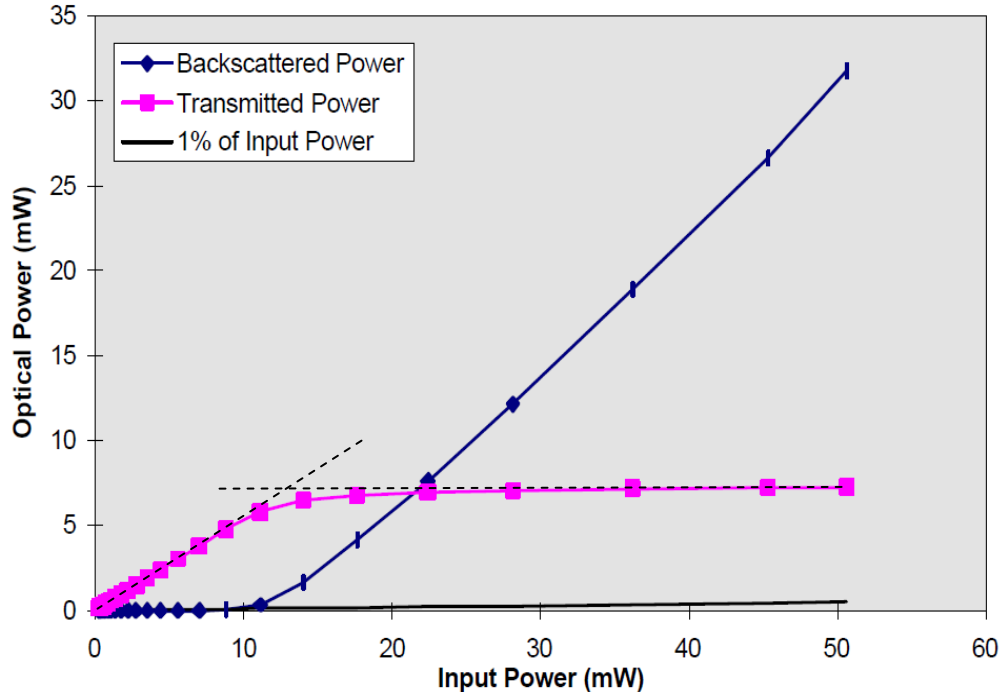

Fig. 3.9: Backscattered Brillouin Stokes and transmitted Brillouin pump (BP) powers against launch BP power are measured. It has been reported that the transmission characteristic power are degraded when the Stokes conversion becomes 1% of the input power [24]. SBS can also be considered the input BP power at which the two fitting dashed lines cross each other [27].

It is important to note that the SBS threshold definitions (1), (2), (4), and (8) have an advantage over (3), (5) and (6) in which BP saturation or BP depletion is the indicator sign. In fact in the former definitions (1), (3), (5) and (6), only two absolute power measurements of the input and the backscattered power are needed rather than three power measurements in methods (2) (and (7) if BP transmitted pump is the indicator) where it is also a requirement to indicate the transmitted power. (5) and (6) also require computations in addition to the experimental results.

In this work, the method (8) will be used since it is possible to analyze the BP Rayleigh reflection and Brillouin Stokes power simultaneously in the reflection

measurement. For the free end 25 km SMF in Fig. 3.1, the peak power of the anti-Stokes, BP Rayleigh scattering and Brillouin Stokes against the BP peak power are shown in Fig. 3.10 (a) and (b) for the different BP linewidth of 124 MHz and 15 MHz, respectively. SBS threshold power is approximately 12 dBm and 4 dBm which are the BP power at the intersections of the BP Rayleigh reflection and the Brillouin Stokes peak power for Fig. 3.10 (a) and (b), respectively.

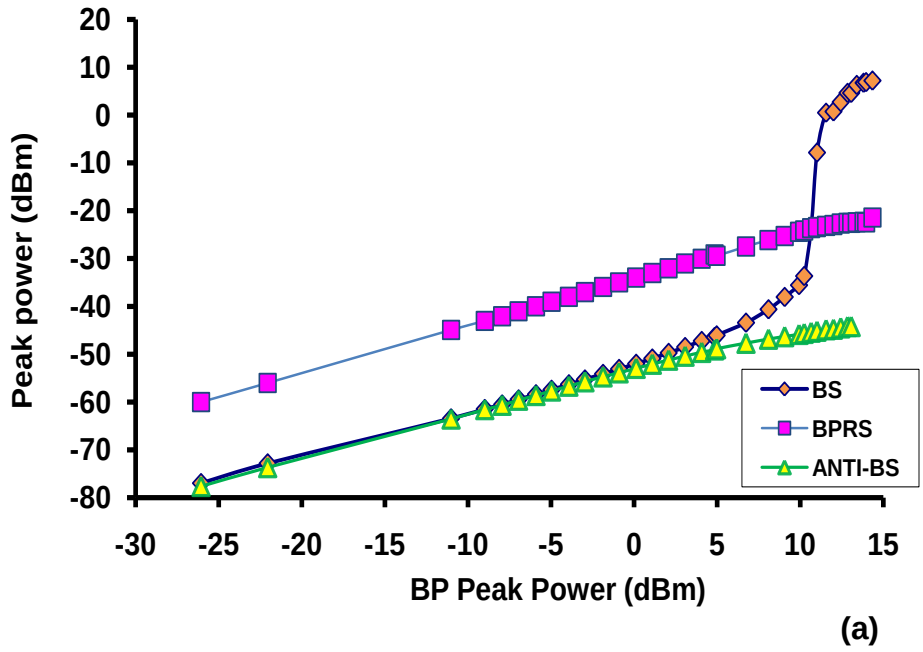

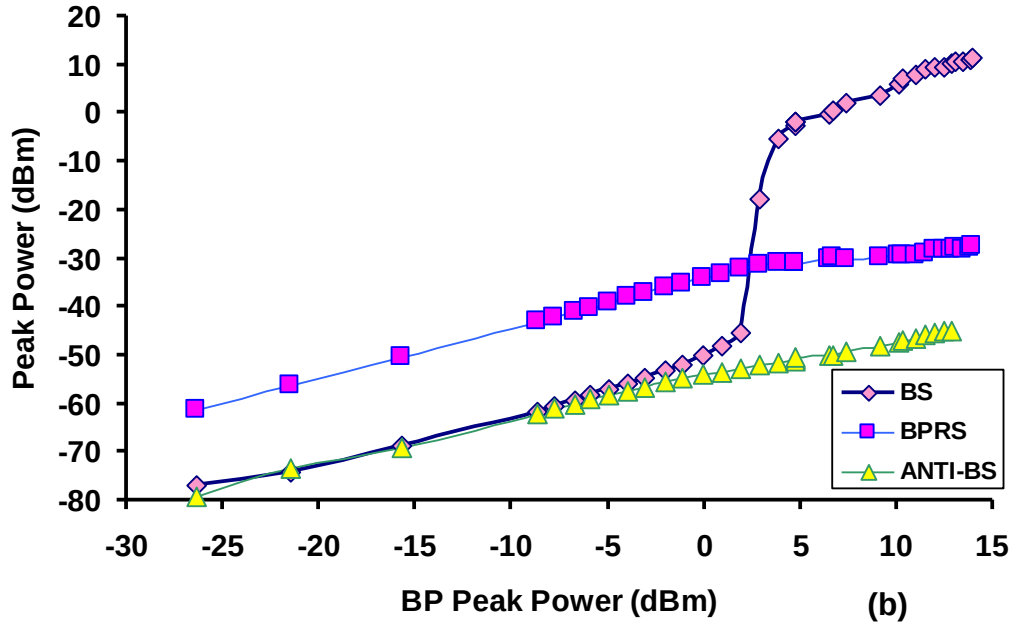

Fig. 3.10: Evaluation of SBS threshold power by using the intersection of BP Rayliegh scattering (BPRS) and Brillouin Stokes (BS) for BP linewidth (a) 124 MHz and (b) 15 MHz. The threshold power is the corresponding BP peak power of the intersection point at about 12 dBm and 4 dBm, for (a) and (b), respectively.

In order to reduce the SBS threshold power and also the fiber length for the usages in compact devices, it is desirable to have a medium with a large Brillouin gain coefficient g_B.Some SBS applications involve Brillouin fiber lasers, Brillouin amplifiers, microwave signal processors, optical sensors, and gyroscopes [30],[31], Although many crystals and organic materials are reported to have a large Brillouin gain coefficient [32], many are difficult to draw in the form of optical fibers. So far a number of non-silica based fibers are successfully drawn into optical fibers, which include Tellurite, Bismuth, and Chalcogenide glass fibers. These optical fibers have large nonlinear Kerr and Raman gain coefficients, and

thus have potential applications in high-speed optical signal processing [33], [34]. A tellurite fiber with a relatively large refractive index of about 2.028 which is about 40% higher than that of silica [35], is expected to exhibit a large Brillouin scattering coefficient since it is proportional to the material refractive index raised to the power of about 7 (n^7) [27]. Chalcogenide fiber is also reported to have a Brillouin gain coefficient about two orders of magnitude larger than of silica-based fibers [36]. For Bismuth-base EDF, it is expected that Brillouin gain coefficient to be about 4×10^{-7} which is four order grater than fused silica [37].

In addition, it is also known that the SBS threshold can be decreased using feedback. Different loop schemes providing the feedback for bulk SBS materials were investigated [37]. In these methods, part of the Brillouin Stokes' light is fed back into the SBS material. Using this feedback, a self-seeding of the SBS process takes place; thus the SBS Stokes' signal increases. At the same time, a part of undepleted residual Brillouin pump light is also fed back into the SBS cell. The injection of the undepleted Brillouin pump also decreases the SBS threshold further due to the intensifying of the injected BP. This is an important issue because fibers, due to the existence of high intensities in their small core have already reduced the SBS threshold by many orders of magnitude compared to the bulk material. Nevertheless, a further SBS threshold reduction which is possible by using a feedback scheme would be of interest especially for continuous wave (CW) and quasi-CW lasers with medium average power in the range of several tens of Watts. It was also shown that even Fresnel reflection at the fiber end surface can decrease the SBS threshold; however, a chaotic behavior of the reflected Brillouin Stokes' light results by using very long fibers in the feedback

mechanism [38]. In the next section, different kinds of feedback mechanism will be discussed.

3.3 Generation of Brillouin Fiber Lasers

The feedback schemes used to decrease the SBS threshold are in the form of ring cavities and linear cavities. If closed-loop gain exceeds unity so that Brillouin amplification overcompensates the cavity loss, Brillouin Stokes' oscillation takes place and, in turn, it causes Brillouin fiber lasers (BFLs) generation. Typical linear and ring cavities which are used for generating linear and ring BFLs are shown in Fig. 3.11 (a) and (b) respectively. In the linear cavity, the linear laser is assumed to have two counter-propagating BFL beams at the laser wavelength whereas in ring cavities, only one unidirectional BFL beam can propagate in the backward direction in comparison to the BP direction due to the Brillouin scattering aspect in optical fibers.

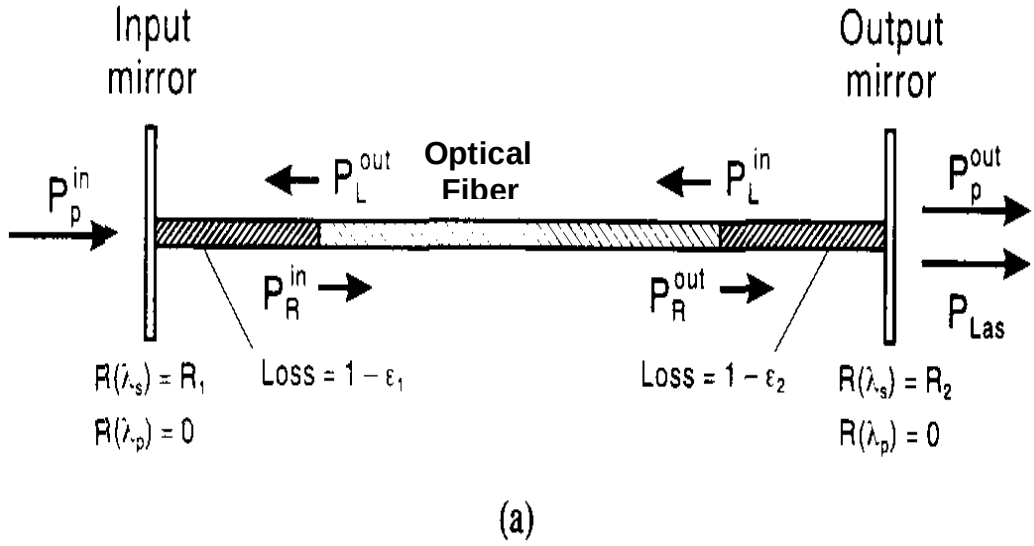

(a)

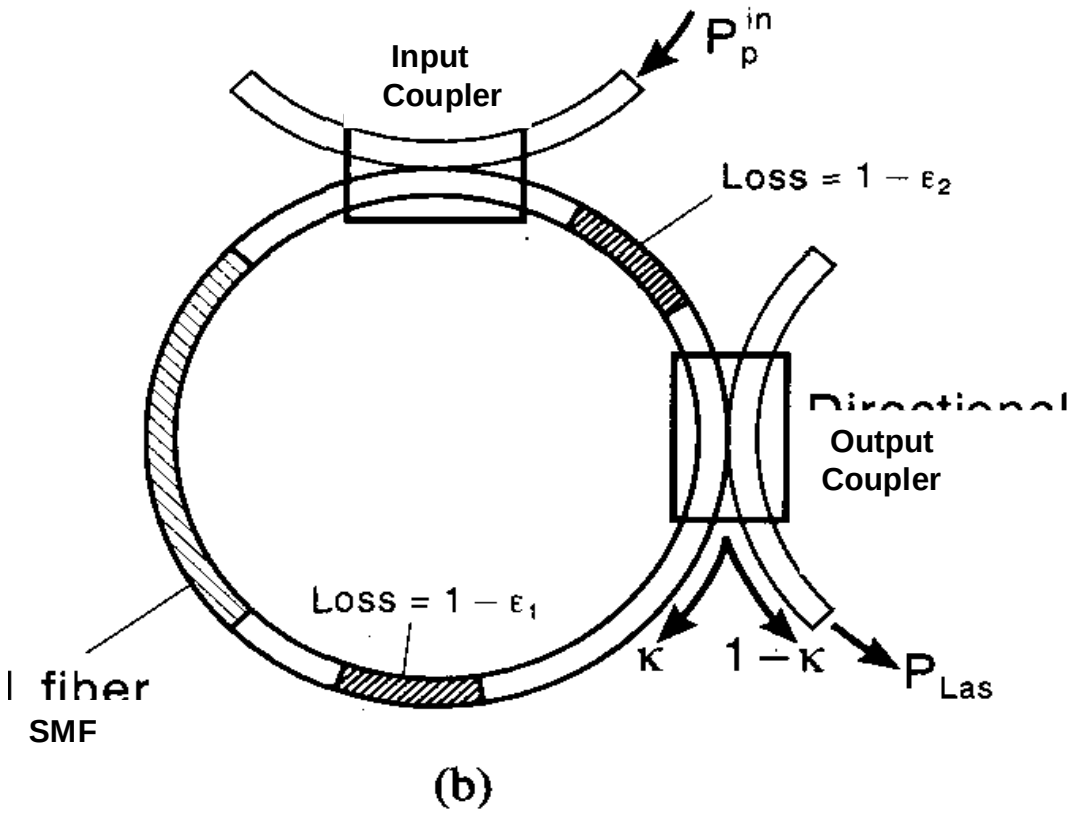

Fig. 3.11: Schematic configurations for (a) linear cavity and (b) ring cavity.

In the linear cavity, shown in Fig. 3.11 (a), R_1 and R_2 are the reflectivity coefficients at the lasing wavelength for the left-hand side and the right-hand side mirrors, respectively. Both mirrors are assumed to be transparent at the pump wavelength so that the pump has only one pass through the fiber. Therefore, there is pump light propagating to the right and a laser light standing wave that is a superposition of right- and left-propagating laser lights at any point in the fiber. P_p^{in} is the pump light power that inputs to the optical fiber. ε_1 and ε_2 are the single-pass transmission coefficients that account for intracavity components such as tuning elements and the fiber-to-mirror coupling loss for each discrete loss elements.

The output laser power P_{Las} is given by

$$P_{Las} = (1 - R_2)\varepsilon_2 P_R^{out} \tag{3.7}$$

where P_R^{out} is the power at the fiber-laser wavelength out from the right hand side end of the optical fiber.

The nonlinear dynamics of Brillouin fiber lasers stands among the richest research area in fiber optics. Under the one-dimensional approximation which is customary in single-mode fibers (SMFs), SBS is understood in the frame of the coherent 3-wave model of SBS as mentioned before in Eqs. (2.66) and (2.67) [39], [40]. This model accounts for perturbative optical Kerr effect and spontaneous noise [41]. Brillouin fiber laser (BFL) devices exhibit periodic, quasi-periodic [42-45], chaotic [46], and even solitonic super- and sub-luminous pulse propagation [47], [48], as well as self-stabilization of the phase which yields ultra-coherent regimes leading to BFL linewidths as narrow as a few hertz [49],[50]. BFLs are fairly simple to operate with only tens of mW of Brillouin pump because of the very high Brillouin gain in a long enough single-mode fiber which allows very low finesse and reinjection rates. According to the modal analysis [51], the linear laser and the ring laser globally exhibit the same dynamics.

By changing the fiber length in the modal analysis [51], three distinct dynamical behaviors can be considered: (1) Lower than a critical value of fiber length L_c, which is 48 m in ring cavities and 11m in ring cavities, the SBS emission is stable for any input pump power. In the framework of a modal analysis, this can be interpreted as the cavity free spectral range (FSR) which is comparable with the width of the Brillouin gain curve so that only a few modes can experience gain. However, near the threshold power, only the mode that

coincides with the center of the gain curve has sufficient gain to overcome the resonator losses and can oscillate. Since the Brillouin curve is homogeneously broadened, the laser always remains monomode as the input power increases [52]. (2) The SBS emission is unstable just beyond the threshold in long enough fibers (comparable to effective length). In other words, the resonator FSR is so small that many of the modes close to the center of the gain curve nearly experience the same gain and can oscillate simultaneously near the threshold. This leads to the unstable behaviors observed in previous works [53-58]. (3) For the intermediate fiber lengths, the transition between the dynamical behaviors observed in the two previous cases for the short and long fibers occurs inside a range of intermediate lengths. The SBS emission, stable and therefore monomode near the threshold, changes to unstable for sufficiently high pumping levels.

For a given fiber length, the Fabry-Perot FSR is half that of the ring cavity. Thus, if the two resonators had the same quality factor, the critical length characterizing the Fabry-Perot would be half that of the ring laser (i.e., 24 m). In the numerical simulations used in the modal analysis [51], however, the Fabry-Perot quality factor is much lower than that of the ring cavity so that the strong overlapping between modes then favors their competition and the critical length is reduced (< 24 m). It is evident that the "Brillouin mirror" regime may be reached by sufficiently increasing the pumping level for any fiber length.

In the next section, the generation of BFL in a ring cavity will be discussed. We propose a new ring-cavity configuration which can result in higher BFL power in comparison to the traditional one [59]. Then we pay attention to our work in the linear cavity BFL generation in which Bragg gratings can also be used

instead of the mirrors [60]. In addition, a new linear cavity configuration is proposed to generate high power linear cavity BFL will be discussed in which the generation of the enhanced BFL will be explained by proposing a new linear cavity configuration in fiber optics [61].

3.3.1 Brillouin Fiber Lasers in Ring Cavities

Great efforts have been spent to improve Brillouin ring fiber lasers (BRFLs) and to study their spectral properties due to increasing interest in optical fibers [62]. Stimulated Brillouin scattering in a continuous wave-pumped low-finesse fiber ring resonator is called BFRL when the closed-loop gain exceeds unity so that Brillouin amplification overcompensates the ring cavity loss. Thus, a cavity length of several meters is required to obtain threshold power in the milliwatt range by preparing the SBS nonlinear gain. The bandwidth of the Brillouin gain is very narrow, typically from 20 to 50 MHz for the wavelength in the near infrared region in single-mode fibers [63]. As soon as the cavity length exceeds a few meters long cavities result in narrow resonance in the frequency domain of cavity modes with sub-Megahertz linewidth. In addition, sub-Megahertz linewidth of cavity modes is also observed as soon as the cavity length exceed a few meter. Narrowing linewidth is observed in Brillouin Stokes as soon as input Brillouin pump power exceeds the Brillouin threshold power [23]. Therefore, BFLs are generally constructed in an all-fiber, high-finesse ring-resonator arrangement to achieve low laser threshold and efficient operation [64]. BRFLs have attracted considerable interest because of their varied type of dynamic behavior [65-70].One of the most important features of BFRLs is the existence of

periodic intensity modulation called self-pulsing in the created Brillouin Stokes signal [65].

When studies of BRFLs were first formulated, no information about the instability of SBS was given since the transient effect of the acoustic wave and optical Kerr effect inducing self- and cross-phase modulations were neglected in this model [71]. A more realistic formulation of the fiber ring laser was given by the coherent three-wave model which was considered in Eqs. (2.66) and (2.67) [56], [72]. Then, the acoustic damping was taken into account and a Hopf bifurcation between steady and pulsed regimes was evident [66]. It is also reported that SBS instabilities including periodic, quasi-periodic and chaotic oscillations may arise only when the length of the fiber cavity is large enough [65], [69]. Moreover, by using a short fiber in a high-finesse cavity, it is generally considered that the SBS instability, especially the self-pulsing phenomenon may be suppressed [69]. Therefore, the physical origin of the instabilities in a BFRL is attributed to the existence of a large number of longitudinal modes beneath the Brillouin gain curve rather than to the optical Kerr effect [54], [58]. Moreover, it is generally considered that the SBS instability, especially the self-pulsing phenomenon may be suppressed by the use of a short and high-finesse cavity [58]. In such a cavity, the threshold of SBS would be greatly reduced [73], [74] and the transient Stokes intensity in the ring could significantly exceed the steady-state value [71].

In most of the previous papers about the SBS effect in a fiber ring resonator, both the pump and Stokes waves have been assumed to be resonant within the cavity. The linear phase detuning of the cavity for either the circulating

pump wave or Stoke wave has been investigated [67],[68]. In fact, the difference between the total linear phase ϕ_p (accumulated by the pump wave) and ϕ_s (accumulated by the Stokes wave) per round trip of the cavity is much larger than the magnitude 2π even if the length of the fiber resonator is several centimeters. In a high-finesse ring resonator, since the circulating pump power depends strongly on the linear phase detuning of the cavity, the difference between ϕ_p and ϕ_s must be considered in the theoretical calculation.

The two configurations for generating BRFL are demonstrated in Fig 3.12. In optical fibers, since the frequency shift of the Brillouin Stokes vanishes in the forward direction which is the direction of the Brillouin pump (BP) propagation, according to Eq. (2.71), Brillouin Stokes propagates only in the backward direction due to the SBS feature in optical fibers. In this study, a new BFRL cavity configuration is proposed using components similar to the conventional BFRL cavity, but the new cavity results in a higher output BFRL power as compared to the conventional BFRL. The experimental setup for the conventional BFRL configuration is shown in Fig. 3.12 (a) in which a 3-dB coupler and a 25 km single-mode fiber (SMF) act as a ring resonator. The anti-clockwise propagating BFRL is routed to the Optical Spectrum Analyzer (OSA) via the 3 port optical circulator. Fig. 3.12 (b) shows the proposed configuration, which uses components similar to the conventional configuration. In this configuration the resonator consists of the same optical circulator, the coupler and the SMF. However, in this configuration, the coupler placed between the SMF and the port 3 of the optical coupler extracts only the counterclockwise output BFRL power detected by the OSA. The SMF which is spliced between ports 2 and 3 of the optical circulator

through the coupler generates the BFL ring resonator. The SMF is 25 km in length and has a cut-off wavelength of 1161 nm with a zero dispersion wavelength of 1315 nm and a mode field diameter of 9.36 μm at 1310 nm. Both BFRLs are pumped by an external cavity tunable laser source (TLS) with a maximum power of approximately 5 dBm. In the Fig. 3.12 (b), the Brillouin pump (BP) with the 15 MHz linewidth is injected into the SMF from port 1 through port 2 of the optical circulator in a clockwise direction. The backward-propagating SBS generated oscillates inside the resonator in anti-clockwise direction to generate the Brillouin laser, which is coupled out using a 3-dB coupler. The optical circulator which protects the TLS from any BP reflection is also used to force the unidirectional operation of the laser in the cavity although SBS in the SMF propagates only in the backward direction due to the SBS feature. The laser output is characterized using an Optical Spectrum Analyzer (OSA) with a resolution of 0.015 nm. All the components are spliced due to the extremely small splice loss.

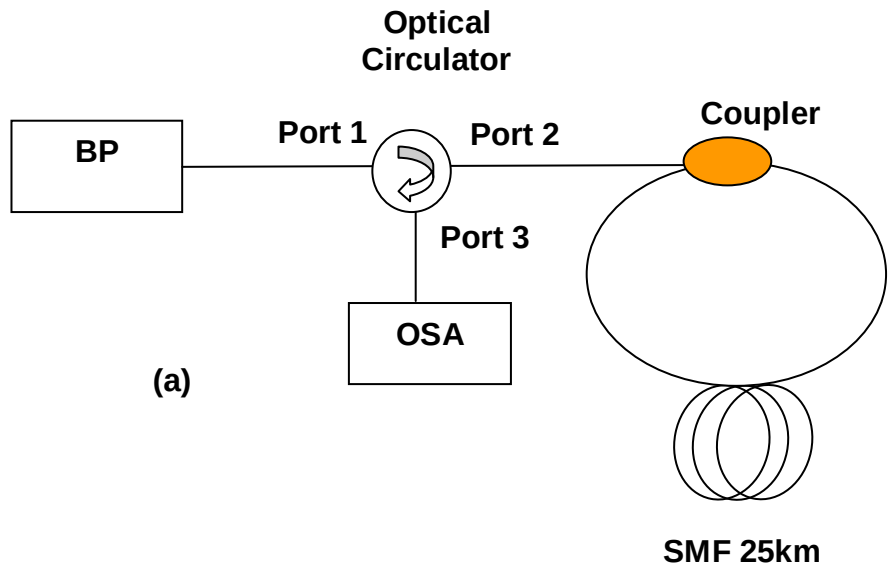

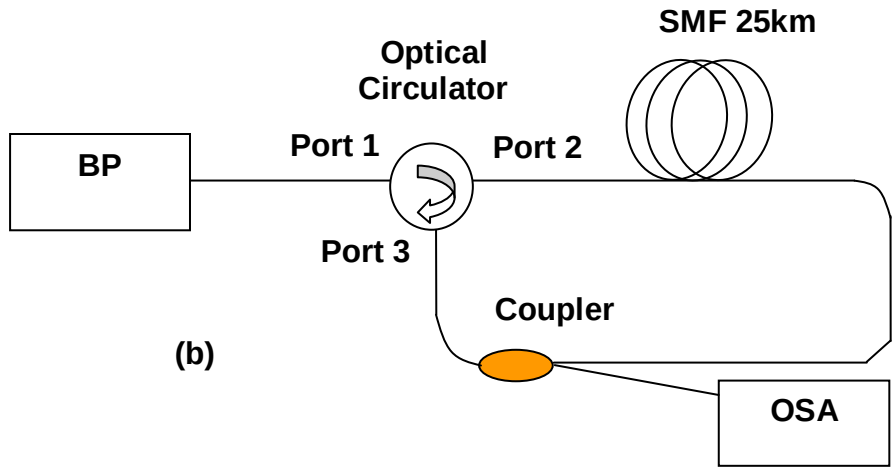

Fig. 3.12: Experimental set up for the generation of (a) a conventional BFRL and (b) the proposed new configuration BFRL [59].

The results are shown in Fig. 3.13 which compares the output spectrum for the conventional BFRL and the proposed new BFRL configuration. The 3-dB coupler (50-50) allows half of the light to oscillate in the cavity and another half to couple out as the output of the BFRL. Both BFRL configurations generate a Brillouin laser at around 1550.1 nm, which is 0.08 nm longer than the BP wavelength. The anti-Stokes signal is also observed at a shorter wavelength due to four-wave mixing between the BP wave and the Brillouin Stokes wave. The proposed BFRL configuration of Fig. 3.12(b) shows an output peak power of -0.5 dBm, which is 5.7 dB higher compared to the conventional configuration in Fig. 3.12(a). The anti-Stokes signal also shows a 1.8 dB increment in signal power. Even though the cavity loss is smaller in the conventional configuration due to using only the SMF and the coupler in the ring resonator, the proposed configuration is configured such that the SMF receives more BP power. In other words, the higher BP power

generates higher back-propagating Brillouin Stokes power and the Brillouin gain in the cavity. Therefore the BFL and the SBS anti-Stokes powers are higher in the proposed BFL configuration as compared to the conventional BFL configuration. The Brillouin crosstalk effect also causes the anti-Stokes and BP Rayleigh reflection power to be transferred to the BFRL power.

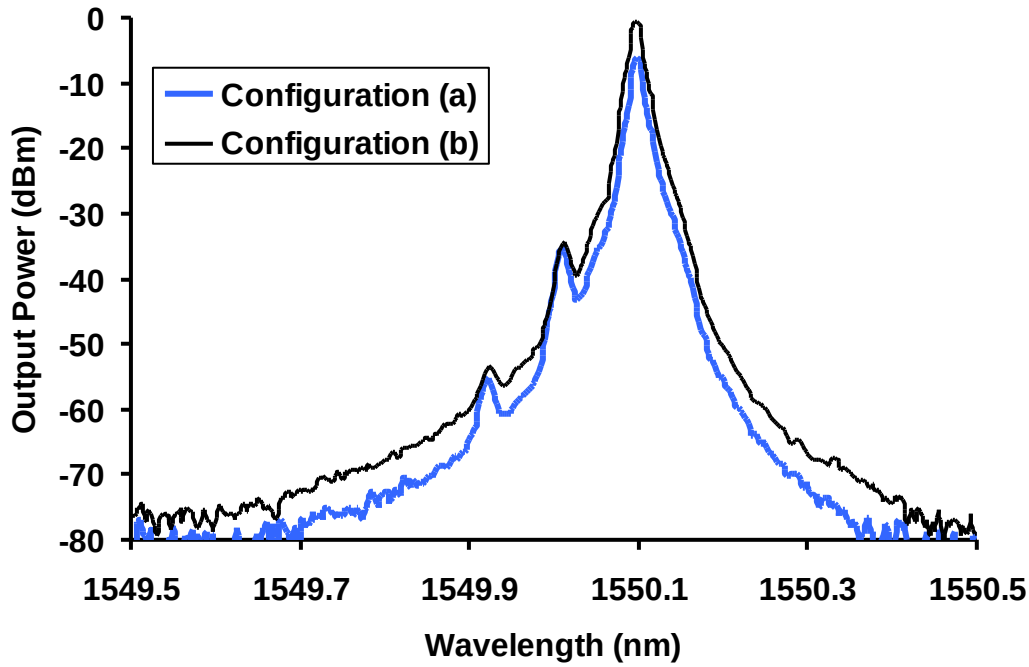

Fig. 3.13: The comparison of the BFRL output spectrum between the conventional configuration (a) and the proposed configuration (b) shown in Fig 3.12 [59].

Fig. 3.14 shows the BFL output spectrum of the proposed new configuration of Fig. 3.12 (b) at the different output coupler ratios. The BP power is fixed at 5.5 dBm and the length of SMF is 25 km in all the measurements. The line spacing is approximately 0.08 nm in the wavelength domain and 11GHz in the frequency domain, as measured by an optical spectrum analyzer with a resolution of 0.015 nm. The 3-dB bandwidth of each BFRL line is less than 0.02nm, limited by the OSA resolution. However, the bandwidth measurement will be done by using the heterodyne method which will be explained in section 3.3. As shown in Fig. 3.14, the laser peak power is increased by decreasing the output leg power ratio due to the increasing BP power which reaches the SMF. However, the output BFRL peak power decreases as the output leg power ratio decreases by 20%. This is attributed to the saturation of the Brillouin Stokes power and the small amount of light being extracted out of the cavity by reducing the coupler ratio. The maximum output power was observed at 0.5 dBm with an output coupler of 20-80 ratio, where 80% of the light is allowed to oscillate in the cavity and 20% of the light is coupled out as output, as shown in Fig. 3.14 [59].

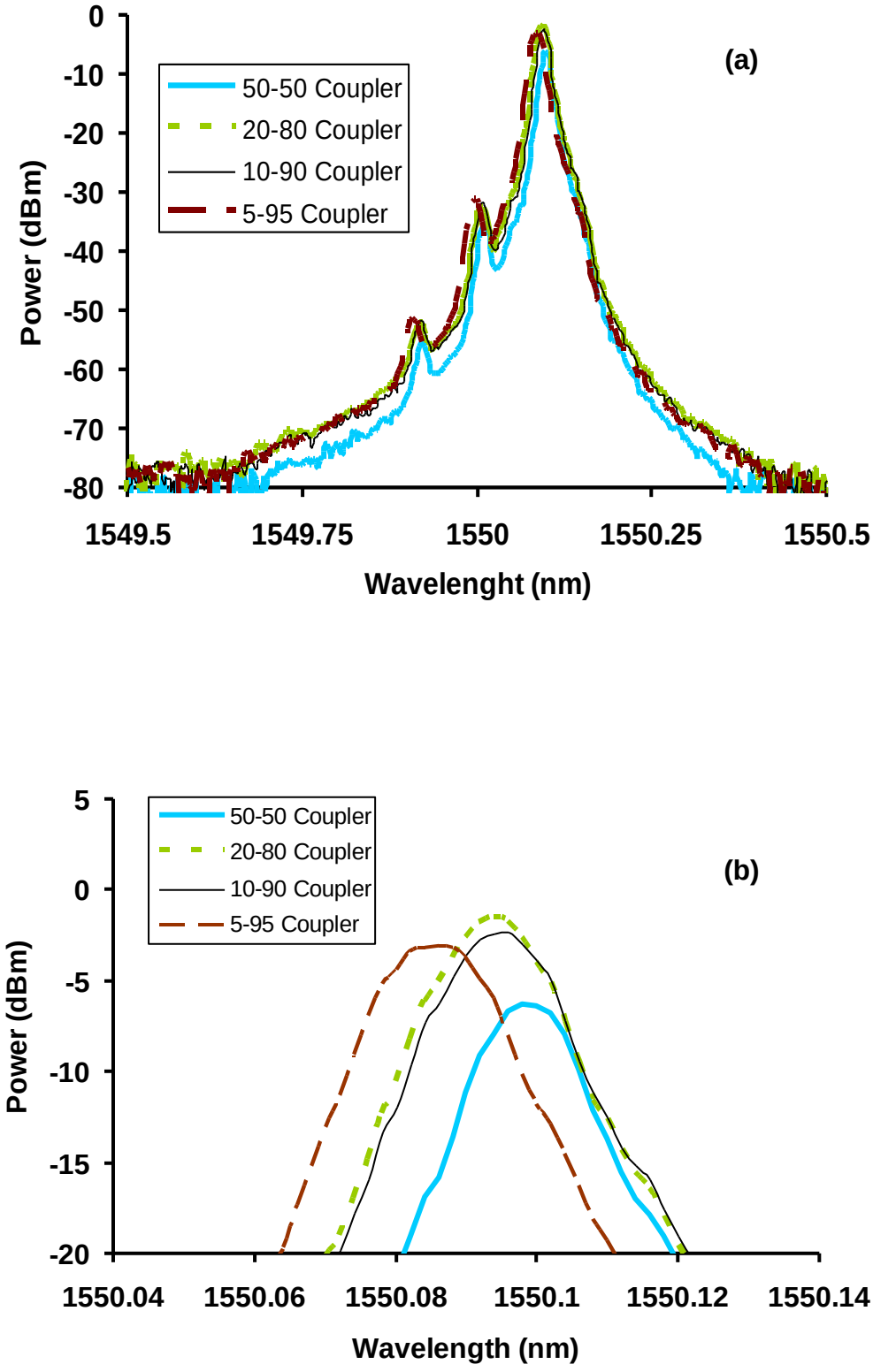

Fig. 3.14: (a) The BFRL output comb at different output coupler ratios. (b) The enlarged figure of the output peak region is shown for the comparison [59].

3.3.2 Generation of Brillouin Fiber Lasers in Linear Cavities

Previous BFLs have been set up using ring cavities and a few BFLs, so far, have been presented using a linear configuration. This is due to the fact that conventional-linear-cavity BFLs suffer from some problems such as the generation of higher-order Stokes and anti-Stokes waves. In the following, we will discuss the linear cavities and propose some linear configurations in order to solve the problems.

In a linear cavity, additional feedback from the boundaries is known to give rise to periodic temporal structures in the experiment [75], [76]. In this paper, we demonstrate a new BFL design with a linear cavity. A stable BFL was obtained at a wavelength of 0.08 nm from the pump wavelength 1550 nm through the careful optimization of the output coupling ratio and the employment of a suitable reflector. The performance of the BFL is done by using different reflectors such as optical circulators and FBGs.

The experimental setup is shown in Fig. 3.15 whereby the linear cavity is formed by two optical circulators in configuration (a), a circulator and a fiber Bragg grating (FBG) in configuration (b) and only a FBG in configuration (c). Here, the SMF characteristics are as the one used before in BFRL generation. The SMF is pumped by the Brillouin pump (BP) which is an external cavity tunable laser source (TLS) amplified by an Erbium-Doped Fiber Amplifier (EDFA). The maximum power of the amplified BP is approximately 14.5 dBm and the BP is injected into the SMF via a 3-dB coupler in the forward direction. The generated backward-propagating SBS oscillates inside the resonator to generate the BFL, which is coupled out via the coupler and the output laser is characterized using an

OSA with a resolution of 0.015 nm. The experiment is carried out using three different couplers ratios; 50/50, 95/5 and 99/1. For each coupler, the port of the lower ratio is connected to the OSA.

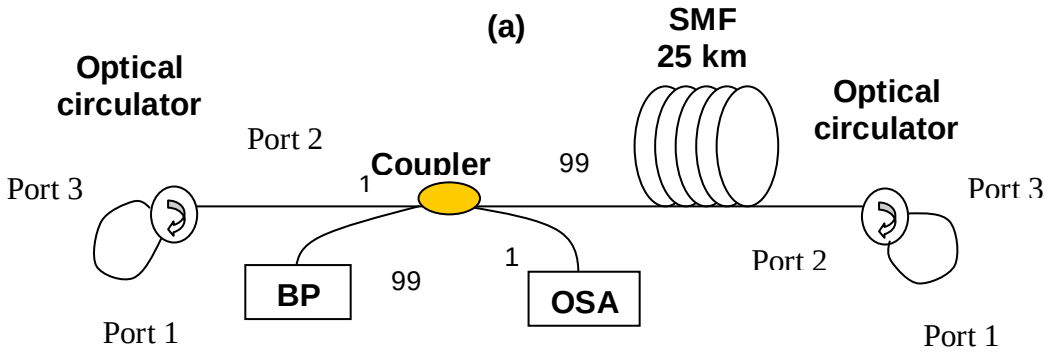

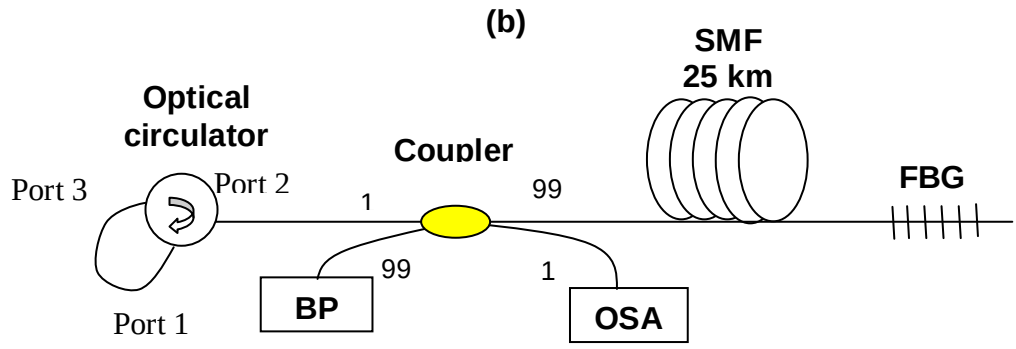

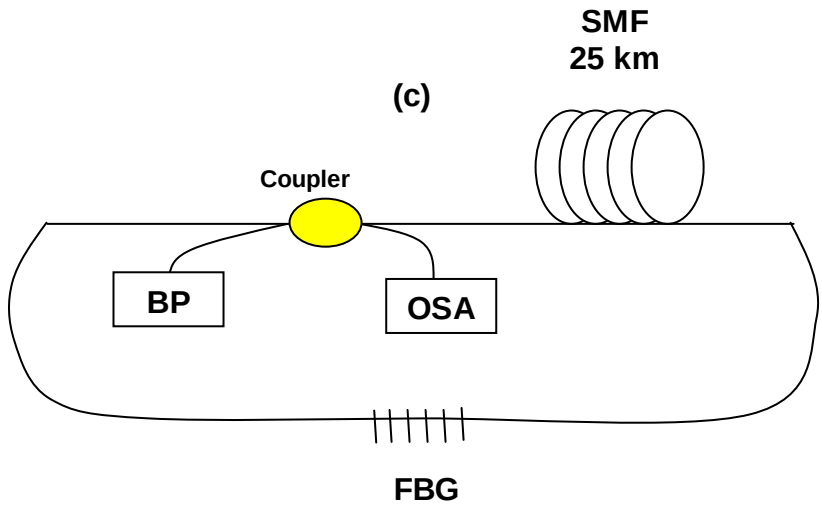

Fig. 3.15: Experimental set up for generating linear cavity Brillouin fiber lasers by using (a) two optical circulators, (b) a circulator and a fiber Bragg grating (FBG), and (c) a FBG [60].

In Fig. 3.16, the BFL output spectrum is demonstrated by using different coupler ratios in the configuration (a) of Fig. 3.15 with the BP power of 14.5 dBm. If the total Brillouin gain is equal to or higher than the cavity loss, BFL laser oscillation can be formed between the two optical circulators. As shown in Fig. 3.16, the BFL is generated with 99/1 coupler, which contributes to higher injected BP power into the SMF and lower cavity loss. However, the laser cannot be generated with a 50/50 coupler due to the injected BP into the SMF which is lower than SBS threshold and the high loss in the cavity. The highest peak is obtained with a 99/1 coupler which has the lowest cavity loss.

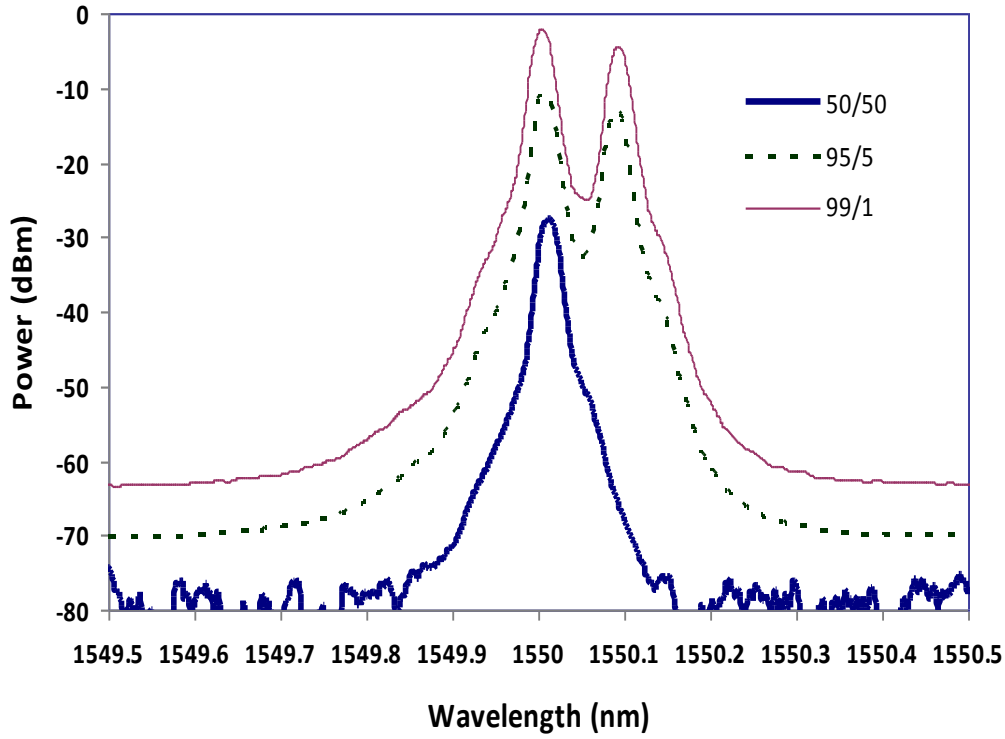

Fig. 3.16: The BFL output spectrum for different coupler ratios used in a linear cavity configuration (a) shown in Fig. 3.14 with the BP power of 14.5 dBm [60].

Fig. 3.17 shows the output spectra of the linear-cavity BFL for each of the mentioned configurations. In this experiment, the coupler ratio is 99/1 and the BP power fixed at 14.5 dBm. The coupler ratio 99/1 is the best ratio for BFL generation according to result obtained in Fig. 3.16. As shown in Fig. 3.17, the two simultaneous lines are obtained with the BP line at approximately 1550.011 nm and the BFL line at approximately 1550.094 nm. The laser is generated by the Brillouin gain which is provided by the 25 km SMF. As the BP is coupled into the SMF, the Brillouin Stokes signal is generated at a frequency shifted by approximately 0.083 nm due to the Brillouin scattering effect. The Stokes

propagates in the opposite direction of the BP and travels to the circulator, acting here as a reflector, before it is rerouted back into the SMF by the circulator. The amplified Stokes then travels back to the other side of reflector and this oscillation continues to generate the BFL. The use of an FBG instead of an optical circulator in configurations B and C also increases the output power of the laser as shown in Fig. 3.17. The highest output power is obtained with the use of only one FBG as in configuration C. This is attributed to the reduced loss in the cavity due to the FBG. The FBG used in the experiment has a reflectivity of more than 99.5% at a wavelength region from 1525 to 1560nm. This contributed to a loss of less than 0.1 dB as compared to the circulator loss which is approximately 1 dB. The maximum laser peak power is obtained at -4.5 dBm.

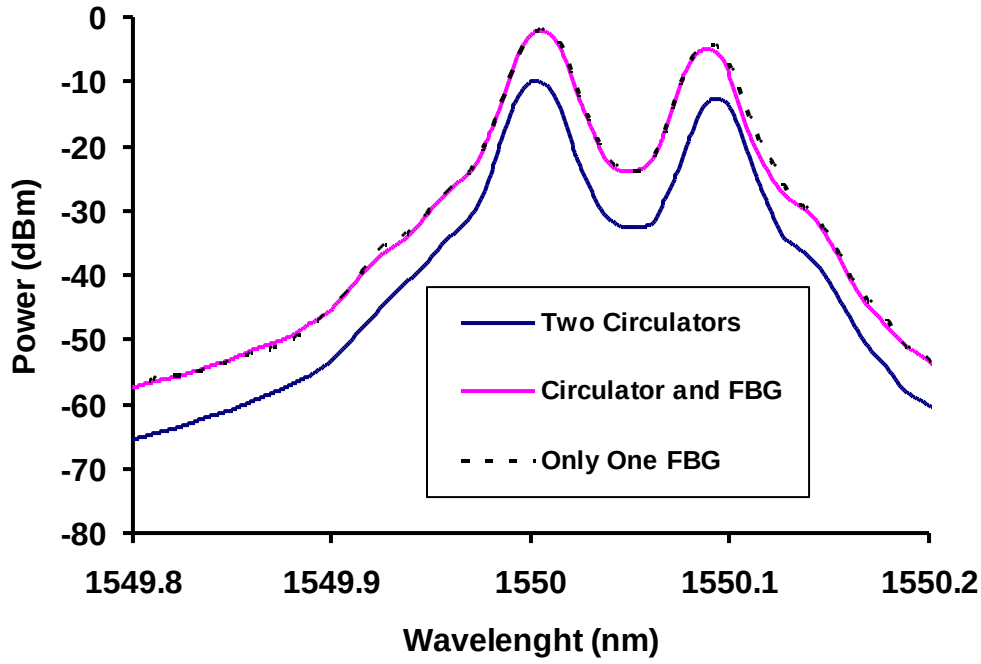

Fig. 3.17: The BFL output spectrum for the different linear cavity configurations at an input BP power of 14.5 dBm [60]**.**

The proposed linear configurations demonstrate new linear-cavity designs for the BFL generation. Stable BFL operation was obtained at an up-shifted wavelength of about 0.08 nm from the pump wavelength through the careful optimization of the output coupling ratio and employment of a suitable reflector. An efficient and low cost linear cavity Brillouin fiber laser (BFL) is demonstrated using only a single fiber Bragg grating (FBG) as a reflector. The laser peak is obtained at -4.5 dBm with a Brillouin pump of 14.4 dBm. The use of a 99/1 optical coupler shows the highest output due to the low loss in the cavity [60].

Fig. 3.18 shows the BP power against the peak power for the both transmitted BP and output BFL. In the experiment, configuration C of Fig. 3.15 was used in conjunction with the 99/1 coupler.

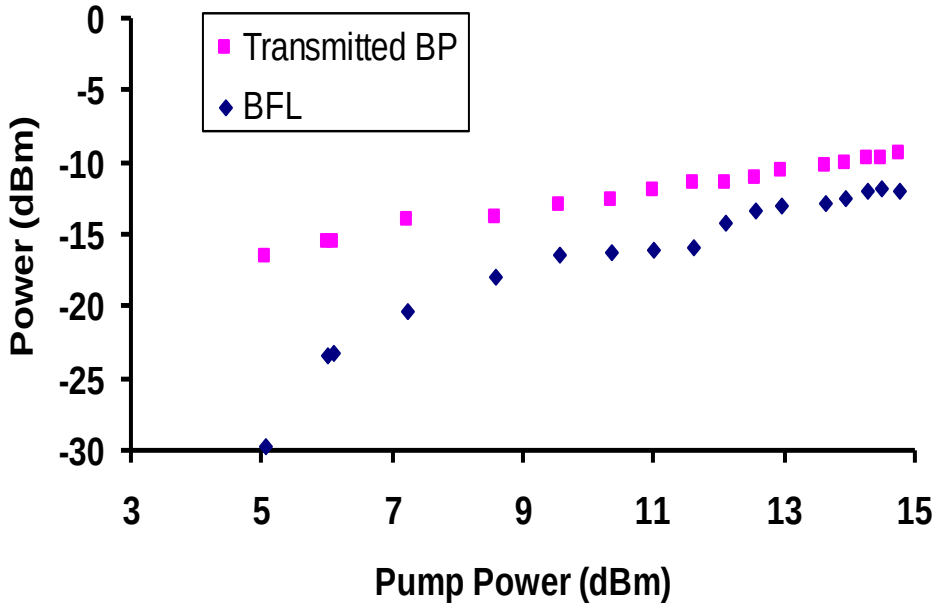

Fig. 3.18: The transmitted BP and BFL peak power in the output of the configuration (c) of Fig. 3.15 against the injected BP peak powers [60].

As shown in this figure, the peak power of the both BP and BFL increases with the BP power. The threshold of the stimulated Brillouin scattering (SBS) is approximately 6 dBm as shown in Fig. 3.18. The SBS increases as the BP power increases and starts to saturate at approximately 9.5 dBm. The Brillouin gain is higher than the cavity loss at a BP above 12 dBm, so that the BFL has been generated and increases with the BP power. As shown in Fig. 3.18, the BFL is always lower than the BP output. Some research has been done to solve this problem in order to improve high power conversion in the BFL generation and to create high power BFL [77], [78]. In this research, a new design for linear cavities is demonstrated in which the BFL peak power can be higher than the transmitted

output BP peak power [61]. In addition, the generated BFL has higher power in comparison to the conventional design by using the same BP power. In other words, very high conversion power efficiency occurs which is new in this field [77],[78],[61]. Stable operation of the BFL is obtained at an up-shifted wavelength of about 0.086 nm from the pump wavelength.

The proposed linear cavity configuration is shown in Fig. 3.19 whereby the linear cavity is formed by two optical circulators (OC1 and OC2), a 3-dB coupler and a 95/5 coupler located between ports 3 and 1 of OC1 and OC2, respectively. As before, a 25 km long SMF is used as a gain medium with an attenuation coefficient of 0.19 dB/km at 1550 nm. The BP is injected into the SMF via the 3-dB coupler and OC1 in a forward (clockwise) direction at $z = 0$ as indicated in Fig. 3.19.

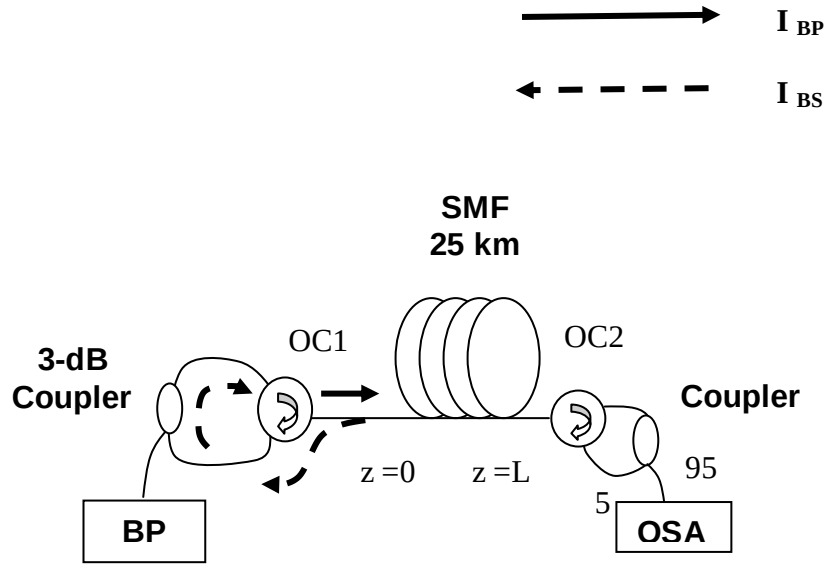

Fig. 3.19: Experimental setup for the proposed conventional linear cavity [61].

The 13 dBm BP is injected into the SMF via the 3-dB coupler and OC1 in a forward (clockwise) direction at $z = 0$ as indicated in Fig. 3.19. The first backward-propagating Stokes, initiated at $z = L$ from spontaneous Brillouin scattering or seed signal, oscillates inside the resonator to subsequently generate the BFL and the second-order forward-propagating Brillouin stokes which is starts at $z = 0$ through cascaded SBS coupled out via the 95/5 coupler. This coupler also suppresses higher-order anti-Stokes and Stokes generation. The first anti-Stokes arises due to four-wave mixing (FWM) between the co-propagating BP and BFL photons. The output laser is characterized using an OSA with a resolution of 0.015 nm.

Fig. 3.20 compares the output BFL spectrum of the proposed configuration and the conventional configuration. As shown in Fig. 3.20, for the proposed configuration, two Stokes lines at approximately 1550.101 nm and 1550.187 nm, and one anti-Stokes at approximately 1549.929 nm are obtained around the oscillated BP at approximately 1550.015 nm whereas we have only the first Stokes in the conventional cavity. However, the first Stokes peak power in the proposed configuration is about 12.3 dB higher than that one resulting in the use the conventional scheme. Also, the BFL peak power is about 0.5 dB higher than the transmitted BP peak power which is a new occurrence encountered in this field [77], [78].

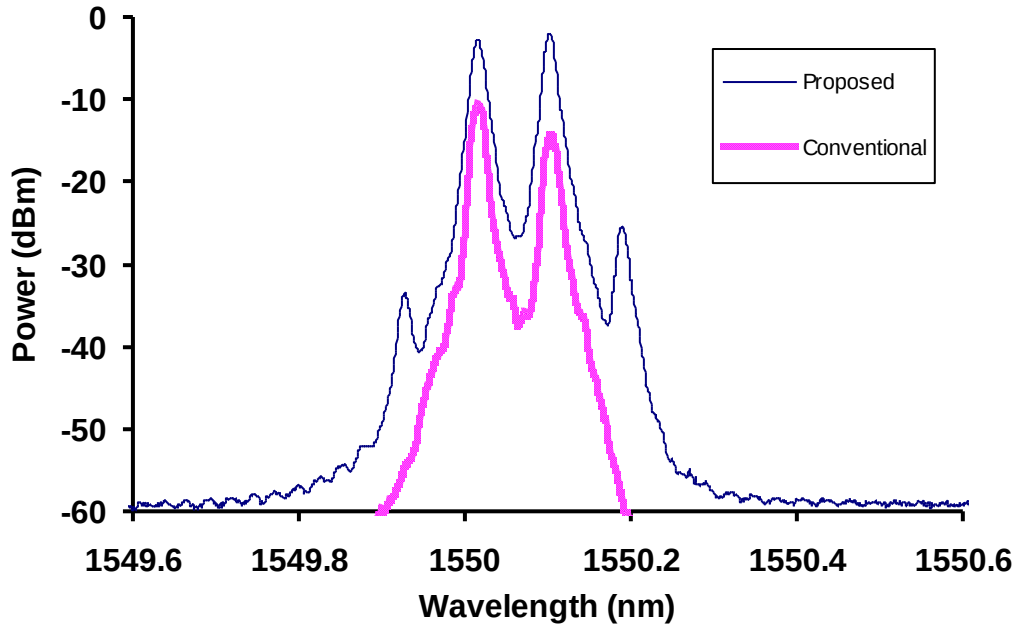

Fig. 3.20: The output spectra for the proposed and conventional configurations at a BP power of 14.4 dBm [61].

Indeed, the generated spectrum is a dual–wavelength Brillouin fiber laser source with the channel spacing 0.08 nm. In the following, the generation of multiwavelength Brillouin fiber lasers will be discussed.

3.4 Generation of Multiwavelength Brillouin Fiber Lasers (MBFLs)

Brillouin fiber lasers (BFLs) have attracted wide attention due to their low threshold and high power conversion efficiency. Among all BFL applications, multiwavelength Brillouin fiber lasers (MBFLs) also known as cascaded Brillouin fiber lasers are able to provide multiple lasing wavelengths which are very useful for wavelength-division-multiplexing (WDM) and dense WDM (DWDM) in optical transmission systems [49], [73], [79]. In pervious WDM and DWDM

systems, separate semiconductor laser sources had been utilized for each channel which required individual wavelength control [80]. The advantages of the MBFLs as sources in WDM and DWDM systems is that channel allocation is done automatically by the Brillouin shift determined by the characteristic properties of the single-mode fiber. The static and dynamical behaviour of MBFLs have been investigated [81], [82], [83]. The generation of Brillouin lasing wavelengths with the assistance of Erbium-doped fiber amplifies (EDFA) have been reported [84], [85]. By using an EDFA in the cavity, the loss can be compensated while still BFL action originates from the Brillouin gain. However, one of the disadvantages of this method is EDFA operational wavelength limitation as it will be discussed in the next chapter.

In the following section, we will discuss the MBFLs generation as a method which is not limited to a special wavelength region.

3.4.1 Generation of MBFLs in Ring Cavities

In this section, the proposed MWBFL utilizes simple components as a 25 km single-mode fiber (SMF) used as the Brillouin gain medium, fiber couplers and an optical circulator to generate necessary feedback for multiwavelength BFL in a ring cavity. Bidirectional multiwavelength operation is obtained, with 20 GHz multiwavelength operation corresponding to the case that even and odd order Stokes waves of BFLs are discriminated in the forward and backward direction respectively. However, 10 GHz BFL optical comb generation can be obtained by the backward and forward combination [86].

The proposed configuration of the multi-wavelength BFL is shown in Fig. 3.21. The elements of the cavity are a 3 dB coupler (2x2), C1, another 3 dB

coupler (1x2), C2, a 4-port optical circulator, OC, and a 25 km SMF as the gain medium. The SMF has a cut-off wavelength of 1167 nm with a zero dispersion wavelength of 1315 nm and a mode field diameter of 9.36 μm. The BFL is pumped by an external cavity tunable laser source (TLS) with a linewidth of approximately 15 MHz which is amplified by an erbium-doped fiber amplifier (EDFA) to provide the maximum power of 14 dBm at an output wavelength of 1560 nm, which in this case is the Brillion Pump (BP).

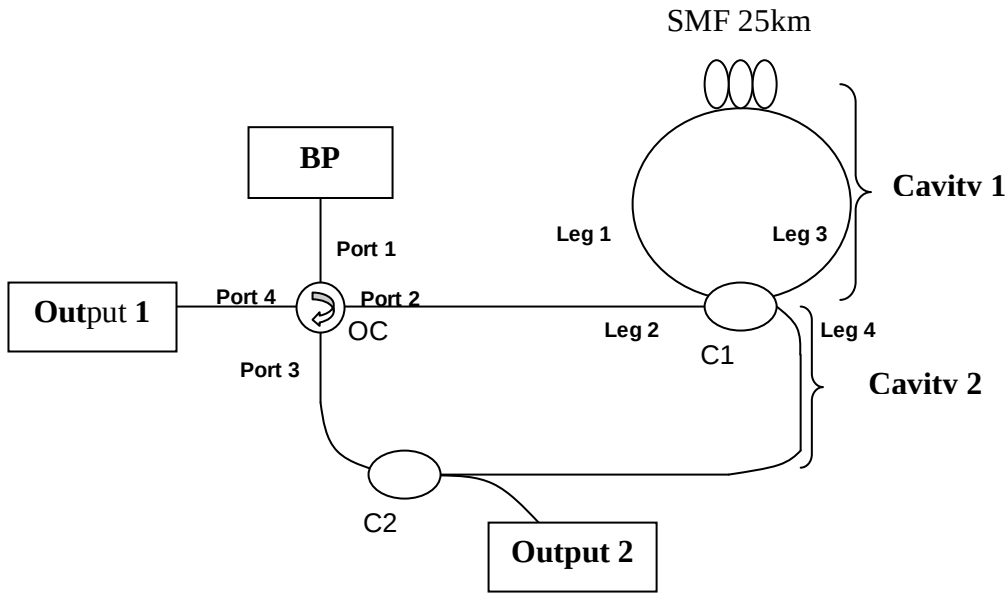

Fig. 3.21: The proposed experiment setup for generation 10 and 20 GHz comb.

The 25 km SMF in Cavity 1 is pumped by the BP that generates the first Stokes that travels in the clockwise direction of Cavity 1 and is emitted at Leg 2 into the second cavity. This provides the required feedback for Cavity 1 whereby this first Stokes travels back into this cavity through Leg 4 and Leg 1 of coupler

C1. This first Stokes will experience amplification from the 25 km SMF acting as a Brillouin gain medium. At the same time, this first Stokes will act as the pump that will generate the second Stokes in the anti-clockwise direction and will oscillate in Cavity 1 until it gains enough power where a portion of this power will be emitted at Leg 4 and will travel in Cavity 2 to be emitted as Output 1 (even Stokes) at Port 4 of the OC. The first Stokes (odd) will be emitted at Output 2 of C2. This process repeats to produce the subsequent odd and even Stokes as mentioned in this experiment. From Fig. 3.21, the odd Stokes can oscillate in both cavities, but the even Stokes will only oscillate in Cavity 1 whereby Cavity 2 provides the means for output extraction.

The BP beam of frequency ω_p generates the first backward propagating Stokes signal of frequency ω_{1s}, a Brillouin frequency down-shifted by $\Delta\omega_B$ with respect to the pump beam (i.e., $\omega_{1s}= \omega_p - \Delta\omega_B$). Then the first Stokes generates the second Stokes which propagates in the opposite direction, as explained earlier in the above section. If a threshold condition is satisfied, this will generate a cascading Brillouin effect as a comb of lines as shown in Fig. 3.22. From the figure, the spacing between two consecutive even or odd Stokes lines is about 0.16 nm (~20 MHz in 1560 nm region). Those lines before the BP line are anti-Stokes lines. This occurs when the various Stokes waves interacts with the pump wave which generates these anti-Stokes through the degenerate FWM process.

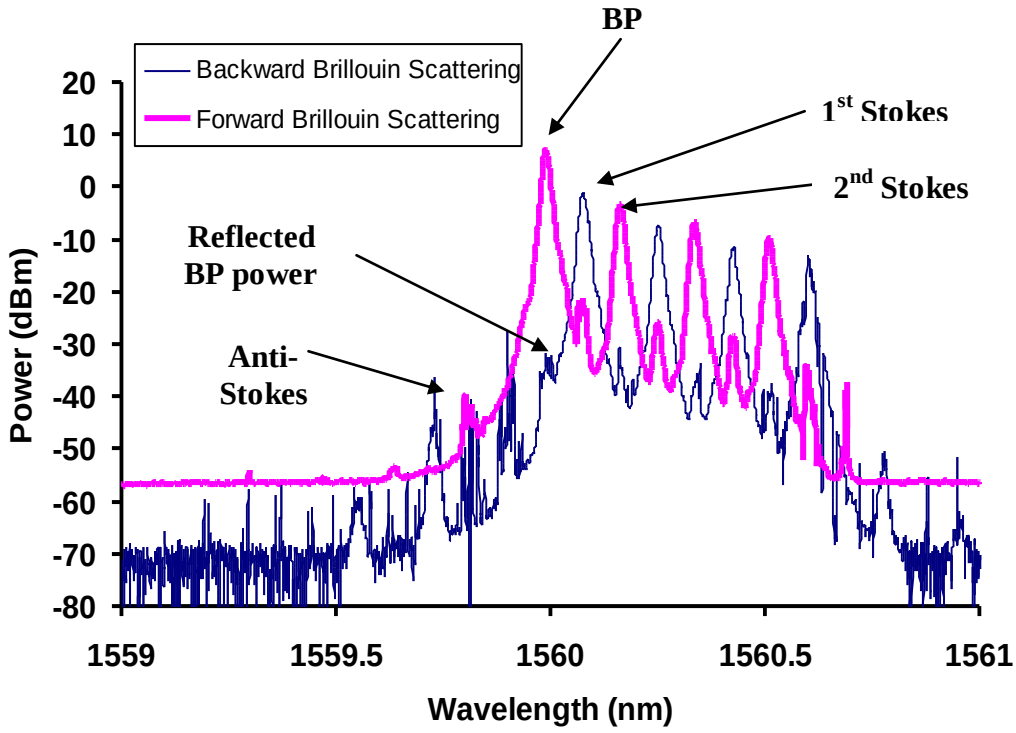

Fig. 3.22: Comb generation with 0.16 nm (~20 GHz) between two consecutive lines in forward and backward directions [86].

By combining the two ports, Output 1 and Output 2, we have a multi-wavelength BFL generation with the spacing 0.08 nm (~10 GHz), between each two adjacent lines as shown in Fig. 3.23. Although there is a power variation between the subsequent Stokes lines, using a gain flattening filter such as the long-period fiber gratings as a suggestion may help to improve and flatten this output, thus making it possible to use this system as a multiple-wavelength output source.

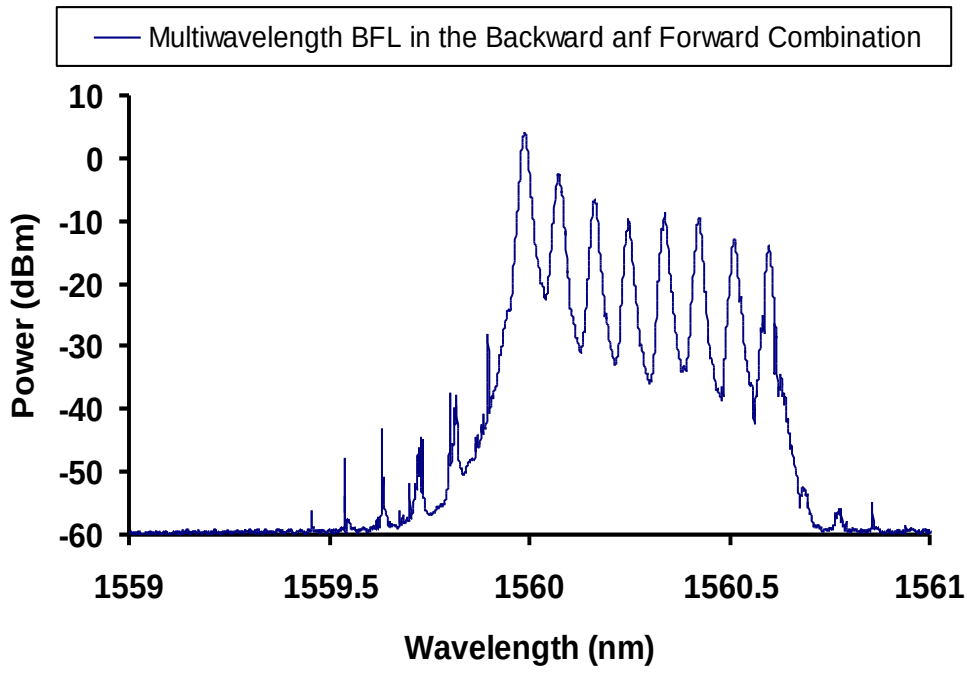

Fig. 3.23: 8 line spacing 0.08 nm (~10 GHz) of BFL Comb Generation [86].

From Fig. 3.23, the peak power of odd and even Stokes and anti-Stokes lines can be measured for different BP powers. These measured peak powers are depicted in Fig. 3.24 for the Stokes and Fig. 3.25 for the anti-Stokes respectively. By using the definition (8) in Section 3.1.3 for the SBS threshold power, the threshold condition of each Brillouin Stokes lines can be defined as the intersection point between the reflected BP power and the Stokes output as shown in Fig. 3.24. The reflected BP power is taken from the backward BP Rayleigh scattering as indicated in Fig. 3.22 for each different BP power. Also, as shown in Fig. 3.24, the Stokes lines begin to saturate as the BP power increases. For instance, the second Stokes line saturates as the threshold for third Stokes is reached. This is due to the power transfer from the second Stokes to the third Stokes, which occurs at when the BP power is approximately at 6.5 dBm. The

same thing can be said for the third and fourth Stokes at 10 dBm of the BP, which is the threshold of the fourth Stokes.

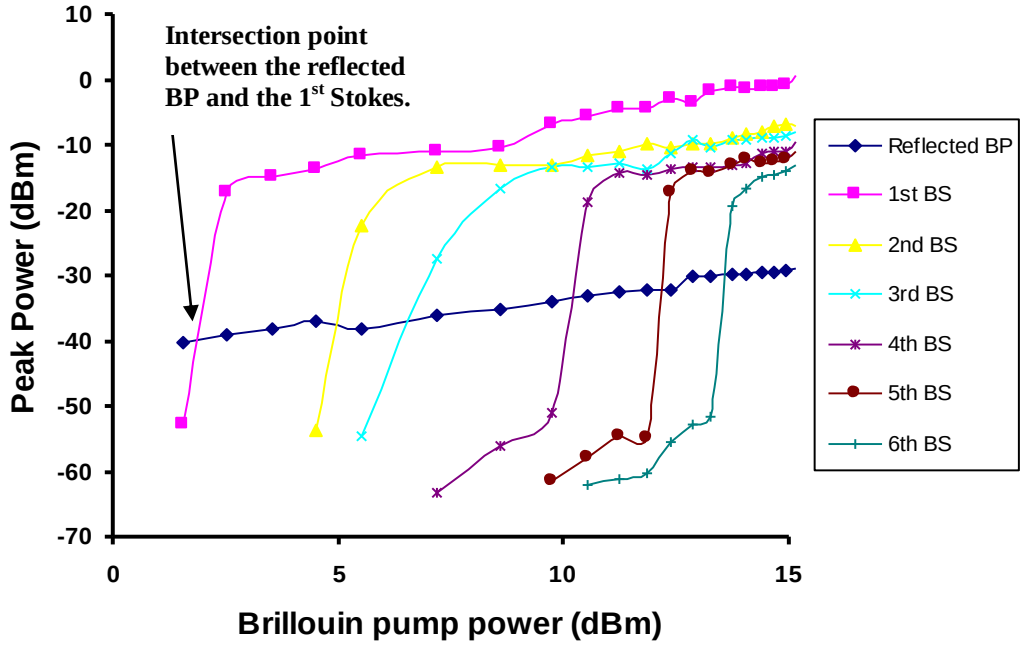

Fig. 3.24: Reflected Brillouin pump and Brillouin Stokes (BS) power against BP power [86].

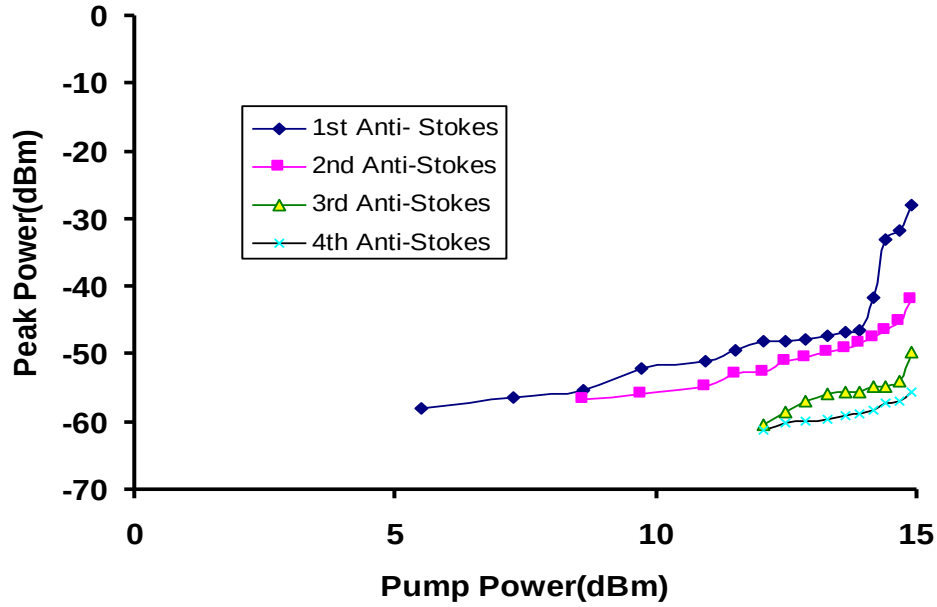

Fig. 3.25: Anti-Stokes Power against BP Power [86].

Fig. 3.25 shows the output peak power of the 1st, 2nd, 3rd and 4th anti-Stokes at different BP powers. For the case of the first Stokes, the peak power of the first anti-Stokes increases linearly with the BP power, but at approximately 13 dBm, the peak power increases significantly. The same effect is observed in the second anti-Stokes, in which the power rises linearly with the increase of the BP until the BP is approximately 13 dBm, whereby the peak power rises significantly. The third and fourth anti-Stokes also shows the same effect, rising linearly with the BP until a BP power of 14 dBm, whereby the rise becomes significant [86].

3.4.2 Generation of MBFLs in Linear Cavities

In this section, a new multi-wavelength Brillouin Fiber Laser (BFL) is demonstrated by using a single-mode fiber (SMF) as the SBS gain medium in a linear cavity. The output multi-wavelength lines are obtained through careful optimization of the output coupling ratio and the employment of an optical circulator as a reflector.

The configuration of the multi-wavelength linear cavity BFL is shown in Fig. 3.26. The Brillouin gain medium is as before the standard 25 km long SMF with cut-off and zero dispersion wavelengths of 1315 nm respectively and a mode field diameter of 9.36 μm. The laser signal generated from an external cavity TLS and amplified by an erbium-doped fiber amplifier (EDFA) is used as the Brillouin laser pump (BP). Here, the BP has a maximum power of approximately 12 dBm with a linewidth of approximately 20 MHz. Two optical circulators, OC1 and OC2, together with the couplers C1 and C2 act as reflectors in the linear cavity as shown in Fig 3.26. The left side reflector has a coupler (C1) with a fixed ratio of 50/50

with one end connected to the BP. The right side reflector coupler (C2) has a variable ratio, with the lower percentage end connected OSA.

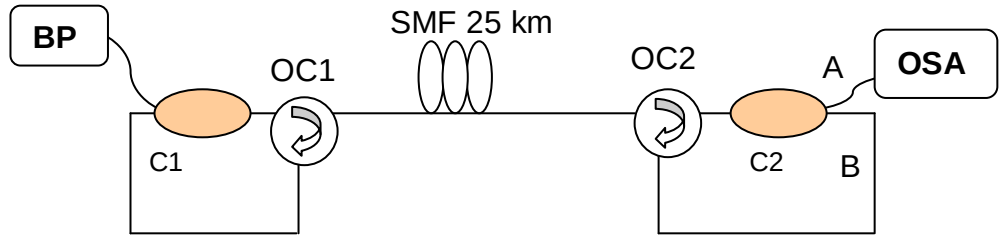

Fig. 3.26: The proposed linear cavity for MBFL generation [112].

The BP is injected into the linear cavity via C1 and OC1. Then, it is coupled into the SMF to generate the first Stokes signal propagating in the opposite direction of the BP signal. The first Stokes travels to OC1 and is re-circulated back into the SMF to be amplified and then moves towards OC2 and is reflected back to complete a round-trip oscillation. This oscillation continues until the intensity of the first Brillouin Stokes is higher than the threshold value for Brillouin gain, upon which the second Brillouin Stokes is generated and then begins to oscillate in the cavity. This process continues and subsequently cascaded Brillouin Stokes can be generated as long as the Brillouin gain is equal or larger than the cavity loss. The multi-wavelength output has a line spacing of approximately 10 GHz, which is equivalent to the Stokes shift in the SMF. The output of the linear cavity BFL is tapped from port A of variable ratio coupler C2, and is measured using the OSA. The coupling ratio of port B of C2 is varied from 70% to 99% (70, 80, 90, 95 and 99%) based on the availability of couplers with these ratios during the experiment.

The impact of the coupling ratio of C2 on the performances of the BFL is depicted in Fig. 3.27. In the experiment, the BP wavelength and power is fixed at 1550 nm and 11.7 dBm, respectively. As shown in Fig. 3.27, more than 9 simultaneous lines are obtained with the line spacing of approximately 0.08 nm for all coupling ratios even though only about 5 lines have nearly the same peak power. The 3-dB bandwidth of each line is lower than 0.02 nm, limited by the OSA resolution. The coupling ratio of C2 controls the amount of light that has been reflected from OC2. A higher ratio of Port B translates to a higher reflectivity at OC2. In the experiment, the minimum coupling ratio of port B is set at 70%, as below this value the reflectivity is very low, which increases the loss inside the laser cavity and thus least number of Stokes and anti-Stokes are observed. At the port B ratio of 95%, 11 simultaneous lines are obtained, which is the highest number of lines and 5 of these lines have a peak power of about -20 dBm. The signal to noise ratio is also largest at this ratio especially at the lines with low peak power. This is attributed to the high reflectivity at OC2 which subsequently reduces the loss inside the cavity to support the cascading process.

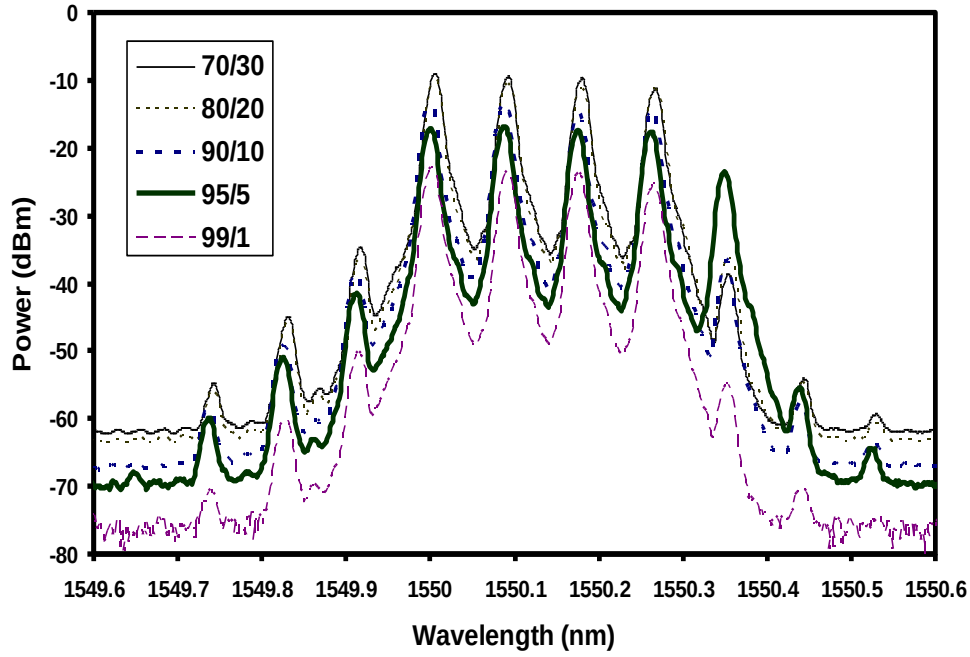

Fig 3.27: Output spectrum of the linear cavity MBFL at using the various output ratios for port B of OC2 [112].

The impact of the BP power on the number of Stokes generated by the MBFL is depicted in Fig. 3.28. The BP wavelength is also set at 1550 nm, while the BP power is varied from 4.1 dBm to 11.7 dBm. The experiment is not continued for BP powers below 4 dBm since the SBS gain cannot sufficiently compensate for the loss inside the laser cavity and thus cannot support multi-wavelength operation. The number of generated Stokes is observed to increase as the BP increases which is attributed to the increment of the nonlinear Brillouin gain with BP power. This situation provides sufficient signal power for higher order Stokes signal to pump the SMF and maintain the cascading of the Stokes into multiple Stokes. The BEFL also generates anti-Stokes as shown in Figures 3.27 and 3.28, especially at the higher BP powers. The anti-Stokes signals arise from the

bidirectional operation and degenerate four-wave mixing in the SMF and they are more obvious when the powers of BP are increased. Additionally, the power of subsequent Stokes lines is typically lower than that of the previous Stokes line as each subsequent Stokes is generated with the energy of the previous Stokes, thus slightly reducing the Stokes line's power. The multiwavelength output of the BFL is observed to be stable at room temperature with only minor fluctuations observed coinciding with large temperature variances. The MBFL has an advantage of being able to operate at any wavelengths depending on the availability of BP. The MBFL design can be made more compact with the use of highly non-linear fibers such as holey fibers for the generation of SBS.

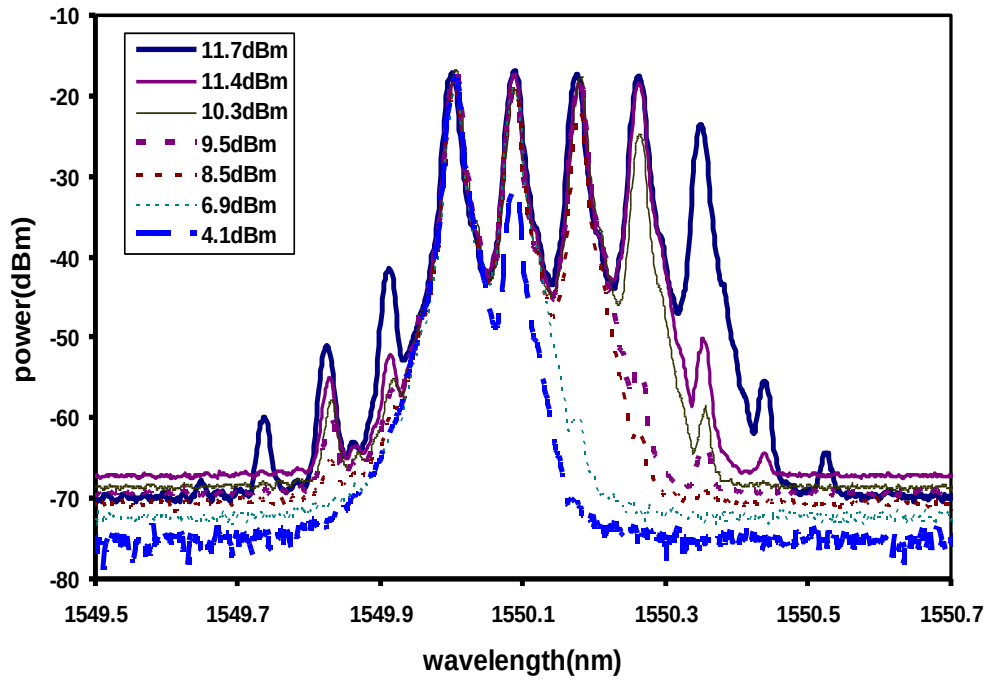

Fig. 3.28: The output spectrum of the proposed MBFL at different BP powers [112].

3.5 Linewidth Measurements Using Brillouin Fiber Lasers

Information can be transmitted by modulating the frequency or the phase of the optical carrier signal in lightwave systems [87-92]. These systems are also known as coherent lightwave systems in which the detection is done by using homodyne or heterodyne detection due to the important role of the phase coherence in the optical carrier. The basic concept behind coherent detection is the coherent combination of the optical signal with a continuous wave (CW) optical field before the detection as shown in Fig. 3.29. The CW field, known also as a local oscillator (LO) in the radio and microwave literature, is generated locally at the coherent detection receiver by using a narrow-linewidth laser.

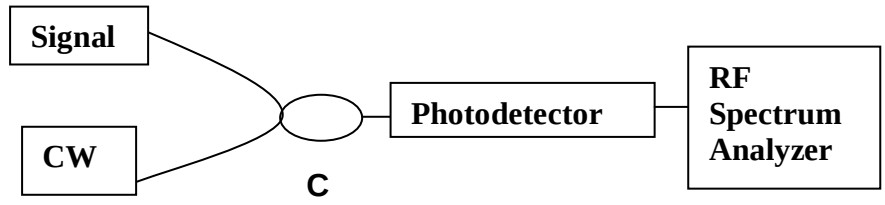

Fig. 3.29: Homodyne and Heterodyne detection for linewidth measurements

The operation behind these techniques can be explained readily. The signal interferes with the LO which is a CW laser in a coupler (C) and the resulting beat response is detected by a photodetector. This beat frequency which is in the radio frequency (RF) region can be analyzed by an RF spectrum analyzer (RFSA). The laser linewidth is usually inferred from the width of this beat spectrum. The optical signal can be written as

$$\psi_s = A_s \exp[-i(\omega_0 t + \varphi_s)] \tag{3.8}$$

in which ω_0, A_s, and φ_s are the angular frequency, amplitude and the phase of the signal, respectively. The optical field of the local oscillator is also expressed similarly by

$$\psi_{cw} = A_{cw}\exp[-i(\omega_{cw}t + \varphi_{cw})] \tag{3.9}$$

with the assumption that the two fields are identically polarized. For any detection, a photodetector responds to the optical intensity so we have to know the incident optical power at the photodetector. It can be shown as

$$P(t) = k|\psi_s + \psi_{cw}|^2 = P_s + P_{cw} + 2\sqrt{P_s P_{cw}}\cos(\omega_{IF}t + \Delta\varphi) \tag{3.10}$$

where k is a factor indicating the photodetector respond, $P_s = kA_s^2$, and $P_{cw} = kA_{cw}^2$ denote the powers of the signal and the CW, respectively and $\Delta\varphi = \varphi_s - \varphi_{cw}$ is the phase difference between the two sources. $\omega_{IF} = (\omega_0 - \omega_{cw})$ is known as the intermediate angular frequency (IF). If the CW power P_{cw} is much larger than the signal power P_s, the first term can be ignorable. The second term represents a large continuous signal which carries no information but does provide a shot noise or a white noise contribution. Basically, there are two different coherent detection techniques; the homodyne and heterodyne detection methods, depending on whether ω_{IF} equals zero or not. These detection methods can be used for the linewidth measurements which will be discussed next.

3.5.1 Linewidth Measurements- Homodyne and Heterodyne Methods

In a homodyne linewidth measurement, a signal is mixed with a time-delayed replica of itself to generate the beat frequency detected by RFSA. Fig. 3.30 shows the configurations for the homodyne linewidth measurement by using an unbalanced Michelson interferometer in (a) a common and (b) a traditional

configuration, respectively. The optical path difference in the fiber interferometer is used to generate the beat frequency. The laser beam is split into two parts. One is the local oscillator and the other is sent to the system to be probed. The scattered light is then mixed with the local oscillator on the detector. The photo detector (PD) and radio frequency spectrum analyzer (RFSA) are used for the beat frequency detection and **C** and **M** also denote a coupler and a mirror, respectively..This arrangement has the advantage of being insensitive to fluctuations in the frequency of the laser. This method can be used to evaluate the coherent length of a laser [93]. This method is sensitive to environment perturbations and the intrinsic loss of the fiber must be considered for the linewidth measurements. Figs 3.31 (a) and (b) show a more effective way of homodyne linewidth measurement by using the ring [94], [95] and the Fabry-Perot cavity [96], respectively. These configurations use a shorter delay fiber due to some roundtrip oscillation of the laser beam in them whereas the resolution is the same as the basic one shown in Fig. 3.30. The resolution of such a measurement is given by the finesse of the interferometer while the largest quantifiable linewidth depends on the free spectral range of the instrument. Commercially, recently Fabry-Perot interferometers have finesse between 100 and 1000, and free spectral ranges between a few 100 MHz to 10 GHz. Thus, Fabry-Perot interferometers are suitable for laser linewidth measurements of the order of MHz to a few GHz. Also, grating spectrometers can measure a spectral width in the region of 10 GHz to 100 GHz. In Fig. 3.30 (a), the laser beam is separated into two by the coupler and a long fiber spliced in one of the ways in order to delay the beam propagating in it. Then the last coupler combines the two beams in order to generate the beat

frequency which in turn will be detected by the photodetector and will be analyzed by the radio frequency spectrum analyzer (RFSA). In the traditional homodyne detection, however, two mirrors are used for reflecting the delayed laser light and the original one. Here the two optical circulators perform the same function as the mirrors when ports 2 and 3 are connected to each other. The combination of the reflected beams is done at the same coupler used for the separation of the original laser. The same process occurs in the other configurations shown in Figs. 3.31 (a) and (b). According to the analysis considered in [96],[97], when the delay time of the fiber τ_d is much larger than the coherence time τ_c, the spectral analysis of the self-homodyne signal gives full information about the linewidth of the laser radiation. The measured full width at the half maximum (FWHM) or bandwidth $\Delta\upsilon_{s.hom.}$ in the self homodyne method is connected with the laser source linewidth $\Delta\upsilon_{\mathrm{L}}$ as

$$\Delta\upsilon_{s.\mathrm{hom}} = 2\Delta\upsilon_{\mathrm{L}} \tag{3.11}$$

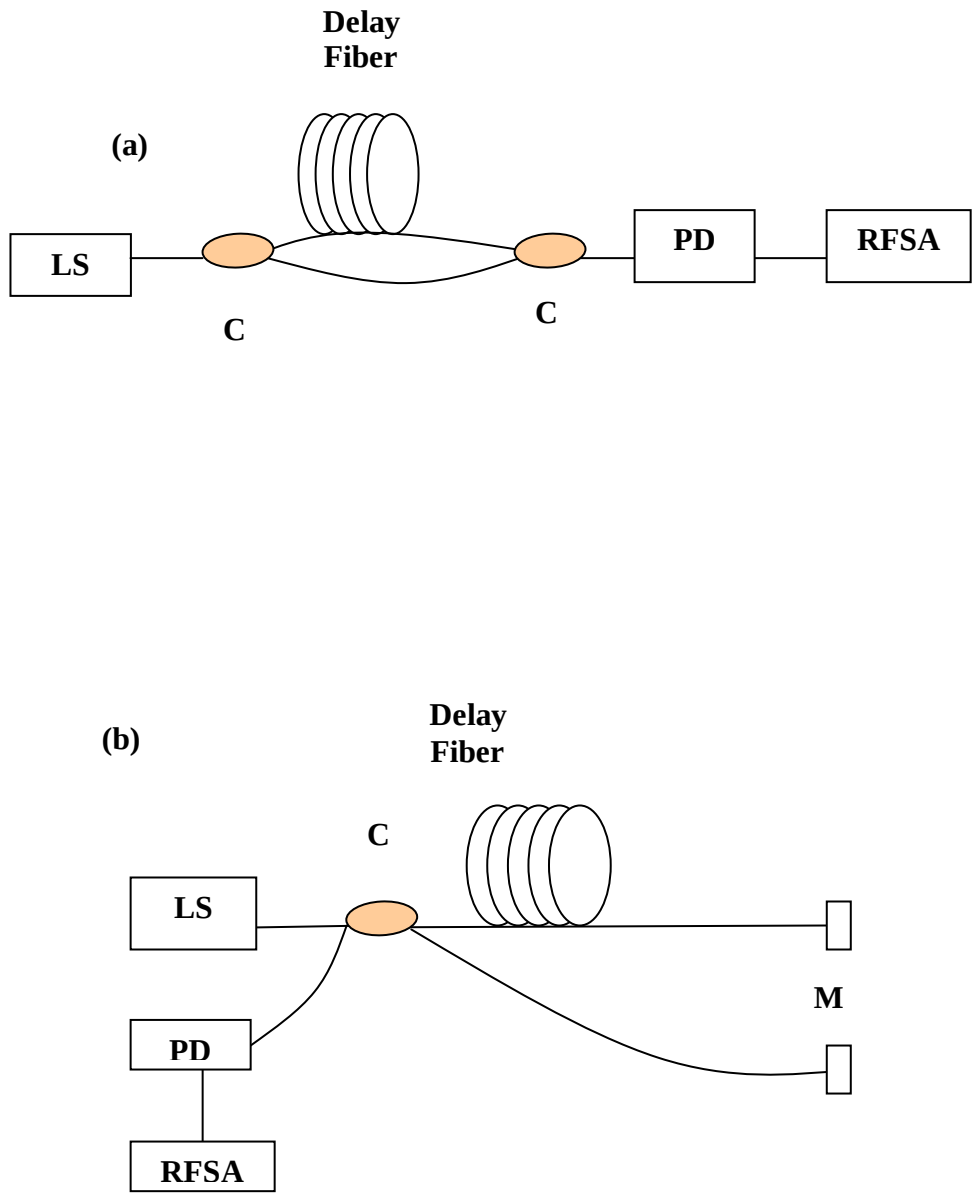

Fig. 3.30: Schematics of the different interferometers used for homodyne linewidth measurement of a laser source (LS) with an unbalanced interferometer in (a) a common Mach Zhender and (b) a traditional Michelson configurations.

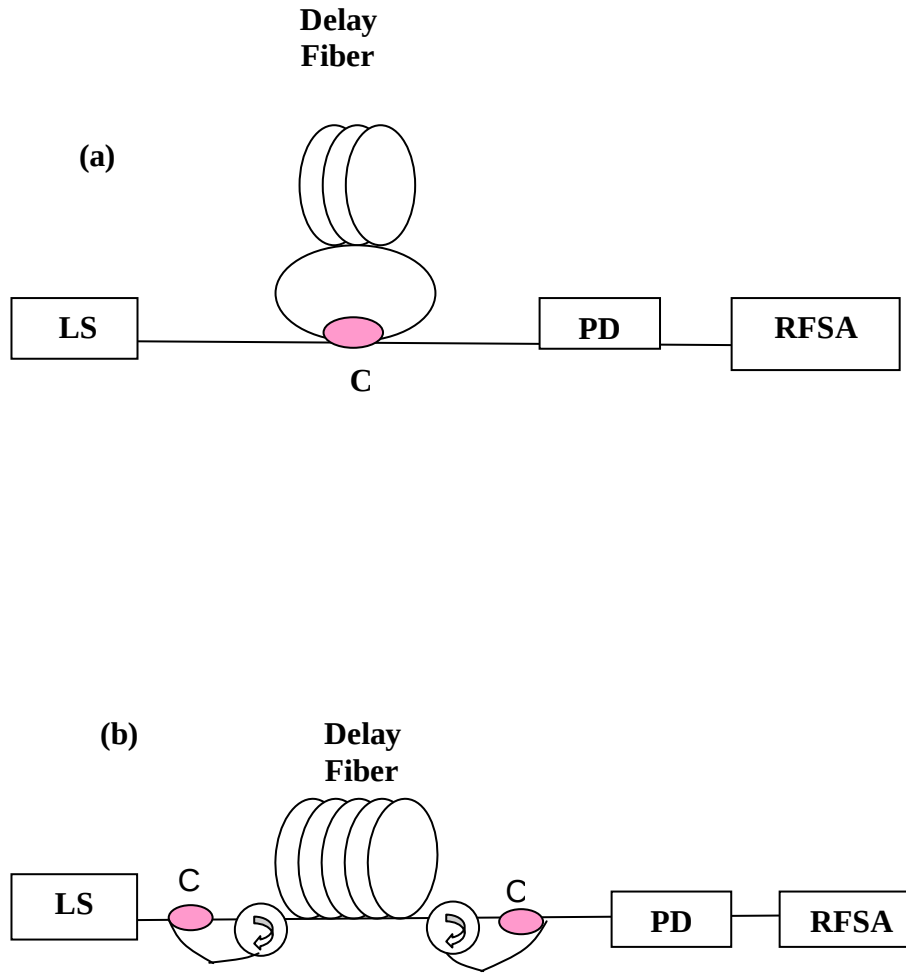

Fig. 3.31: The more effective way of the homodyne linewidth measurement of the laser source (LS) by using (a) a ring, and (b) a Fabre-Perot cavity. C and OC refer to a coupler and an optical circulator, respectively.

According to Eqs. (2.2) and (2.3), if the loop has a free spectral range (FSR) $\Delta\upsilon$ and a finesse F, the system can measure the minimum linewidth as

$$\delta\upsilon = \frac{\Delta\nu}{\mathrm{F}} \tag{3.12}$$

where $\Delta\upsilon$, the FSR can be obtained by

$$\Delta\upsilon = \frac{c}{nL} \tag{3.13}$$

in which L is the length of the fiber in the loop and n is the refractive index of the fiber in the loop. In the Fabry-Perot cavity, $2L$ must be used instead of L in Eq. (4.6) due to the distance doubling in a roundtrip. The finesse of the ring cavity can be shown to be

$$\mathrm{F} = \frac{\pi}{2}\left\{\sin^{-1}\left(\sqrt{\frac{(1-bL)^2}{4bL}}\right)\right\} \tag{3.14}$$

where L and b are obtained as

$$L = \exp\left[-(\alpha l + s)\right] \tag{3.15}$$

$$b = (1-k)^{\frac{1}{2}}(1-\delta)^{\frac{1}{2}} \tag{3.16}$$

in which α is the loss coefficient of the fiber, s the loss experienced by the electric field at the splices, k the intensity coupling ratio of the coupler, and α the excess intensity loss of the coupler. Since the resolution is proportional to the finesse, the resolution is influenced by the coupler strength, the excess loss introduced by the couplers, the fiber and the splices [94]. To measure an ultra-narrow linewidth we have to use a longer fiber and access lower finesse due to increased loss in fibers. Using a ring resonator with a free spectral range of 8.5 MHz, a linewidth 100 KHz corresponding to a finesse value of 85 was obtained.

Due to the limitation on the available light source, we have to use longer fibers to measure narrower linewidths. In order to compensate the fiber loss, an optical amplifier can be placed in the fiber loop. This method is not suitable for the ultra-narrow linewidth lasers since it needs very long fibers (>10 km). This is a drawback for homodyne linewidth measurement; when the coherence time of the laser is greater than the storage time of the resonator, there is a limitation on the resolution [98]. In addition, the amplitude noise and the phase noise are mutually overlapped in this detection; this is also known as the delayed self-homodyne detection due to using a laser source.

Another more effective method for linewidth measurement is the heterodyne method which can be formally done in two ways. Different setups are employed for different linewidth regimes. One method so called the delayed self-heterodyne measurement is attractive for narrow bandwidth laser measurements in the region of a few 100 kHz to 100 MHz. In the simplest way of this method as shown in Fig. 3.32(a), an asymmetric Mach-Zehnder is formed in such a way that one path is significantly longer than the other. Here, an acousto optical modulator (AOM) such as an acousto-optical Bragg frequency shifter is spliced in the longer path in order to shift the frequency. Then the delayed-frequency-shifted signal in the long path is combined with the signal in the short path by using a coupler. The resulting beat frequency can similarly be detected by using a fast-response photodiode and an RF spectrum analyzer [99]. By forming a ring resonator as shown in Fig 3.32 (b), the effective fiber length can also be increased in the heterodyne linewidth measurement as the homodyne counterpart.

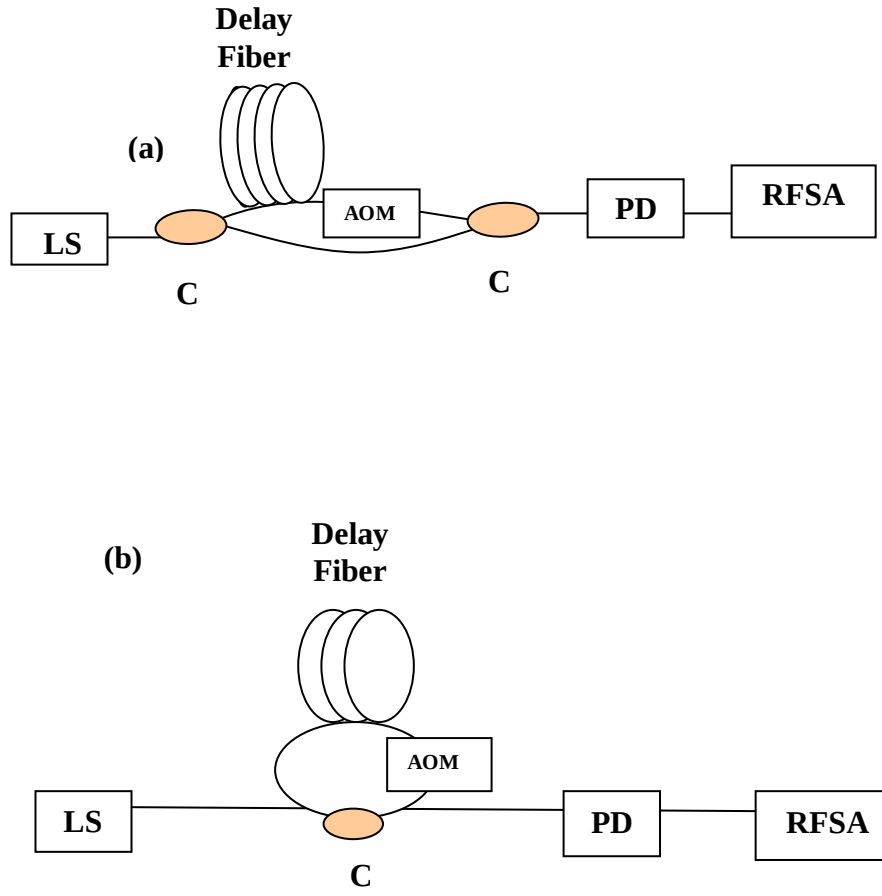

Fig. 3.32: The delayed-self heterodyne method for narrow linewidth measurement of a laser source (LS) using (a) an unbalanced Michelson interferometer and (b) a ring cavity. The acoustic optical modulator (AOM) is used to shift the frequency.

This linewidth measurement can be true if the delayed time τ_d imposed in the long path is much greater than the laser coherence time τ_c so that the two fields incident on the detector are not coherent. Thus, the validity of this method is often cited as [100]:

$$\tau_c << \tau_d \tag{3.17}$$

where the delayed time τ_d and the resolution of the interferometric method $\Delta\nu_{res}$ are related through

$$\tau_d = \frac{nL_d}{c} \cong \frac{1}{\Delta\nu_{res}} \tag{3.18}$$

in which L_d is the fiber delay length.

In other words, the coherence length must be shorter than the fiber length. Otherwise, measurements are still possible, but the interpretation of the beat signal becomes more difficult and requires intricate data post-processing routines. In fact, the analyses are generally based on a white frequency noise spectrum as the dominant contribution to the laser linewidth. For diode lasers, this is a valid assumption, as the optical linewidth stems primarily from spontaneous emission-induced refractive index changes in the semiconductor [101]. However, in the case of fiber lasers, the spontaneous emission contribution is extremely small, i.e. in the region of a few hertz and the linewidth behavior is instead overwhelmingly dominated by frequency noise and the linewidth is no longer white-noise in nature, but has a low frequency spectrum in the region of kHz [101],[102],[103]. In fact, condition in Eq. (3.17) is not sufficient for the delayed self-heterodyne interferometer to be accurate when applied to the linewidth measurement of fiber lasers since their noise behavior is not frequency-independent [104]. In addition, fiber delay lines with lengths 100 km or more are not used commonly in the delayed self heterodyne interferometry linewidth measurement due to increased propagation losses although a 11 km delay fiber length incorporating an erbium doped fiber amplifier for compensating the loss was experimentally demonstrated for determining a fiber laser characterization [102],[103]. Measurements on narrower laser linewidths around a few hertz or less are accomplished by detecting the beat signal of two identical uncorrelated lasers which will be discussed in the following section for measuring the linewidth of Brillouin fiber lasers.

3.5.2 Application of Brillouin Fiber Lasers for Laser Linewidth Measurement

Improved laser sources recently indicate narrow linewiths in the sub-megahertz range with enhanced coherence properties. Among all fiber lasers, the linewidth of Brillouin fiber lasers has been experimentally determined in various ranges from 3.84 Hz to 2.8 kHz [105], [106],[107]. The ultra-narrow linewidth measurement is a challenge because the self- homodyne or self-heterodyne techniques require long delaying fibers which is impractical for fiber lasers due to propagation losses. However, the laser linewidth measurement can also be done by evaluating the beat signal resulting from the interference of the laser with another uncorrelated laser as has been done in [105], [106],[107]. This method requires another laser either with a comparable well-known spectrum or with an extremely narrow and ignorable linewidth. In this thesis, by using the later method, a Brillouin fiber laser is applied to measure the linewidth of an uncorrelated tunable laser source (TLS) which has two organized wide and narrow linewidths. The linewidth of the Brillouin Stokes $\Delta\upsilon_{\mathrm{BS}}$ is proportional to the Brillouin pump linewidth $\Delta\upsilon_{\mathrm{p}}$ as shown theoretically [108]:

$$\Delta\upsilon_{\mathrm{BS}} = \Delta\upsilon_{\mathrm{p}}\left(1-\frac{\pi\ l\Delta\upsilon_{B}}{\mathrm{v}\ \mathrm{Ln}(R)}\right) \tag{3.19}$$

where $\Delta\upsilon_{B}$ is the Brillouin gain bandwidth , l is the fiber length, v the velocity of light in the fiber and R is the coupling ratio. Therefore, a narrow linewidth TLS is used to generate a narrow BFL linewidth. By using the narrow linewidth BFL instead of the CW laser in the heterodyne configuration as shown in Fig. 3.29, the

linewidth of the wide and narrow uncorrelated TLS can be measured. Here, the TLS and the narrow BFL are used to replace the signal and CW in Fig. 3.29.

The experimental setup for generating a BFL is shown in Fig. 3.33 with a coupler and a long single-mode fiber (SMF) acting as a traditional ring resonator. The BFL is pumped by an external cavity tunable laser source (TLS) which is amplified by an erbium-doped fiber amplifier. The maximum power of the amplified Brillouin pump (BP) is approximately 14.3 dBm. The BP is injected into the resonator from port 1 through port 2 of the optical circulator in an anti-clockwise direction. The generated backward-propagating SBS oscillates inside the resonator in a clockwise direction to generate the backward BFL, which is coupled out via a 3-dB coupler. From port 2, the BFL is then routed into an optical spectrum analyzer (OSA) through port 3 by the optical circulator. The SMF used in the experiment is 25 km in length and has a cut-off wavelength of 1161 nm with a zero dispersion wavelength of 1315 nm and a mode field diameter of 9.36 μm. The output laser is characterized using an OSA with a resolution of 0.015 nm while the linewidth of the laser is measured using a radio frequency spectrum analyzer (RFSA) and the heterodyne beat technique [109].

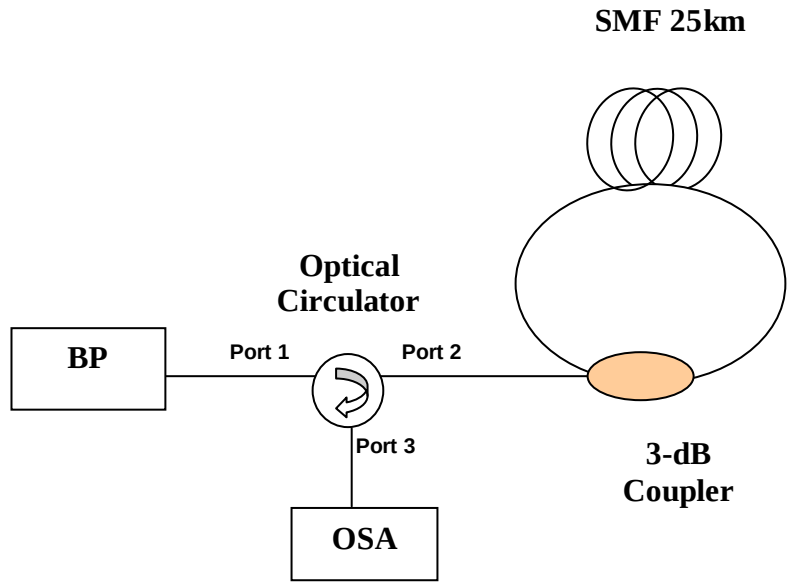

Fig. 3.33: The Experimental set up for generating a Brillouin fiber laser in using a Brillouin pump (BP) which is a tunable laser source (TLS) amplified by an EDFA in the narrow TLS linewidth setting.

Fig. 3.34 (a) and (b) compares the BFL output spectrum at different BP linewidth settings with BP powers of 4.5 dBm and 14.3 dBm respectively. Both figures show three simultaneous lines: anti-Stokes at around 1549.9 nm, BP reflections at 1550 nm, and BFLs at around 1550.1 nm so that the Brillouin shift is about 0.086 nm. The anti-Stokes signal is observed at a shorter wavelength due to four-wave mixing between the BP and the Stokes line. Although the anti-Stokes power is almost unchanged, the powers of the BP reflections and BFL lines increase as the BP power increases due to Brillouin-induced crosstalk between the lines [110]. With the BP wide linewidth setting, the BFL power as shown in Fig. 3.34 (b) is relatively lower as compared to the BP narrow linewidth setting in Fig. 3.34 (a).

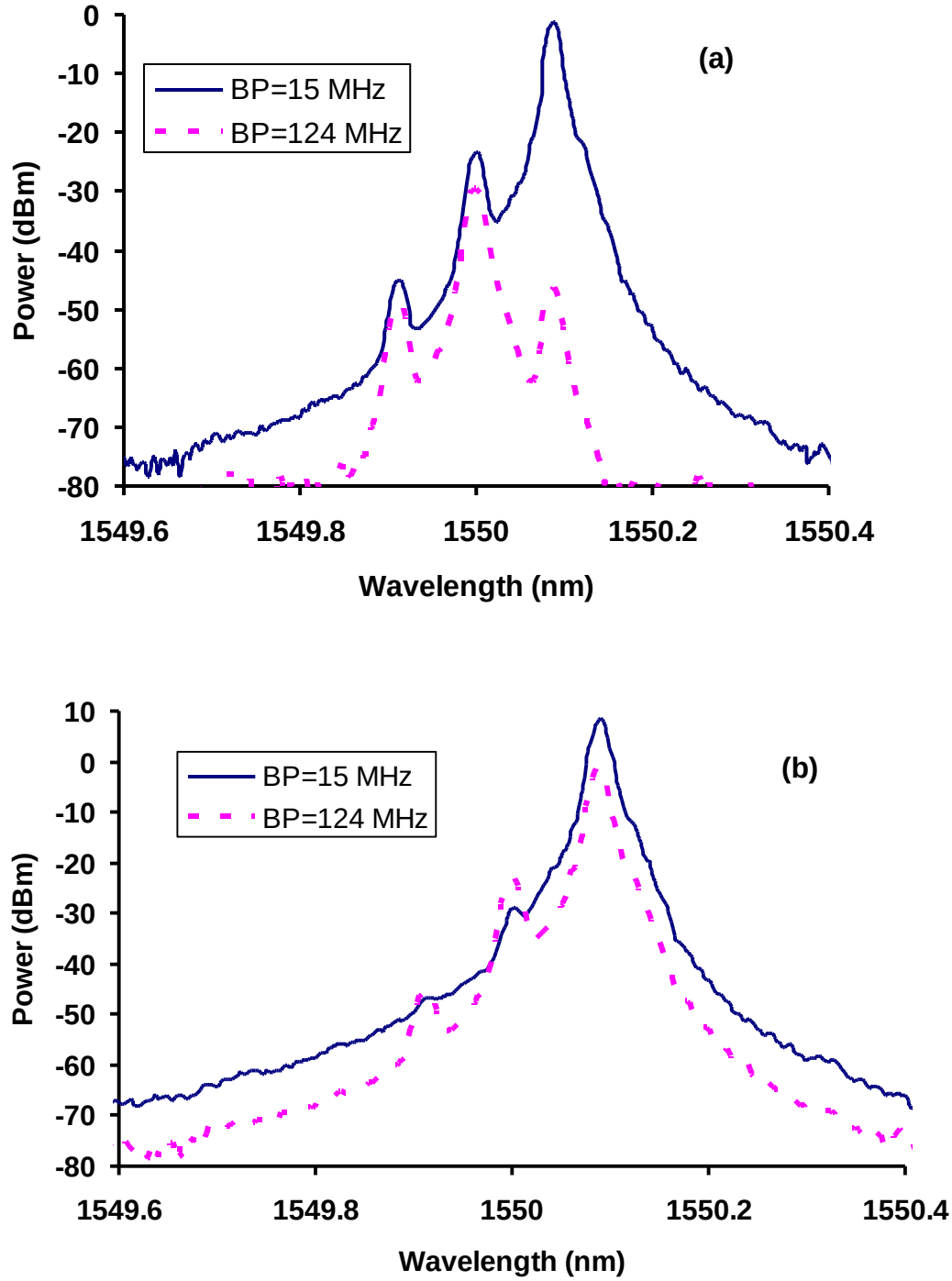

Fig. 3.34: The BFL output spectrum for different narrow and wide BP linewidths (15 MHz and 124 MHz) at BP power (a) 4.5 dBm and (b) 14.3 dBm [111].

For measuring the TLS linewidth, the power of the Brillouin pump (BP) and the BFL are set to be equal at around -5 dBm whereas their frequencies are slightly different but around 1550 nm to generate the beat frequency. The (2×2) 3-dB coupler is used to combine the both BP and BFL waves as shown in Fig 3.35. The heterodyne beat spectrum between the TLS and the narrow independent BFL is shown in Fig. 3.36 for (a) a wide and (b) a narrow TLS linewidth setting, respectively. The measured TLS linewidths are obtained at 124 MHz and 15 MHz for wide and narrow TLS linewidth setting, respectively.

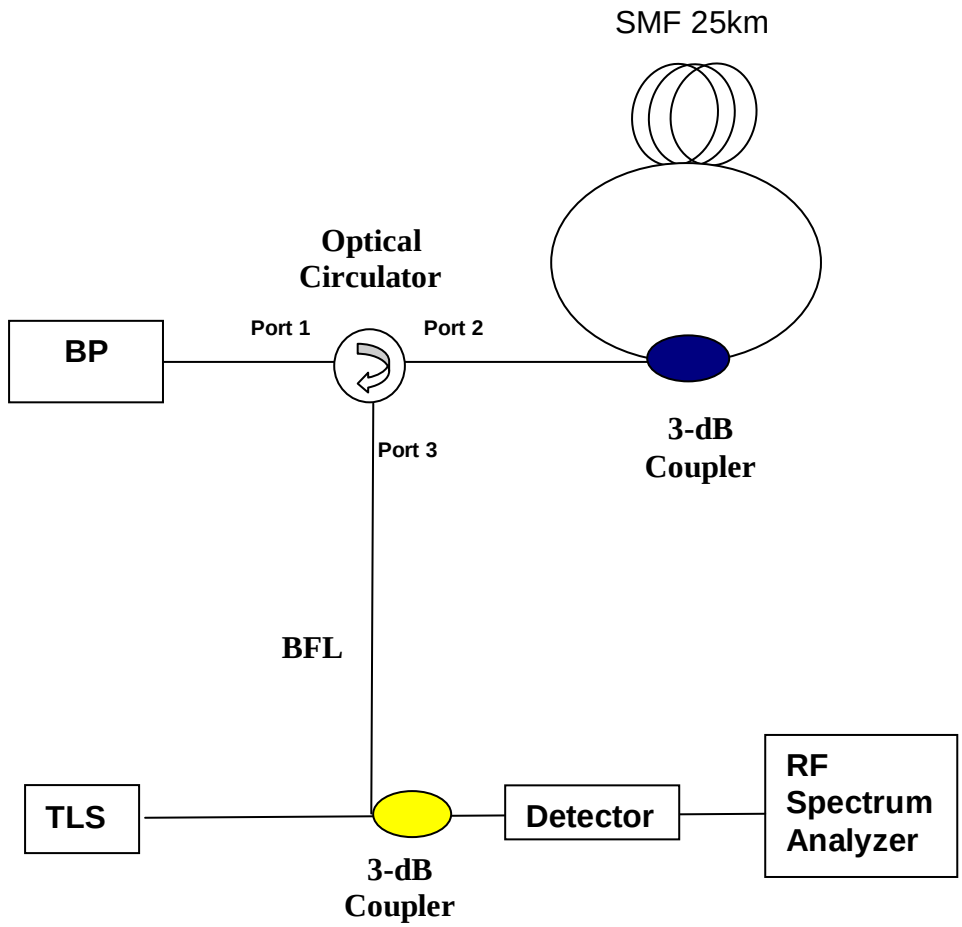

Fig. 3.35: The experimental setup for heterodyne linewidth measurement of a tunable laser source (TLS) by using a Brillouin fiber laser (BFL) in the heterodyne technique.

(a)

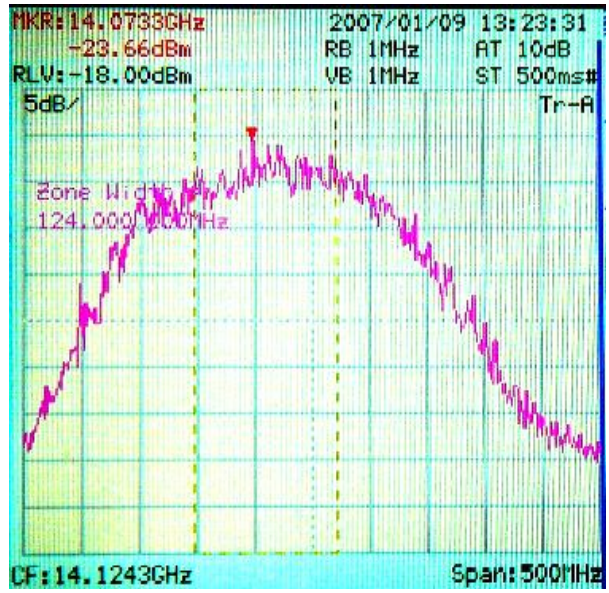

(b)

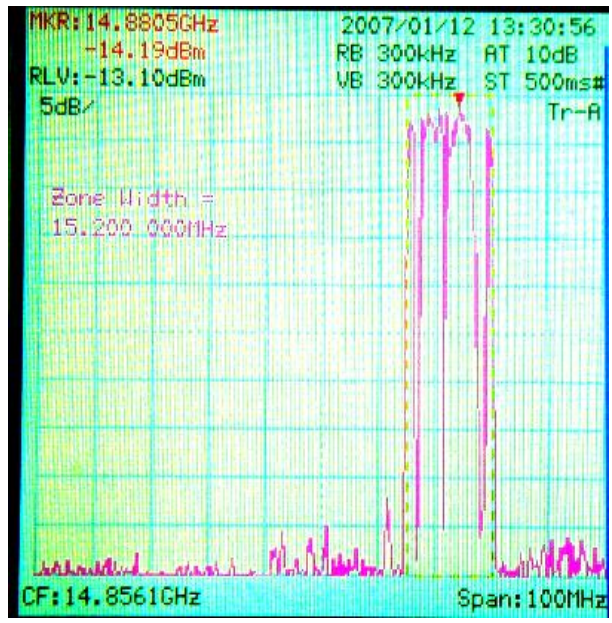

Fig. 3.36: Heterodyne beat spectra between the narrow BFL and the TLS at (a) a wide and (b) a narrow linewidth setting which are measured 124 MHz and 15 MHz, respectively [111].

In order to obtain BFL linewidth, two similar but independent BFLs are used to generate the heterodyne beat spectrum using an experimental setup as shown in Fig 3.37. A (1×2) 3-dB coupler is used to combine both BFL spectra. As before, the two BFLs are the same in power but have slightly different frequencies to generate the beat frequency in the detection range of the RF spectrum analyzer shown in Fig. 3.37.

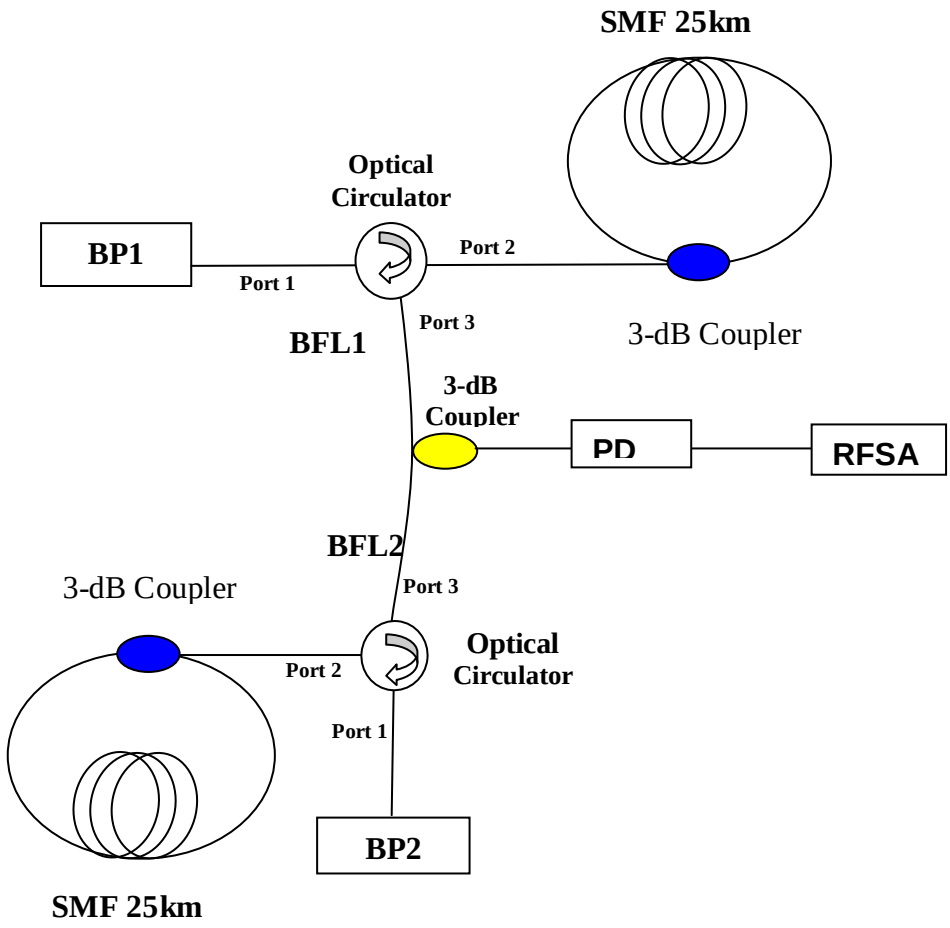

Fig. 3.37: The experimental setup for measuring the BFL linewidth by using two independent BFLs in the heterodyne technique.

Fig. 3.38 shows the measured beat frequency spectrum at the different BP linewidth setting 124 MHz and 15 MHz, respectively. As shown in Fig. 3.38 (a) and (b), the BFL linewidth is obtained at about 8 Hz and 24 Hz using the BP linewidth 15 MHz and 124 MHz, respectively. The smaller BP linewidth generates the smaller BFL linewidth as expected from the theory [108].

(a)

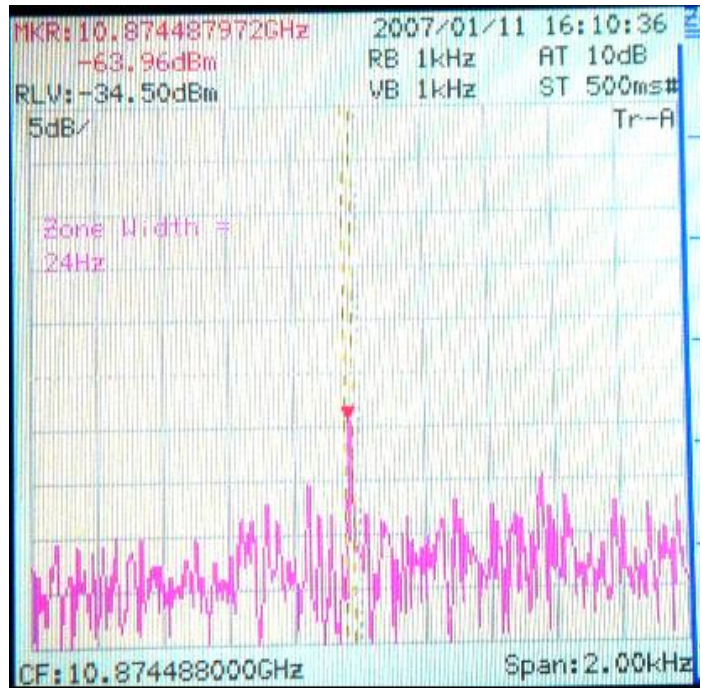

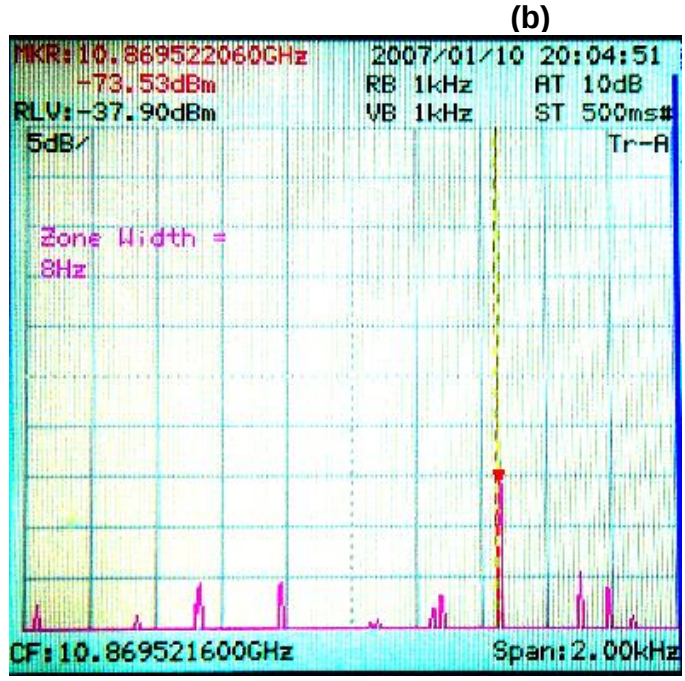

Fig. 3.38: The heterodyne beat spectra between the two similar independent BFLs generated by the TLS linewidths (a) 124 MHz and (b) 15 MHz [111].

3.6 Summary

New BFLs with higher output power in ring and linear cavities are proposed. By using the same components and the same BP power 5 dBm**,** the proposed BFRL configuration shows an output BFL peak power of -0.5 dBm, which is 5.7 dB higher compared to the conventional configuration [59]. The proposed linear cavity BFL configuration has been demonstrated by incorporating a 3-dB coupler, a 95/5 coupler, two optical circulators, and a 25 km SMF that allows very high conversation efficiency energy from BP to BFL compared with the previous works [77], [78]. Stable BFL operation is obtained at an up-shifted wavelength of 0.086 nm from the BP wavelength with the BFL peak power at -1

dBm, which is 12.3 dB higher than the conventional BFL peak power by using the same BP peak power 13 dBm. The BFL peak power is about 0.5 dB higher than the BP transmitted peak power [61]. As an important application of BFL, the generation of MBFLs is also demonstrated by using ring and linear BFL cavities. More than 14 and 9 BFL lines are obtained in the ring and linear cavities by using BP power 14 dBm and 11.7 dBm, respectively. In the ring cavity, the both wavelength spacing 0.08 nm (~10 GHz) and 0.16 nm (~20 GHz) are produced with the bi-directional multi-wavelength generation whereas in the linear cavity only the wavelength spacing 0.08 nm (~10 GHz) is obtained. These MBFLs are suitable for some applications such as WDM and DWDM optical network systems and optical sensors. In the generated MBFLs especially in the ring cavity, the peak powers of lines are not comparable to each other and the number of lines is also depended on using higher BP power. This cause to use a compact Bi-EDFA in the BFL cavities to increase number of lines and to generate a multiwavelength Brillouin Erbium laser comb with more flatness in the line peak power as will be discussed in the next chapter. Nevertheless, MBFLs have the benefit that they can be generated at any wavelength by using a simple cavity configuration as soon as the BP power is available. In addition, the number of lines in the generated MBFLs is comparable to that one in some reported MBEFLs even though we use only a laser source (BP).

In addition, the Brillouin fiber laser has experimentally demonstrated its ability for laser linewidth measurements of values less than a few 100 MHz to a few Hz regions due to its extra narrow and nearly negligible linewidth. The major advantage of this linewidth measurement system seems to be widely independent

of the source wavelength by generating the uncorrelated BFL at a fixed frequency around the frequency of the source which is the TLS or other independent BFLs in this work. The other advantage of this method is its simplicity which only requires widely available standard optical components. Although the BFL linewidth has been reported to be 3.84 Hz with the BP linewidth at 100 kHz [107], here, BFL linewidth is measured at 8 Hz and 24 Hz by using the BP linewidth measured about 15 MHz and 124 MHz, respectively [111]. The demonstrated BP linewidth is acceptable according to our provided instrument information and the determined BFL linewidth reported by the others [106], [107], [108].

References

[1] R. G. Smith, "*Optical power handling capacity of low loss optical fibers as determined by stimulated Raman and Brillouin scattering*", App. Opt., Vol. 11, 1972, pp. 2489-2494.

[2] N. Shibata, R. G. Waarts, and R. P. Braun, "*Brillouin-gain spectra for single-mode fibers having pure-silica, GeO_2-doped, and P_2O_5-doped cores*," Opt. Lett., Vol. 12, 1987, pp. 269-271.

[3] Y. Azuma, N. Shibata, T. Horiguchi, and M. Tateda, "*Wavelength dependence of Brillouin-gain spectra for single-mode optical fibers*," Electron. Lett., Vol. 24, 1988, pp. 250-252.

[4] N. Shibata, K. Okamoto, and Y. Azuma, "*Longitudinal acoustic modes and Brillouin-gain spectra for GeO2-doped-core single-mode fibers*," J. Opt. Soc. Am. B, Vol. 6, 1989, pp. 1167-1174.

[5] Y. Nobuyuki and T. Imai, "*Stimulated Brillouin scattering suppression by means of applying strain distribution to fiber with cabling*", J. Lightwave Technol., Vol. 11, 1993, pp. 1519-1522.

[6] M. Nicklès, Luc Thévenaz, and Philippe A. Robert, "*Simple distributed fiber sensor based on Brillouin gain spectrum analysis*", Opt. Lett., Vol. 21, 1996, pp. 758-761.

[7] L. Thevenaz, Luc Th´evenaz, and Philippe A. Robert, "*High-accuracy Brillouin gain spectrum measurements of single-mode fibers*", Proceedings of the Symposium on Optical Fiber Measurements, NIST, Boulder Co., 1994, pp. 211-214.

[8] R. W. Tkach, A. R. Chraplyvy, and R. M. Derosier, "*Spontaneous Brillouin scattering for single-mode optical-fibre characterisation*", Electron. Lett., Vol. 22, 1986, pp. 1011-1013.

[9] R. St. Pierre, D. W. Mordaut, and H. Injeyan, J. G. Bery, R. C. Hilyard, M. E. Weber, M. G. Wickham, G. M. Harpole, R. Senn, "*Diode array pumped kilowatt laser*," J. Sel. Topics Quant. Electron., QE-3, 1997, pp. 53-58.

[10] E. A. Kuzin, M. P. Petrov, B. E. Davydenko, "*Phase conjugation in an optical fibre*," Opt. Quant. Electron., QE-17, 1985, pp. 393-397.

[11] H. J. Eichler, J. Kunde, B. Liu, *"Quartz fibre phase conjugators with high fidelity and reflectivity*," Opt. Commun., Vol. 139, 1997, pp. 327-334.

[12] R. G. Harrison, V. I. Kovalev, W. Lu, D. Yu, "*SBS self-phase conjugation of CW Nd:YAG laser radiation in an optical fibre*," Opt. Commun., Vol. 163, 1999, pp. 208-211.

[13] D. C. Jones, M. S. Mangir, and D. A. Rockwell, "*A stimulated Brillouin scattering phase-conjugate mirror having a peak-power threshold < 100 W* ," Opt. Commun., Vol. 123, 1995, pp. 175-181.

[14] Y. Aoki, K. Tajima, and I. Mito, "*Input Power Limits of Single-Mode Optical Fibers due to Stimulated Brillouin Scattering in Optical Communication Systems*", J. Lightwave Technol., Vol. 6, 1988, pp. 710-719.

[15] G. P. Agrawal, "*Nonlinear Fiber Optics*," Academic Press, London, p. 333, 2007.

[16] A. Gaeta A. and R. W. Boyd, "*Stochastic Dynamics of Stimulated Brillouin Scattering in an Optical Fiber*", Phys. Rev. A, Vol. 44, 1991, pp. 3205-3209.

[17] G. P. Agrawal, "*Nonlinear Fiber Optics*," 3rd ed., Academic Press, New York, chap. 9, 2001.

[18] A. B. Ruffin, M. –J. Li, X. Chen, A. Kobyakov, F. Annunziata, "*Brillouin gain analysis for fibers with different refractive induces*," Opt. Lett., Vol. 30, 2005, pp. 3123-3125.

[19] M. Nikles, L. Thevenaz, P. A. Robert, "*Brillouin gain spectrum characterization in single-mode optical fibers*," J. Lightwave Technol., Vol. 15, 1997, pp. 1842-1851.

[20] K. Shiraki et al., "*SBS threshold of a fiber with a Brillouin frequency shift distribution*," J. Lightwave Technol., Vol.14, 1996, pp. 55-57.

[21] A. R. Chraplyvy, "*Limitation on lightwave communications imposed by optical fiber nonlinearities*," J. Lightwave Technol., Vol. 8, 1990, pp. 1548-1557.

[22] P. Bayvel and P. M. Radmore, "*Solutions of the SBS equations in single mode optical fibers and implications for fiber transmission system*," Electron. Lett., Vol. 26, 1990, pp. 434-436.

[23] R. D. Esman, K. J. Williams, "*Brillouin scattering: beyond threshold*," IEEE Proceeding of the Optical Fiber Communications Conference, 1996, pp. 227-228.

[24] W. B. Gardner, "*Appendix on Nonlinearities for G. 650*", ITU Document COM 15-273-E, ITU, 1996.

[25] T. C. E. Jones, "*The validity of single mode optical fiber transfer standard for the calibration of fibers for high power uses*," National Physical Laboratory (NPL) Report COEM 10, 1998.

[26] T. Shimizu, K. Nakajima, K. Shiraki, K. Ieda, I. Sankawa, "*Evaluation methods and requirments for the stimulated Brillouin scattering thresholdin a single-mode fiber*," Opt. Fiber Technol., Vol. 14, 2008, pp. 10-15.

[27] D. Cotter, "*Observation of stimulated Brillouin scattering in low-loss silica fiber at 1.3-μm*,"Electron. Lett., Vol.18, 1982, pp. 495-496.

[28] X. P. Mao, R. W. Tkach, A. R. Chraplyvy, R. M. Jopson, and R. M. Derosier, "*Stimulated Brillouin threshold dependence on fiber type and uniformity*," IEEE Proceeding of the Optical Fiber Communications Conference, Tech. Dig. OFC/IOOC'91, San Diego USA, TuK4, 1991, p. 41.

[29] X. P. Mao, R. W. Tkach, A. R. Chraplyvy, R. M. Jopson, and R. M. Derosier, "*Stimulated Brillouin threshold dependence on fiber type and uniformity*," Photon. Technol. Lett., Vol. 4, 1992, pp. 66-68.

[30] S. Norcia, S. Tonda-Goldstein, D. Dolfi, and J. –P. Huignard, "*Efficient single-mode Brillouin fiber laser for low-noise optical carrier reduction of microwave signals*," Opt. Lett., Vol. 28, 2003, pp. 1888-1890.

[31] F. Zarinetchi, S.P. Smith, and S. Ezekiel, "*Stimulated Brillouin fiber optic laser gyroscope*," Opt. Lett., Vol.16, 1991, pp. 229-231.

[32] H. Yoshida, M. Nakatsuka, H. Fujita, T. Sasaki, and K. Yoshida, "*High-engery operation of a stimulated Brillouin scattering mirror in an L-Arginine phosphate monohydrate crystal*," Appl. Opt., Vol. 36, 1997, pp. 7738- 7787.

[33] J. H. Lee, T. Tanemura, T. Nagashima, T. Hasegawa, S. Ohara, N. Sugimoto, and K. Kikuchi, "*Use of 1-m* Bi_2O_3 *nonlinear fiber for 160-Gbit/s optical-time division demultiplexing based on polarization rotation and wavelength shift induced by cross-phase modulation*," Opt. Lett., Vol. 30, 2005, pp. 1267-1269.

[34] M. Asobe, T. Kanamori, and K. I. Kubodera, "*Applications of highly nonlinear chalcogenide glass fiber in ultrafast all-optical switches*," J. Quantum Electron., Vol. 29, 1993, pp. 2325-2333.

[35] G. Ghosh, "*Sellmeier coefficients and chromatic dispersions for some tellurite glasses*," J. Am. Ceramic. Soc., Vol. 78, 1995, pp. 2828-2830.

[36] K. S. Abedin, "*Observation of strong stimulated Brillouin scattering in single-mode* As_2Se_3 *chalcogenide fiber*," Opt. Express, Vol. 13, 2005, pp. 10266-10271.

[37] G. K. N. Wong, M. J. Damzen, "*Investigations of Optical Feedback Used to Enhance Stimulated Scattering*," J. Quant. Electron. QE-26, 1990, pp. 139-148.

[38] M. Dämmig, G. Zinner, F. Mitschke, H. Welling, "*Stimulated Brillouin scattering in fibers with and without external feedback*," Phys. Rev. A, Vol. 48, 1993, pp. 3301-3309.

[39] J. Botineau, C. Leycuras, C. Montes, E. Picholle,"*Stabilization of a stimulated Brillouin fiber ring laser by strong pump modulation*," J. Opt. Soc. Am. B, Vol. 6, 1989, pp. 300-312.

[40] C. Montes, D. Bahloul, I. Bongrand, J. Botineau, G. Cheval, A. Mahmoud, E. Picholle, A. Piccozi, "*Self-pulsing and dynamic bistability in cw-pumped Brillouin fiber ring lasers*," J. Opt. Soc. Am. B, Vol. 16, 1999, pp. 932-951.

[41] R. W. Boyd, K. Rzazewski, P. Narum, "*Noise Initiation of Stimulated Brillouin Scattering*, "Phys. Rev. A, Vol. 42, 1990, pp. 5514-5521.

[42] I. Bar-Joseph, A. A. Friesem, E. Lichtman, R. G. Waarts, "*Steady and relaxation oscillations of stimulated Brillouin scattering in single-mode optical fibers* ," J. Opt. Soc. Am. B, Vol. 2, 1985, pp. 1606-1611.

[43] A. L. Gaeta, R. W. Boyd, "*Stimulated Brillouin scattering in the presence of feedback*," Int. J. Nonlinear Opt. Phys., Vol. 1, 1992, pp. 581-594.

[44] C. Montes, A. Mamhoud, E. Picholle, "*Bifurcation in a cw-pumped Brillouin fiber-ring laser: Coherent soliton morphogenesis*," Phys. Rev. A, Vol. 49, 1994, pp. 1344-1349.

[45] S. Randoux, V. Lecoeuche, B. Segard, J. Zemmouri, "*Dynamical analysis of Brillouin fiber lasers: An experimental approach*," Phys. Rev. A, Vol. 51, 1995, R4345 -R4348.

[46] D. Yu, W. Lu, R. G. Harrison, "*Observation and characterization of deterministic chaos in stimulated Brillouin scattering with weak feedback*,"Phys. Rev. A, Vol. 49, 1994, R24-R27.

[47] E. Picholle, C. Montes, C. Leycuras, O. Legrand, J. Botineau, "*Observation of dissipative superluminous solitons in a Brillouin fiber ring laser*," Phys. Rev. Lett., Vol. 66, 1991, pp. 1454-1457.

[48] C. Montes, A. Picozzi, D. Bahloul, "*Dissipative three-wave structures in stimulated backscattering. II. Superluminous and subluminous solitons*," Phys. Rev. E, Vol. 55, 1997, pp. 1092-1105.

[49] S. P. Smith, F. Zarinetchi, S. E. Ezekiel, "*Narrow-linewidth stimulated Brillouin fiber laser and applications*," Opt. Lett., Vol. 16, 1991, pp. 393-395.

[50] M. Nikles, L. Thevenaz, Ph. A. Robert, "*Brillouin gain spectrum characterization in single-mode optical fibers*," J. Lightwave Technol. Vol. 15, 1997, pp. 1812- 1851.

[51] S. Randoux, V. Lecoeuche, B. Segard, and J. Zemmouri, "*Dynamical analysis of Brillouin fiber lasers: An experimental approach*," Phys. Rev. A, Vol. 51, 1995, pp. 4345-4348.

[52] O. Svelto, "*Principle of Lasers*," 3 rd Ed. New York, Plenum Press, 1989.

[53] M. Dämming, G. Zinner, F. Mitschke, and H. Welling, "*Stimulated Brillouin scattering in fibers with and without external feedback*," Phys. Rev. A, Vol. 48, 1993, pp. 3301-3308.

[54] R. G. Harrison, P. M. Ripley, and W. Lu, "*Observation and characterization of deterministic chaos in stimulated Brillouin scattering with weak feedback*," Phys. Rev. A, Vol. 49, 1994, pp. R24-R27.

[55] E. Picholle, C. Montes, C. Leycuras, O. Legrand, and J. Botineau, "*Observation of dissipative superluminous solitons in a Brillouin fiber ring laser*," Phys. Rev. Lett., Vol. 66, 1991, pp. 1454-1457.

[56] J. Botineau, C. Leycuras, C. Montes, and E. Picholle, "*Stabilization of a stimulated Brillouin fiber ring laser by strong pump modulation*," J. Opt. Soc. Am. B, 1989, pp. 300-312.

[57] I. Bar-Joseph, A. A. Friesem, E. Lichtman, and R. G. Waarts, "*Steady and relaxation oscillations of stimulated Brillouin scattering in single-mode optical fibers*," J. Opt. Soc. Am. B, Vol. 2, 1985, pp. 1606-1611.

[58] C. Montes, A. Mamhoud, and E. Picholle, "*Bifurcation in a cw-pumped Brillouin fiber-ring laser: Coherent soliton morphogenesis*," Phys. Rev. A, Vol. 49, 1994, pp. 1344-1349.

[59] M. R. Shirazi, S. W. Harun, K. Thambiratnam, M. Biglary, H. Ahmad, "*New Brillouin fiber laser configuration with high output power*," Microwave and Optical Technology Letters, Vol. 49, 2007, pp.2656-2658.

[60] H. Ahmad, M. R. Shirazi, M. Biglary, S. W. Harun, "*Linear cavity Brillouin fiber laser using a fiber Bragg grating*," Microwave and Optical Technology Letters, Vol. 50, 2008, pp. 265-266.

[61] M. R. Shirazi, S. W. Harun, M. Biglary, and H. Ahmad, "*Linear cavity Brillouin fiber laser with improved characteristics*," Opt. Lett., Vol. 33, 2008, pp. 770-772.

[62] L. F. Stokes, M. Chodorow, and H. J. Shaw, "*All-fiber stimulated ring laser with submilliwatt pump threshold*," Opt. Lett., Vol. 7, 1982, pp. 509-511.

[63] N. Nikles, L. Thevenaz, and P. A. Robert, "*Brillouin gain spectrum characterization in single-mode optical fibers*," J, Lightwave Technol., Vol. 15, 1997, pp. 1842-1851.

[64] S. P. Smith, F. Zarinetchi, and S. Ezekiel, "*Narrow-linewidth stimulated Brillouin fiber laserand applications*," Opt. Lett., Vol. 16, 1991, pp. 393-395.

[65] C. Montes, D. Bahloul, I. Bongrand, J. Botineau, G. Cheval, A. Mamhoud, E. Picholle, and A. Picozzi, "*Self-pulsing and dynamic bistability in cw-pumped Brillouin fiber ring lasers*,"J. Opt. Soc. Am. B, Vol.16, 1999, pp. 932-951.

[66] C. Montes, A. Mamhoud, E. Picholle, "*Bifurcation in a cw-pumped Brillouin fiber-ring laser: Coherent soliton morphogenesis*," Phys. Rev. A., Vol. 49, 1994, pp. 1344- 1349.

[67] S. Randoux, V. Lecoeuche, B. Segard and J. Zemmouri, "*Dynamical analysis of Brillouin fiber lasers: An experimental approach*," Phys. Rev. A, Vol. 51, 1995, pp. R4345-4348.

[68] S. Randoux, V. Lecoeuche, B. Segard and J. Zemmouri, "*Dynamical behavior of a Brillouin fiber ring laser emitting two Stokes components* ," Phys. Rev. A, Vol. 52, 1995, pp. 2327-2334.

[69] V. Lecoeuche, B. Segard, and J. Zemmouri, "*Modes of destabilization of Brillouin fiber ring lasers*,"Opt. Commun. Vol. 134, 1997, pp. 547- 558.

[70] E. Picholle and A. Piccozi,"*Guided-acoustic-wave resonances in the dynamics of a stimulated Brillouin fiber ring laser*," Opt. Commun., Vol. 135, 1997, pp. 327- 330.

[71] P. Bayvel, I. P. Giles and P. M. Radmore, "*Transient and steady-state characteristics of a Brillouin amplifier based on an all-fiber single-mode ring resonator,"* Opt. Quantum Electron., Vol. 21, 1989, pp. S113-S128.

[72] J. Bontineau, C. Leycuras, C. Montes, "*CW-pumped polarization-maintaining Brillouin fiber ring laser: I. Self-structuration of Brillouin Solitons*," Opt. Commun., Vol. 257, 2006, pp. 319-333, and "*CW-pumped polarization-maintaining Brillouin fiber ring laser: II. Active mode-locking by phase modulation*," Opt. Commun., Vol. 257, 2006, pp. 311-318.

[73] L. F. Stokes, M. Chodorow, and H. J. Shaw, "*All-fiber stimulated Brillouin ring laser with submilliwatt pump threshold*," Opt. Lett., Vol. 7, 1982, pp. 509-511.

[74] R. Kadiwar and I. P. Giles, "*Effects of stimulated Brillouin scattering on the performance of polarization-maintaining all-fiber ring resonators*," Opt. Lett., Vol. 14, 1989, pp. 332-334.

[75] R. V. Johnson, and J. H. Marburger, "*Relaxation Oscillations in Stimulated Ruman and Brillouin Scattering*," Phys. Rev. A, Vol. 4, 1971, pp. 1175-1182.

[76] I. Bar-Joseph, A. A. Friesem, E. Lichtman, and R. G. Waarts, "*Steady and relaxation oscillations of stimulated Brillouin scattering in single-mode optical fibers*," J. Opt. Soc. Am. B, Vol. 2, 1985, pp. 1606-1611.

[77] V. Lecoeuche, P. Niay, M. Douay, P. Bernage, S. Randoux and J. Zemmouri, " *Bragg grating based Brillouin fiber laser*," Opt. Commun., Vol. 177, 2000, pp. 303-306.

[78] Y. Shen, X. Zhang, and K. Chen, "*All-Optical Generation of Microwave and Millimeter wave using a two-frequency Bragg grating-based Brillouin fiber laser*," J. Lightwave Technol., Vol. 23, 2005, pp. 1860- 1865.

[79] K. O. Hill, B. S. Kawasaki, and D. C. Johnson, "*CW Brillouin laser*," Appl. Phys. Lett., Vol. 28, 1976, pp. 608-609.

[80] K. Nosu, H. Toba, K. Inoue, and K. Oda, "*100 channel optical FDM technology and its applications to optical FDM channel-based networks*," J. Lightwave Technol., Vol. 11, 1993, pp. 764-776.

[81] K. Ogusu, "*Analysis of steady-state cascaded stimulated Brillouin scattering in a fiber Fabry-Perot resonator*," Photon. Technol. Lett., Vol. 14, 2002, pp. 947-949.

[82] S. Randoux, V. Lecoeuche, B. Segard, and J. Zemmouri, " *Dynamical behaviour of a Brillouin fiber ring laser emitting two Stokes components*," Phys. Rev. A, Vol. 52, 1995, pp. 2327-2334.

[83] K. Ogusu and A. Sakai, "*Generation and dynamics of cascaded stimulated Brillouin scattering in a high finesse fiber Fabry-Perot resonator*," Jpn. J. Appl. Phys., Vol. 41, 2002, pp. 609-616.

[84] L. Zhan, J. H. Ji, J. Xia, S. Y. Luo, and Y. X. Xia, "*160-line multiwavelength generation of linear cavity self-seeded Brillouin-Erbium fiber laser*," Opt. Express, Vol. 14, 2006, pp. 10233-10283.

[85] S. Shahi, S. W. Harun, N. S. Shahabuddin, M. R. Shirazi, and H. Ahmad, "*Multiwavelength generation using a bismuth-based EDF and Brillouin effect in a linear cavity configuration*," Opt. Laser Technol., Vol. 41, 2008, pp.198-201.

[86] M R Shirazi, M Biglary, S W Harun, K Thambiratnam and H Ahmad, "*Bidirectional multiwavelength Brillouin fiber laser generation in a ring cavity*," J. Opt. A: Pure Appl. Opt., Vol. 10, 2008, 055101, 3pp.

[87] M. Shwartz, "*Information Transmission, Modulation, and Noise*," 4th ed., Mc Graw-Hill, New York, 1990.

[88] R. E. Ziemer, "*Principles of Communications; Systems*," Modulation and Noise, Wiley, New York, 1994.

[89] L. W. Couch II, "*Digital and Analog Communication Systems*," 5th ed., Prentice Hall, Upper Saddle River, NJ, 1995.

[90] M. S. Roden, "*Analog and Digital Communication Systems*," Prentice Hall, Upper Saddle River, NJ, 1995.

[91] B. P. Lathi, "*Modern Digital and Analog Communication Systems*," Oxford University Press, New York, 1995.

[92] W. R. Bennet, "*Communication Systems and Techniques*," IEEE Press, Piscataway, NJ, 1995.

[93] R. Louden in: "*The quantum Theory of Light*," Oxford University Press, Oxford, 1991.

[94] C. Yue, J. D. Peng, Y. B. Liao, B. K. Zhou, "*Fiber ring lasers with finesse 1260*," Electron Lett., Vol. 24, 1988, pp. 622-623.

[95] H. Okamura, K. Iwatsuki, "*Er-doped fibre ring resonator applied to optical spectrum analyser with less than 100 kHz resolution*," Electron. Lett., Vol. 27, 1991, pp.1047-1049.

[96] A. Yariv, "*Optical Electronics in Modern Communication*," Oxford University Press, New York, chapter 10.7, pp. 393-401, 1997.

[97] T. Ikegami, S. Sudo, Y. Sakai, "*Frequency stabilization of semiconductor laser diodes*," Artech House Inc., Boston, chapters 2-3, pp. 18-56, 1995.

[98] K. Hsu, C. M. Miller, J. W. Miller "*Speed-of- light effect in high-resolution long-cavity fiber Fabre-Perot scanning interferometers*," Opt. Lett., Vol.18, 1993, pp. 235-237.

[99] T. Okoshi, A. Kikuchi, A. Nakayama, "*Novel method for high resolution measurment of laser output spectrum*," Electron. Lett., Vol. 16, 1980, pp. 630-631.

[100] L. R. Richter, H. I. Mandelburg, M. S. Kruger and P. A. McGrath, "*Linewidth determination from self-heterodyne measurments with subcoherence delay times*," J. Quantum Electron., QE-22, 1986, pp. 2070-2074.

[101] G. A. Ball, C. G. Hull-Allen and J. Livas, "*Frequency noise of a Bragg grating fiber laser*," Electron. Lett., Vol. 30, 1994, pp. 1229-1230.

[102] J. W. Dawson, N. Park, and K. J. Vahala, "*An improved delay self-heterodyne interferometer for linewidth measurements*," Photon. Technol. Lett., Vol. 4, 1992, pp. 1063-1066.

[103] P. Horak, N. Y. Voo, M. Ibsen and W. H. Loh, "*Pump-noise induced linewidth contributions in distributed feedback fiber lasers*," Photon. Technol. Lett., Vol. 18, 2006, pp. 998-1000.

[104] P. Horak, and W. H. Loh, "*On the delayed self-heterodyne interferometric technique for determining the linewidth of fiber lasers*," Opt. Express, Vol.14, 2006, pp. 3923-3928.

[105] J. Geng, S. Staines, Z. Wang, J. Zong, M. Blake, and S. Jiang, "*Highly stable low-noise Brillouin fiber laser with ultranarrow spectral linewidth*," Photon. Technol. Lett., Vol. 18, 2006, pp.1813-1815.

[106] S. P. Smith, F. Zarinetchi, and S. Ezekiel, "*Narrow-linewidth stimulated Brillouin fiber laser and applications*," Opt. Lett., Vol.16, 1991, pp.393-395.

[107] J. Boschung, L. Thevenaz, and P. A. Robert, "*High-accuracy measurement of the linewidth of a Brillouin fiber ring laser*," Electron. Lett., Vol.30, 1994, pp. 1488-1489.

[108] A. Debut, S. Randoux, and J. Zemmouri, "*Linewidth narrowing in Brillouin Lasers: Theoretical analysis*," Phys. Rev. A, Vol. 62, 2000, pp.023803-1 023803-4.

[109] W. V. Sorin, "*Fiber Optic Test and Measurement,*" D. Derickson, Ed. Upper Saddle River, NJ: Prentice Hall, ch. 10, 1998,

[110] G.P. Agrawal, "*Fiber Optic Communication System,"* 3rd ed., New York, Wiley Interscience, John Wiley & Sons INC, 2001.

[111] M. R. Shirazi, S. W. Harun, M. Biglary, K. Thambiratnam, and H. Ahmad, "*Effect of Brillouin Pump Linewidth on the Performance of Brillouin Fiber Lasers*,"ISAST transaction on Electron. and Signal processing, Vol. 1, 2007, pp. 30-32,.

[112] M. R. Shirazi, N. S. Shahabuddin, S. N. Aziz, K. Thambiratnam, S. W. Harun, and H. Ahmad, "*A linear cavity Brillouin fiber laser with multiple wavelength output*," Laser Phys. Lett., Vol. 5, 2008, pp. 361-363.

Chapter 4:

Multiwavelength Brillouin Erbium Fiber Laser Generation

4.1 Introduction

In an optical system, the propagating signal is attenuated by all optical components such as the optical and couplers. After some distance, the cumulative loss causes the signal to become too weak to be detected. Before the advent of optical amplifier, the only option was to regenerate the signal. In other words, before the signal becomes too weak, the signal has to be regenerated. This was done by regenerators which convert the optical signal to an electrical signal, amplify it up electrically, and convert it back into an optical signal for the retransmission. Regenerators are suitable for the specific bit rate and modulation format applied by the optical system. Optical amplifiers, however, are independent on the bit rate or signal formats. Furthermore, having fairly large gain bandwidths, optical amplifiers can simultaneously amplify several signals whereas a regenerator is required for each special wavelength. Therefore, optical amplifiers have become an essential element in high-performance optical systems even though they introduce additional noise, and this noise accumulates as the signal passes through multiple amplifiers along its path.

The spectral shape of the gain, the output power, and the transient behavior of an optical amplifier are important parameters. A sufficiently high output power,

the flat gain over the operating wavelength range, and the insensitive gain to variations in input power of the signal are important factors for amplifiers.

In this chapter, Erbium-doped fiber amplifiers (EDFAs) will be discussed and used for increasing number of lines in multiwavelenth Brillouin fiber lasers cited in the section 3.3.2. The generated comb is called multiwavelength Brillouin Erbium fiber laser (MBEFL).

4.2 Principle of Operation in Erbium-Doped Fiber Amplifiers (EDFAs)

An EDFA scheme is depicted in Fig. 4.1. It consists of about 14 m length of silica fiber whose core is doped with ionized atoms (ions), Er 3+, of the rare earth element erbium. This fiber is pumped using a laser diode, typically at a wavelength of 980 nm or 1480 nm. In order to combine the output of the pump laser with the input signal, the doped fiber is preceded by a wavelength division multiplexing (WDM) coupler. At the output, another WDM coupler is used to separate the amplified laser signal (LS) from any remaining EDFA pump signal power. As shown in Fig. 4.1, the EDFA is pumped in the forward direction means that the EDFA pump signal and the LS are in the same direction. The isolator is used at the input and the output to not only prevent the generation of fiber lasers by the reflections into the amplifier but also protect LS and EDFA pump from any reflection power.

The EDFA has some benefits in optical systems. Firstly, the EDFA can be used as a compact amplifier using reliable high-power laser diodes. Secondly, the fact that EDFA is a simple all-fiber device makes it easy to couple light in and out of it readily. In addition, the fact that it introduces no crosstalk as a Raman amplifier

when it is used as an amplifier in WDM systems. The crosstalk will be discussed in the next chapter for Raman amplifiers.

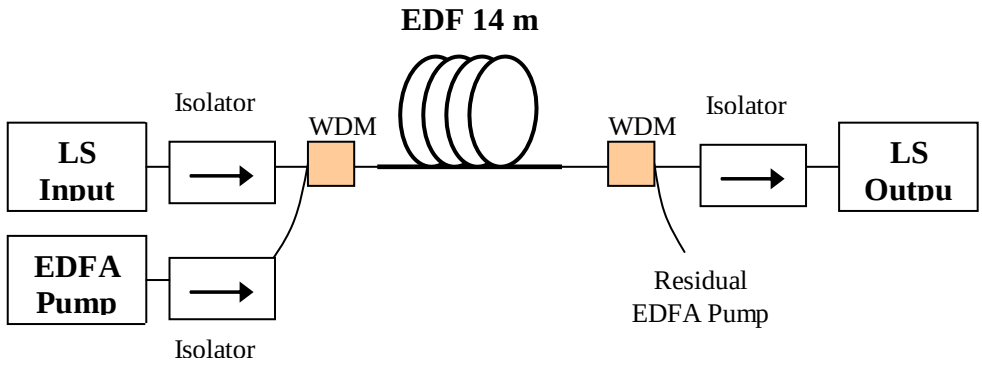

Fig. 4.1: An erbium-doped fiber amplifier (EDFA) in forward pumping.

In EDFA, the physical key phenomenon behind the signal amplification is stimulated emission of radiation by atoms in the presence of an electromagnetic field. This field is an optical signal of the LS in the case of the optical amplifiers. According to the principles of quantum mechanics, any physical system is found in one of its discrete number of energy levels. However, at thermal equilibrium, lower energy levels are more highly populated. Therefore, at thermal equilibrium, we have only absorption of the input signal. In order for amplification to occur, we must *invert* the relationship between the populations that prevails under thermal equilibrium. The population inversion can be achieved by using EDFA pump energy in an EDFA.

Three of the energy levels of erbium ions in silica glass are shown in Fig. 4.2. Each of the energy level that is indicated as a discrete line in an isolated ion of Erbium (Er 3+) is split into multiple energy levels when these ions are intended into silica glass. This process is termed Stark splitting. Moreover, glass does not have a regular structure. Thus the Stark splitting levels are slightly different for

individual EDF depending on the local surroundings observed by those ions. As a result of the Stark splitting, each discrete energy level of Er 3+ ion spreads into a continuous energy level band. In Fig. 4.2, the 980 nm transition corresponds to the band gap between the first and the third levels (E_1 and E_3). The 1480 nm transition corresponds to the gap between the bottom of the first band (E_1) to the top of the second band (E_2). In silica glass doped by Er 3+ ions, the set of frequencies that can be amplified by stimulated emission from the E_2 band to the E_1 band corresponds to the wavelength range 1525 - 1570 nm. The dashed line shows fast decay of ions from the E_3 energy level to the E_2 by the spontaneous emition.

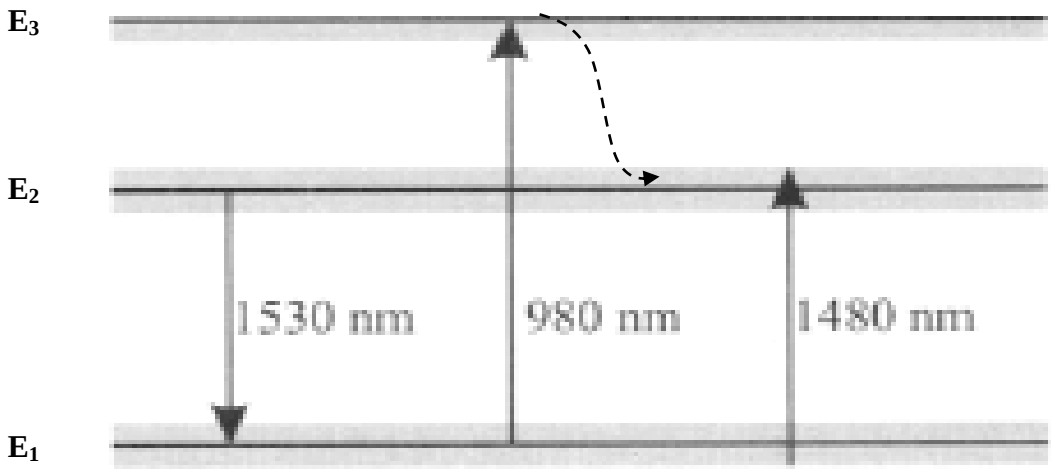

Fig. 4.2: Three energy level bands in silica glass doped by Er 3+ ions. The energy levels are spread into bands by the Stark splitting effect. The upward arrows denote wavelengths at which the amplifier can be pumped to excite the Er 3+ ions into the higher energy level whereas the downward transition represents the wavelength of photons emitted due to spontaneous and stimulated emission.

Indeed, this spreading of energy levels is a useful characteristic for increasing the frequency or wavelength range of the signals that can be amplified. Within each energy band, the erbium ions are distributed in the various levels within that band

in a nonuniform manner by a process known as thermalization. It is due to this thermalization process that an amplifier is capable of amplifying several wavelengths simultaneously. Thermalization refers to the process by which the Erbium ions are distributed within the various (split) levels constituting an energy band.

In thermal equilibrium, $N_1 > N_2 > N_3$ where N_i denotes the ionic population in level E_i, i = 1, 2, 3. The population inversion condition for stimulated emission from E_2 to E_1 is $N_2 > N_1$. It can also be accompanied by a combination of absorption and spontaneous emission as follows. The energy difference between the E_1 and E_3 levels corresponds to a wavelength of 980 nm. So if optical power at 980 nm known as EDFA pump power is injected into the amplifier, it will cause transitions of the ions from E_1 to E_3 and vice versa. Since $N_1 > N_3$, there will be a net absorption of the 980 nm pump power. The ions that have been raised to level E_3 by this process will quickly transit to level E_2 by the spontaneous emission process. The lifetime for this process is about 1μs whereas the spontaneous emission process from level E_2 to level E_1 is about 10 ms, which is four orders larger than the E_3 to E_2 lifetime. Furthermore, if the EDFA pump power is sufficiently large, ions that transit to the E_1 level are rapidly raised again to the E_3 level and the process will be repeated. There are also several levels other than E_3 and higher than E2. Although these levels can be used for pumping an EDFA, the pumping process is less efficient than pump power for a given gain at 980 nm. Although the wavelength 1480 nm is another possible option for the pump wavelength, which corresponds to absorption from the bottom sublevel of the E_1 band to the top sublevel of the E_2, EDFA pumping at 1480 nm is not as efficient as 980 nm pumping. Furthermore, the degree of population inversion that can be

achieved by 1480 nm pumping is lower which, in turn, it causes higher noise figure.

However, higher-power pump lasers are available at 1480 nm, compared to 980 nm, and thus 1480 nm pumps find applications in amplifiers designed to yield high output powers. Another advantage of the 1480 nm pump is that the pump power can also propagate with low loss in the silica fiber due to low loss of silica fiber in 1480 nm in comparison to 980 nm. Therefore, an EDFA pump laser with the wavelength 1480 nm can be set up remotely from the amplifier itself.

As a result of spreading Er 3+ ion levels into bands, all frequencies that correspond to the energy difference between some energy in the E_2 band and some energy in the E_1 band can be amplified. In the case of erbium ions in silica glass, the set of frequencies that can be amplified by stimulated emission corresponds to the wavelength in the range about 1525-1570 nm with a peak around 1530 nm which is exactly one of the low-attenuation wavelength region of standard optical silica fiber. Fig. 4.3 shows the gain of a typical EDFA as a function of the wavelength for different values of the pump power. When such an EDFA is used in a WDM communication system, different WDM channels undergo different degrees of amplification. This is called the gain flatness problem, which is a critical issue particularly in WDM systems with cascaded EDFA amplifiers [1-3].

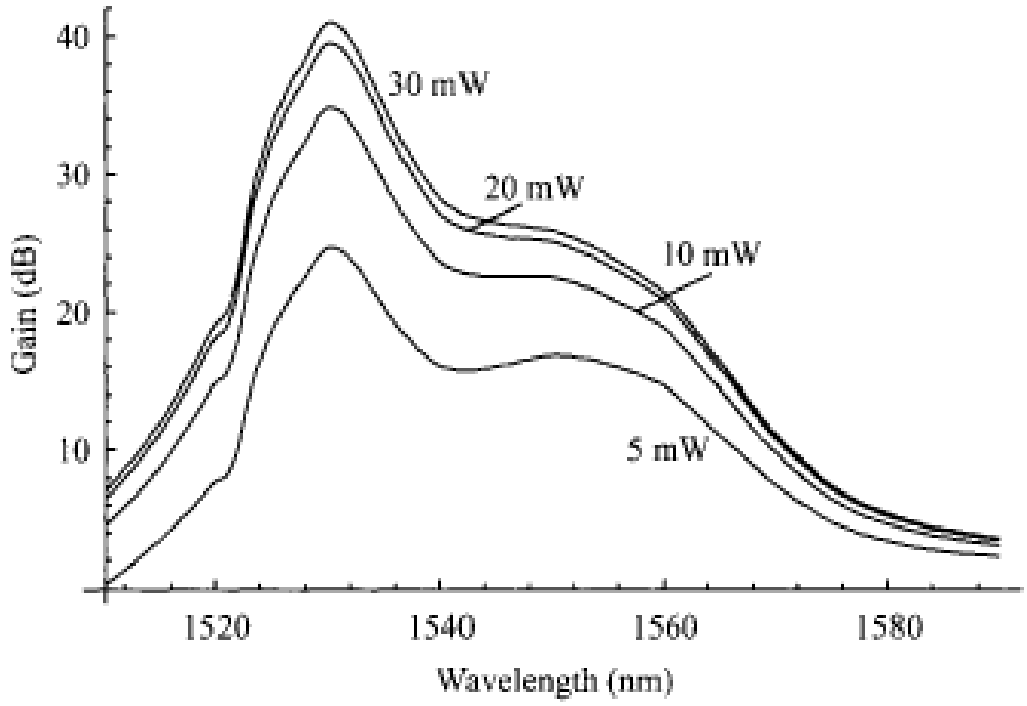

Fig. 4.3: The gain of a typical EDFA as a function of the wavelength for four different values of the EDFA pumps power. The length of the doped fiber is taken to be 14 m and 980 nm pumping is assumed [4].

4.3 Application of EDFAs in L-Band wavelength region (1565-1625 nm)

Traditional EDFAs operate only in the C-band wavelength (1530-1565 nm). However, the gain shape of EDF has a relatively long tail extending well beyond this range to about 1605 nm as shown in Fig. 4.3. This has stimulated a lot of researches to develop the optical systems in the so-called L-band from 1565 to 1625 nm. L-band EDFAs operate on the same principle as C-band EDFAs. However, there are significant differences in the design of L- and C-band EDFAs. The gain spectrum of erbium is much flatter intrinsically in the L-band than in the C-band. However, the gain coefficient of Erbium in the L-band is about three times smaller than in the C-band. This requires the use of either much longer doped fiber lengths or fiber with higher erbium doping concentrations.

It is reported that the length of EDF is around 7 to 8 times longer than that in the conventional amplifier in order to exploit the L band region to achieve high gain although longer EDF leads to lower power conversion efficiency caused by the higher fiber loss [5]. In addition, some researches have been carried out to develop EDF with high Er^{3+} concentration and thus, exhibits low loss characteristic [6], [7], [8]. Central Glass & Ceramic Research Institute of India managed to fabricate silica EDF with Er^{3+} concentration of 900 ppm using a Modified Chemical Vapor Deposition (MCVD) process in conjunction with a solution doping technique [9]. The 15 m of this silica EDF could provide gain from wavelength of 1565 until 1595 nm [9-12]. However, the previous EDFA consists of 50 m silica EDF with concentration of 400 ppm to provide the same amplification in L-band region [13]. In addition, the pump powers required for L-band EDFAs are much higher than their C-band counterparts. Due to the smaller absorption cross sections in the L-band, these amplifiers also have higher amplified spontaneous emission. Finally, many of the other components used inside the amplifier, such as isolators and couplers, exhibit wavelength-dependent loss and so are specified different for the L-band than for the C-band [14]. In practice, due to the significant differences between C- and L-band amplifiers, these amplifiers are usually realized as separate devices, rather than as a single device.

On the other hand, Bismuth-EDFs (Bi-EDFs) exhibits wide emission bandwidth with strong emission probability in 1550 nm region as shown in Fig. 4.4 [15], [16]. As shown in this figure, the amplification range can extend to above 1600 nm easily by using Bismuth. In addition, the Bi-EDFA gain spectrum is nearly flat in L band in comparison to the traditional EDFA. EDFAs have been widely studied [17-23] and applied in fiber lasers [24-26].

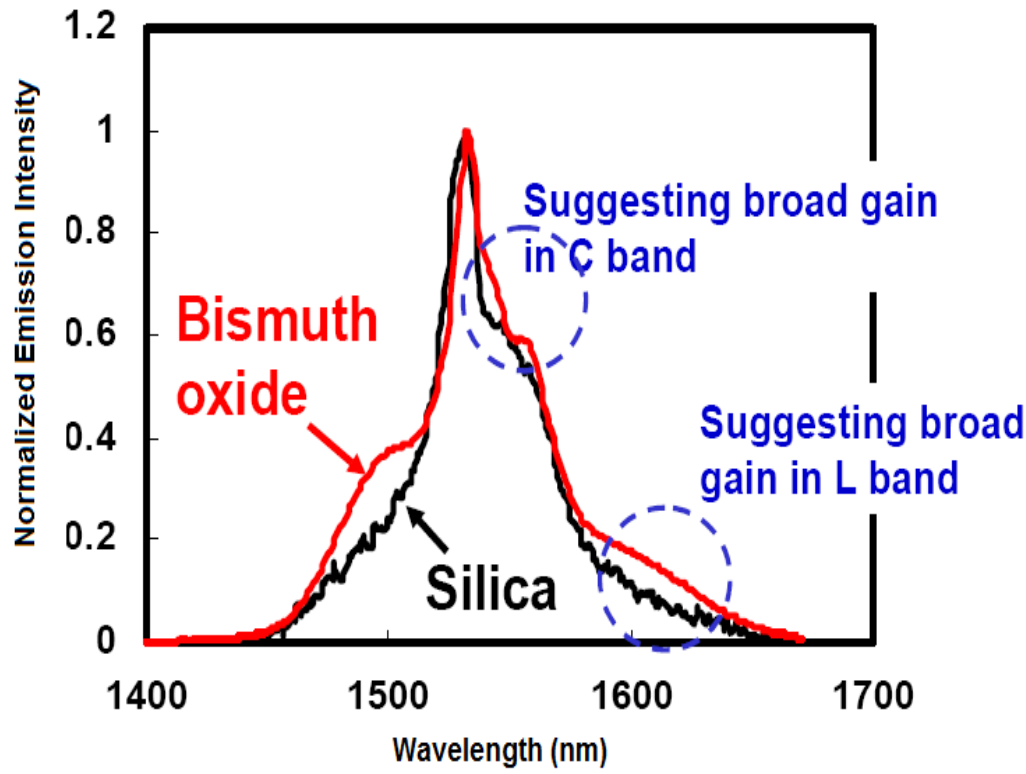

Fig. 4.4: The gain of a typical Bismuth oxide based EDFA as a function of the wavelength in comparison with the traditional EDFA in the same condition. Bismuth oxide glass exhibits broader emission than the traditional Silica based EDF [16].

In this work, after reviewing the principal theory of Bi-EDFA, MBEFLs will be demonstrated by using a Bi-EDFA to increase the number of lines of the linear cavity MBFL proposed in the section 3.2.2.

4.4 Theory of Bismuth Based Erbium Doped Amplifiers (Bi-EDFA)

As mentioned before, the rate equations can be expressed by the energy-level diagrams in Fig. 4.2. The levels are numbered in a particular manner that allows one set of rate equations to be used for both systems. The fiber is doped

with $N_t(r,\phi,z,t)$ total population density or active ions per unit volume with $N_i(r,\phi,z,t)$ ions per unit volume in the itch level in every time at a position in cylindrical coordinates. Rate equations are written for the EDFA pump and signal beams with the propagation vectors $\mathbf{K}_P$ and $\mathbf{K}_S$, respectively. In contrast to the theory of the two-levels [27], it is needed to differentiate between pump and signal beams due to their different interaction with different energy levels. A signal beam is defined as one that interacts with the metastable level and the terminal lasing level, and a pump beam is assumed that interacts with the ground state and the pump level. For direct pumping to the metastable level of a three-level ion, such as for 1480 nm pumping of Er3+, the pump is theoretically considered as an additional signal beam.

For clarity, powers are described in photons per second and symbols indicating the time and positional dependencies of intensities and ion populations are not shown in the rate equations. Assume N_1, N_2, and N_3 represent the population densities of Er 3+ ions at the E1 E_2 and E_3 levels, respectively. Then, the total population density of Erbium, N, is expressed as

$$N = N_1 + N_2 + N_3 \tag{4.1}$$

They can be obtained by solving the steady-state assumed rate equations as [3], [28]:

$$\frac{dN_1}{dt} = (A_{21} + R_{S21} + R_{P21} + R_{ASE21})N_2 - (R_{S12} + R_{P12} + R_{ASE12})N_1 + BN_2^2$$

$$\frac{dN_2}{dt} = -(A_{21} + R_{S21} + R_{P21} + R_{ASE12})N_2 + (R_{12} + R_{P12} + R_{ASE12})N_1 - 2BN_2^2 + W_{32}N_3$$

$$\frac{dN_3}{dt} = -W_{32}N_3 + BN_2^2 \tag{4.2}$$

where the irradiative decay rate of the E_2 level and the spontaneous emission of E_3 level are ignored respectively to the spontaneous emission probability A_{12} of the E_2 level and is the fast decay rate from the E_3 level to the E_1 level W_{12}. A_{12} can be calculated by Fuchtbauer-Ladenburg formula [29]. B is corporative upconversion coefficient evaluated by Snoek's method [30]. R denotes the radiative decay rate of the signal under amplification, EDFA pump and ASE as following:

$$R_{S21} = (\frac{\sigma_S^E}{A_{eff} h\upsilon_S})P_S$$

$$R_{S12} = (\frac{\sigma_S^A}{A_{eff} h\upsilon_S})P_S$$

$$R_{P21} = (\frac{\sigma_P^E}{A_{eff} h\upsilon_P})(P_p^+ + P_P^-)$$

$$R_{P12} = (\frac{\sigma_P^A}{A_{eff} h\upsilon_P})(P_p^+ + P_P^-)$$

$$R_{ASE21} = (\frac{\sigma_P^E}{A_{eff} h\upsilon_S})(P_{ASE}^+ + P_{ASE}^-)$$

$$R_{ASE12} = (\frac{\sigma_P^A}{A_{eff} h\upsilon_S})(P_{ASE}^+ + P_{ASE}^-)$$

(4.3)

where $A_{eff} = \pi d_m^2 / 4$ is the effective area of the mode field diameter d_m in the fiber. $P_P^{\pm}$ are forward and backward propagating EDFA pump power in the multistage bi-directional EDFA as shown in Fig. 4.5. P_S is the signal power and $P_{ASE}^{\pm}$ are forward and backward amplified spontaneous emission (ASE) power. σ_P^E and σ_P^A are the emission and absorption cross sections at the pump wavelength, respectively. The optimal length of Bi-EDF in a multistage configuration can be

found by investigating the pump, signal and ASE power propagating along the core of the Bi-EDF as the following equations:

$$\frac{dP_P^{\pm}}{dz} = (\sigma_P^E N_2 \mp \sigma_P^A)\Gamma_P P_P \mp \alpha_P P_P$$

$$\frac{dP_S}{dz} = (\sigma_S^E N_2 - \sigma_S^A N_1)\Gamma_S P_S - \alpha_S P_S$$

$$\frac{dP_{ASE}^{\pm}(\upsilon)}{dz} = (\pm\sigma_\upsilon^E N_2 \mp \sigma_\upsilon^A N_1)\Gamma_\upsilon P_{ASE}^{\pm} \pm \sigma_\upsilon^E N_2 \Gamma_S h\upsilon\Delta\upsilon \mp \alpha_\upsilon P_{ASE}^{\pm} \qquad (4.4)$$

In Eqs. (4.4), α_p and α_s are, respectively, the attenuation coefficients of the fiber for the pump and signal. $\Delta\upsilon$ implies the effective ASE bandwidth. Γ_P and Γ_S are corresponding overlapping factors for pump and signal power respectively and h is Plank's constant. It is supposed that all exited ions upon the E_3 level decays immediately to E_3. In the reported work for the simulation Bi-EDFA, the typical parameters used for the calculation are listed according to the Table 1 [31].

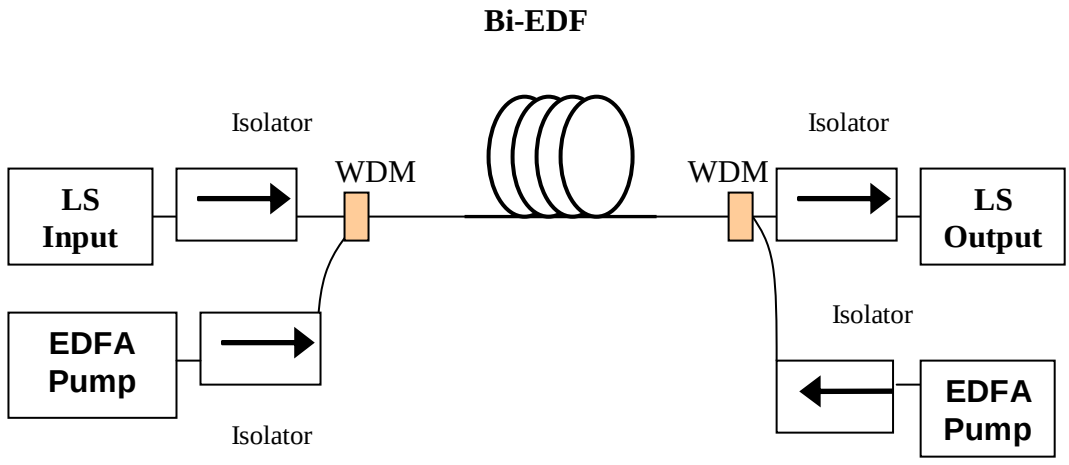

Fig. 4.5: Bi-directional Bismuth based Erbium-doped amplifier (Bi-EDFA).

Table 1: Typical parameters used for Bi-EDFA simulation [31].

Parameter	Symbol	Unit	Value
Spontaneous emission rate	A_{12}	s^{-1}	300
Irradiative decay rate	W_{12}	s^{-1}	7500
Cooperative upconversion coefficient	B	m^3s^{-1}	8.5×10^{-24}
Emission cross section of pump	σ_P^E	cm^2	1.19×10^{-21}
Emission cross section of signal	σ_S^E	cm^2	1.60×10^{-21}
Absorption cross section of pump	σ_P^A	cm^2	3.61×10^{-21}
Absorption cross section of signal	σ_S^A	cm^2	4.99×10^{-22}
Confinement factor of pump	Γ_P		0.5
Confinement factor of signal	Γ_S		0.47
Background loss	α	ms^{-1}	0.6
ASE effective bandwidth	$\Delta\upsilon$	nm	6.7×10^{-9}
Er density	N	cm^{-3}	7.9×10^{19}

In the next section, a new multi-wavelength MBEFL configuration based on the linear cavity BFL mentioned in Fig. 3.26 is proposed to increase the number of lines by using Bi-EDFA in the linear cavity.

4.5 Generation of Multiwavelength Brillouin Erbium Fiber lasers (MBEFLs)

The configuration of the proposed MBEFL is shown in Fig. 4.6. It consists of a short bismuth-based EDF (Bi-EDF) approximately 2.15m in length with an erbium concentration of 3250 ppm and a cut-off wavelength of 1440 nm as well as a pump absorption rate of 83 dBm at 1480 nm. The fiber is manufactured by Asahi Glass in Japan and is supplied with angled AC/PC connectors. The Bismuth based fiber is connected to the single-mode fiber (SMF) and is pumped bi-directionally using

two 1480 nm lasers to generate a Bi-EDFA. A SMF of 25 km in length is used as a non-linear gain medium and two WDM couplers are used to combine the pump Bi-EDFA power and laser wavelengths in a bi-directional amplifier configuration. An external cavity tunable-laser source (TLS) with the maximum power of 6.5 dBm is used as the Brillouin pump (BP). Two optical circulators, OC1 and OC2, are used to create the linear cavity and are placed at both ends to act as reflectors. The coupler C1 is used to inject the BP signal and C2 is used to tap the output power for detection by an optical spectrum analyzer (OSA).

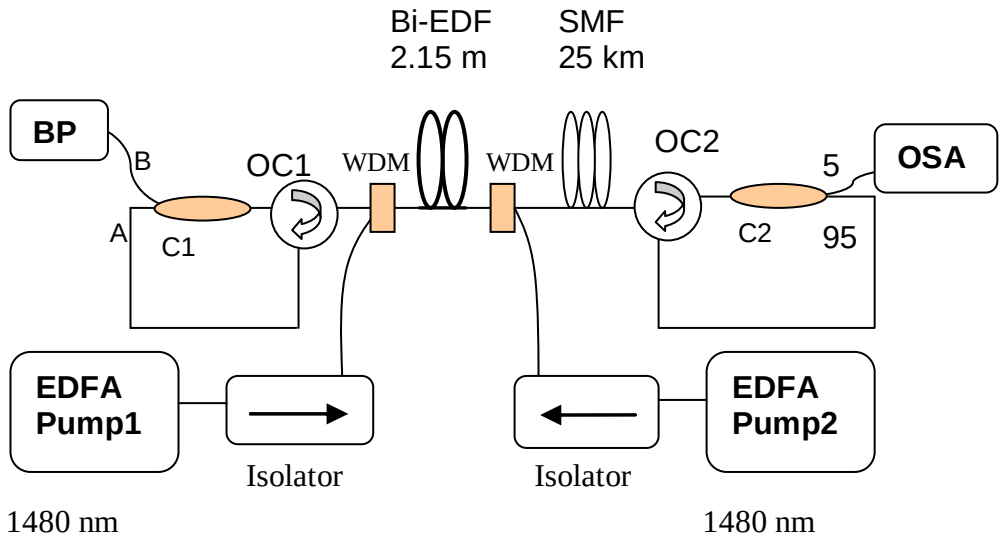

Fig. 4.6: The proposed linear cavity for MBEFL generation by using a Bi-EDFA [26].

The BP is injected into the linear cavity via C1 at the leg B and is then amplified by the bi-directionally pumped Bi-EDF. Then, the amplified BP is coupled into the SMF to generate the first Stokes signal propagating in the opposite direction of the

BP signal. The Stokes signal is then amplified by the bismuth-based EDF (Bi-EDF) amplifier before being re-circulated by the OC1 ring cavity back towards the SMF. The 1st Stokes then travels towards OC2 where it is tapped by the coupler C2 for viewing at the OSA. As it travels, the 1st Stokes will also generate the 2nd Stokes in the SMF, which will also travel towards OC1 and be re-circulated into the system, much like the 1st Stokes. This generation process continues as long as the incoming Stokes exceeds the threshold values for Brillouin gain, thereby providing cascaded Brillouin Stokes. The number of Stokes generated depends on the total gain of the Brillouin Bi-EDF amplifier over the cavity loss. The output of the linear cavity BEFL is tapped from the 5% port of C2 at OC2 and characterized by the OSA with a resolution of 0.015 nm. The linewidth of the BP signal is 15 MHz, which is measured by using the heterodyne technique as mentioned in last chapter.

The operating wavelength of the MBEFL is determined by the gain of the bi-directionally pumped Bi-EDFA over its cavity loss and this covers the L-band region (1560–1600 nm). The free-running spectrum, which is taken when BP is off, is shown in Fig. 4.7 at the Bi-EDFA pump power of 120 mW for both the two 1480 nm pumps. In Fig. 4.7, C2 is a 99/1 coupler with the 99% output designated as Port B. The wavelength of the peak power is generated at the 1570 nm region, which is where the difference between the Bi-EDF gain spectrum and cavity loss is the largest.

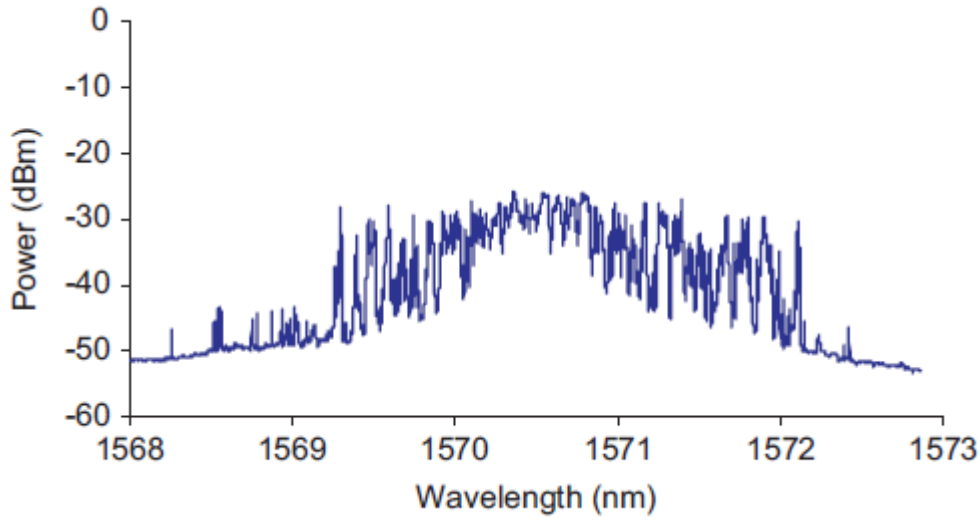

Fig. 4.7: Free-running spectrum of the BEFL (without BP). The powers of the two Bi-EDFA pumps (P1 and P2) are fixed at 120mW [26].

The free-running BEFL exhibits a peak power of approximately -30 dBm with bandwidth of approximately 4 nm centered at 1570.5 nm. The chosen BEFL operating wavelength must be within or as close as possible to the bandwidth of the free-running BEFL.

The impact of the coupling ratio of C1 on the number of Stokes and anti-Stokes lines generated by the BEFL is depicted in Fig. 4.8. The 1480nm pump and BP powers are fixed at 120mW and 5 dBm, respectively. The BP wavelengths are optimized to 1570.7, 1570.3 and 1568.5nm for the coupling ratios of 50/50, 80/20 and 99/1, respectively. The coupling ratio of C1 controls the amount of BP power that is injected into the cavity. A higher ratio at Port B translates into a higher injected BP power and lower reflectivity of OC1.

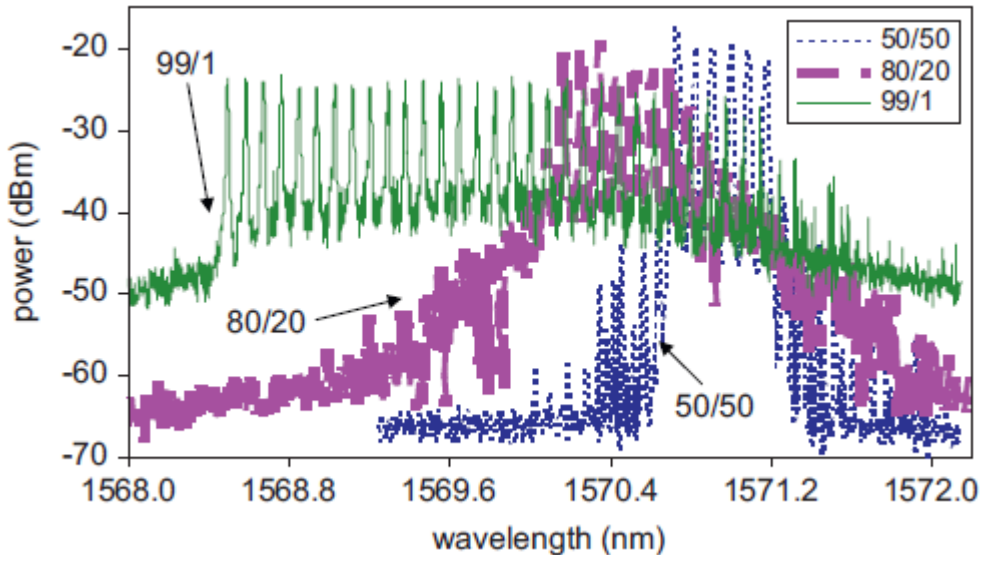

Fig. 4.8: Output spectrum of MBEFL at different coupling ratios of C1. The both EDFA pump powers (P1 and P2) and the BP powers are fixed at 120mW, 120mW and 5 dBm, respectively [26].

As shown in Fig. 4.8, an increment of the Port B ratio (50%, 80% and 99%) increases the number of lines of the BEFL output, but reduces the peak power of these lines. The reduction of the peak powers are due to the reflectivity of the OC1 ring, which subsequently increases the cavity loss by reducing ratio of the Port A. This also has the effect of shifting the operating wavelength of the BEFL travels to the shorter wavelength region.

The impact of the 1480nm pump power on the number of Stokes generated by the BEFL is depicted in Fig. 4.9. The BP is set at a wavelength of 1569.0 nm, which is close to the lasing wavelength of the free-running BEFL and the BP power is fixed at 5 dBm. Both the 1480nm pump powers are varied from 60 and 120mW. Lower pump powers will not give any Stokes due to the low EDFA gain,

and thus the minimum pump power is 60mW. At a pump power combination of 60 and 100mW, the least number of lines are generated as shown in Fig. 4.9. However, as the combination pump power increases, the number of lines generated also increases. This can be attributed to the increment of the erbium gain with increase in the pump power as this situation provides sufficient signal power for higher order Stokes signal to pump the SMF and maintain the cascading of the Stokes into multiple Stokes. As shown in Fig. 4.9, the highest number of lines is obtained at a pump power of 120mW. The number of lines is higher in Fig. 4.9 (d) as compared with that in Fig. 4.9 (c) even though two pump power combinations are almost similar, due to gain characteristics of the bi-directionally pumped Bi-EDF amplifier. A higher gain is obtained if the signal is injected from the side with higher pump power.

(a)

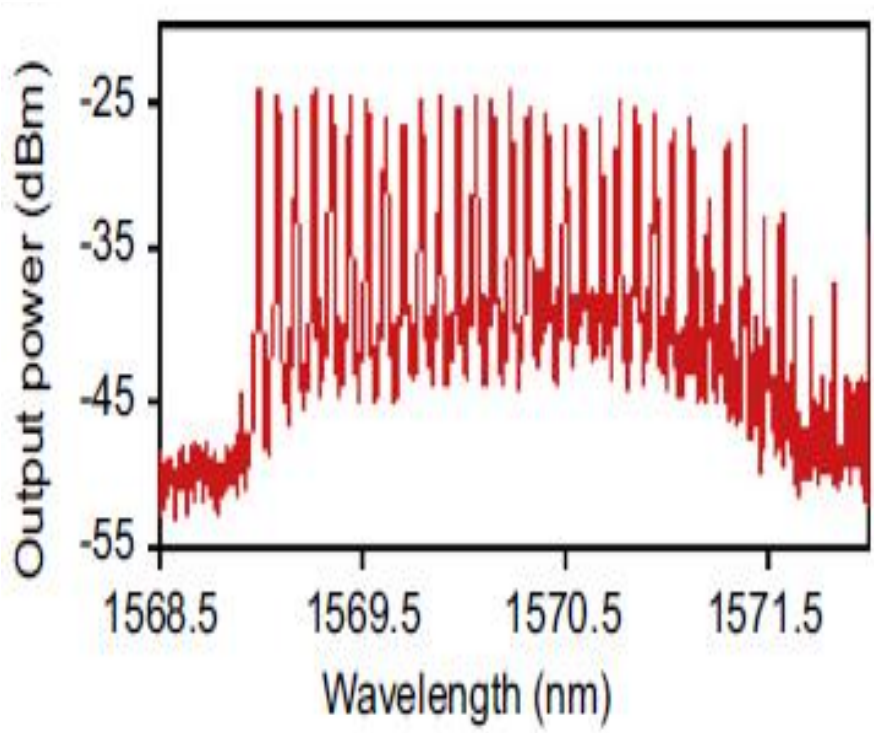
Output power (dBm)
-25
-35
-45
-55
1568.5
1569.5
1570.5
1571.5
Wavelength (nm)

(b)

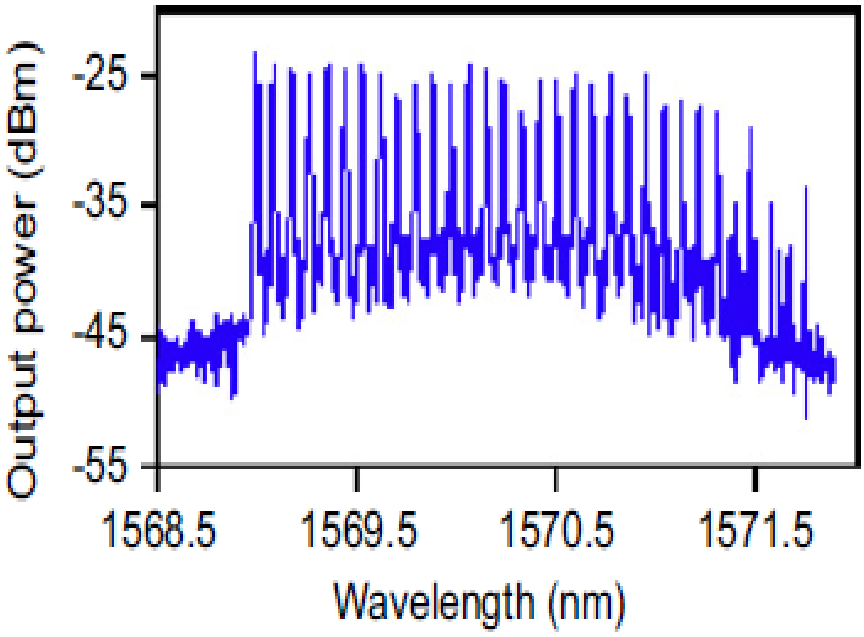
Output power (dBm)
-25
-35
-45
-55
1568.5
1569.5
1570.5
1571.5
Wavelength (nm)

(c)

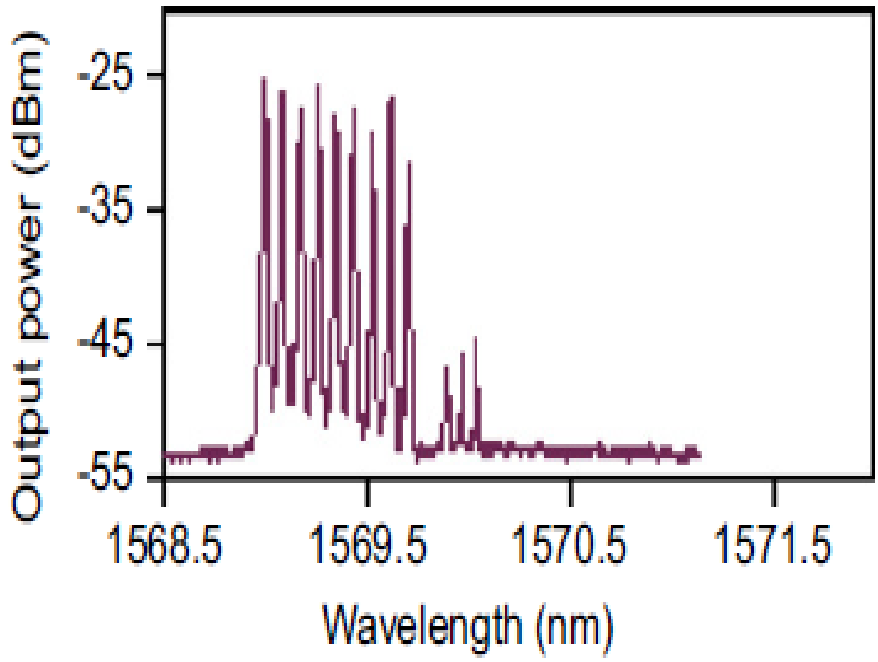

(d)

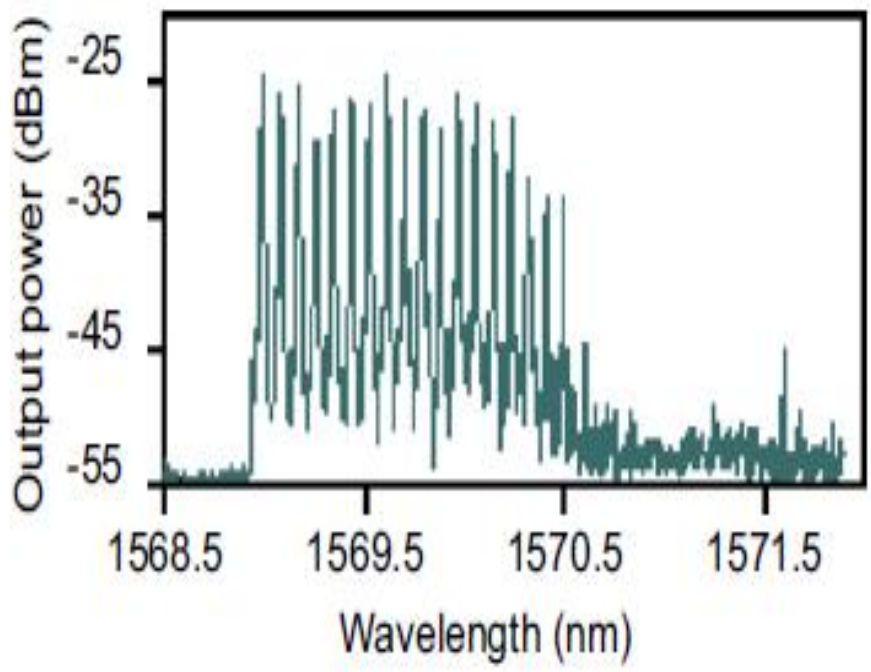

Fig. 4.9: MBEFL spectra at fixed wavelength 1480 nm and different Bi-EDFA pump powers (a) P1=P2=120mW, (b) P1=P2=105mW, (c) P1=60mW, P2= 100mW and (d) P1=105mW, P2=60mW. The BP power and wavelength is also fixed at 6.5 dBm and 1569.0 nm, respectively [26].

Fig.4.10 shows the output spectrum of the MBEFL at BP wavelength of 1568.2nm and the BP power of 5 dBm. In this experiment, 50 multi-wavelength lines are obtained at the maximum pump power of 120mW. However, a higher number of Stokes lines are expected at a higher pump power. The line spacing is approximately 0.09nm in the wavelength domain (~11GHz) while the 3 dB bandwidth of each line is about 0.02 nm, limited by the OSA resolution of 0.015 nm. In the MBEFL generation, anti-Stokes lines are also generated due to the degenerate four wave-mixing processes between BP and Stokes waves especially at the higher Bi-EDFA pump and BP powers. Additionally, the power of each subsequent Stokes lines is typically lower than that of the previous Stokes line, as each subsequent Stokes is generated with the energy of the previous Stokes, slightly reducing the Stokes line's power. However, some of the lines have a peak power, which is higher than the previous lines as shown in Fig. 4.10. This is attributed to other phenomenon such as four-wave mixing and Brillouin crosstalk which will transfer energy from neighboring lines to these lines. The generated MBEFL is observed to be stable at room temperature with only minor fluctuations observed coinciding with large temperature variances.

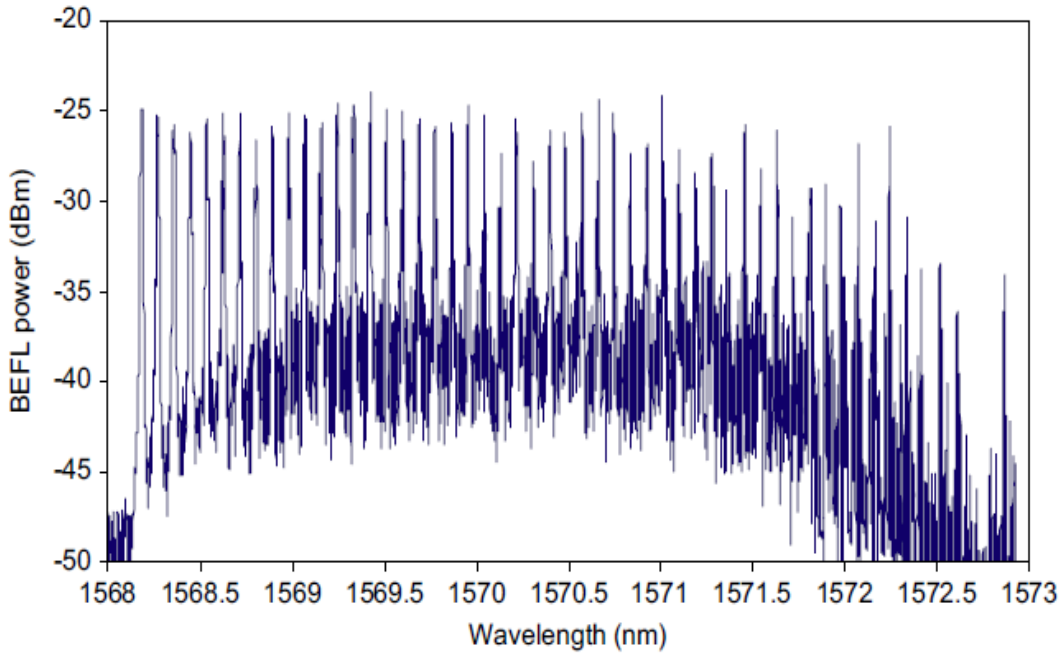

Fig. 4.10: The generated MBEFL output spectra by using BP wavelength of 1568.2 nm and BP power of 5 dBm and two bi-directional Bi-EDFA pump power 120 mW [26].

The linear cavity MBEFL allows the lasing wavelength to passing the Bi-EDF gain twice per one oscillation and thus increases the net gain per oscillation. This results in the linear cavity to exhibit a lower threshold power and achieves a larger number of Stokes and anti-Stokes compared with the ring configuration [25], [26]. The proposed MBEFL using a short-length bismuth-based EDF gain medium will allow for the development of compact BEFL devices. Further reductions in size can be obtained if the SMF is replaced with highly non-linear fibers such as holey fibers. A holey fiber with a core diameter of about 1.6 μm would require less than 100 m to obtain the SBS effect desired [32].

4.6 Summary

A multiple wavelength source using a Bi-EDF in a linear cavity configuration is proposed and demonstrated in this work. The configuration uses a pair of optical circulators at both the input and output ends of the cavity to form a linear resonator for multiwavelength generation, and also one optical coupler to inject the BP at one end and another optical coupler to tap the output at the other end of the linear cavity. A short length of 2.15 m of Bi-EDF together with an SMF optical fiber has generated the multiwavelength BEFL with a wavelength spacing of 0.09 nm in the L-band region. A stable output laser comb of 50 lines is obtained at a BP of 1568.2 nm and 6.5 dBm and two 1480 nm pumps at 120 mW. The injected BP wavelength and power together with the 1480 nm pump laser has a great effect on the number and output peak power of the BEFL lines. Using the Bi-EDF, a compact MBEFL can be realized. With the existence of highly non-linear fibers such as holey fibers, a more compact BEFL can be designed using the proposed configuration. The generated MBFL is depended to Bi-EDFA operational wavelength region. Although, Bi-EDFA has a wide operational region than the traditional EDFA, the proposed MBEFL can only be generated in C and L band. In addition, the lines in the MBEFL have the peak power of about -25 dBm even though two Bi-EDFA pump power of 120 mW and a BP power 6.5 dBm have been used. These problems cause to investigate multiwavelength Brillouin Raman fiber lasers which will be considered in the next chapter.

References

[1] E. Desurvire, "*Erbium-Doped Fiber Amplifiers: Principles and Applications."* John Wiley, New York, 1994.

[2] E. Desurvire, D. Bayart, B. Desthieux, S. Bigo, "*Erbium-Doped Fiber Amplifiers, Device and System Developments*," John Wiley, New York, 2002.

[3] P.C. Becker, N. A. Olsson, and J. R. Simpson. "*Erbium-Doped Fiber Amplifiers: Fundamentals and Technology,"* Academic Press, San Diego, CA, *1999.*

[4] C. R. Giles and E. Desurvire, "*Propagation of signal and noise in concatenated Erbium –doped Fiber optical amplifiers*," J Lightwave Technol., Vol. 9, 1991, pp. 147-154.

[5] M. A. Mahdi, "*Novel broadband Erbium-doped fiber amplifiers for WDM transmission systems*,"Ph. D Thesis, Photonics Research Center, Physics Department, University of Malaya, 2001.

[6] S. Ishikawa, M. Kakui, M. Nishimura and Y. Makio, "*High gain per unit lengths silica-based erbium-doped fiber for 1580 nm band amplification*," Proc. Optical Amplifiers and Their Applications OAA '98, 1998, pp. 64-67.

[7] S. Endo, S. Ishikawa, M. Kakui, N. Nishimura and Y. Makio, "*High concentration Er-doped fiber for efficient L-band amplification with short length*," Proc. Optoelectronics and Communication Conference OECC, 1999, pp. 1356-1357.

[8] L. Jie, Y. Peida, C. Shuling, W. Shujian, L. Shiyu and W. Yanliang, "*High concentration erbium-doped fiber for wide-band EDFA*," Optoelectronics and Communication Conference OECC, 2000, pp. 262-263.

[9] S. W. Harun, M. C. Paul, M. Pal, A. Dhar, R. Sen, S. Das, S. K. Bhadra, N. S. Shahabuddin and H. Ahmad, "*An efficient and flat-gain Erbium-doped fiber amplifier in*

the region of 1550 nm to 1590 nm," Optoelectronics and Advanced Materials – Rapid Communications, Vol. 2, no. 8, 2008, pp. 455 – 458.

[10] R. Sen, T. Bandyopadhyay, S. K. Bhadra, K. Dasgupta, M. C. Paul, "*A method for fabricating rare earth doped optical fibre*," PCT WO 02/060830 A1

[11] M. Pal, R. Sen, M. C. Paul, S. K. Bhadra, S. Chatterjee, D. Ghosal, K. Dasgupta, "*Investigation of the deposition of porous layers by the mcvd method for the preparation of rare-earth-doped cores of optical-fibers*," Opt. Commun., Vol. 254, no. 88, 2005, pp. 88-95.

[12] M. Chatterjee, R. Sen, M. Pal, M. Naskar, M. Paul, S. Bhadra, K. Dasgupta, D. Ganguli, T. Bandyopadhyay, A. Gedanken, R. Reisfeld, "*Rare-earth doped optical fiber from oxide nanoparticle*," Acta. Opt. Sin., Vol. 23, 2003, pp. 35-36.

[13] S. W. Harun, "*Designs of Enhanced L-band Erbium-doped Fiber Amplifiers*," Ph. D Thesis, Photonics Research Center, Physics Department, University of Malaya, 2004.

[14] E A. Flood, "*L-band erbium-doped fiber amplifiers*," IEEE proceeding In OFC Technical Diges, 2000, pp. WG 1-1 - WG 1-4.

[15] "*Introduction of high performance EDF based on bismuth oxide host glass*", Technical Bulletin Bi-EDF, Asahi Glass co. Ltd., Nov 2002.

[16] S. Ohara, N. Sugimoto, K. Ochiai, H. Hayashi, Y. Fdasawa, T. Hirose, M. Reyes, "*Extra-Broadband and Highly Eficient Short length* $Bi_2\ 0_3$ *-based EDF*," IEEE, OFC, 2003, Vol. 2, pp. 635-636.

[17] N. Sugimoto, Y. Kuroiwa, K. Ochiai, S. Ohara, Y. Fukusawa, and S. Ito, "*Novel Short-Length EDF for C+L Band Amplification*," in Optical Amplifiers and Their Applications, A. Mecozzi, M. Shimizu, and J. Zyskind, eds., Vol. 44 of OSA Trends in Optics and Photonics, 2000, paper OTuA6.

[18] N. Sugimoto, "*Ultrafast Optical Switches and Wavelength Division Multiplexing (WDM) Amplifiers Based on Bismuth Oxide Glasses*," J. Am. Ceram. Soc. Vol. 85, 2002, pp. 1083-1088.

[19] N. Sugitomo, "*Recent Progress in Bi-EDF Technology*", Asahi Glass Co. Ltd., 2005.

[20] B. O. Guan, H. Y. Tam, S. Y. Liu, P. K. A. Wai and N. Sugimoto, "*Ultra-wideband bismuth-based EDFA for DWDM systems*", Optoelectronics Proceedings of the Sixth Chinese Symposium, 2003, pp. 147–149.

[21] B. O. Guan, H. Y. Tam, S. Y. Liu, P. K. A. Wai and N. Sugimoto, "*Ultrawide-Band La-codoped Bi2O3-Based EDFA for L-Band DWDM Systems*", Photon. Technol. Lett., Vol. 15, no. 11, pp. 1525-1527, 2003.

[22] K. Taira, K. Kikuchi, and N. Sugimoto, "*Dispersion and pulse amplification characteristics of Bismuth Oxide based Erbium doped fiber amplifiers*," in Proc. Optical Amplifies and Applications Conference (OAA), Vancouver, July 2002, paper OTuC2.

[23] H. Sotobayashi, J.T. Gopinath, and E. P. Ippen, "*23 cm long Bi2O3-based EDFA for picosecond pulse amplification with 80 nm gain bandwidth*", Electron. Lett., Vol. 39, no. 19, 2003, pp. 1374-1375.

[24] H. Ahmad, N. S. Shahabuddin, K. Dimyati, Z. Jusoh and S. W. Harun, "*An Enhanced Bismuth-Based Brillouin Fiber Laser with Linear Cavity Configuration*", Fiber and Intergrated Optics, Vol. 27, no. 1, 2008, pp. 35-40.

[25] N. S. Shahabuddin, S. W. Harun, K. Thambiratnam and H. Ahmad, "*Bismuth-based Brillouin/Erbium fiber laser*", J. Modern Optics, Vol. 55, no. 8, 2008, pp. 1345-1351.

[26] S. Shahi, S. W. Harun, N. S. Shahabuddin, M. R. Shirazi, H. Ahmada, "*Multi-wavelength generation using a bismuth-based EDF and Brillouin effect in a linear cavity configuration*," Elsevier, Optics & Laser Technology, Vol. 41, 2008, pp. 198 - 201,.

[27] A. A. M. Saleh, R. M. Jopson, J. D. Evankow, and J. Aspell, "*Modeling of gain in erbium doped fiber amplifier*," Photon. Technol. Lett., Vol. 2, 1990, pp. 714-717.

[28] C. R. Giles and E. Desurvire, "*Modeling erbium-doped fiber amplifiers*," J. Lightwave Technology, Vol. 9, 1991, pp. 271-283.

[29] W. L. Barnes, R. I. Laming, E. J. Tarbox, P. R. Mokel, "*Absorption and emission cross section of Er^{3+} doped silica fiber,*" J. Quantum Electron., Vol. 27, 1991, pp. 1004-1010.

[30] E. Snokes, G. N. van den Hoven, A. Polman, "*Cooperativeupconversion in erbium – implanted soda-lime silicate glass optical waveguides*," J. opt. Soc. Am. B, Vol. 12, 1995, pp. 1468-1474.

[31] H. Hayashi, N. Sugimoto, S. Tanabe, "*High-performance and wideband amplifier using bismuth-oxide-based EDF with cascade configurations*," Opt. Fiber Thechnol., Vol. 12, 2006, pp. 282-287.

[32] J. H. Lee, Z. Yusoff, W. Belardi, M. Ibsen, T. M. Monro, D. J. Richardson, "*Investigation of Brillouin effects in small-core holey optical fiber: lasing and scattering*," Opt. Lett., Vol. 27, 2002, pp. 927–929.

Chapter 5:

Mutiwavelength Brillouin Raman Fiber Lasers

5.1 Introduction

Although Erbium-doped fiber amplifiers (EDFAs) can be designed to amplify the C band (1530 – 1565 nm) and the L band (1565-1625 nm) wavelength regions, Raman amplifiers can work in any wavelength as long as the Raman pump is available. The Raman amplifiers use stimulated Raman scattering (SRS) effect which is a nonlinear phenomenon arises from inelastic Raman scattering. In Raman scattering effects, energy gets transferred from one light wave to another wave called the Raman Stokes wave at a longer wavelength (or lower energy). The lost energy is absorbed by the molecular vibrations, or phonons, in the medium. The same as stimulated Brillouin scattering (SBS), photon-phonon interaction involves in this nonlinear process. However, optical phonons participate in SRS whereas acoustic phonons involve in SBS. Different dispersion relations of acoustic and optical phonons lead to some differences between SBS and SRS. SBS occurs only in the backward direction in an optical fiber and the SBS threshold power is a few miliwatts whereas SRS can occur in the both directions with the SRS threshold power ~ 1 W [1]. The peak value of Brillouin gain occurs at about 10 GHz for the Brillouin Stokes shift but 13 THz for the Raman Stokes shift. Thus, the scattered light is downshifted in frequency by about 10 GHz for SBS but by about 13 THz for SRS. The Raman gain spectrum extends up to 30 THz; however,

the Brillouin gain spectrum is extremely narrow of about tens of MHz [2]. The first wave can be thought of as being a Raman pump wave that causes amplification of the Raman Stokes wave. As the Raman pump propagates in the fiber, it loses power and the Stokes wave gains power. However, In the a Raman amplifier, the Raman pump wave is a high-power wave, and the Raman Stokes wave is the signal wave is to be amplified at the expense of the pump wave power.

5.2 Basic Concepts of Stimulated Raman Scattering (SRS) and Raman Gain

Fig. 5.1 shows the Raman gain coefficient as a function of wavelength spacing in fused silica. The peak gain coefficient g_R is approximately 6×10^{-14} m/W at 1.55 μm, which is much smaller than the gain coefficient for SBS (6×10^{-11} m/W) [3]. However, channels up to 15 THz (125 nm) apart will be amplified effectively by SRS. Also SRS can be used in both the direction of signal propagation (forward) and the reverse direction (backward).

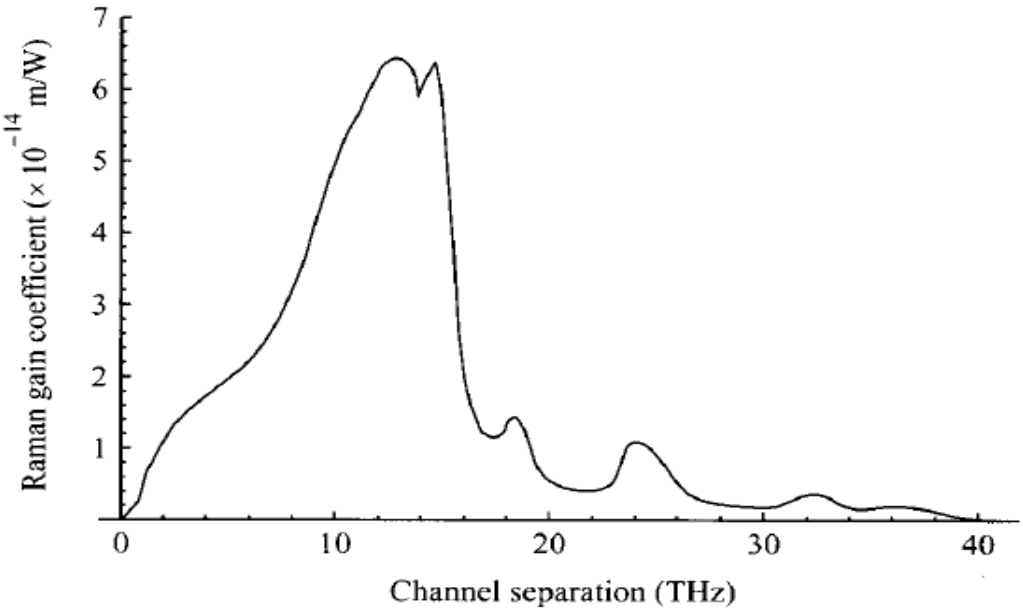

Fig. 5.1: Raman gain spectrum as a function of channel separation in fused silica [1].

SRS can also be detrimental in WDM systems in which the optical fiber acts as a Raman amplifier. In these systems, the long wavelength channels are amplified by the short-wavelength channels which are in the bandwidth of the Raman gain spectrum with the peak at 13 THz (~100 nm in 1550 nm wavelength region). Therefore, the shortest-wavelength channel in the Raman gain spectrum is the most depleted channel since it can pump simultaneously many channels placed in the Raman gain spectrum region. This phenomenon is known as Raman crosstalk which can degrade the performance of the optical systems and must be considered especially in WDM systems [4-8].

A quantum mechanical description of the SRS effect is depicted in Fig. 5.2. The incident photon loses its energy during the interaction with an optical phonon. Therefore, the molecule energy from the ground state with the energy level E1 rises to the virtual energy level E3. Spontaneously, the molecule decays to the vibrational state with the energy level E2 and a photon whose energy is (E3-E2) is emitted. Therefore, an optical phonon of energy (E2-E1) is remained and the frequency of the phonon is

$$\upsilon = (E2 - E1)/h \tag{5.1}$$

where h is the Plank's constant. This resonant frequency is about 13 THz for silica fibers as mentioned before. The conservation of energy requires that

$$\upsilon_P = \upsilon_S + \upsilon \tag{5.2}$$

where υ_P and υ_S denotes the frequency of the incident (pump) photon and the Stokes photon, respectively. The Raman gain spectrum has a nearly bandwidth 6 THz. As a result, E2 is a band of energy rather than a discrete line.

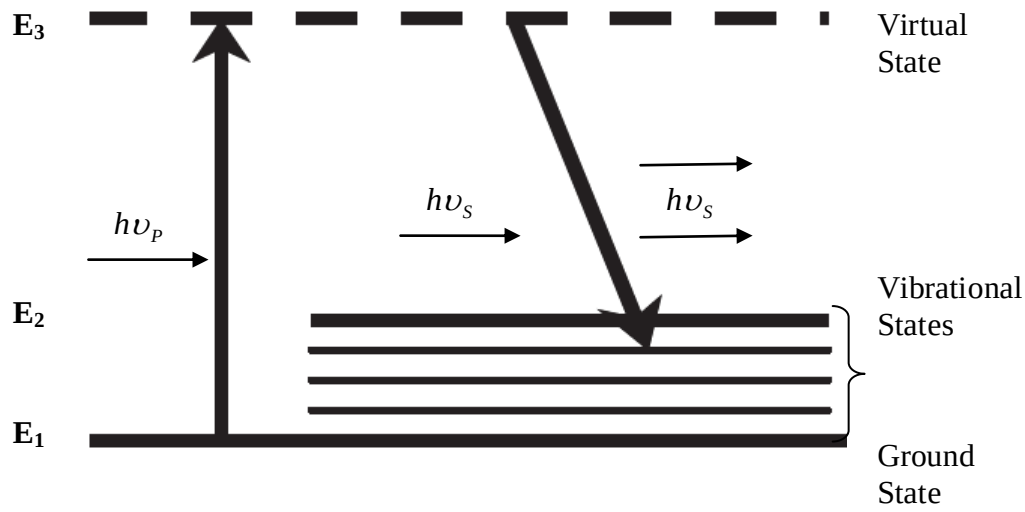

Fig. 5.2: Schematic of the energy levels of a molecule involved during stimulated Raman scattering (SRS).

Once the two waves (Raman pump and signal) are presented, the pump prepares the power for Raman amplification of the signal as shown in Fig. 5.2. The frequency of the pump and signal waves are supposed to be υ_P and υ_S, respectively. The excited molecule in the virtual state is stimulated by the signal to emit a photon of the same frequency and phase as the signal so that Raman amplification takes place. The main difference of a Raman amplifier and an EDFA is that population inversion which is not required for Raman amplification. In addition, the wavelength at which the Raman amplification takes place is determined by the wavelength of the Raman pump and the vibrational frequency of the molecule. As a result, Raman amplification can be operated at any wavelength as long as the suitable Raman pump is provided.

As EDFAs, Raman amplifiers can be pumped in the both direction forward and backward. Due to using high power Raman pumps and the typically small attenuation, Raman pump waves can propagate in a great distance along the fiber. Thus, the backward Raman pumping protects receivers from Raman pump waves.

Besides, the noise sources in Raman amplifiers are somewhat different from EDFAs. The Raman gain responds instantaneously to the Raman pump power. Therefore fluctuations in the Raman pump power, $P_P(z)$, causes the optical gain $g(z)$ to vary and will appear as Raman crosstalk to the desired signals. The optical gain $g(z)$ is related to the Raman gain as

$$g(z) = g_R \frac{P_P(z)}{A_{eff}} \tag{5.3}$$

In which A_{eff} is the effective area of the pump beam inside the fiber. The Raman gain is shown in Fig. 5.3 (a) against the amplifier length for forward and backward Raman pumping [9]. As shown in the figure, the average gain is slightly higher in forward Raman pumping. The solid and dashed lines correspond to copolarized and orthogonally polarized cases, respectively (the two lines are indistinguishable in the case of backward pumping). Physically, it takes some distance for the orthogonally polarized signal to be adjusted before it can experience the full Raman gain.

According to Eq. (5.3), it is also important to keep the pump at a constant power. However, this is not occur in EDFAs where the response time of the EDFA gain is on the order of milliseconds much slower than the Raman gain responds. On the other hand, having the pump propagates in the opposite direction to the signal (backward Raman pumping) reduces the Raman gain fluctuation due to the Raman pump fluctuation. This can be understood since fluctuations in Raman pump power are then averaged over the propagation time over the fiber in backward Raman pumping. In order to explain this, first suppose the case where the Raman pump propagates along with the signal in the same direction (forward Pumping). The two waves travel at nearly the same velocity. In this case, when the

pump power is high or low at the input, there is a high or low gain for the signal. However, in the backward Raman pumping, as the signal propagates through the fiber, whenever it overlaps with the pump signal in the high power state, it sees a high gain. When it overlaps with the pump signal in the low power state, it sees a lower gain. If the pump fluctuations are relatively fast compared to the propagation time of the signal across the fiber, the gain variations average out, and by the time the signal exits the fiber, it has seen only a constant optical gain. As shown in Fig. 5.3 (b) the fluctuation in signal under Raman amplification is higher in forward pumping in comparison to the backward pumping [9]. Another major concern in Raman amplifiers which can be solved by the backward Raman pumping is crosstalk between the WDM signals due to Raman amplification. A modulated signal at a specific wavelength depletes the pump power and imposes effectively the same modulation on the Raman pump signal. This modulation on the pump, in turn, affects the optical gain seen by the next wavelength effectively appearing as crosstalk on that wavelength. Again, having the backward pumping reduces this effect dramatically. For these reasons, most Raman amplifiers use backward or counterpropagating pump geometry.

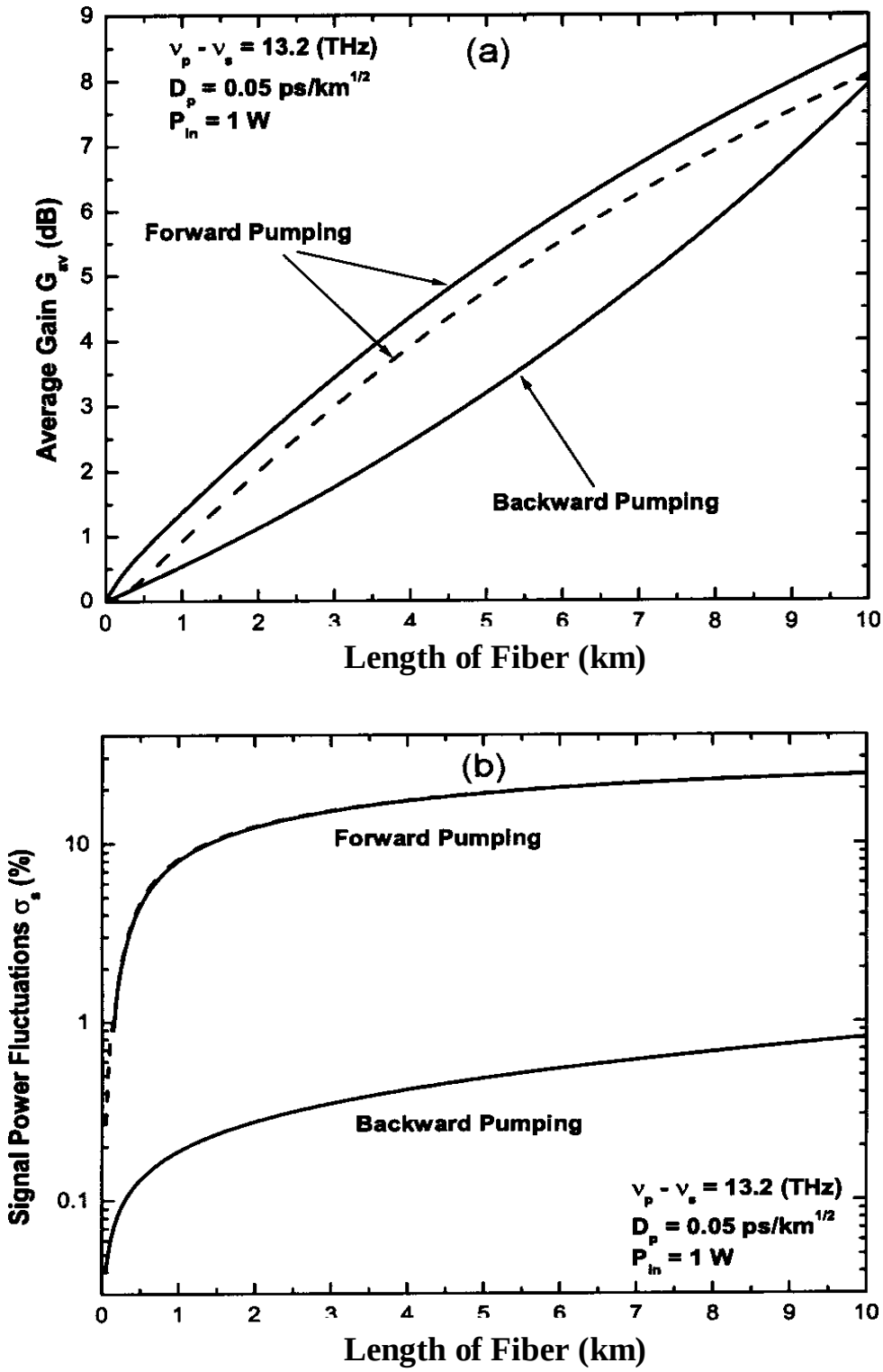

Fig. 5.3: (a) Average gain and (b) level of signal fluctuations as a function of amplifier length for a fiber with polarization-mode dispersion $D_P = 0.05\ ps/\sqrt{km}$. The solid and dashed curves correspond to the cases of copolarized and orthogonally polarized signal, respectively. The two carves are indistinguishable in the case of backward pumping and in forward pumping in (b). The two curves nearly coincide in the case of backward pumping [9].

In Eq. (5.3), the ratio g_R / A_{eff} is a measure indicating Raman-gain efficiency [10]. This ratio is depicted in Fig. 5.4 for the three fibers standard silica single-mode fiber (SMF), dispersion-shifted fiber (DSF), and dispersion-compensating fiber (DCF). As shown in Fig. 5.4, a DCF can be 8 times more efficient than SMF in Raman amplification due to the sufficient smaller core diameter of DCF. In addition, the frequency dependence of the Raman gain is nearly the same for all the three fibers as evident from the normalized gain profile in the figure. The gain bandwidth $\Delta\upsilon_g$ which is the full width at half maximum (FWHM) of the dominant peak is about 6 THz.

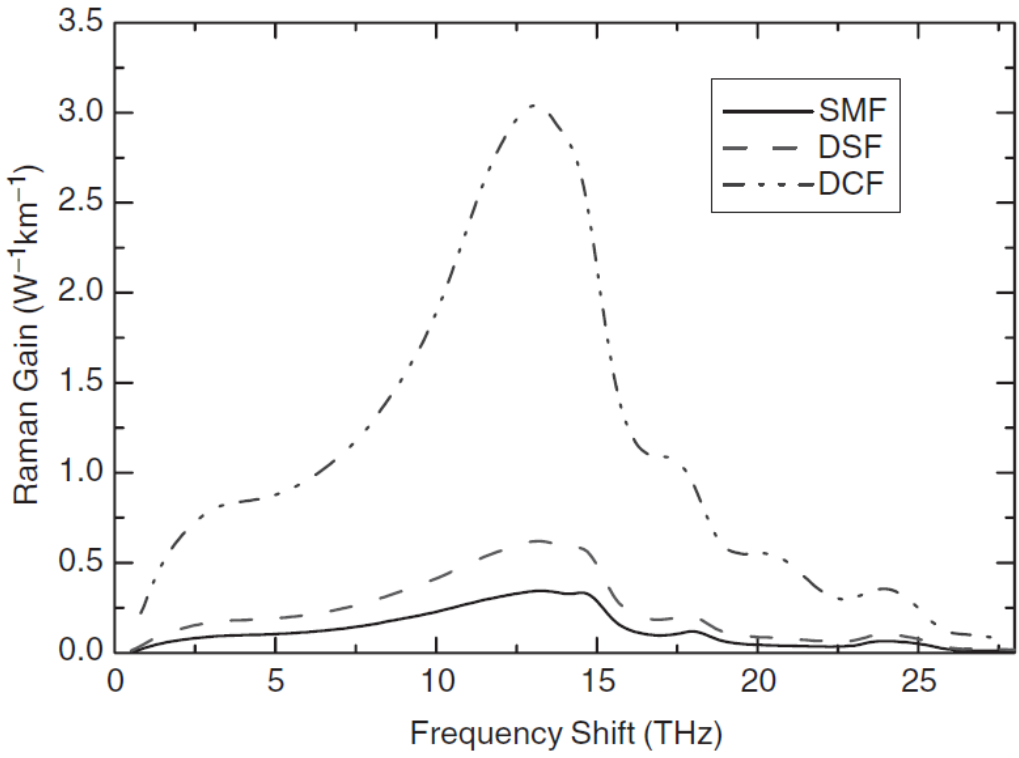

Fig. 5.4: Raman gain profiles (g_R / A_{eff}) for a 1510-nm Raman pump in three different fiber types, standard single mode fiber (SMF), dispersion shifted fiber (DSF), and dispersion compensating fiber (DCF) [10].

An interesting aspect of the Raman amplifiers is their large bandwidth that can be extended by using multiple Raman pump sources in various frequencies. This method can be extended to produce a broadband amplification operating a wavelength region grater than 100 nm, for example 1500 -1600 nm. The wide bandwidth of Raman amplifiers in comparison to the other optical amplifiers makes them attractive especially in optical transmission communication systems although a relatively high power Raman pump of about a few Watts is required to generate a high Raman amplification. In the following section, the theory of Raman amplifiers will be discussed.

5.3 The Theory of Raman Amplifiers

Nonlinear polarization vectors at the Raman Stokes and Raman pump frequencies (ω_S and ω_P) are proportional to products of the Raman Stokes and Raman pump fields that is $P_{NL}^{\omega s} = \left|E_2^{\omega p}\right|^2 E_1^{\omega s}$ and $P_{NL}^{\omega p} = \left|E_2^{\omega s}\right|^2 E_1^{\omega p}$. These relations are known as the Raman Stokes generation and the inverse Raman effect. In the similar way led to Eqs. (2.118) and (2.119), the following equations involving the Raman Stokes and Raman pump powers (P_S and P_P) can be deduced by substituting the two nonlinear polarization vectors into the fundamental wave equation Eq. (2.8) and by using the slowly varying envelope approximation (SVEA) introduced in Eq. (2.83) [11]

$$\xi \frac{dP_P}{dz} = -\alpha_P P_P - (\frac{\omega_P}{\omega_S})(\frac{g_R}{A_{eff}})P_P P_S \tag{5.4}$$

$$\frac{dP_S}{dz} = -\alpha_S P_S + (\frac{g_R}{A_{eff}})P_P P_S \tag{5.5}$$

where α_P and α_S denotes fiber losses for the Raman pump and Raman Stokes, respectively. $\xi = \pm 1$ depending on the pumping configuration; the plus and minus sign should be used in the forward and backward-pumping case, respectively. It is also supposed that the pump and the Stokes fields are copolarized. Equation (5.4) and (5.5) can not be readily solved analytically due to their nonlinear-coupled nature.

In the absence of the losses α_P and α_S, It can be easily indicated that

$$\frac{d}{dz}\left(\frac{P_S}{\omega_S} + \frac{P_P}{\omega_P}\right) = 0 \tag{5.6}$$

Therefore, total number of photons during the SRS process is constant in the absence of the losses. In many practical situations, pump power is so large compared with the signal power that pump depletion can be neglected.

In the absence of the fiber losses, Eq. (5.4) in the forward pumping ($\xi = +1$) results in

$$P_P(z) = P_P^0 \exp(-\alpha_P z) \tag{5.7}$$

where P_P^0 represents the input pump power of the optical fiber. By using Eqs. (5.5) and (5.7), it can be deduced

$$P_s(L) = P_S(z=0)\exp\left(g_R \frac{P_P^0}{A_{eff}} L_{eff} - \alpha_S L\right) \tag{5.8}$$

where L is the fiber length and L_{eff} is the effective length given by Eq. (2.60). Due to the fiber loss at the pump wavelength, the effective length of the Raman amplifier is less than the actual length of the optical fiber; indeed, $L_{eff} \approx 1/\alpha_P$ for a long fiber in which $\alpha_P L >> 1$. In our case, $\alpha_P \cong 0.192$ (dB/km) $= 0.0437$ (km)$^{-1}$. Therefore, regarding Eqs. (2.60) and

(2.61), $L_{eff} \cong 22.87\ km$. In the absence of Raman amplification ($g_R = 0$), the pump power is in the form

$$P_S(L) = P_S(z=0)\exp(-\alpha_S L) \tag{5.9}$$

Therefore, by using Eqs. (5.8) and (5.9), the amplifier gain can be obtained as

$$G_A = \frac{P_{S-ON}}{P_{S-OFF}} = \exp(g_R \frac{P_P^0}{A_{eff}} L_{eff}) = \exp(g_0 L) \tag{5.10}$$

where g_0 is the small-signal gain given by

$$g_0 = g_R(\frac{P_P^0}{A_{eff}})(\frac{L_{eff}}{L}) \approx \frac{g_R P_P^0}{A_{eff} L \alpha_P} \tag{5.11}$$

For a long fiber with the condition $\alpha_P L >> 1$, the amplification gain factor G_A is the fiber length independent.

The backward Raman pumping ($\xi = -1$) can be considered in a similar way. In this case, Eq. (5.4) can also be solved in the undepletion pump approximation. By using the boundary condition $P_P(L) = P_P^0$ the result is

$$P_P(z) = P_P^0 \exp(-\alpha_P(L-z)) \tag{5.12}$$

By using Eq. (5.12) and the integration of Eq. (5.5), the same solution as Eq. (5.8) will be obtained. It indicates that the amplified signal power at a given pumping level is the same in both the forward- and the backward-pumping configurations in the undepletion pump approximation. However, Fig 5.3 (a) shows, this approximation is not completely correct.

The case of bidirectional pumping can also be analyzed by considering that the pump power is the sum of the both forward and backward pump powers that is

$$P_P = P_P^F + P_P^B \tag{5.13}$$

since the two Raman laser pumps are located at the two opposite sides of the fiber. The pump power in the ignorable pump depletion will be obtained by solving the following equations

$$\frac{dP_P^F}{dz} = -\alpha_P P_P^F \tag{5.14}$$

$$\frac{dP_P^B}{dz} = -\alpha_P P_P^B \tag{5.15}$$

Thus, total pump power P_P is easily in the form as

$$P_P(z) = P_0[R\ \exp(-\alpha_P z) + (1-R)\exp(-\alpha_P(L-z))] \tag{5.16}$$

where P_0 is the total pump power lunched into the fiber from the both sides and R is the ratio of the forward power per the total lunched pump power

$$R = \frac{P_0^F}{P_0^F + P_0^B} \tag{5.17}$$

The amplifier gain G can also be deduced by using the Eq. (5.15) and (5.5).

The SBS behaviour in Raman-pumped fibers can also be studied by an approach similar to that used in the unpumped fibers [1], [12]:

$$\xi\frac{dP_{RP}}{dz} = -\alpha_{RP}P_{RP} - (\frac{\omega_{RP}}{\omega_S})(\frac{g_R}{A_{eff}})P_{RP}(P_{BS} + P_{BP})$$

$$\frac{dP_{BS}}{dz} = -(\frac{g_B}{A_{eff}})P_{BS}P_{BP} + \alpha_{BS}P_{BS} - (\frac{g_R}{A_{eff}})P_{BS}P_{RP}$$

$$\frac{dP_{BP}}{dz} = -(\frac{g_B}{A_{eff}})P_{BS}P_{BP} - \alpha_{BP}P_{BP} + (\frac{g_R}{A_{eff}})P_{BP}P_{RP} \tag{5.18}$$

where P_{PR}, P_{BP}, and P_{BS} represent , in turn, Raman pump power, Brillouin pump power, and Brillouin Stokes power. α_{BP}, α_{BS}, and α_{BP} also denote the attenuation coefficients of the optical fiber for the Raman pump, the Brillouin

Stokes, and Brillouin pump, respectively. g_B is the Brillouin gain in the fiber and all the other parameters are the same as Eqs. (5.4) and (5.5).

In the next chapter, we will discuss multiwavelength Brillouin-Raman fiber lasers by preparing a forward Raman pumping in a BFL ring cavity.

5.4 Generation of Multiwavelength Brillouin Raman Fiber Lasers

Homogeneous nature of gain medium (EDFA) limits the bandwidth and amplitude envelope profiles of the output MBEFL comb spectrum [13]. In addition, in order to provide cost effectiveness, good stability, and higher number of lines in multiwavelength Brillouin fiber lasers, a Raman amplifier can be used to generate multiwavelength Brillouin/Raman fiber laser (MBRFL) comb spectrum [13-16].

In this work, a multiple-wavelength Brillouin fiber laser (BFL) is demonstrated by the injection of intense light. This technique uses Raman gain in conjunction with Rayleigh scattering to help the Brillouin Stokes cascading process [19].

The experimental setup for the multiple-wavelength BFL is shown in Fig.5.5. The ring resonator is formed using a 3-dB coupler and a 25 km long single-mode fiber (SMF) as the gain medium. The SMF has a cut-off wavelength of 1161 nm, zero dispersion wavelength of 1315 nm and a mode field diameter of 9.36 μm. The BFL is pumped by the Brillouin laser pump (BP) which is an external cavity tunable laser source (TLS) with a maximum power of approximately 5.5 dBm. A wavelength division multiplexing coupler (WDM) is used to inject the 1465 nm intense light into the system to assist the cascading process. The power of the Raman pump laser diode is fixed at 150 mW.

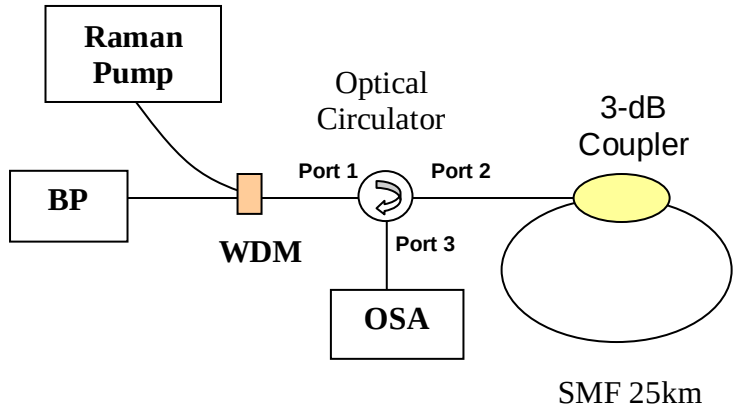

Fig. 5.5: Experimental set up for multiwavelength Brillouin Raman fiber laser generation [19].

The Brillouin pump (BP) is sent through the WDM (which is also used to inject the 1480nm intense light) and a 3-port circulator to generate backward-propagating path for stimulated Brillouin scattering (SBS). The backward-propagating SBS oscillates inside the ring produced by the 3-dB coupler and the 25 km SMF to generate the first Brillouin Stokes.The Stokes power is simultaneously amplified by Raman gain created through the forward injection of 1465 nm intense light in the SMF. The feedback by the Rayleigh scattering helps the cascading process to generate a higher order Stokes. The first Brillouin Stokes oscillating in the backward direction in the SMF generates the second Brillouin Stokes in forward direction when its power reaches the second Stokes threshold power. The other Stokes lines will be generated in the same way through the so-called Billouin cascading process. Four-wave mixing also causes fluctuation in the peak power of the lines. The multiwavelength laser output is characterized using an optical spectrum analyzer (OSA) which is located at port 3 of optical circulator.

Fig. 5.6 compares the output spectrum with and without the injection of intense Raman pump light. Without the injection of Raman pump, a 5.5 dBm BP produces one Brillouin Stokes with -6 dBm peak power. In spite of the fact that the threshold of first-order SBS in a SMF is very low, the generation of second order SBS is not usually achieved at the BP power 5.5 dBm. When there is no feedback, there are two factors that make the cascading process in SMF ineffective. First, as the pump power increases above the first-order threshold, the SBS power distribution inside the fiber becomes increasingly concentrated near the fiber input, subsequently decreasing the fiber length available for the SBS interaction. Second, in contrast to the first-order SBS process which is initiated using a monochromatic pump, second-order SBS is pumped by first-order Stokes radiation that is essentially non-monochromatic: its spectrum is only 4 times narrower than the SBS gain spectrum in the fiber [17]. The situation becomes very different in the presence of feedback to the SBS process that can cause considerable narrowing of the first-order SBS spectrum. Therefore second-order SBS generation can be observed with the feedback [18].

When 1465 nm Raman pump power is injected, the second and the third Stokes are generated. However, in the backward direction, the BP Rayleigh reflection and the second Stokes reflection can be observed as shown in Fig. 5.6. The second stokes Rayleigh reflection and the third Stokes are generated by the injection of the Raman pump with no significant changes in the output power of the first Stokes due to crosstalk phenomenon which transfers energy from the shortest wavelength to the longest one. The odd Stokes lines are observed in the backward direction whereas the transmitted Brillouin pump (BP) and even stokes

lines can be observed in the forward direction as it is obvious in the same setup in Fig. 3.22 [19].

The 1465 nm injection also increases the amplified spontaneous emission in the 1560 nm region due to Raman amplification. Rayleigh scattering (RS) occurring within the fiber can provide feedback to the SBS process to increase the Brillouin gain and help in the cascading process. This feedback provides very effective linewidth narrowing of the laser radiation creating the condition required for SBS. The growth of SBS in the ring resonator then causes a series of cascaded SBS processes leading to generation of higher order modes.

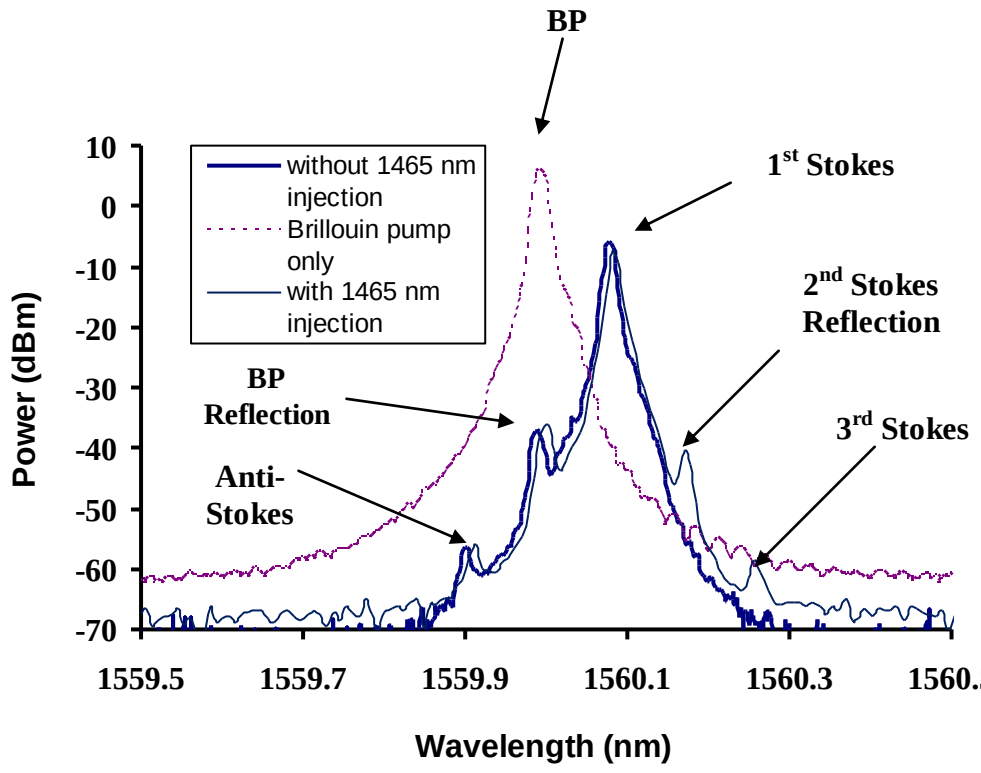

Fig. 5.6: Comparison of BFL output spectrum with and without the Raman pump light injection. The generation of the second Stokes reflection and the third Stokes after the injection Raman pump is obvious.

Fig. 5.7 shows the BFL output spectrum at different BP wavelengths. The BP and 1465 nm Raman pump powers are fixed at 5.5 dBm and 150mW respectively. There are no significant changes in power of the first Stokes as shown in the figure. However, the powers of higher-order Stokes are seen to be highest at a wavelength of 1560 nm due to the higher Raman gain in this wavelength. The number of Stokes is expected to be higher if the Raman pump power is higher or if we use a fiber such as dispersion compensating fiber (DCF) having higher Raman gain. The spacing between the lines is about 0.08 nm which is the Brillouin shift in the experiment, as measured by an optical spectrum analyzer with 0.015 nm resolution. Anti-Stokes line is also generated through degenerate four-wave mixing between the Brillouin pump and the first Stokes line as shown in Figs 5.6 and 5.7.

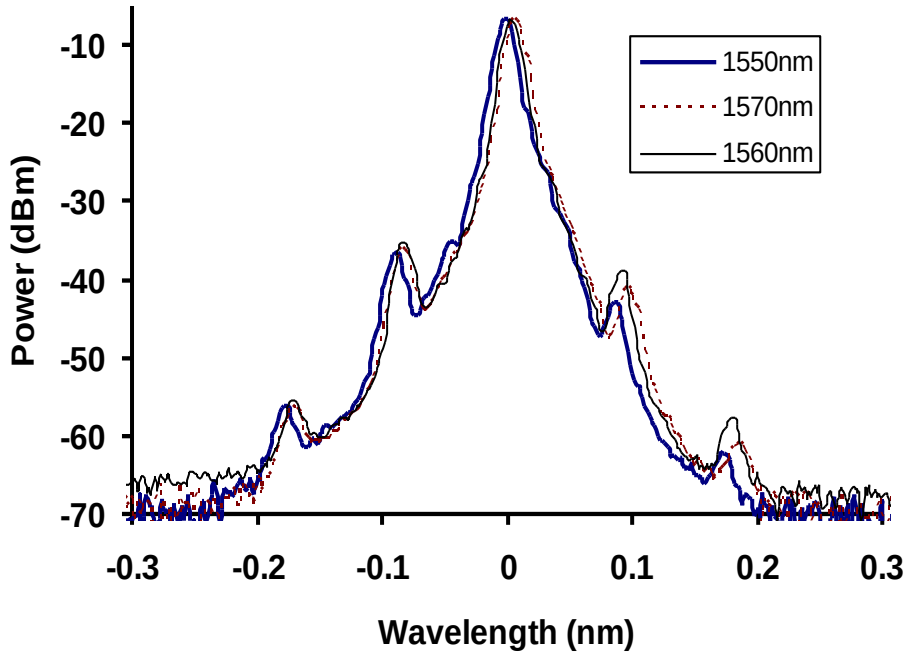

Fig. 5.7: The BFL output comb at different Brillouin pump wavelength of [19].

In this experiment, the effect of Forward Raman amplification on the cascading Brillouin Stokes generation has been studied [19]. In the following section, the effect of Raman amplification on Brillouin fiber lasers will be explained.

5.5 Effect of Raman Amplification on Brillouin Fiber Larers

Both stimulated Raman and Brillouin scattering are nonlinear phenomena that can affect to each other performance. SBS behaviour in optical fibers with Raman amplification has been studied [20-23].

In this thesis, the effects of the backward, forward, and bi-directional Raman gains on SBS performance in a linear cavity are studied. Here, we use linear cavity in order to use leftover Brillouin pump (BP) and Raman pump (RP) power after each transmission through a 25 km SMF used as a gain medium. The results show that the change in SBS threshold power is also interestingly related linearly to the total Raman gain appeared on SBS, and this relationship is independent of Raman pumping schemes. In addition, Raman amplification on the SBS is highly increased around the SBS threshold especially in the forward and bi-directional Raman pumping [24].

Fig. 5.8 shows the experimental setup, where a 25 km SMF used as a gain medium located between ports 2 of two optical circulators (OC1 and OC2) to form a linear cavity. A (2x2) 1/99 coupler located between Port 3 and Port 1 of OC1 helps to inject BP into the cavity, to send a feedback signal, and at the same time to extract part of output. The BP signal is performed using an external cavity tunable laser source (TLS) amplified by an erbium-doped fiber amplifier (EDFA) to obtain the maximum power of 13 dBm at wavelength of 1580 nm with linewidth of 15 MHz. The generated backward propagating Brillouin Stokes, and the transmitted BP signal reflected by OC2, are coupled from port 2 to 3 in the

circulator OC1 and 99% of that signal are re-injected back into the system. Wavelength-division multiplexing couplers WDM1 and WDM2 are used simultaneously to inject Raman pump light into the system in bi-directional Raman amplification. However, in order to decrease loss in the cavity, we remove WDM2 in the setup for forward Raman pumping and connect port 3 and Port1 of OC2 together. Similarly, WDM1 is removed for backward Raman pumping and BP is injected directly into the cavity through the 1/99 coupler. The SMF has a cut-off wavelength of 1161 nm with a zero dispersion wavelength of 1315 nm, a mode field diameter of 9.36 μm, and attenuation coefficient of 0.19 dB/km at 1580 nm.

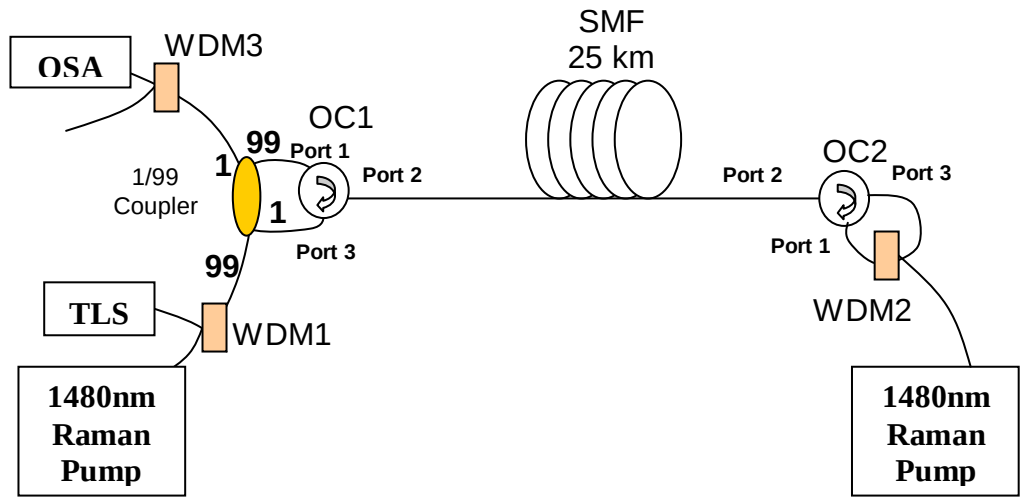

Fig. 5.8: Experimental setup for bi-directional Raman pumping. To decrease loss, WDM2 and WDM1 will be removed in the configuration for forward and backward Raman pumping, respectively [24].

The backward-propagating SBS is coupled out via the coupler and is characterized using an OSA with a resolution of 0.015 nm. The OSA is used instead of power

meter to avoid additional noises involved in this measurement. In addition, WDM3 is incorporated in front of the OSA to suppress the residual Raman pump light in the output.

The output Brillouin Stokes and transmitted BP power against input signal BP peak power are shown in Fig. 5.9 with and without 1480 nm RPs in various pumping schemes. Figs. 5.9(a), 5.9(b) and 5.9(c) represent backward, forward and bi-directional pumping respectively. Before transmitted BP power starts to saturate quickly around -5 dBm in these schemes, the output power of the SBS increases in accordance with an increase in the BP power. The SBS threshold power, P_{th}, is defined as the input BP power at which the transmitted BP peak power equals to the output peak power of the SBS. In the experiment, the RP power is varied from 0 to 150 mW. However, due to different loss in the Raman pumping schemes, SBS threshold is different in each scheme when RP power is off. It should also be noted that the SBS threshold power decreases as the Raman pump power is increased. The change in SBS threshold power (ΔSBS) induced by Raman amplification is examined and compared for different pumping schemes. It is maximum with the bi-directional and minimum with the backward Raman pumping scheme. ΔSBS is also proportional to the Raman pump power as shown in Fig. 5.9. The SBS threshold power is reduced by 2.5 dB, 1.75 dB, and 2.75 dB in the forward, backward, and bi-directional Raman amplifiers, respectively; by the same Raman pump power 150 mW at 1480 nm with the Brillouin pump wavelength 1580 nm.

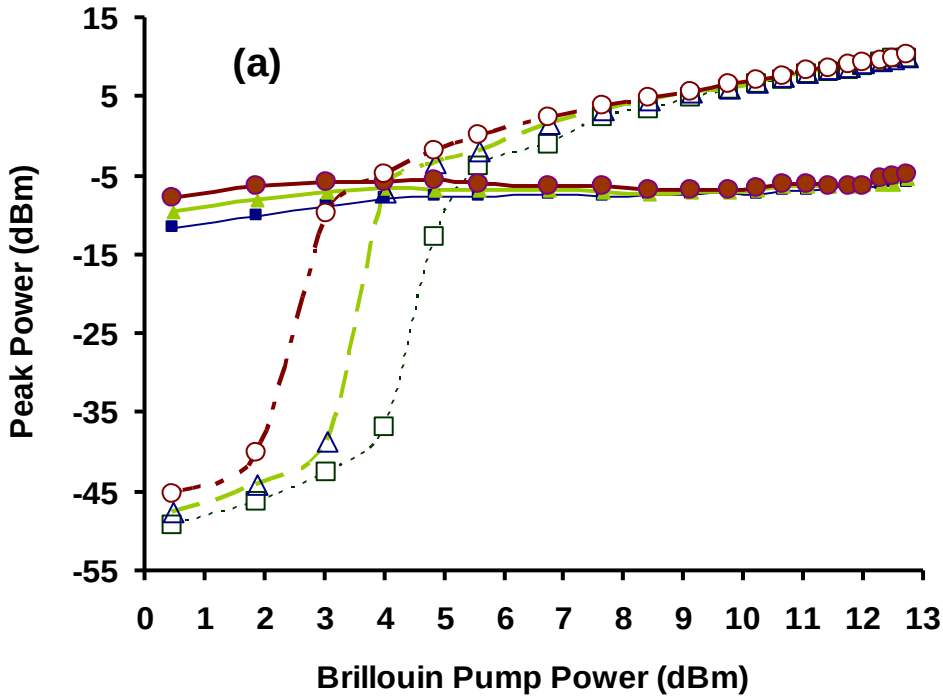
(a)
Peak Power (dBm)
15
5
-5
-15
-25
-35
-45
-55
0 1 2 3 4 5 6 7 8 9 10 11 12 13
Brillouin Pump Power (dBm)

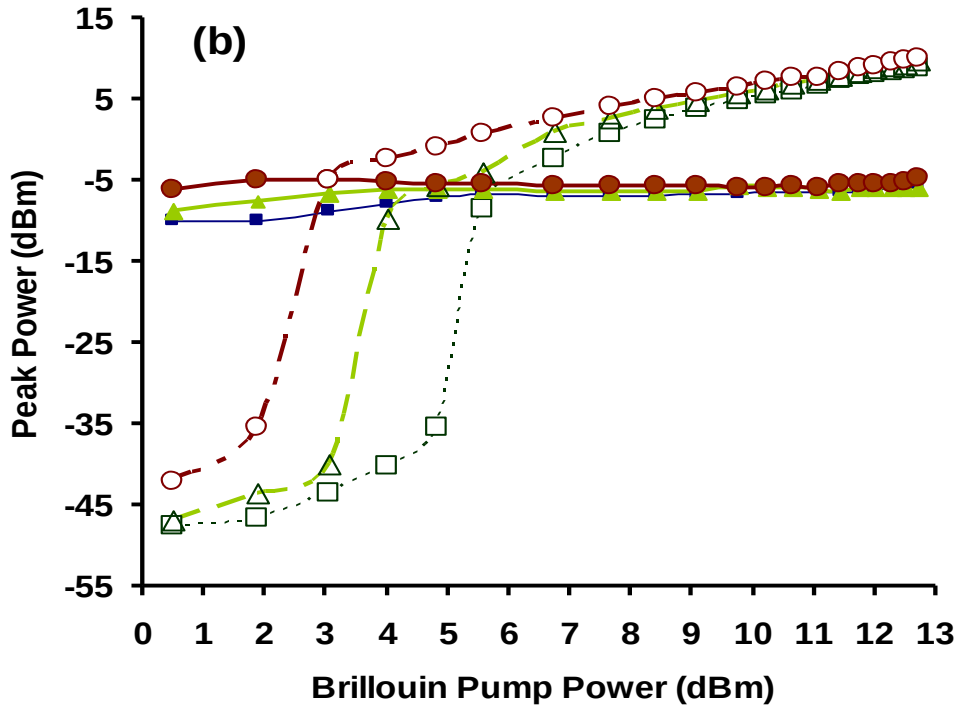
(b)
Peak Power (dBm)
15
5
-5
-15
-25
-35
-45
-55
0 1 2 3 4 5 6 7 8 9 10 11 12 13
Brillouin Pump Power (dBm)

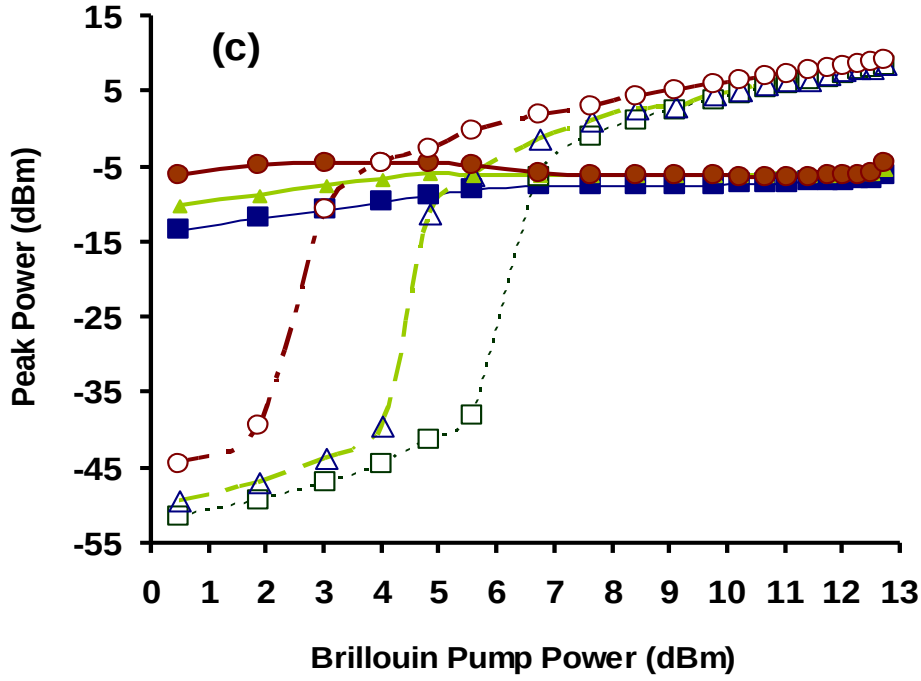

Fig. 5.9: Output transmitted BP power, solid lines, and Brillouin Stokes power, dashed lines, as a function of the input BP power in the case of (a) backward, (b) forward, and (c) bidirectional Raman pumping. The rectangles, triangles, and circles represent the cases where RP power is 0, 75, and 150mW, respectively [24].

In order to investigate further the effect of Raman amplification on SBS, we analyze the Raman on-off gain affected on Brillouin Stokes, as a function of the input peak power of BP signal as shown in Fig. 5.10 (a). As expected, a decrease in P_{th} is observed with increase in the Raman pump power, especially in the case of the forward and bi-directional Raman pumping schemes. However, around SBS threshold, the gain is also higher within a wider region for both the forward and bi-directional pumping schemes in comparison with the backward pumping scheme. The gain starts to show saturation with the appearance of the SBS and is eliminated completely beyond the SBS threshold power. Finally, the relationship between the change in the SBS threshold and Raman on-off gain on

Brillouin Stokes is shown in Fig. 5.10 (b). It is interesting that the relationship is simple and almost linear independent of the Raman pumping schemes.

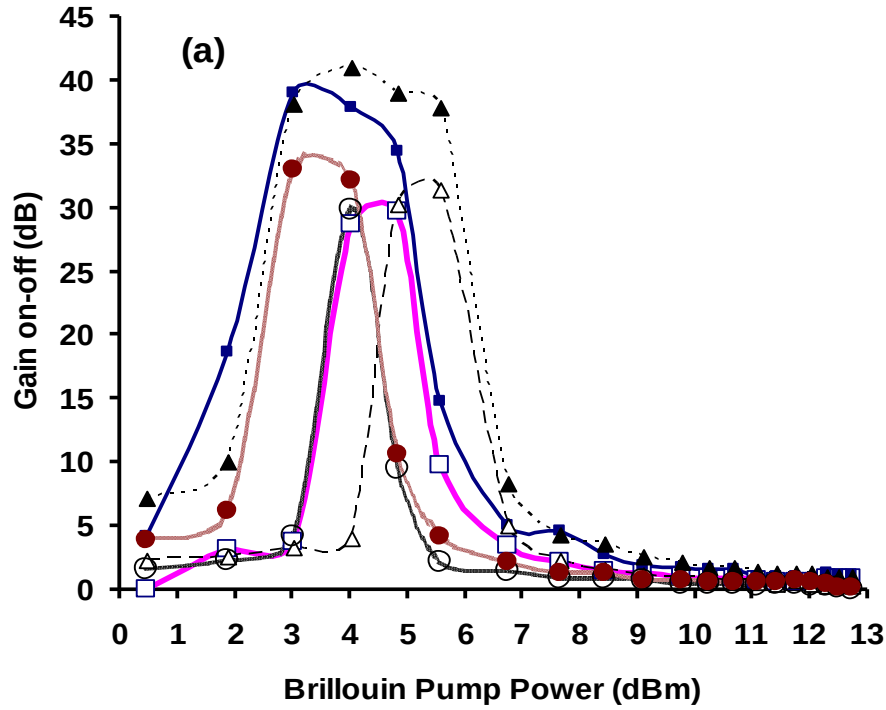

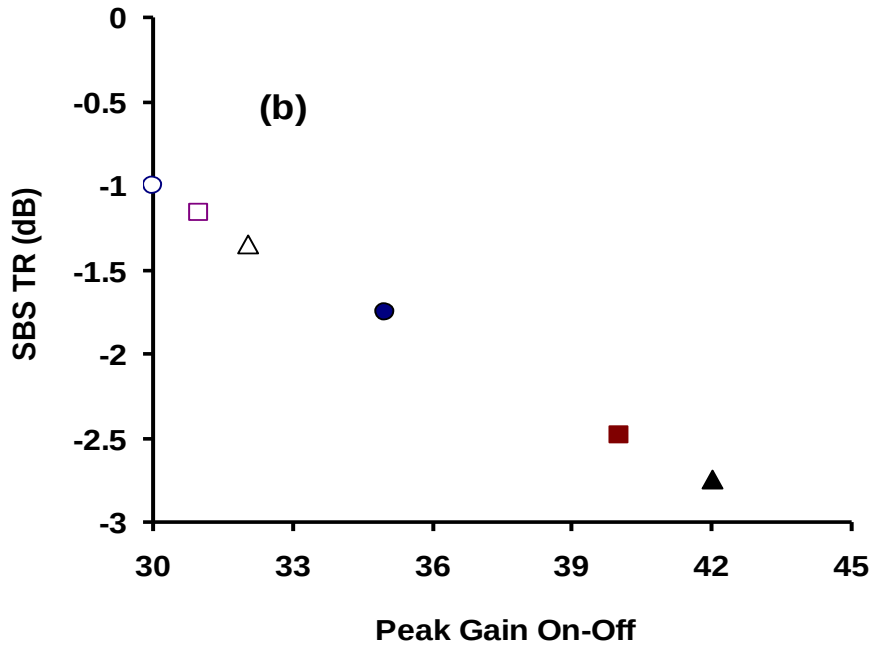

Fig. 5.10: (a) shows effect of Raman on–off gain on the peak power of Brillouin Stokes against various input BP and RP powers. SBS threshold reduction (SBS TR) against peak Raman on–off gain can also be deduced, as shown in (b). Different Raman pumping schemes are indicated by markers, i.e., backward (circle), bidirectional (triangle), and forward (square). Solid lines and solid markers represent RP power at 150 mW, whereas dashed lines and hollow markers represent RP power at 75 mW [24].

5.6 Summary

Raman amplifiers are able to provide multiwavelength Brillouin Raman fiber lasers (MBRFL). The line spacing is equal to the Brillouin shift which is about 0.08 nm. By using higher Raman pump and by choosing the Brillouin pump near the Raman peak gain, the peak power of MBRFL lines is higher. In addition, under different Raman pumping schemes, the reduction of the SBS threshold power is highest for the bi-directional Raman amplification and is the lowest for the backward Raman pumping scheme. The result shows that SBS threshold decreases with the increase of Raman gain affected on SBS and this decrease is

much faster for bi-directional and forward pumping than backward pumping. However, the amount of reduction depends strongly and solely on the Raman gain, independent of Raman pumping scheme.

References:

[1] R. G. Smith, "*Optical power handling capacity of low loss optical fibers as determined by stimulated Raman and Brillouin scattering*," Appl. Opt., Vol. 11, 1972, pp. 2489-2494.

[2] R. H. Stolen, E. P. Ippen, and A. R. Tynes, "*Raman oscillation in glass optical waveguide*," Appl. Phys. Lett., Vol. 20, 1972, pp. 62- 64.

[3] E. P. Ippen, and R. H. Stolen, "*Stimulated Brillouin Scattering in Optical Fibers*," Appl. Phys. Lett., Vol. 21, 1972, pp. 539-541.

[4] A. G. Grandpierre, D. N. Christodoulides, and J. Toulouse, "*Theory of Stimulated Raman Scattering Cancellation in Wavelength-Division-Multiplexed Systems via Spectral Inversion*," Photon. Technol. Lett., Vol. 11, 1999, pp. 1271-1273.

[5] K. P. Ho, "*Analysis of Homodyne Crosstalk in Optical Networks Using Gram–Charlier Series*," J. Lightwave Technol., Vol. 17, 1999, pp. 149-154.

[6] C. M. Mclntosh, A. G. Grandpierre, D. N. Christodoulides, J. Toulouse, and J. M. P. Delvaux, "*Eliminating SRS Channel Depletion in Massive WDM Systems via Optical Filtering Techniques*," Photon. Technol. Lett., Vol. 13, 2001, pp. 302-304.

[7] X. Zhou, and M. Brik, "*Performance limitation due to statistical Raman crosstalk in a WDM system with multiple-wavelength bidirectionally pumped Raman amplification*," J. Lightwave Technol., Vol. 21, 2003, pp. 2194-2202.

[8] T. Yamamato and S. Norimatsu, "*Statistical analysis on stimulated Raman crosstalk in dispersion-managed fiber links*," J. Lightwave Technol., Vol. 21, 2003, pp. 2229-2239.

[9] Q. Lin and G. P. Agrawal, "*Vector theory of stimulated Raman scattering and its application to fiber based Raman amplifiers*," J. Opt. Soc. Am. B., Vol. 20, 2003**,** pp. 1616-1631.

[10] S. Namiki and Y. Emori, "*Ultrabroad band Raman amplifiers pumped and gain-equalized by wavelength-division-multiplexed high-power laser diodes*," J. Sel. Topics Quantum Electron., Vol. 7, 2001, pp. 3-16.

[11] G. P. Agrawal, "*Nonlinear Fiber Optics*," 4th Ed., Academic Press, New York, 2007, ch.8.

[12] A. Kobyakov, M. Mehendale, M. Vasilyev, S. Tsuda, and A. F. Evans, "*Stimulated Brillouin scattering in Raman-pumped fibers: A Theroretical Approach*," J. Lightwave Technol., Vol. 20, 2002, pp.1635-1643.

[13] B. Min, P. Kim, and N. Park, "*Flat Amplitude Equal Spacing 798-Channel Rayleigh-Assisted Brillouin/Raman Multiwavelength Comb Generation in Dispersion Compensating Fiber*," Photon. Technol. Lett., Vol. 13, 2001, pp. 1352-1354.

[14] K. D. Park, B. Min, P. Kim, N. Park, J. H. Lee, J. S. Chang, "*Dynamics of cascaded Brillouin-Rayliegh scattering in a distributed fiber Raman amplifier*," Opt. Lett., Vol. 27, 2002, pp. 155-157.

[15] A. K. Zamzuri, M. A. Mahdi, A. Ahmad, M. I. Md Ali, and M. H. Al-Mansoori, "*Flat amplitude multiwavelength Brillouin-Raman comb fiber laser in Rayleigh-scattering-enhanced linear cavity*," Opt. Express, Vol. 15, 2007, pp. 3000-3005.

[16] Y. G. Liu, and D. Wang, "*Wavelength tunable and amplitude-equilibrium dual-wavelength lasing sources with dual-pass Raman/Brillouin amplification configuration*," Opt. Express, Vol. 16, 2008, pp. 3583-3588.

[17] A. A. Fotiadi, R. Kiyan, O. Deparis, P. Megret, and M. Blondel, "*Statistical properties of stimulated Brillouin scattering in single-mode optical fibers above threshold*,"Opt. lett., Vol. 27, 2002, pp. 83-85.

[18] Randoux ,S.; Lecoeuche, V.; Segard, B. and Zemmouri, "*Dynamical behavior of a Brillouin fiber ring laser emitting two Stokes components*," J. Phys. Rev. A, Vol. 52, 1995, pp. 2327-2334.

[19] S.W. Harun, M.R. Shirazi, and H. Ahmad, "*Multiple wavelength Brillouin fiber laser from injection of intense signal light*," Laser Phys. Lett., Vol. 4, 2007, pp. 678-680.

[20] T. Okuno and M. Nishimura, "*Effect of stimulated Raman amplification in optical fibre on stimulated Brillouin scattering threshold power*," Electron. Lett. Vol. 38, 2002, pp. 14-16.

[21] M. Mehendale, A. Kobyakov, M. Vasilyev, S. Tsuda and A. F. Evans, "*Effect of Raman amplification on stimulated Brillouin scattering threshold in dispersion compensating fibres*," Electron. Lett., Vol. 38, 2002, pp. 268-269.

[22] R. Engelorecht, M. Bayer, L. P. Schmidt, "*Numerical calculation of stimulated Brillouin scattering and its suppression in Raman fiber amplifiers*," IEEE proceeding conference, Laser and Electro-Optics Euro, CLEO/ Euro, 2003, p. 641.

[23] G. Ravet. A. F. Fotiadi, M. Blondel, P. Megret, "*Suppression of stimulated Brillouin scattering with a Raman fiber amplifier*," IEEE/LEOS proceeding Symposium Benelux Chapter, 2004, pp. 199-202.

[24] M. R. Shirazi, M. Biglary, S. W. Harun, K. Thambiratnam, and H. Ahmad, "*Effects of different Raman pumping schemes on stimulated Brillouin scattering in a linear cavity*," Appl. Opt., Vol. 47, 2008, pp.3088-3091.

Chapter 6:

Conclusion and Future Works

In this chapter, we summarize all the presented works done to generate multiwavelength Brillouin fiber laser sources. Then, some suggestions for future works will also be presented.

6.3 Conclusion

At first, the work is focused on increasing power conversion from the input Brillouin pump (BP) to the backward-propagating Brillouin fiber lasers (BFLs) to generate high power BFLs in ring and linear cavities. Due to the reduction of loss in the proposed ring cavity, the generated BFL has a peak power which is 5.7 dB higher than that one produced in the conventional ring cavity by using the same components and the same BP power. The BFL generation in linear cavities is also mentioned with fiber Bragg gratings (FBGs) and optical circulators (OCs) where Ports 3 and 1 are connected to each other so that the OCs can reflect the wave injected in Port 2.

In linear cavities, although some researches have been done on producing high power BFLs, the generated Brillouin peak power is lower than the transmitted BP peak power. In other words, the energy conversion from the BP to the generated BFL is low as a problem in the reported literatures. In this work, after reviewing the conventional BFL linear cavities, we try to solve the problem. In the proposed linear cavity, even though the second Brillouin Stokes has been generated, the generated BFL peak power is higher than the transmitted Brillouin

laser pump peak power. Indeed, considering the Brillouin Pump in the output, the generated spectrum is a dual–wavelength fiber laser source with the channel spacing 0.08 nm. The BFL peak power generated in the proposed linear cavity is 12.3 dB higher than the BFL peak power in the conventional one using the same input Brillouin laser pump with the peak power 14.4 dBm.

MBFLs are also demonstrated by using ring and linear cavities as an application of BFLs. More than 14 and 9 BFL lines are demonstrated in the ring and linear cavities, respectively. In the ring cavity, the both wavelength spacing 0.08 nm (~10 GHz) and 0.16 nm (~20 GHz) can be obtained with the bi-directional multi-wavelength generation. The transmitted BP and even Stokes are propagating in the forward direction whereas the odd Stokes are in the backward direction. The consecutive odd and even Stokes have the wavelength spacing 0.16 nm. The combination of the forward and backward direction generates MBFL with the 0.08 nm wavelength spacing. In the linear cavity, however, only the wavelength spacing 0.08 nm (~10 GHz) is obtained. In addition, the peak powers of lines in the linear cavity are more comparable and the generated comb is more flat than that obtained in the ring cavity. The generated MBFLs are suitable for some applications such as optical sensors. Since BFLs are very coherent light sources with ultra-narrow linewidths, BFLs have also been used in various applications such as microwave generation and gyroscopes.

In this work, the BFL linewidth is also measured using the heterodyne method. BFL linewidth measurements have been a challenge due to the ultra-narrow BFL linewidth. In addition, BFLs can be used for laser linewidth measurement due to their ultranarrow linewidth. The tunable laser source (TLS) linewidth measurement is done using an independent Brillouin fiber ring laser

(BFRL) in the heterodyne configuration. The BFRL is generated in a conventional ring cavity by using a TLS in the narrow linewidth setting. In the heterodyne configuration, the BFRL is emitted as the local oscillator or the continuous wave to measure the linewidths of an independent TLS in the narrow and wide linewidth settings. It is revealed that the TLS has the linewidth values of 15 MHz and 124 MHz in the narrow and wide linewidth settings, respectively. In the same configuration, the BFRL linewidths are determined to be 8 Hz and 24 Hz by using two uncorrelated BFRLs generated by a BP linewidth of 15 MHz and 124 MHz, respectively. The measured BFL linewidths are in the range of a few hertz as expected.

In order to increase number of lines in MBFLs, we use a Bismuth based Erbium doped fiber amplifier (Bi-EDFA) in the linear cavity. More than 50 of lines have been generated only by using 2.15 m Bi-EDF in the proposed linear cavity. The applied Brillouin pump and Bi-EDFA pump are 5 dBm, and 120 mW, respectively. The resulted MBFL can operate in the C band and the L band wavelength region due to the wider operational wavelength of the Bi-EDF in comparison with the traditional MBEFL. In addition, the generated comb of MBEFL is more flat.

MBEFls cannot be generated in any wavelength due to the limited operational wavelength of EDFAs in the C and L band wavelength regions. Therefore, in order to generate a multiwavelength at any wavelength, a Raman amplifier is used instead of an EDFA in a MBFL cavity. The other method to generate a multiwavelength laser source, a Raman amplifier is prepared in the cavity to increase number of lines. Here, in a ring cavity, we injected the Raman pump power 150 mW in the same direction as the Brillouin pump through the

single-mode fiber. Therefore, the SMF operate simultaneously as the Brillouin and Raman gain medium to preparing the Raman gain for amplifying the Brillouin Stokes and to increase number of lines. By using 150 mW Raman pump power and 5.5 dBm Brillouin pump power, only the second and the third Brillouin Stokes are generated in the resulted multiwavelength Brillouin Raman fiber laser (MBRFL). The used SMF and the Brillouin and Raman pumps are according to our available components. In spite of the MBEFL and MBRFL generation, MBFLs have the benefit that they can be generated in any wavelength by using a simple cavity configuration as soon as only the BP power is available.

The interaction between Raman amplification and stimulated Brillouin scattering is also investigated in the last part of this thesis. The results show that the reduction in the SBS threshold power occurs under different Raman pumping schemes in a linear cavity with 25km SMF. The SBS threshold decreases with the increase of Raman-gain On-Off and this decrease is much faster for bi-directional and forward pumping than for backward pumping due to the lower Raman gain at this Raman pumping scheme. It is revealed that the amount of SBS threshold reduction depends strongly and solely on the gain effect on it, independent of Raman pumping scheme.

6.4 Future Works

For future works, the theoretical understanding on high efficiency BFL is required towards further improvement of the proposed linear cavity BFL. This understanding should also focus particularly on the four-wave mixing and the initial noise on the BFL which seems to be important factors in generating a stable BFL. By using a polarization controller (PC) in MBFL generation, the number of lines is expected to be increased since the evolution of the polarization state of the

Brillouin Stokes wave becomes self-consistent which is an important requirement for effective Brillouin fiber laser.

Compact devices for MBEFL generation can be realized with the existence of highly non-linear fibers such as holey fibers instead of SMF, a more compact BEFL can be designed using the proposed configuration. Using higher Raman pumps and fibers having higher Raman gain such as DCF, the proposed method for generating MBRLs can be used to produce multiwavelength laser source at any wavelength as long as the Raman and Brillouin pump are available.

The theoretical work is required for the understanding of the reduction in the SBS threshold power under different Raman pumping schemes in a cavity BFL. Why the amount of SBS threshold reduction depends strongly and solely on the Raman gain seems to be a challenging theoretical work. Having a lot of experimental information about the Brillouin pump linewidth and the generated BFL linewidth, it seems that further theoretical work is also necessary to be done on the BFL linewidth and its dependence to the BP linewidth.

As an active area of research in nonlinear fiber optics, it seems that BFLs, MBFLs, MBEFLs, and MBRFLs remain as an important issue of the future.

General Characteristics

Optical sources such as fiber lasers can be evaluated based on a number of characteristics which are briefly introduced here as the basis of most of the theoretical and experimental works that are carried out in the subsequent chapters. These characteristics include output power, operational wavelength, spectral linewidth, finesse, modulation bandwidth, stability, threshold, efficiency and side mode suppression ratio (SMSR) or the signal to noise ratio (SNR) as will be discussed in what is to follow.

A.1 Output Power

The most important characteristic of an optical source especially in nonlinear optics is its output power. In both linear and nonlinear optics, it is useful to express received power I (and also the transmitted power for all components) in decibel units defined as

$$I \text{ (in dBm)} = 10 \, \text{Log}_{10} \, I \text{ (in mW)} \qquad \text{(A.1)}$$

The letter m in dBm is a reminder of the reference level of 1 mW chosen for convenience. In this decibel scale for the absolute power, 1 mW corresponds to 0 dBm, whereas powers less than 1 mW are expressed as negative numbers. The amount of power required depends on the applications. In fiber optics communications for example, the launched power is normally less than a few miliwatts due to SBS generation [1] whereas large powers are used commonly in experiments on nonlinear fiber optics. Higher power optical sources are now available at reasonable prices; however, the maximum optical power is limited by

a few factors, such as nonlinear phenomena (scattering especially SBS as cited before), the damage threshold of the components and the safety of the users. The damage threshold power of components must be considered particularly when amplifiers are used. For example, damage to the connector's ferrule has been reported to occur at a source power of about 16 dBm [2].

A.2 Operational Wavelength

At the time of writing, the 1550 nm wavelength is the most widely used wavelength since the minimum loss of single-mode fibers is about 0.2 dB/km near 1550 nm as shown in Fig A.1. The advantage of using a single-mode optical fiber is that this type of fiber has less internal (Rayleigh) scattering in comparison to multimode optical fibers. A secondary minimum less than 0.35 dB/km occurs near the 1310nm wavelength region. Note that the peak near 1.4 μm and a smaller peak near 1.23 μm seen in Fig. A.1 occur due to absorption caused by hydroxyl (OH) impurities or residual water vapour in the silica fiber [1]. Therefore, it is only logical that the operational wavelength of most commercial optical components and also optical sources to be near 1550 nm. However, in special works such as Erbium and Ytterbium optical amplifiers where we have to use other wavelengths of 980 nm and 1060 nm respectively, optical sources and optical components suitable in these regions of operational wavelengths should be made available.

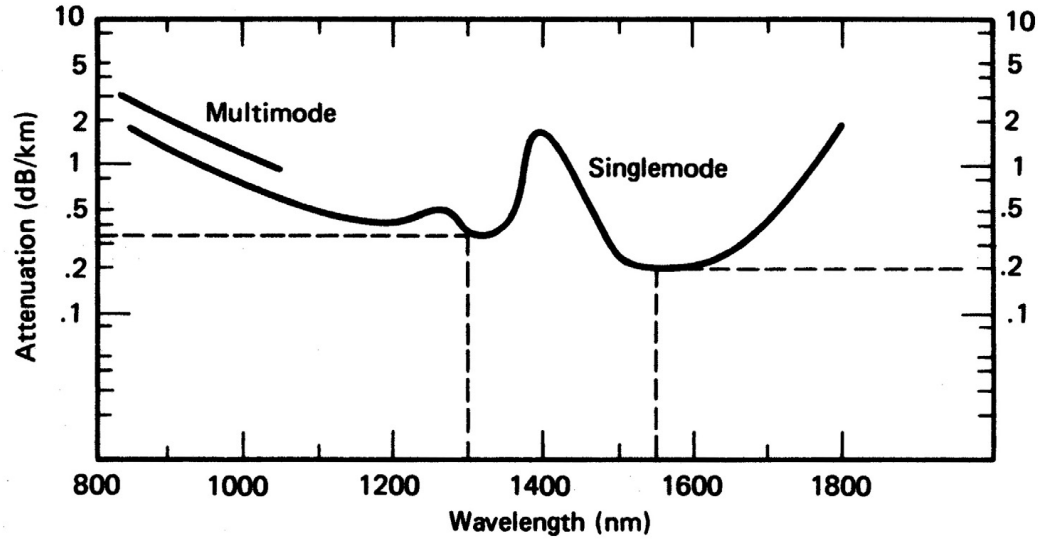

Fig. A.1: Fiber attenuation as a function of wavelength for standard single-mode optical fiber [1].

A.3 Linewidth

Linewidth is defined as the full width at half maximum (FWHM) of a power spectrum. In the decibel scale, it is equal to the width of the spectrum at -3 dB of the maximum power. In nonlinear optics, SBS threshold power depends on the linewidth or spectral width of the source or pump power; in other words, the SBS threshold increases when the spectral width of the pump power increases with the condition that the spectral width of the pump is much greater than the spectral width of the Brillouin gain spectrum [3]. In optical fiber communication systems, the smaller the spectral width, the better the condition for communication; however, this requirement is reversed in sensor systems. That's to say, a smaller spectral width source contributes to a smaller material dispersion in a silica fiber optics, so that a broader bandwidth is allowed in optical communication [4]. In contrast, the smaller spectral width in a sensor system contributes to a higher coherent noise [5]. The coherent noise is not a factor in optical communication because the transmission distance is long enough that the coherency noise is lost.

In chapter 4, we discuss the method used in this work to measure the ultra-narrow BFL linewidth which is reported from to be in the range of a few Hz to a few kHz.

A.4 Threshold Power

The minimum amount of pump power required for a laser source to begin lasing is defined as the threshold power. When the pump power is below the threshold power, the output power of the laser source is incoherent and spontaneous. Pumping above the threshold results in a narrowing of the spectral width. Lower lasing threshold is preferred for a laser source since lower optical pump power consumption is required. In an optical transmission system, however, to increase the transmission distance by using a high-input power requires the SBS threshold to be increased. In a cavity, a low threshold power requires low cavity losses and high gain efficiency. The question of what values are most appropriate for the threshold pump power is one of the fundamental issues of laser design. The threshold can be characterized by three phenomena; the sudden increment in power, the significant reduction in the spectral width, and the clamping of the amplified spontaneous emission (ASE) level.

A.5 Finesse

The spectral width $\delta\upsilon$ of each mode in a cavity can be given by:

$$\delta\upsilon = \frac{\Delta\upsilon}{\mathrm{F}} \tag{A.2}$$

where $\Delta\upsilon$, the free spectrum range, is the separation between modes in the frequency domain and F is referred to as the finesse of the cavity. The greater the

finesse, the sharper the bands of transmitted frequency are relative to their separation. For a conventional Fabry-Perot cavity, $\Delta\upsilon$ is readily calculated as:

$$\Delta\upsilon = \frac{c}{2nL} \tag{A.3}$$

where c is the speed of light in vacuum, n is the refraction index of the medium in the cavity and L is the cavity length. The factor 2 will be omitted in a ring cavity with the same length L. In addition, F is determined by the following equation:

$$F = \frac{\pi(Re^{-\alpha L})}{1 - Re^{-\alpha L}} \tag{A.4}$$

in which $R = \sqrt{R_1 R_2}$ is the geometric mean of the two mirror irradiance reflectivities and α is the internal power loss coefficient.

A.6 Modulation Bandwidth

Optical data modulation involves the conversion of an electrical data signal into an optical data signal by using the electrical data to temporally alter one or more physical properties of the optical signal. The intensity, phase and frequency of the optical signal can all be altered in this way [6]. Semiconductor laser diodes as an example of optical sources can be directly modulated through their driving currents. However, fiber lasers can only be externally modulated for high speed external modulation due to its long atomic carrier lifetime [7]. This characteristic however, is not covered in this study as we are only concentrating on the device study rather than the transmission where the modulation rate is extremely important.

A.7 Laser Stability

Laser stability is one of the important elements for a laser source and sensor applications. It refers to the temporal stability of the peak power and wavelength of the laser source in the condition that variation in the peak power and the wavelength of the laser source is minimized. Many factors influence a source's stability, such as temperature, pump condition and the gain dynamics. On the other hand, the stability of a BFL depends on the Brillouin pump power level, polarization control, total laser cavity length, temperature and the output coupling ratio [8]. By improving these parameters and especially applying a polarization controller, we can improve the BFL stability. In addition, semiconductor laser diodes are very much temperature dependent whereas fiber lasers are less severely affected [9].

A.8 Slope Efficiency

An important characteristic of a pumped laser source is its slope efficiency, also called differential efficiency. It is obtained by plotting the laser output power against the input pump power. The plotting curve is usually close to a straight line above the threshold power and the slope efficiency is the slope of this line. This characteristic is due to the same optical loss for all input powers in a cavity. However, the curve may be nonlinear especially for high power lasers, typically with lower slope at high input powers.

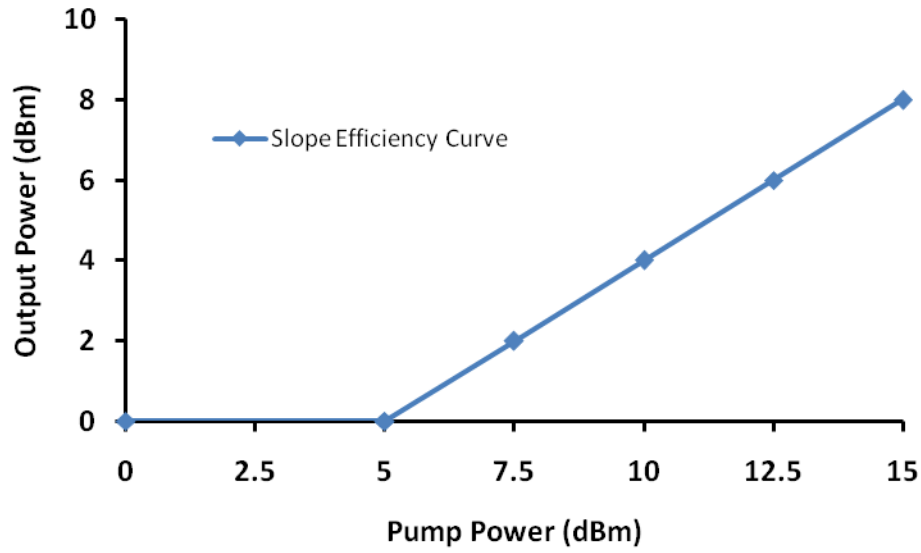

Fig. A.2: Output power versus input pump power for an optical pumped laser. It shows that the threshold pump power is 5 W, and the slope efficiency is 80%.

For an optical laser source, efficiency represents the ratio of the lasing output power over the pump power, in other words, the conversion of the pump energy to the lasing energy. For example, efficiency of a BFL system has been reported to be about 80%. This value can be obtained from the slope of the transfer characteristic curve as shown in Fig. A.2. Efficiency is also being used to refer to the power launching or power coupling efficiency between the source and the input end of the fiber. The direct (without lenses) coupling efficiency for the LD is about 30% however, fiber lasers have the best coupling efficiency of more than 97% [10].

There are still some lingering questions about efficiency. Why is the efficiency of most lasers limited to values of anything from 0.1% to 30%? What are the limiting factors? What are some ways presently being researched to increase efficiency? In this work, we are going to increase the efficiency in a linear cavity BFL generation which will be discussed in chapter 3.

A.9 Side Mode Suppression Ratio (SMSR)

An expression of the quality of a single-mode laser is the SMSR defined as the difference in amplitude between the main spectral mode to the most dominant side mode. A source is more generally characterized by the SMSR, however, SMSR can be confused with the signal to noise ratio, SNR [11]. SNR actually refers to the ratio between the peak signal point and the noise level shown in Fig. A.3.

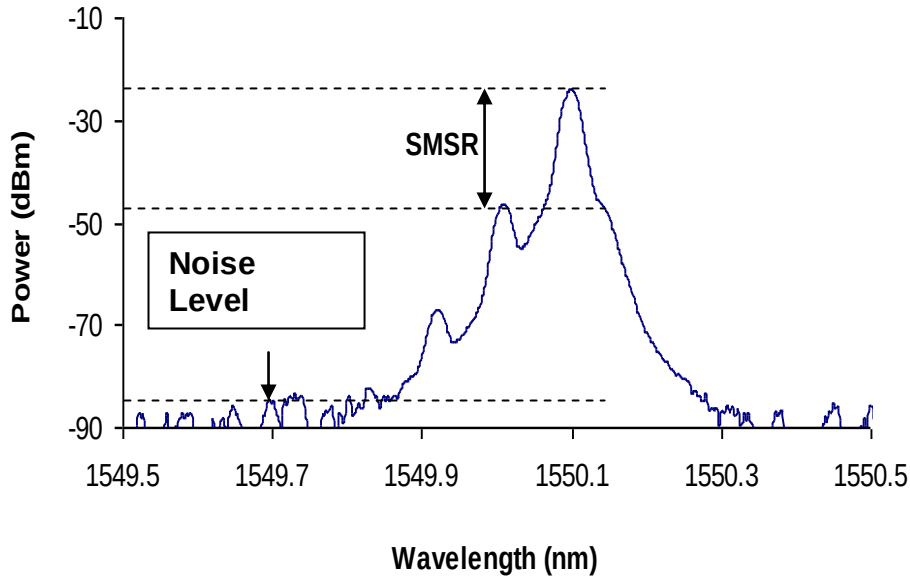

Fig. A.3: Definition of the SMSR and SNR in BFL generation at about 1550.1 nm with a Brillouin pump at approximately 1550 nm.

A.10 Noise Figure

A measure of the noise characteristic of an amplifier is the noise figure (F). It is defined by the ratio of the input signal to noise (S/N) ratio to the output S/N ratio as

$$F = \frac{(S/N)_{INPUT}}{(S/N)_{OUTPUT}} \tag{A.5}$$

It is a factor of the degradation in the signal under the amplification. Amplification increases the signal power to a suitable level; however, it degrades the information of the signal. The amplifier's noise figure is often express in the decibel unit as

$$F_{dB} = LogF \tag{A.6}$$

All amplifiers show noise figure more than unity ($F_{dB} > 0$). Thus, they diminish the signal quality. Nevertheless, optical amplification improves the signal performance when it is compared with that of systems in which the receiver amplifies the signal electrically after the detection. Typically, semiconductor optical amplifiers have the poorest noise figure of about 8 dB, EDFAs have the noise figure around 5-6 dB whereas good Raman amplifiers have noise figures less than 4.5 dB.

A.11 Single-Mode Optical Fibers

In order to eliminate intermodal dispersion, single-mode fibers are proposed in the 1.3 μm wavelength band around the year 1984. Single-mode fiber has a relatively small core diameter of about 8 to 10 μm, which is a small multiple of the operating wavelength range of the light signal. This forces all the energy in a light signal to travel in the form of a single mode. Single-mode optical fibers are preferred for long haul, large bandwidth and for using with integrated optic components. However, single-mode fibers are not completely single mode since they can simultaneously support two modes of orthogonal polarizations corresponding to the fundamental mode HE_{11} (LP_{01}) [11]. In addition, these two orthogonally polarized modes are degenerate under ideal conditions because they have the same propagation constant. In practice, however, this degeneracy breaks

slightly due to some irregularities such as random variations in the core shape and its size along the length of the fiber. This mixes randomly the two polarization components, and scrambles the polarization of the incident light as it propagates through the single-mode fiber. Nevertheless, for some applications, it is required that fibers maintain state of polarization for transmission light. Such fibers called polarization-maintaining fibers (PMFs) or polarization-preserving fibers do this requirement [12]. Random fluctuations in the core shape and size of the PMFs are not the governing parameters in state of polarization in these fibers since such fibers can preserve the linear polarization if the light is launched with its polarization along one of the principal axes of the fiber.

References for Appendix A

[1] G. P. Agrawal, *Fiber-Optics Communication Systems*, 3rd ed., Academic, New York, 2002.

[2] B. E. A. Saleh, and M. C. Teich, Fundamentals of Photonics, John Wiley, New York, 1991.

[3] G. P. Agrawal, *Nonlinear Fiber Optics*, 3 rd ed., Academic, New York, 2001.

[4] J. C. Palais, *Fiber Optic Communication, 5th* ed., Prentice Hall, 2002.

[5] P. F. Wysocki, M. J. F. Digonnet, B. Y. Kim and H. J. Shaw "Characteristics of Erbium-doped superfluorescent fiber source for interferometric sensor application," J. Lightwave Technol. vol. 12, pp. 550-567, 1994.

[6] P J. Winzer and R-J Essiambre, "Advanced modulation formats for high capacity optical transport networks," *J. Lightw. Technol.*, vol. 24, pp. 4711- 4728, 2006.

[7] S. Norcia, S. Tonda-Goldstein, R. Frey, D. Dolfi, J. P. Huignard, "Efficient single-mode 1.5 /spl mu/m Brillouin fiber laser for radiofrequency applications," IEEE CLEO/Europe Conference, pp. 247 – 248, 2003.

[8] K. S. Abedin, "Single-frequency Brillouin lasing using single-mode As_2Se_3 chalcogenide fiber," Optics Express, vol. 14, pp. 4037-4042, 2006.

[9] H. Li and K. Ogusu, "Instability of stimulated Brillouin scattering in a fiber ring resonator," Optical Review, vol. 7, pp. 303-308, 2000.

[10] D. Derickson, *Fiber Optic Test and Measurement*, Hewlett-Packard Professional Books, Prentice Hall, New Jersey, 1998.

[11] A. W. Snyder and J. D. Love, *Optical Waveguide Theory*, Chapman and Hall, 1983.

[12] R. B. Dyott, *Elliptical Fiber Waveguides*, Artec House, Boston, 1995.

B.1 Journal Papars

[1] S. Shahi, S.W. Harun, N.S. Shahabuddin, **M.R. Shirazi**, H. Ahmad, "Multi-wavelength generation using a bismuth-based EDF and Brillouin effect in a linear cavity configuration," Optics & Laser Technology vol. 41, pp. 198– 201, 2009.

[2] **M R Shirazi**, M Biglary, S W Harun, K Thambiratnam and H Ahmad, "Bidirectional multiwavelength Brillouin fiber laser generation in a ring cavity," IOP, J. Opt. A: Pure Appl. Opt. vol. 10, 055101 (3pp), 2008.

[3] **M. R. Shirazi**, S. W. Harun, M. Biglary, and H. Ahmad, "Linear cavity Brillouin fiber laser with improved," OSA, Opt. Lett. vol. 33, pp. 770-772, 2008.

[4] **M. R. Shirazi**, M. Biglary, S. W. Harun, K. Thambiratnam, and H. Ahmad, "Effects of different Raman pumping schemes on stimulated Brillouin scattering in a linear cavity," OSA, Appl. Opt. vol. 47, pp. 3088-3091, 2008.

[5] **M. R. Shirazi**, N. S. Shahabuddin, S. N. Aziz, K. Thambiratnam, S. W. Harun, and H. Ahmad, "A linear cavity Brillouin fiber laser with multiple wavelengths output," Laser Phys. Lett. vol. 5, pp. 361–363, 2008.

[6] S. W. Harun, **M. R. Shirazi**, and H. Ahmad, "A new configuration of multi-wavelength Brillouin fiber laser," Laser Phys. Lett. vol. 5, pp. 48–50, 2008.

[7] H. Ahmad, **M. R. Shirazi**, M. Biglary, S. W. Harun, "Linear cavity Brillouin fiber laser using a fiber Bragg grating," Wiley InterScience, Microwave and Optical Technology Letters vol. 50, pp. 265-266, 2008.

[8] S. W. Harun, **M. R. Shirazi**, H. A. Abdul-Rashid and H. Ahmad, **"**Multiwavelength source using a Brillouin fiber laser," Journal of Nonlinear Optical Physics & Materials (JNOPM)**,** vol. 17, pp. 199 – 203, 2008.

[9] **M. R. Shirazi**, S. W. Harun, K. Thambiratnam, M. Biglary, H. Ahmad, "New Brillouin fiber laser configuration with high output power," Wiley InterScience, Microwave and Optical Technology Letters vol. 49, pp.2656-2658, 2007.

[10] **M. R. Shirazi**, S. W. Harun, M. Biglary, K. Thambiratnam, and H. Ahmad, "Effect of Brillouin Pump Linewidth on the Performance of Brillouin Fiber Lasers," ISAST, Transaction on Electron. and Signal Processing, vol. 1, pp.30-32, 2007.

[11] S. W. Harun, **M. R. Shirazi**, and H. Ahmad, "Multiple wavelength Brillouin fiber laser from injection of intense signal light," Laser Phys. Lett. vol. 4, pp. 678-680, 2007.

B.2 Conference Papers

[1] **M. R. Shirazi**, S. W. Harun, M. Biglary, K. Thambiratnam, and H. Ahmad, "10 and 20 GHz Optical Comb Generation of Brillouin Fiber Lasers," The National Physics Conference (PERFIK), Kuala Terengganu, Malaysia, 26-28 December 2007.

[2] K. Thambiratnam, S. W. Harun, **M. R. Shirazi**, A. H. Sulaiman, S. N. Aziz and H. Ahmad, "A Compact Dual Wavelength Ring Laser Using a SOA and an AWG," The National Physics Conference (PERFIK), Kuala Terengganu, Malaysia, 26-28 December 2007.

[3] **M. R. Shirazi**, S. W. Harun, M. Biglary, K. Thambiratnam, H. Ahmad "Generation of Higher-Order SBS in Optical Fibers through Injection of Intense Signal Light," Mathematics and Physical Science Graduate Congress (MPSGC), University of Malaya, Kuala Lumpur, Malaysia, 12-14 August 2007.

[4] S. W. Harun, **M. R. Shirazi**, H. A. Abdul-Rashid and H. Ahmad, **"**Multiwavelength source using a Brillouin fiber laser," The 6th International Symposium on Modern Optics and Its Applications (ISMOA), Bandu, Indonesia, 6-10 August 2007.

Selected Papars

In this appendix, some of the various publications used to do this research are presented. These publications were obtained from the research data directly related to this work and also as an extention of the work done in this thesis. I hope this appendix help to the readers of this work.

Linear cavity Brillouin fiber laser with improved characteristics

M. R. Shirazi,[1,*] S. W. Harun,[2] M. Biglary,[1] and H. Ahmad[1]

[1]Department of Physics, Photonics Research Center, University of Malaya, 50603 Kuala Lumpur, Malaysia
[2]Department of Electrical Engineering, Faculty of Engineering, University of Malaya, 50603 Kuala Lumpur, Malaysia
*Corresponding author: behshirazi@yahoo.com

Received November 26, 2007; revised February 21, 2008; accepted March 6, 2008;
posted March 11, 2008 (Doc. ID 90133); published April 8, 2008

A configuration for linear cavity Brillouin fiber laser (BFL) generation is demonstrated using a standard single-mode fiber, two optical circulators, a 3 dB coupler, and a 95/5 coupler to allow high efficiency. With a Brillouin pump (BP) power of 13 dBm, the laser peak power is 12.3 dB higher than a conventional linear cavity BFL at an upshifted wavelength of 0.086 nm from the BP wavelength. In addition, it is revealed that the BFL peak power can be higher than the transmitted BP peak power when the BP power exceeds the second Brillouin Stokes threshold power. © 2008 Optical Society of America

OCIS codes: 290.5900, 060.2310, 060.3510, 230.5750.

Stimulated Brillouin scattering (SBS) arises from a common interaction between the intense pump light and acoustic waves in a single mode fiber (SMF) that gives rise to backward-propagating frequency-downshifted light [1]. The thermally excited acoustic waves generate an index grating that copropagates with the pump at the acoustic velocity in the SMF. This moving grating reflects the pump light and causes the backscattered light to experience a downshift in the frequency as a result of the Doppler effect. SBS has potential applications in sensors [2,3] and in the realization of very narrow linewidth Brillouin fiber lasers (BFLs), whereby the Stokes linewidth becomes significantly narrower than the pump linewidth with reductions of up to a few hertz [4–6]. Moreover, a BFL can be designed for virtually any wavelength, provided that the required pump laser is available, thus showing a high potential for applications in metrology and spectroscopy.

Typically, most BFLs operate in a ring configuration, but to our knowledge until now there have been only a few reports on linear cavity BFLs. The main reason for this is that conventional linear cavity BFLs suffer from problems such as the generation of high-order Stokes and anti-Stokes waves and the performance of the output transmitted BP power higher than the Brillouin laser [7,8]. In this Letter, we demonstrate a new design for a linear cavity or Fabry–Perot cavity BFL in which the BFL peak power can be higher than the transmitted output BP peak power when the BP power exceeds the second Brillouin Stokes threshold power of 12 dBm. Stable operation of the BFL is obtained at an upshifted wavelength of 0.086 nm from the pump wavelength.

The proposed configuration is shown in Fig. 1(a), whereby the linear cavity is formed by two optical circulators (OC1 and OC2), a 3 dB (50/50) coupler, and a 95/5 coupler located between ports 3 and 1 of OC1 and OC2, respectively. A 25 km long SMF is used as a gain medium and has an attenuation coefficient of 0.19 dB/km at 1550 nm, a cutoff wavelength of 1161 nm with a zero dispersion wavelength of 1315 nm, and a mode field diameter of 9.36 μm. The SMF is pumped by an external cavity tunable laser source (TLS) that is amplified by an erbium-doped fiber amplifier (EDFA) and fed into the system. The maximum power of the amplified BP is ~13 dBm. The BP is injected into the SMF via the 3 dB coupler and OC1 in a forward (clockwise) direction at $z=0$ as indicated in Fig. 1(a). The first backward-propagating Stokes, initiated at $z=L$ from spontaneous Brillouin scattering or a seed signal, oscillates inside the resonator to subsequently generate the BFL and the second-order forward-propagating Brillouin Stokes that is started at $z=0$ through cascaded SBS. The 95/5 coupler extracts the output power and suppresses higher-order anti-Stokes and Stokes generation. The first anti-Stokes wave arises due to four-wave mixing (FWM) between copropagating BP and BFL photons. The output laser is characterized using an optical spectrum analyzer (OSA) with a resolution

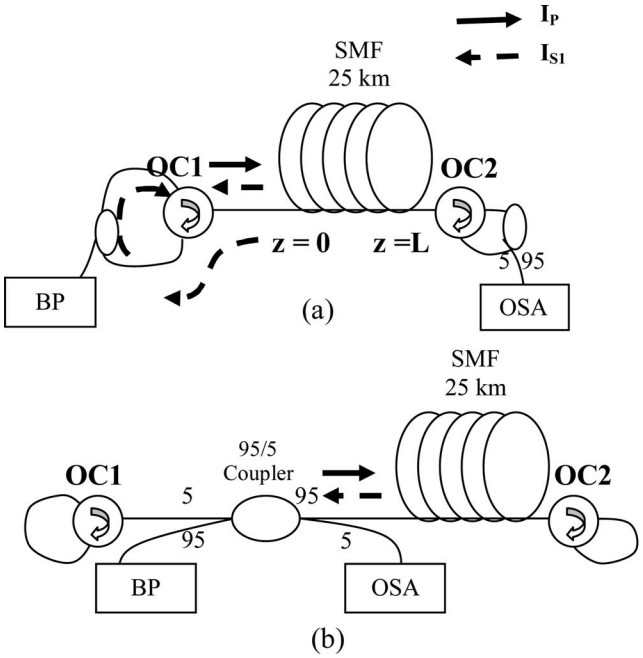

Fig. 1. Experimental setup for (a) proposed and (b) conventional linear cavity configurations.

0146-9592/08/080770-3/$15.00

of 0.015 nm. The experiment is also carried out for the conventional configuration [8] in which a (2×2) 95/5 coupler is placed before the SMF as depicted in Fig. 1(b) for comparison purposes.

Operational principles of the BFL system can be described as the following. The steady-state interaction between the BP and Stokes waves are governed by the nonlinear coupled equations [9]

$$\frac{dI_P(z)}{dz} = -g_B I_P(z) I_{S1}(z) - \alpha I_P(z),$$

$$\frac{dI_{S1}(z)}{dz} = -g_B [I_P(z) I_{S1}(z) - I_{S1}(z) I_{S2}(z)] + \alpha I_{S1}(z),$$

$$\frac{dI_{S2}(z)}{dz} = g_B I_{S1}(z) I_{S2}(z) - \alpha I_{S2}(z), \quad (1)$$

where $I_P(z)$, $I_{S1}(z)$, and $I_{S2}(z)$ are the pump and first- and second-order Stokes intensities, respectively, as functions of the distance in the fiber; g_B is the Brillouin gain parameter that depends on the fiber; and α is the fiber attenuation coefficient. Since considerations (in this Letter) are restricted to a weak-reflectivity limit of the exit face, interactions of the reflected fields with the initial pump and the already present Stokes fields in the fiber can be neglected. To determine the effect of feedback, the following boundary conditions must hold:

$$I_P(0) = I_0(1-R_1) + R_1 I_P^R(0),$$

$$I_P^R(L) = R_2 I_P(L),$$

$$I_{S1}^R(0) = R_1 I_{S1}(0),$$

$$I_{S1}(L) = R_2 I_{S1}^R(L),$$

$$I_{S2}(0) = R_1 I_{S2}^R(0),$$

$$I_{S2}^R(L) = R_2 I_{S2}(L), \quad (2)$$

where $I_P^R(z)$, $I_{S1}^R(z)$, and $I_{S2}^R(z)$ determine the reflected pump and the reflected first and second Stokes waves, respectively. I_0 is the maximum pump power coupled into the fiber, and R_1 and R_2 are the intensity reflectivities of the entrance and exit faces of the cavity, respectively. Opposite to $I_P(z)$, $I_{S2}(z)$, and $I_{S1}(z)$, the reflected waves $I_P^R(z)$ and $I_{S2}^R(z)$, starting at $z=L$, travels in $-z$, whereas $I_{S1}^R(z)$, initiated at $z=0$, travels in $+z$, so that, in a similar way to the derivation of Eq. (1), we can readily write equations governing the reflected waves. The equations for the reflected waves in addition to Eqs. (1) and (2) govern the dynamics of the linear cavity BFL system that enable it to operate on the first two Stokes components. There are still two questions that have to be considered. First it is FWM that especially describes anti-Stokes generation. Second, the seeding noise that initiates laser emission, although above the lasing threshold, this noise is much weaker than all the other factors, so we ignore it in our analytical calculation.

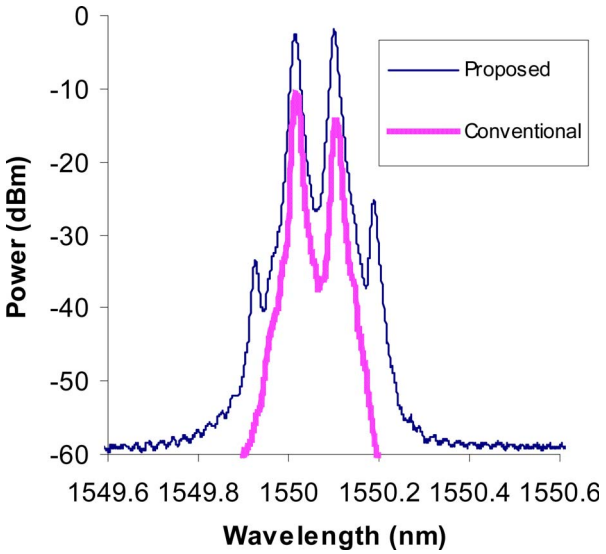

Fig. 2. (Color online) BFL output spectra for different configurations at a BP power of 13 dBm.

Figure 2 compares the output BFL spectrum of the proposed and conventional configurations. As shown in Fig. 2, for the proposed configuration, two Stokes waves at 1550.101 and 1550.187 nm and one anti-Stokes wave at 1549.929 nm are obtained around the oscillated BP at 1550.015 nm, whereas we have only the first Stokes wave in the conventional cavity. The laser is generated by the Brillouin gain in the SMF. As the BP is coupled into the SMF, the first Stokes signal is generated at an upshifted wavelength of 0.086 nm owing to the Brillouin scattering effect. Also, with the BP power of 13 dBm in both configurations, Fig. 2 shows that the BFL peak in the proposed configuration is −1 dBm; in other words, it is 12.3 dB higher as compared to the conventional configuration owing to the reduction of round-trip loss in the proposed BFL configuration, where the couplers are set

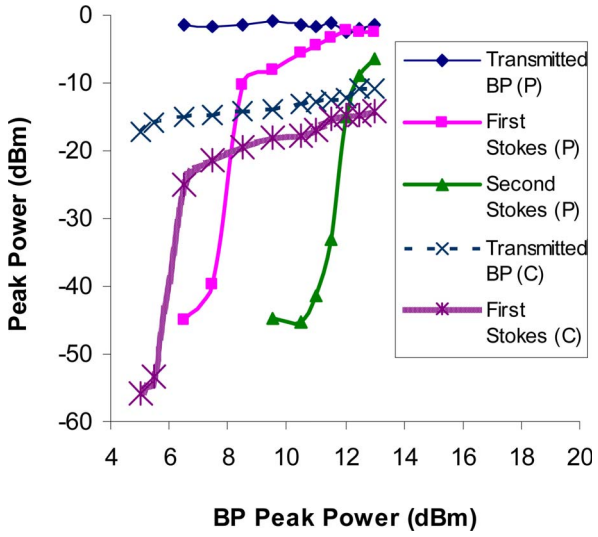

Fig. 3. (Color online) SBS and the transmitted output BP peak powers against input BP peak power for both conventional (C) and proposed (P) configurations.

between ports 1 and 3 of the circulators. In the conventional configuration, the BP and SBS light beams propagate twice into the 95/5 coupler to complete one oscillation inside the cavity, and thus the cavity loss is increased. In addition, as shown in Fig. 3, it is revealed that when the BP power exceeds the second SBS threshold power of 12 dBm, the peak power of the BFL shows a distinct saturation behavior in its output power and can be ~0.5 dB higher than the transmitted BP peak power.

In conclusion, a linear cavity BFL configuration has been demonstrated by incorporating a 3 dB coupler, a 95/5 coupler, two OCs, and a 25 km SMF that allow a very high conversion efficiency. A stable BFL operation was obtained at an upshifted wavelength of 0.086 nm from the pump wavelength with the BFL peak power of –1 dBm, which is 12.3 dB higher than the conventional BFL with the same BP power of 13 dBm owing to the reduced cavity loss in the proposed configuration. When the pump power exceeds the second SBS threshold power, it is revealed that the BFL peak power can be higher than the transmitted BP peak power so that a very high conversion efficiency can be obtained.

References

1. G. P. Agrawal, *Nonlinear Fiber Optics*, 3rd ed. (Academic, 2001).
2. T. Kurashima, T. Horiguchi, and M. Tateda, Opt. Lett. **15**, 1038 (1990).
3. Y. Tanaka and K. Hotate, J. Lightwave Technol. **15**, 838 (1997).
4. S. P. Smith, F. Zarinetchi, and S. Ezekiel, Opt. Lett. **16**, 393 (1991).
5. J. Boschung, L. Thevenas, and P. A. Robert, Electron. Lett. **30**, 1488 (1994).
6. M. R. Shirazi, S. W. Harun, M. Biglary, K. Thambiratnam, and H. Ahmad, ISAST Trans. Elec. Signal Proc. **1**, 30 (2007).
7. V. Lecoeuche, P. Niay, M. Douay, P. Bernage, S. Randoux, and J. Zemmouri, Opt. Commun. **177**, 303 (2000).
8. H. Ahmad, M. R. Shirazi, M. Biglary, and S. W. Harun, Microwave Opt. Technol. Lett. **50**, 265 (2008).
9. S. Randoux, V. Lecoeuche, B. Segard, and J. Zemmouri, Phys. Rev. A **52**, 2327 (1995).

J. Opt. A: Pure Appl. Opt. **10** (2008) 055101 (3pp) doi:10.1088/1464-4258/10/5/055101

Bidirectional multiwavelength Brillouin fiber laser generation in a ring cavity

M R Shirazi[1], M Biglary[1], S W Harun[2], K Thambiratnam[1] and H Ahmad[1]

[1] Photonics Laboratory, Department of Physics, University of Malaya, 50603 Kuala Lumpur, Malaysia
[2] Department of Electrical Engineering, Faculty of Engineering, University of Malaya, 50603 Kuala Lumpur, Malaysia

E-mail: behshirazi@yahoo.com, swharun@um.edu.my and harith@um.edu.my (H Ahmad)

Received 11 January 2008, accepted for publication 28 February 2008
Published 27 March 2008
Online at stacks.iop.org/JOptA/10/055101

Abstract
Bidirectional multiwavelength Brillouin fiber laser (BFL) generation is demonstrated using a 25 km long single-mode fiber as a Brillouin gain medium in a ring cavity. Odd-order Brillouin Stokes waves appear in the backward direction whereas Brillouin pump and the even Stokes orders are in the forward direction with the line spacing 0.16 nm (∼20 GHz) between each two consecutive waves in forward and backward directions. In addition, by a combination of the backward and forward outputs, we have a higher number comb generation of a multiwavelength BFL with the line spacing 0.08 nm (∼10 GHz). The proposed configuration can work at any wavelength which is a benefit to the others.

Keywords: fiber optics, stimulated Brillouin scattering, fiber lasers, multiwavelength light source, BFLs

(Some figures in this article are in colour only in the electronic version)

1. Introduction

Laser sources capable of producing more than one wavelength with an accurate wavelength difference between the signals are of significant importance for applications in optical sensors, microwave signal processing, optical spectroscopy instrumentation and high capacity communication networks. The requirements for this type of laser source should have the criteria for closely spaced multiwavelength line spacing and stabilized flattened peak powers between adjacent lines. Operation of these lasers at low threshold powers would also be of significant advantage. In order to fulfill the above requirements, different approaches have been taken such as multiwavelength erbium-doped fiber lasers (MWEDFLs), multiwavelength Brillouin erbium fiber lasers (MWBEFLs), multiwavelength Brillouin–Raman fiber lasers (MWBRFLs), and multiwavelength Brillouin fiber lasers (MWBFLs) [1–4]. Stable multiwavelength sources based on erbium-doped fibers (EDFs), such as MWEDFLs, are difficult to obtain due to the homogeneous broadening of laser modes, which in turn results in mode competition. As such, MWEDFLs so far have only been demonstrated by cooling of the gain medium of an erbium-doped fiber to liquid-nitrogen temperature [1], or by using a specially designed twin-core EDF [2], so as to reduce the homogeneous linewidth of the gain medium and therefore to prevent mode competition between adjacent laser lines. Hybrid MWBEFLs with a feedback scheme are one of the most common candidates for realizing ultra-dense wavelength operation, although they have a wavelength limitation due to EDFA amplification bandwidth [3, 4]. Special fibers such as dispersion compensating fibers (DCFs) have been used to increase the Raman gain in MWBRFLs generation, limited only by the available Raman and Brillouin pump sources [5, 6]. Of the various approaches, the use of BFLs has not been considered seriously because of the limited number of lasing lines and undesirable power flatness [7, 8]. In this paper, a proposed MWBFL utilizes Brillouin gain from a single-mode fiber (SMF), fiber couplers and an optical circulator so as to generate necessary feedback for multiwavelength BFL performance. Bidirectional multiwavelength operation can be obtained, with 20 GHz multiwavelength operation corresponding to the case that even-and odd-order Stokes

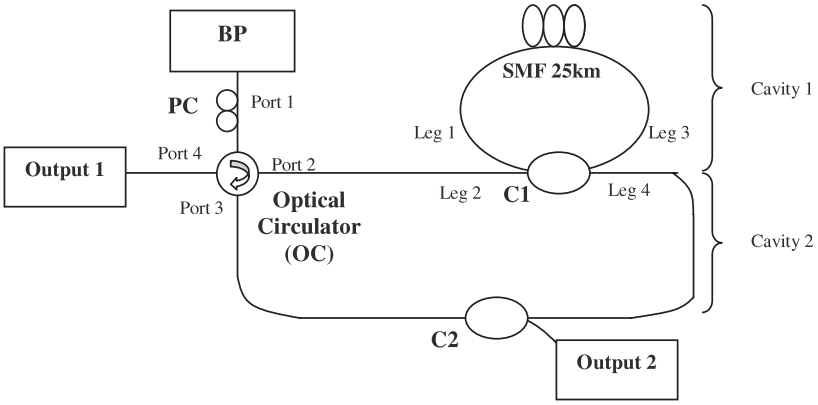

Figure 1. The proposed experimental set-up for generation of 10 and 20 GHz combs.

waves of BFLs are discriminated in the forward and backward direction, respectively. However, 10 GHz BFL optical comb generation can be obtained by the backward and forward combination.

2. Experimental set-up

The proposed configuration of the multiwavelength BFL is shown in figure 1. The elements of the cavity are a 3 dB coupler (2 × 2), C1, another 3 dB coupler (1 × 2), C2, a four-port optical circulator, OC, and a 25 km SMF as the gain medium. The SMF has a cutoff wavelength of 1167 nm with a zero dispersion wavelength of 1315 nm and a mode field diameter of 9.36 μm. The BFL is pumped by an external cavity tunable laser source (TLS) with a linewidth of approximately 15 MHz which is amplified by an erbium-doped fiber amplifier (EDFA) to provide the maximum power of 14 dB m at an output wavelength of 1560 nm, which in this case is the Brillouin pump (BP). A polarization controller (PC) is used to control the polarization of the pump wave so that the evolution of the polarization state of the Stokes wave becomes self-consistent, an important requirement for effective Brillouin lasing output.

The 25 km SMF in cavity 1 is pumped by the BP that generates the first Stokes wave that travels in the clockwise direction of cavity 1 and is emitted at leg 2 into the second cavity. This provides the required feedback for cavity 1 whereby this first Stokes travels back into this cavity through leg 4 and leg 1 of coupler C1. This first Stokes will experience amplification from the 25 km SMF acting as a Brillouin gain medium. At the same time, this first Stokes will act as the pump that will generate the second Stokes in the anti-clockwise direction and will oscillate in cavity 1 until it gains enough power where a portion of this power will be emitted at leg 4 and will travel in cavity 2 to be emitted as output 1 (even Stokes) at port 4 of the OC. The first Stokes (odd) will be emitted at output 2 of C2. This process repeats to produce the subsequent odd and even Stokes as mentioned in this experiment. From figure 1, the odd Stokes can oscillate in both cavities, but the even Stokes will only oscillate in cavity 1 whereby cavity 2 provides the means for output extraction.

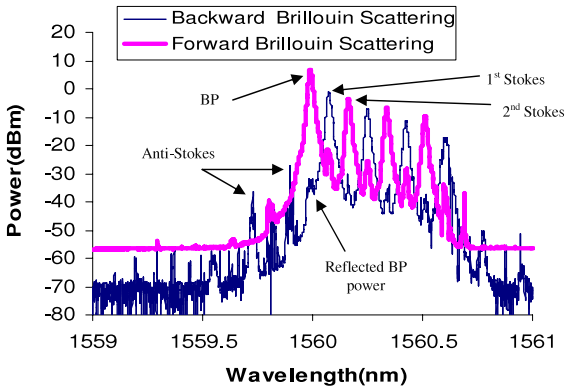

Figure 2. Comb generation with 0.16 nm (∼20 GHz) between two consecutive lines in the forward and backward directions.

3. Results and discussion

A strong pump beam of frequency ω_p generates the first backward propagating Stokes signal of frequency ω_{1s}, a Brillouin frequency down-shifted by $\Delta\omega_B$ with respect to the pump beam (i.e. $\omega_{1s} = \omega_p - \Delta\omega_B$). Then the first Stokes generates the second Stokes which propagates in the opposite direction, as explained earlier in the above section. If a threshold condition is satisfied, this will generate a cascading Brillouin effect as a comb of lines as shown in figure 2. From the figure, the spacing between two consecutive even or odd Stokes lines is about 0.16 nm. Those lines before the BP line are anti-Stokes lines. This occurs when the various Stokes waves interact with the pump wave which generates these anti-Stokes $\omega\omega\Delta$ through the degenerate FWM process.

By combining the two ports, output 1 and output 2, we have a multiwavelength BFL generation with the spacing 0.08 (nm), 10 (GHz), between each two adjacent lines as shown in figure 3. Although there is a power variation between the subsequent Stokes lines, using a gain flattening filter such as the long-period fiber gratings may help to improve and flatten this output, thus making it possible to use this system as a multiple-wavelength output source.

From figure 3, the peak power of odd and even Stokes and anti-Stokes lines can be measured for different BP powers. These measured peak powers are depicted in figure 4 for

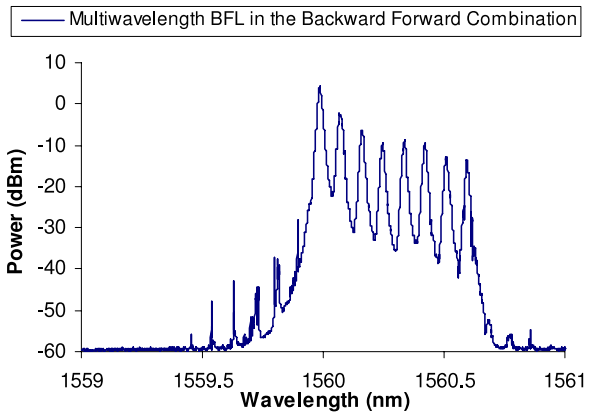

Figure 3. Eight-line spacing 0.08 nm (∼10 GHz) of BFL comb generation.

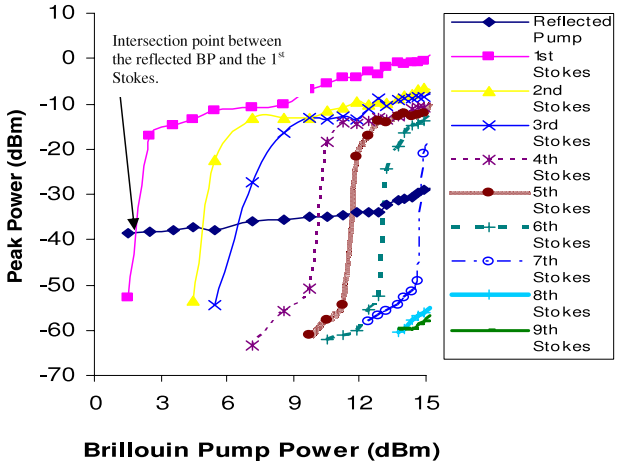

Figure 4. Reflected Brillouin pump and Stokes waves power plotted against BP power.

the Stokes and figure 5 for the anti-Stokes, respectively. From [9, 10], the threshold condition of each Brillouin Stokes line can be defined as the intersection point between the reflected BP power and the Stokes output as shown in figure 4. The reflected BP power is taken from the backward scattering as indicated in figure 2 for each different BP power. Also, as shown in figure 4, the Stokes lines begin to saturate as the BP power increases. For instance, the second Stokes line saturates as the threshold for the third Stokes is reached. This is due to the power transfer from the second Stokes to the third Stokes, which occurs when the BP power is approximately at 6.5 dB m. The same thing can be said for the third and fourth Stokes at 10 dB m of the BP, which is the threshold of the fourth Stokes.

Figure 5 shows the peak output power of the first, second, third and fourth anti-Stokes at different BP powers. For the case of the first Stokes, the peak power of the first anti-Stokes increases linearly with the BP power, but at approximately 13 dB m, the peak power increases significantly. The same effect is observed in the second anti-Stokes, in which the power rises linearly with the increase of the BP until the BP is approximately 13 dB m, whereby the peak power rises significantly. The third and fourth anti-Stokes also show the same effect, rising linearly with the BP until a BP power of 14 dB m, whereby the rise becomes significant.

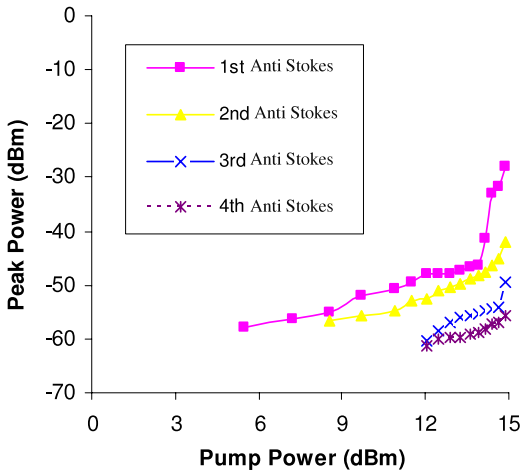

Figure 5. Anti-Stokes power plotted against BP power.

4. Conclusion

We have demonstrated a bidirectional multiwavelength BFL generation using a 25 km single-mode fiber by the cascaded Brillouin scattering and four-wave mixing processes. The wavelength spacing 0.08 (nm) and 0.16 (nm) are obtained with the bidirectional multiwavelength generation suitable for some applications such as optical sensors. Depending only on the BP wavelength, the proposed configuration can work at any wavelength which is a benefit to the others.

References

[1] Yamashita S and Hotata K 1992 Multiwavelength erbium-doped fiber laser using intracavity etalon and cooled by liquid nitrogen *Electron. Lett.* **32** 1298–9
[2] Graydon O, Loh H W, Laming R I and Dong L 1996 Triple-frequency operation of an Er-doped twincore fiber loop laser *IEEE Photon. Technol. Lett.* **8** 63–5
[3] Harun S W, Cheng X S, Saat N K and Ahmad H 2005 S-band Brillouin erbium fiber laser *Electron. Lett.* **4** 174–6
[4] Fok M P and Shu C 2006 Spacing-adjustable multi-wavelength source from a stimulated Brillouin scattering assisted erbium-doped fiber laser *Opt. Express* **14** 2618–24
[5] Guy M J, Chernikov S V and Taylor J R 1998 Lossless transmission of 2 ps pulses over 45 km of standard fiber at 1.3 μm using distributed Raman amplification *Electron. Lett.* **34** 793–4
[6] Zamzuri A K, Mahdi M A, Ahmad A, Md Ali M I and Al-Mansoori M H 2007 Flat amplitude multiwavelength Brillouin–Raman comb fiber laser in Rayleigh-scattering-enhanced linear cavity *Opt. Express* **15** 3000–5
[7] Cowle G J, Loh W H, Laming R J and Stepanov D Y 1997 Multiwavelength operation of Brillouin/erbium fiber laser with injection-locked seeding *Optical Fiber Communication Conf. OFC 97* pp 34–5
[8] Park D D, Park J H, Park N, Lee J H and Chang J S 2000 53-line multi-wavelength generation Brillouin/erbium fiber lasers with enhanced Stokes feedback coupling *Optical Fiber Communication Conf.* vol 3, pp 11–3
[9] Smith R G 1972 Optical power handling capacity of low loss optical fibers as determined by stimulated Raman and Brillouin scattering *Appl. Opt.* **11** 2489–94
[10] Shimizu T, Nakajima K, Shiraki K, Ieda K and Sankawa I 2008 Evaluation methods and requirements for stimulated Brillouin scattering threshold in a single-mode fiber *Opt. Fiber Technol.* **14** 10–5

LASER PHYSICS LETTERS

www.lphys.org

Abstract: A linear cavity Brillouin fiber laser (BFL) is proposed and demonstrated for multi-wavelength operation. The BFL uses a single mode fiber (SMF) as a non-linear gain medium and an optical circulator to generate a linear cavity resonator. Two couplers are used to inject the Brillouin Pump (BP) and tap the BFL output respectively. The effect of the coupler ratio on the BFL performance is studied by keeping constant the ratio of the first coupler and varying the ratio of the second coupler. 11 simultaneous lines with a line spacing of 0.8 nm are obtained at a BP of 11.7 dBm and a coupler ratio of 95:5. The laser output is stable at room temperature with 5 lines obtained at above −30 dBm, and has the largest signal to noise ratio observed at the remaining lines. The proposed BFL has the advantage of being able to operate at any wavelength and is only dependent on the available BP wavelength.

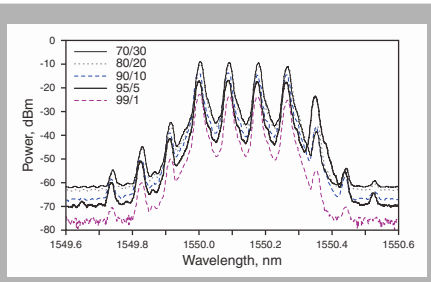

Output spectrum of the linear cavity BFL at various C2 coupling ratios

A linear cavity Brillouin fiber laser with multiple wavelengths output

M.R. Shirazi, [1] *N.S. Shahabuddin,* [1] *S.N. Aziz,* [1] *K. Thambiratnam,* [1] *S.W. Harun,* [2] *and H. Ahmad* [1]

[1] Photonics Laboratory, Department of Physics, University of Malaya, 50603 Kuala Lumpur, Malaysia
[2] Department of Electrical Engineering, Faculty of Engineering, University of Malaya, 50603 Kuala Lumpur, Malaysia

Received: 21 December 2007, Revised: 24 December 2007, Accepted: 26 December 2007
Published online: 11 January 2008

Laser Phys. Lett. **5**, No. 5, 361–363 (2008) / **DOI** 10.1002/lapl.200710134

Abstract: A linear cavity Brillouin fiber laser (BFL) is proposed and demonstrated for multi-wavelength operation. The BFL uses a single mode fiber (SMF) as a non-linear gain medium and an optical circulator to generate a linear cavity resonator. Two couplers are used to inject the Brillouin Pump (BP) and tap the BFL output respectively. The effect of the coupler ratio on the BFL performance is studied by keeping constant the ratio of the first coupler and varying the ratio of the second coupler. 11 simultaneous lines with a line spacing of 0.8 nm are obtained at a BP of 11.7 dBm and a coupler ratio of 95:5. The laser output is stable at room temperature with 5 lines obtained at above −30 dBm, and has the largest signal to noise ratio observed at the remaining lines. The proposed BFL has the advantage of being able to operate at any wavelength and is only dependent on the available BP wavelength.

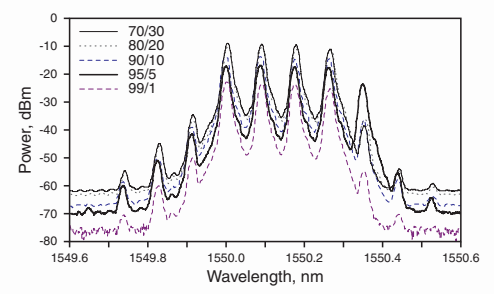

Output spectrum of the linear cavity BFL at various C2 coupling ratios

A linear cavity Brillouin fiber laser with multiple wavelengths output

M.R. Shirazi, [1,*] *N.S. Shahabuddin,* [1] *S.N. Aziz,* [1] *K. Thambiratnam,* [1] *S.W. Harun,* [2,**] *and H. Ahmad* [1]

[1] Photonics Laboratory, Department of Physics, University of Malaya, 50603 Kuala Lumpur, Malaysia
[2] Department of Electrical Engineering, Faculty of Engineering, University of Malaya, 50603 Kuala Lumpur, Malaysia

Received: 21 December 2007, Revised: 24 December 2007, Accepted: 26 December 2007
Published online: 11 January 2008

Key words: Brillouin fiber laser; multi-wavelength laser; non-linear gain; stimulated Brillouin scattering

PACS: 42.60.Da, 42.81.-i, 42.81.Wg, 42.81.Uv

1. Introduction

Multi-wavelength fiber lasers have garnered considerable attention due to their potential in wavelength division multiplexing (WDM) systems, optical fiber sensor systems, optical component testing and spectroscopy applications. These lasers have been developed with various mechanisms such as erbium doped fiber lasers (EDFLs) [1–3], amplified spontaneous emission (ASE) slicing [4] and Brillouin/Erbium fiber lasers (BEFLs) [5–7]. Recently, we reported a multi-wavelength laser, which uses stimulated Brillouin scattering (SBS) in a single mode fiber (SMF) as a non-linear gain medium in a ring configuration [8,9]. SBS is a nonlinear effect that results from the interaction between intense pump light and acoustic waves in a SMF, thus giving rise to backward propagating frequency shifted light. The thermally excited acoustic waves generate an index grating that co-propagates with the pump at the acoustic velocity in the SMF. This moving grating reflects the pump light and causes the backscattered light to experience a frequency downshift equal to $\nu_B = 2n\nu_A/\lambda_P$, where ν_A is the acoustic velocity, n is the refractive index, and λ_P is the pump wavelength as a result of the Doppler effect. In the case of a standard SMF, the shift is determined to be approximately 0.08 nm at the 1550 nm wavelength region.

In this paper, we demonstrate a new multi-wavelength Brillouin Fiber Laser (BFL) using an SBS gain medium in linear cavity. The proposed system has the advantage that it does not use an erbium-doped fiber as a gain medium as reported earlier by other works [4–7]. The output multi-

* Corresponding author: e-mail: behshirazih@yahoo.com, ** swharun@um.edu.my

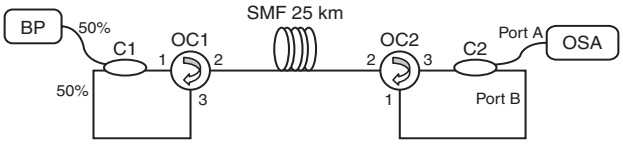

Figure 1 The proposed linear cavity BEFL

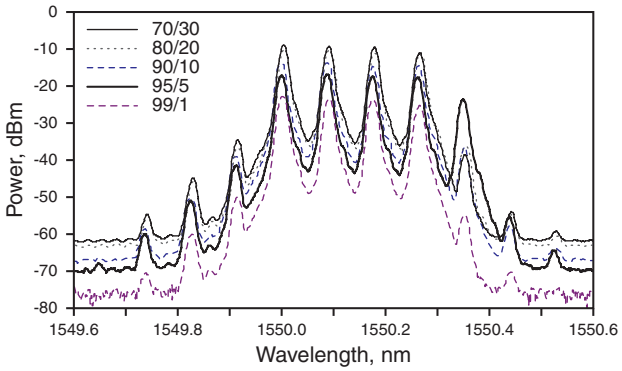

Figure 2 (online color at www.lphys.org) Output spectrum of the linear cavity BFL at various C2 coupling ratios, with the higher ratio biased to port B, which is connected to port 1 of OC2

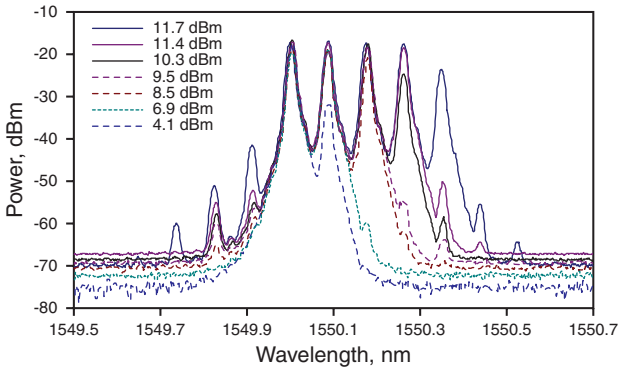

Figure 3 (online color at www.lphys.org) Output spectrum of the proposed BFL at different BP powers

wavelength lines are obtained through careful optimization of the output coupling ratio and the employment of an optical circulator as a reflector, which is relatively more than those obtained earlier as in references [8,9].

2. Experimental setup

The configuration of the multi-wavelength linear cavity BFL is shown in Fig. 1. The Brillouin gain medium is a standard 25 km long SMF-28 with cut-off and zero dispersion wavelengths of 1161 nm and 1315 nm respectively and a mode field diameter of 9 μm. A signal from an external cavity tunable laser source (TLS) amplified by an erbium-doped fiber amplifier (EDFA) is used as the BP. The BP has a maximum power of approximately 11.7 dBm with a linewidth of approximately 20 MHz. Two optical circulators, OC1 and OC2, together with the couplers C1 and C2 act as reflectors in the linear cavity as shown in Fig. 1. The left side reflector has a coupler (C1) with a fixed ratio of 50:50 with one end connected to the BP. The right side reflector coupler (C2) has a variable ratio, with the lower percentage end connected to the optical spectrum analyzer (OSA).

The BP is injected into the linear cavity via C1, OC1 and is then coupled into the SMF-28 to generate the first Stokes signal propagating in the opposite direction of the BP signal. The first Stokes travels to OC1 and is recirculated back into the SMF-28 to be amplified and then moves towards OC2 and is reflected back to complete a round-trip oscillation. This oscillation continues until the intensity of the first Brillouin Stokes is higher than the threshold value for Brillouin gain, upon which the second Brillouin Stokes is generated and then begins to oscillate in the cavity. This process continues and subsequently cascaded Brillouin Stokes can be generated as long as the Brillouin gain is equal or larger than the cavity loss. The multi-wavelength output has a line spacing of approximately 10 GHz, which is equivalent to the Stokes shift in the SMF-28. The output of the linear cavity BFL is tapped from port A of variable ratio coupler C2, and is measured using an OSA with a resolution of 0.015 nm. The coupling ratio of port B of C2 is varied from 70% to 99% (70, 80, 90, 95, and 99%) based on the availability of couplers with these ratios during the experiment.

3. Result and discussion

The impact of the C2 coupling ratio on the performance of the BFL is depicted in Fig. 2. In the experiment, the BP wavelength and power is fixed at 1550 nm and 11.7 dBm, respectively, and the higher C2 ratio is looped back into the system through port B of C2. As shown in Fig. 2, 9 to 11 simultaneous lines are obtained with a line spacing of approximately 0.08 nm for all coupling ratios tested. The 3 dB bandwidth of each line is about 0.02 nm, limited by the OSA resolution of 0.015 nm. The coupling ratio of C2 controls the amount of light that has been reflected from OC2 and a higher Port B ratio translates to a higher OC2 reflectivity. In the experiment, the minimum coupling ratio of port B is set at 70%, as below this value the OC2 reflectivity becomes very low, thus increasing the loss inside the laser cavity and inhibiting the generation of cascaded Brillouin Stokes, which limits the number of Stokes and anti-Stokes. At a port B ratio of 95%, 11 simultaneous lines are obtained with 5 of the lines having a peak power of above -30 dBm, which is the highest number of lines observed in this experiment. The signal to noise ratio is also largest at

this ratio, especially at lines with lower peak powers. This is attributed to the high reflectivity at OC2, which subsequently reduces the loss inside the cavity and promotes the generation of cascaded Brillouin Stokes and at the same time reducing the noise at this region.

The impact of the BP power on the number of Stokes generated by the BFL is shown in Fig. 3. The BP wavelength is set at 1550 nm, while the BP power is varied from 4.1 dBm to 11.7 dBm. Below BP power of 4 dBm, the experiment is not continued as the SBS gain cannot sufficiently compensate for the loss inside the laser cavity and thus cannot support multi-wavelength generation. The number of generated Stokes is observed to increase as the BP increases and this can be attributed to the increase of the nonlinear Brillouin gain as the BP power rises. This situation provides sufficient signal power for higher order Stokes signals to pump the SMF and maintain the cascading process of the Stokes into multiple Stokes. However, the power of each subsequent Stokes line is typically lower than that of the previous Stokes line as each subsequent Stokes is generated with the energy of the previous Stokes, thus slightly reducing the Stokes line's power. The BFL also generates anti-Stokes as shown in Fig. 2 and Fig. 3, especially at the higher BP powers. The anti-Stokes signals arise from the bidirectional operation and four-wave mixing in the SMF and are more obvious when the BP power is increased. The multi-wavelength output of the BFL is observed to be stable at room temperature with only minor fluctuations observed due to external temperature variances. The BFL is advantageous as it is able to operate at any wavelength, depending only on the availability of the BP. Furthermore, the BFL can be made compact with the use of highly non-linear fibers such as holey fibers for the generation of SBS.

4. Conclusion

A new multi-wavelength BFL is demonstrated using linear cavity configuration using two optical circulator and coupler pairs as resonators with an SMF-28 as a gain medium. The proposed BFL is able to generate up to 11 Stokes and anti-Stokes lines with a line spacing of 0.08 nm at the 1550 nm region at a BP power of 11.7 dBm. The number of Stokes lines obtained depends on the BP power as well as the coupler ratio at the reflectors. At a coupler ratio of 95:5, optimum BFL operation is achieved with 5 lines obtained at above – 30 dBm with the largest signal to noise ratio observed at the other lines. The multi-wavelength BFL is stable at room temperature and is capable of operating at any wavelength, dependent only on the BP wavelength.

References

[1] O. Graydon, W.H. Loh, R.I. Laming, and L. Dong, IEEE Photon. Technol. Lett. **8**, 63–65 (1996).
[2] F. Abdullah, A.S.M. Noor, M.A. Mahdi, H.A.A. Rashid, and M.K. Abdullah, Laser Phys. Lett. **2**, 535–537 (2005).
[3] S.-P. Chen, L. Ding, S.-M. Wang, Y.-G. Li, K.-C. Lu, and S.-H. Zhou, Laser Phys. Lett. **3**, 584–587 (2006).
[4] S.W. Harun, F.A. Rahman, K. Dimyati, and H. Ahmad, Laser Phys. Lett. **3**, 495–497 (2006).
[5] M.H. Al-Mansoori, A.W. Naji, S.J. Iqbal, M.K. Abdullah, and M.A. Mahdi, Laser Phys. Lett. **4**, 371–375 (2007).
[6] S.W. Harun, M.Z. Zulkifli, and H. Ahmad, Laser Phys. Lett. **3**, 369–371 (2006).
[7] S.W. Harun, S.D. Emami, F. Abd Rahman, S.Z. Muhd-Yassin, M.K. Abd-Rahman, and H. Ahmad, Laser Phys. Lett. **4**, 601–603 (2007).
[8] S.W. Harun, M.R. Shirazi, and H. Ahmad, Laser Phys. Lett. **4**, 678–680 (2007).
[9] S.W. Harun, M.R. Shirazi, and H. Ahmad, Laser Phys. Lett. **5**, 48–50 (2008).

Optics & Laser Technology 41 (2009) 198–201

Contents lists available at ScienceDirect

Optics & Laser Technology

journal homepage: www.elsevier.com/locate/optlastec

Multi-wavelength generation using a bismuth-based EDF and Brillouin effect in a linear cavity configuration

S. Shahi [a], S.W. Harun [b], N.S. Shahabuddin [a], M.R. Shirazi [a], H. Ahmad [a,*]

[a] Photonics Laboratory, Department of Physics, University of Malaya, 50603 Kuala Lumpur, Malaysia
[b] Department of Electrical Engineering, Faculty of Engineering, University of Malaya, 50603 Kuala Lumpur Malaysia

ARTICLE INFO

Article history:
Received 23 January 2008
Received in revised form
23 April 2008
Accepted 7 May 2008
Available online 19 June 2008

Keywords:
Fiber laser
Multiple wavelength fiber lasers
Brillouin erbium fiber laser

ABSTRACT

The generation of a multiple wavelength source using a bismuth-based erbium-doped fiber (Bi-EDF) in a linear cavity configuration is demonstrated. The configuration uses a pair of optical circulators at the input and output ends of the cavity to form a resonator for multi-wavelength generation in conjunction with optical couplers to inject the Brillouin pump (BP) and to tap the output at the two ends. The Brillouin erbium fiber laser (BEFL) comb with a 2.15 m of Bi-EDF has a wavelength spacing of 0.09 nm and operates in long-wavelength (L-) band region. A stable output laser comb of 50 lines is obtained at a BP of 1568.2 nm and 5 dBm and two 1480 nm pumps at 120 mW. The injected BP wavelength and power as well as the 1480 nm pump powers have a great effect on the number of lines and output power of the BEFL. This configuration is compact due to the use of the significantly shorter Bi-EDF as the linear gain medium, and can be made more compact by replacing the single-mode fiber with highly non-linear fibers such as holey fibers.

1. Introduction

The recent demand for multi-wavelength fiber lasers has increased due to their potential applications in wavelength division multiplexing (WDM), sensors, component testing and spectroscopy. Multi-wavelength sources have been reported and investigated using various gain mediums such as erbium-doped fibers (EDFs) [1,2], semiconductors [3], stimulated Raman scattering [4], stimulated Brillouin scattering [5] or hybrid gain mediums [6,7]. Fiber lasers using EDFs have been widely investigated due to their advantages such as the higher power conversion efficiency and lower threshold powers. Stimulated Brillouin scattering (SBS) in optical fibers is also an interesting phenomenon for optical amplification due to its low threshold power and narrow bandwidth. Thus far, several effective methods based on the hybrid EDF and SBS gain mediums have been proposed for multi-wavelength fiber lasers [8–10].

Recently, bismuth-based EDFs have been extensively studied for use in compact amplifiers with short gain medium lengths. These fibers incorporate lanthanum (La) ions to decrease the concentration quenching of the erbium ions in the fiber [11], which in turn allows the erbium ion concentration to be increased to above 1000 ppm. A fiber with such a high erbium dopant concentration is expected to have enormous potentials in realizing compact EDFAs and EDFA-based devices. In our previous works, we have demonstrated a multi-wavelength source using a hybrid Brillouin erbium-doped fiber laser (BEFL) with a bismuth-based EDF in both a ring and linear cavity configuration [12,13], with the linear cavity BEFL exhibiting a lower threshold power compared with the ring configuration. In this paper, a new multi-wavelength BEFL configuration based on linear cavity is proposed to increase the number of Stokes and anti-Stokes. This BEFL incorporates an optical circulator at both ends to form a linear cavity for multi-wavelength light generation. Compared with the previous linear cavity BEFL [13], this configuration is designed to have a lower cavity loss by injecting (tapping) a Brillouin pump (BP) (output) from the side of the cavity.

2. Experimental set-up

The configuration of the proposed BEFL is shown in Fig. 1. It consists of a short bismuth-based EDF (Bi-EDF) approximately 2.15 m in length with an erbium concentration of 3250 ppm and a cut-off wavelength of 1440 nm as well as a pump absorption rate of 83 dBm at 1480 nm. The fiber is manufactured by Asahi Glass in Japan and is supplied with angled AC/PC connectors. The bismuth-based fiber is connected to the single-mode fiber (SMF) and is pumped bi-directionally using two 1480 nm lasers. A SMF of 25 km in length is used as a non-linear gain medium and WDM

* Corresponding author. Tel.: +60 3 79674828; fax: +60 3 79674290.
E-mail addresses: swharun@um.edu.my (S.W. Harun), harith@um.edu.my (H. Ahmad).

0030-3992/$ - see front matter © 2008 Published by Elsevier Ltd.
doi:10.1016/j.optlastec.2008.05.009

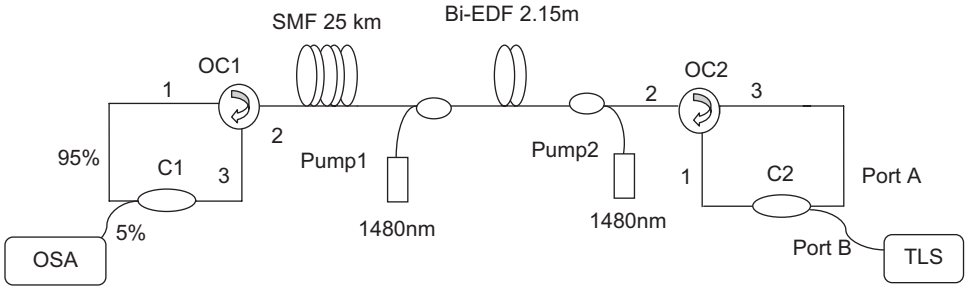

Fig. 1. Experimental configuration of the proposed linear cavity BEFL.

coupler is used to combine the pump and laser wavelengths. An external cavity tunable-laser source (TLS) with the maximum power of 8 dBm is used as the BP. Two optical circulators, OC1 and OC2, are used to create ring cavities that are placed at both ends to act as reflectors. The coupler C1 is used to inject the signal BP form the TLS and C2 is used to tap the output signal for the optical spectrum analyzer (OSA).

The BP is injected into the linear cavity via C2 and is then amplified by the bi-directionally pumped Bi-EDF. The amplified BP is then coupled into the SMF to generate the first Stokes signal propagating in the opposite direction of the BP signal. The Stokes signal is then amplified by the bismuth-based EDF (Bi-EDF) amplifier before being re-circulated by the OC2 ring cavity back towards the SMF. The 1st Stokes then travels towards OC1 where it is tapped by the coupler C1 for viewing at the OSA. As it travels, the 1st Stokes will also generate the 2nd Stokes in the SMF, which will also travel towards OC1 and be re-circulated into the system, much like the 1st Stokes. This generation process continues as the incoming Stokes exceeds the threshold values for Brillouin gain, thereby providing cascaded Brillouin Stokes. The number of Stokes generated depends on the total gain of the Brillouin/Bi-EDF amplifier over the cavity loss. The output of the linear cavity BEFL is tapped from the 5% port of C1 at OC1 and characterized by an OSA with a resolution of 0.015 nm. The linewidth of the BP signal is 15 MHz, which is measured using a heterodyne technique.

3. Result and discussion

The operating wavelength of the BEFL is determined by the gain of the bi-directionally pumped Bi-EDF over its cavity loss and this covers the L-band region (1560–1600 nm). The free-running spectrum of the BEFL, which is taken without BP at a pump power of 120 mW for the two 1480 nm pumps is shown Fig. 2. In the experiment, C2 is a 99/1 coupler with the 99% output designated as Port B. The peak wavelength is generated at the 1570 nm region, which is where the difference between the Bi-EDF gain spectrum and cavity loss is the largest. The free-running BEFL exhibits a peak power of approximately −30 dBm with bandwidth of approximately 3 nm centered at 1570.5 nm. The chosen BEFL-operating wavelength must be within or as close as possible to the bandwidth of the free-running BEFL.

The impact of the coupling ratio of C2 on the number of Stokes and anti-Stokes generated by the BEFL is depicted in Fig. 3. The 1480 nm pump and BP powers are fixed at 120 mW and 8 dBm, respectively. The BP wavelengths are optimized to 1570.7, 1570.3 and 1568.5 nm for the coupling ratios of 50/50, 80/20 and 99/1, respectively. The coupling ratio of C2 controls the amount of BP power that is injected into the cavity provides the reflectivity of ring 2. A higher ratio at Port B translates into a higher injected BP power and lower reflectivity of OC2. As shown in Fig. 3, an

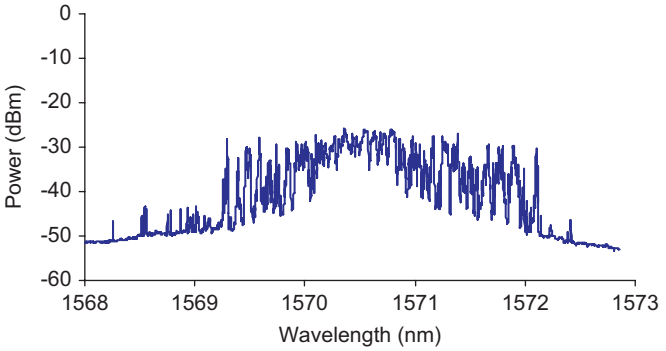

Fig. 2. Free-running spectrum of the BEFL (without BP). The powers of P1 and P2 are fixed at 120 mW.

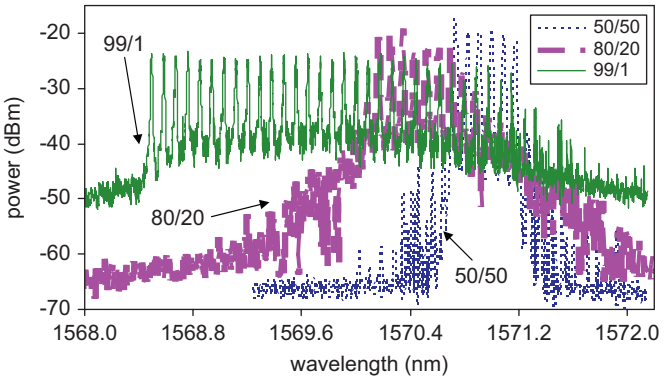

Fig. 3. Output spectrum of BEFL at different C2 coupling ratios. The P1, P2 and BP powers are fixed at 120 mW, 120 mW and 8 dBm, respectively.

increment of the Port B ratio (50%, 80% and 99%) increases the number of lines of the BEFL output, but reduces the peak power of these lines. The reduction of the peak powers are due to the reflectivity of the OC2 ring, which subsequently increases the cavity loss. This also has the effect of shifting the operating wavelength of the BEFL travels to the shorter wavelength region.

The impact of the 1480 nm pump power on the number of Stokes generated by the BEFL is depicted in Fig. 4. The BP is set at a wavelength of 1569.0 nm, which is close to the lasing wavelength of the free-running BEFL and the BP power is fixed at 8 dBm. Both the 1480 nm pump powers are varied from 60 and 120 mW. Lower pump powers will not give any Stokes due to the low EDFA gain, and thus the minimum pump power is 60 mW. At a pump power combination of 60 and 100 mW, the least number of lines are generated as shown in Fig. 4. However, as the combination pump power increases, the number of lines generated also increases. This can be attributed to the increment of the erbium gain with

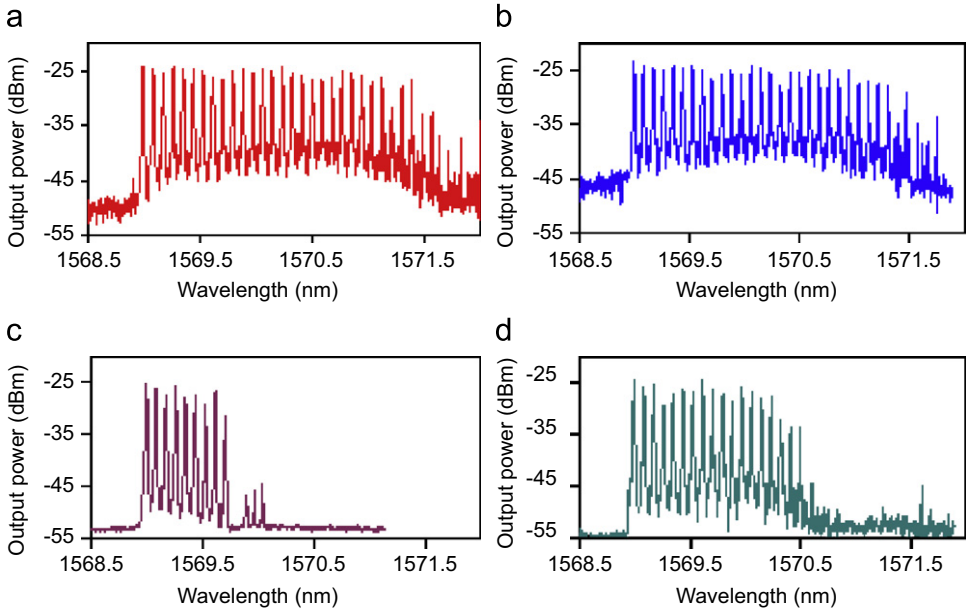

Fig. 4. Multi-wavelength spectra at different combination 1480 nm pump powers. The BP power and wavelength is fixed at 8 dBm and 1569.0 nm, respectively. (a) P1 = P2 = 120 mW, (b) P1 = P2 = 105 mW, (c) P1 = 60 mW, P2 = 100 mW and (d) P1 = 105 mW, P2 = 60mW.

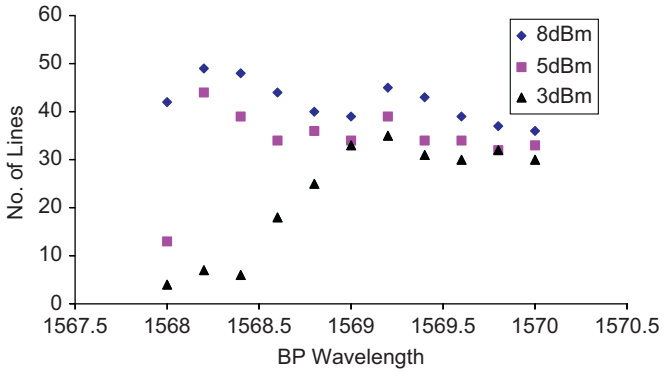

Fig. 5. Number of BEFL lines against BP wavelength at different injected BP power. Both the P1 and P2 pump powers are fixed at 120 mW.

increase in the pump power as this situation provides sufficient signal power for higher order Stokes signal to pump the SMF and maintain the cascading of the Stokes into multiple Stokes. As shown in the figure, the highest number of lines is obtained at a pump power of 120 mW. The number of lines is higher in Fig. 4(d) as compared with that in Fig. 4(c) even though two pump power combinations are almost similar, due to gain characteristics of the bi-directionally pumped Bi-EDF amplifier. A higher gain is obtained if the signal is injected from the side with higher pump power.

Fig. 5 shows the number of multi-wavelength lines as a function of BP wavelength at different BP power. In the experiment, the BP wavelength is varied from 1568 to 1570 nm, which is close to the lasing bandwidth of the free-running BEFL and the BP power is varied from 3 to 8 dBm. Both of the pump powers are fixed at 120 mW. Below a BP power of 3 dBm, the BEFL system operates with the presence of the free-running Bi-EDF laser cavity modes within the cascaded Stokes bandwidth. Therefore, the experiment is not continued for BP powers below this power since the BEFL system is observed to be working under an instable domain. The optimum BP wavelength is moving towards longer wavelength as the BP power reduces. The maximum multi-wavelength line of 50 is obtained at BP wavelength of 1568.2 nm and BP power of 5 dBm. As the BP moves farther away from this wavelength (1568.2 nm), less and less Stokes and anti-Stokes lines are observed as the gain decreases and becomes less and less sufficient to support the cascading process. If the BP is considerable far from the lasing bandwidth of the free-running BEFL, there is no gain to support the cascading process, and thus no Stokes lines are observed. The number of lines increases as the BP power increases from 3 to 8 dBm as is expected when the BP power is increased as now more Stokes can be generated before the cascading process stops.

Fig. 6 shows the output spectrum of the multi-wavelength BEFL at BP wavelength of 1568.2 nm and a BP power of 5 dBm. In this experiment, 50 multi-wavelength lines are obtained at the maximum pump power of 120 mW. However, a higher number of Stokes is expected at a higher pump power. The line spacing is approximately 0.09 nm in the wavelength domain and 11 GHz in the frequency domain while the 3 dB bandwidth of each line is about 0.02 nm, limited by the OSA resolution of 0.015 nm. The BEFL also generates anti-Stokes as shown in Fig. 3, especially at the higher pump powers. The anti-Stokes signals arise from the bi-directional operation and four-wave mixing in the SMF and they are more obvious when the powers of the 1480 nm pumps and the BP are increased. Additionally, the power of each subsequent Stokes lines is typically lower than that of the previous Stokes line, as each subsequent Stokes is generated with the energy of the previous Stokes, slightly reducing the Stokes line's power. However, some of the lines have a peak power, which is higher than the previous lines as shown in Fig. 6. This is attributed to other phenomenon such as four-wave mixing, which will transfer energy from neighboring lines to this line. The multi-wavelength output of the BEFL is observed to be stable at room temperature with only minor fluctuations observed coinciding with large temperature variances.

The number of lines obtained in the proposed BEFL is higher as compared with the previous ring cavity BEFL configuration [12].

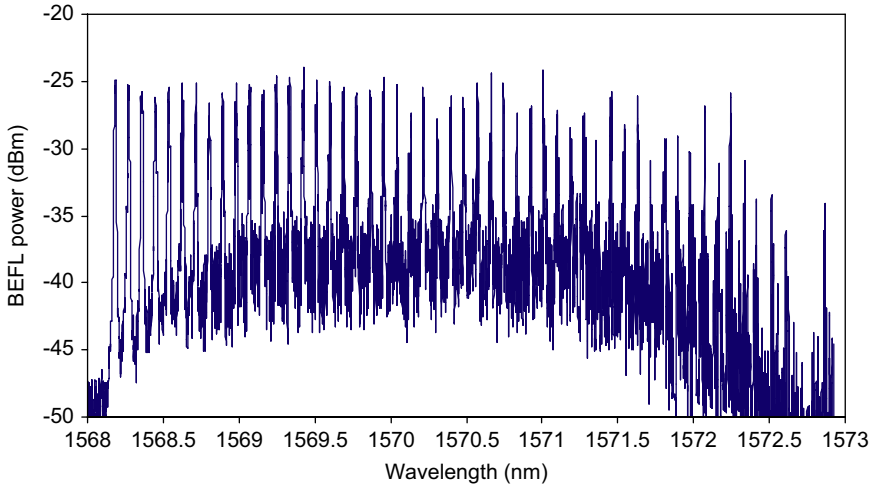

Fig. 6. BEFL output spectra at BP wavelength of 1568.2 nm and BP power of 5 dBm.

The linear cavity BEFL allows the lasing wavelength to passing the Bi-EDF gain twice per one oscillation and thus increases the net gain per oscillation. This resulted in the linear cavity BEFL to exhibit a lower threshold power and achieves a larger number of Stokes and anti-Stokes compared with the ring configuration. The proposed BEFL using a short-length bismuth-based EDF gain medium will allow for the development of compact BEFL devices. Further reductions in size can be obtained if the SMF is replaced with highly non-linear fibers such as holey fibers. A holey fiber with a core diameter of $\sim$1.6 μm would require less than 100 m to obtain the SBS effect desired [14].

4. Conclusion

A multiple wavelength source using a Bi-EDF in a linear cavity configuration is proposed and demonstrated in this paper. The configuration uses a pair of optical circulators at both the input and output ends of the cavity to form a resonator for multi-wavelength generation, and also one optical coupler to inject the BP at one end and another optical coupler to tap the output at the other end of the linear cavity. A short length of 2.15 m of Bi-EDF together with an SMF optical fiber has generated the multi-wavelength BEFL with a wavelength spacing of 0.09 nm in the L-band region. A stable output laser comb of 50 lines is obtained at a BP of 1568.2 nm and 5 dBm and two 1480 nm pumps at 120 mW. The injected BP wavelength and power together with the 1480 nm pump laser has a great effect on the number and output peak power of the BEFL lines. Using the Bi-EDF, a compact BEFL can be realized. With the existence of highly non-linear fibers such as holey fibers, a more compact BEFL can be designed using the proposed configuration.

References

[1] Dong XP, Li S, Chiang KS, Ng MN, Chu BC. Multiwavelength erbium-doped fiber laser based on a high-birefringence fiber loop mirror. Electron Lett 2000; 36:1609–10.
[2] Moon DS, Paek UC, Chung Y. Multiwavelength lasing oscillations in an erbium-doped fiber laser using few-mode fiber bragg grating. Opt Express 2004;12:6147–52.
[3] Qureshi KK, Tam HY, Chung WH, Wai PK. Multiwavelength laser source using linear optical amplifier. IEEE Photon Technol Lett 2005;17:1611–3.
[4] Han YG, Kim CS, Kang JU, Paek UC, Chung Y. Multiwavelength Raman fiber ring laser based on tunable cascaded long-period fiber gratings. IEEE Photon Technol Lett 2003;15:383–5.
[5] Harun SW, Shirazi MR, Ahmad H. A new configuration of multi-wavelength Brillouin fiber laser. Laser Phys Lett 2008;5:48–50.
[6] Wang DN, Tong FW, Fang X, Jin W, Wai PKA, Gong JM. Multiwavelength erbium-doped fiber ring laser source with a hybrid gain medium. Opt Commun 2003;228:295–301.
[7] Qin S, Chen DR, Tang Y, He S. Stable and uniform multiwavelength fiber laser based on hybrid Raman and erbium-doped fiber gains. Opt Express 2006; 14:10522–7.
[8] Ahmad H, Saat NK, Harun SW. S-band erbium-doped fiber ring laser using a fiber bragg grating. Laser Phys Lett 2005;2:369–71.
[9] Abdullah F, Noor ASM, Mahdi MA, Rashid HAA, Abdullah MK. Intracavity loss control effect on tuning range of tunable dual erbium-doped fiber laser. Laser Phys Lett 2005;2:535–7.
[10] Chen SP, Ding L, Wang SM, Li YG, Lu KC, Zhou SH. Switchable dual-wavelength erbium-doped fiber ring laser using bending dependent loss to switch the operating wavelength. Laser Phys Lett 2006;3:584–7.
[11] Sugimoto N, Ochiai K, Hirose T, Ohara S, Fukasawa Y, Hayashi, et al. Ultracompact gain block with Bi_2O_3-based erbium-doped fiber. Jpn J Appl Phys 2004;43:2551–2.
[12] Shahabuddin NS, Harun SW, Zulkifli MZ, Thambiratnam K. Ahmad H. Bismuth-based Brillouin/erbium fiber laser. J Modern Opt 2007, accepted for publication.
[13] Ahmad H, Shahabuddin NS, Dimyati K, Jusoh Z, Harun SW. An enhanced bismuth-based Brillouin/erbium fiber laser with linear cavity configuration. Fiber Integrated Opt 2008;27:35–40.
[14] Lee JH, Yusoff Z, Belardi W, Ibsen M, Monro TM, Richardson DJ. Investigation of Brillouin effects in small-core holey optical fiber: lasing and scattering. Opt Lett 2002;27:927–9.

ISAST Transactions on Electronics and Signal Processing, No. 1, Vol. 1, 2007

Effect of Brillouin Pump Linewidth on the Performance of Brillouin Fiber Lasers

M. R. Shirazi[1,] S. W. Harun, M. Biglary[1], K. Thambiratnam[1], and H. Ahmad[1]

Abstract— **The effect of the pump linewidth on the performance parameters of Brillouin fiber lasers (BFLs) such as the linewidth, output power, and threshold, as well as the suitability of the BFL in measuring narrow laser linewidths is demonstrated. For the Brillouin pump (BP) linewidths of 15.2 MHz and 124 MHz, BFL linewidths of 8 Hz and 24 Hz respectively were obtained from heterodyne beat signals. Due to the BFL linewidth decrease, the corresponding BFL threshold also decreases, resulting in the BFL power for the BFL linewidth of 8 Hz being 9.7 dBm higher than the power of the BFL linewidth of 24 Hz at the same BP power of 14.3 dBm in a pure silica single-mode fiber. These results demonstrate ultra-narrow BFL linewidths and the role of the narrow BP linewidth in the development of high performance BFLs.**

Index Terms—**Brillouin scattering, fiber laser, linewidth, BFL**

I. INTRODUCTION

Stimulated Brillouin Scattering (SBS) is a nonlinear effect that results from the interactions between the intense pump light and acoustic waves in a single-mode fiber (SMF), subsequently giving rise to backward propagating frequency-downshifted light [1]. The thermally excited acoustic waves generate an index grating that co-propagates with the pump at the acoustic velocity in the SMF. This moving grating reflects the pump light and causes the backscattered light to experience a downshift in the frequency as a result of Doppler Effect. The shift in frequency with respect to the pump is given by $\Delta\nu_{BS} = (2V_A / c)\,\nu_P$, where V_A is the acoustic velocity in the fiber and ν_P is the optical frequency of the pump beam. The frequency shift in the 1550 nm region is approximately 10 GHz (0.08 nm). Although SBS generation can be detrimental in coherent optical communication systems [2], it does serve useful purposes, for instance in producing Brillouin fiber lasers (BFL) [3]. BFLs are highly coherent light sources and have generated increasing interest for a number of applications such as gyroscopes and sensors due to their extremely narrow linewidths [4].

Manuscript received May 7, 2007.This work was done in the Department of Physics, Faculty of Science, University of Malaya, Malaysia.

Authors[1] are with the Photonics Research Center, Department of physics, University of Malaya, 50603 Kuala Lumpur, Malaysia.(Phone & fax: 603-79674290; e-mails: behshirazi@yahoo.com, harith@um.edu.my).

S.W. Harun is now with the Department of Electrical Engineering, Faculty of Engineering, University of Malaya, 50603 Kuala Lumpur, Malaysia. (e-mail: swharun@um.edu.my).

In this paper, the effect of the pump linewidth on the performance of the BFL is demonstrated after measuring the narrow and wide Brillouin pump linewidths. The output power, linewidth, and threshold of the BFL are compared for the two different Brillouin pump linewidths.

II. EXPERIMENTAL SETUP

The experimental setup is shown in Fig. 1 with a coupler and a long single-mode fiber (SMF) acting as a resonator. The BFL is pumped by an external cavity tunable laser source (TLS) which is amplified by an erbium-doped fiber amplifier. The maximum power of the amplified Brillouin pump (BP) is approximately 14.3 dBm. The BP is injected into the resonator from port 1 through port 2 of the optical circulator in a clockwise direction. The generated backward-propagating SBS oscillates inside the resonator in an anti-clockwise direction to generate the backward BFL, which is coupled out via a 3-dB coupler. From port 2, the BFL is then routed into an optical spectrum analyzer (OSA) through port 3 of the optical circulator. The SMF used in the experiment is 25 km in length and has a cut-off wavelength of 1161 nm with a zero dispersion wavelength of 1315 nm and a mode field diameter of 9.36 μm. The output laser is characterized using an OSA with a resolution of 0.015 nm while the linewidth of the laser is measured using an optical spectrum analyzer and the heterodyne beat technique [5].

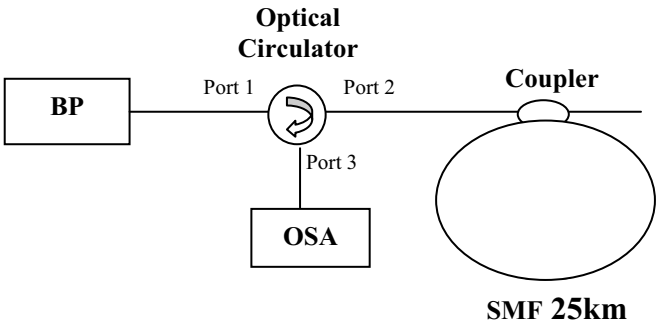

Fig. 1: Experimental set up

III. RESULTS AND DISCUSSION

Fig. 2 and Fig. 3 compare the BFL output spectrum at different BP linewidth settings with the BP powers of 4.5 dBm and 14.3 dBm, respectively. Both figures show three

simultaneous lines: anti-Stokes at approximately 1549.9 nm, BP reflections at 1550 nm and BFL lines at around 1550.1 nm so that the Brillouin shift is approximately 0.086 nm. The anti-Stokes signal is observed at a shorter wavelength due to four-wave mixing between the BP and Stokes line. Although the anti-Stokes power remains almost unchanged, the powers of the BP reflections and BFL lines increase as the BP power increases due to Brillouin induced crosstalk between the lines [6]. With the BP wide linewidth setting, the BFL power is relatively lower as compared to the BP narrow linewidth setting as depicted in Fig. 2.

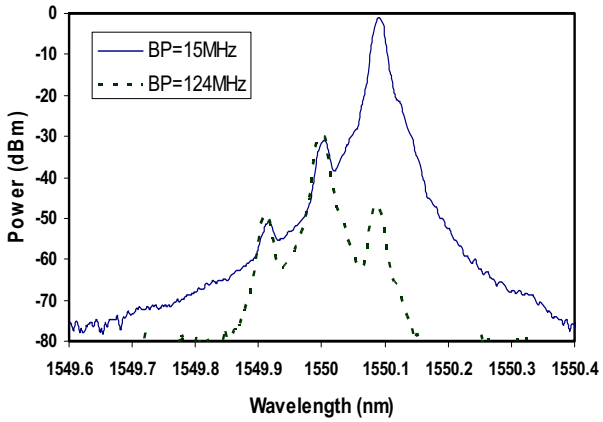

Fig. 2: The BFL output spectrum for different BP linewidths (15 MHz and 124 MHz) at BP power 4.5 dBm.

The maximum BFL power as shown in Fig. 3 is obtained 8.5 dBm using the BP narrow linewidth setting (15 MHz) at the BP power of 14.3 dBm, which is 9.7 dB higher than the maximum BFL power obtained using the BP wide linewidth setting (124 MHz) at the same BP power. Thus the pump conversion efficiency increases from 2.82% to 26.3% by changing the BP linewidth from wide to narrow.

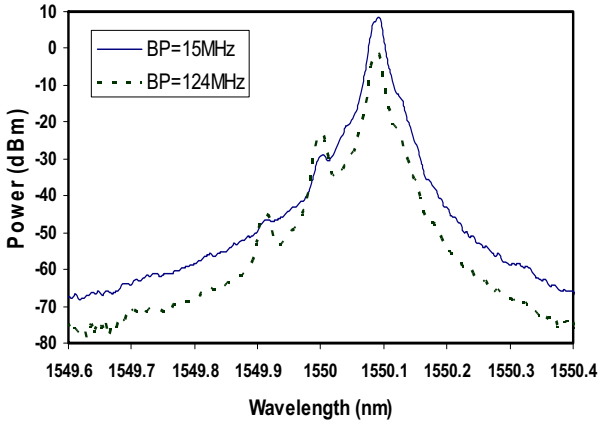

Fig. 3: The BFL output spectrum for different BP linewidths (15 MHz and 124 MHz) at a BP power of 14.3 dBm.

In the BP linewidth measurement, we use a 3-dB coupler to obtain the heterodyne beat frequency between the pump and the narrow BFL generated by the narrow linewidth pump setting. In accordance with the theory [7], this approximation is allowed for as the BFL linewidth is ignorable in comparison to the BP linewidth. While the powers of the pump and the BFL are the same, their frequencies are slightly different. The heterodyne beat spectrum between the pump and the BFL is shown in Fig. 4 for the narrow and wide linewidth pump settings. The pump linewidths are obtained at 15 MHz and 124 MHz.

(a)

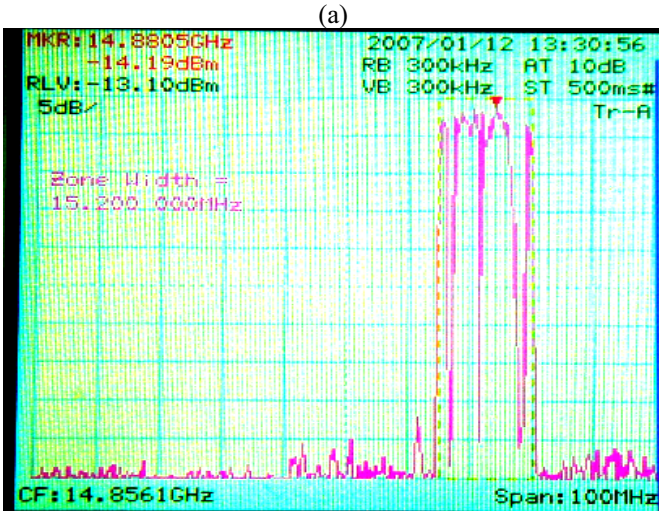

(b)

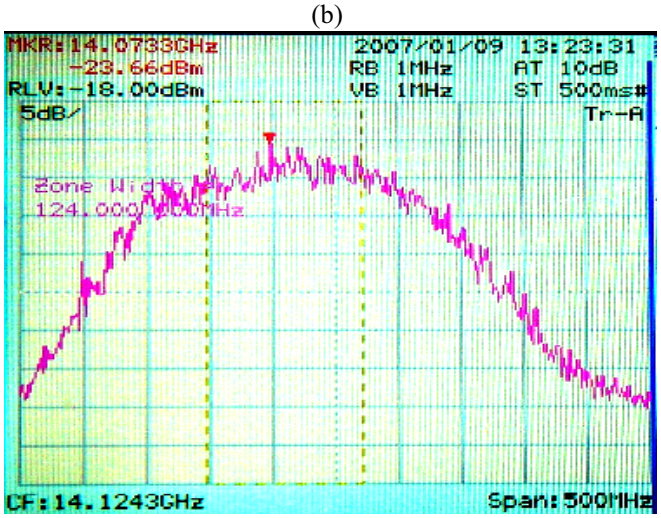

Fig. 4: Heterodyne beat spectra between the narrow BFL and the BP at (a) narrow (15 MHz) and (b) wide (124 MHz) BP linewidth settings.

In order to obtain BFL linewidth, two similar but independent BFL configurations are used to generate the heterodyne beat spectum in the 3-dB coupler. As before, the two BFLs have the same power but slightly different frequencies. Fig. 5 shows the heterodyne beat spectra of the two BFLs generated by the two different BP linewidths at 15 MHz and 124 MHz with measured BFL linewidths of 8 Hz and 24 Hz respectively.

(a)

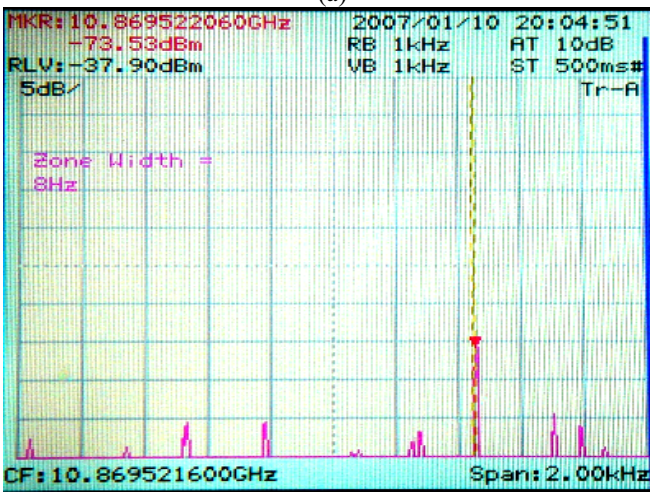

(b)

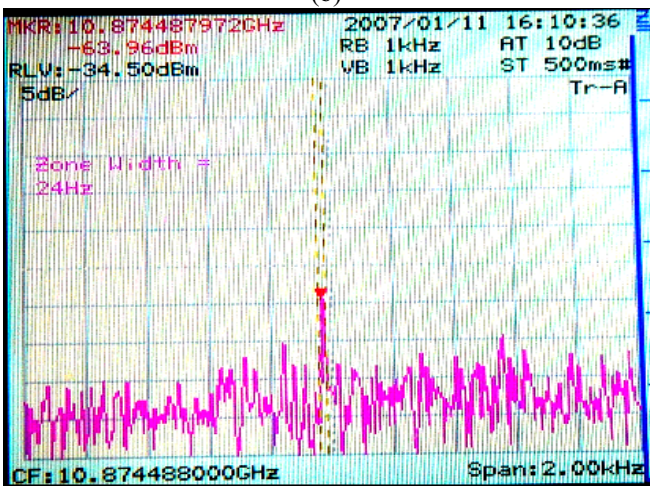

Fig. 5: Heterodyne beat spectra between the two similar independent BFLs generated by the BP linewidths (a) 15 MHz and (b) 124 MHz.

Finally, Fig. 6 shows the BFL power against the BP power at the BP linewidths of 15 MHz and 124 MHz respectively. As shown in Fig. 5, the narrow linewidth contributes to the higher output power of the BFL and the lower BFL operation threshold. In the low–BP power range, BFL power for both BP linewidths 15 MHz and 124 MHz increase linearly as BP power increases. However, as the power exceeds a given critical power, the BFL power rapidly increases. The slope of the graph is measured to be about to 1.24 and 1.21 before the critical power levels, and also having approximately same values after the levels for the BFL linewidths 15 MHz and 124 MHz, respectively. The SBS threshold power is defined the BP power at this critical power level, therefore, the SBS thresholds, and so the BFL thresholds are observed at approximately 2 dBm and 11 dBm at BP linewidths of 15 MHz and 124 MHz respectively.

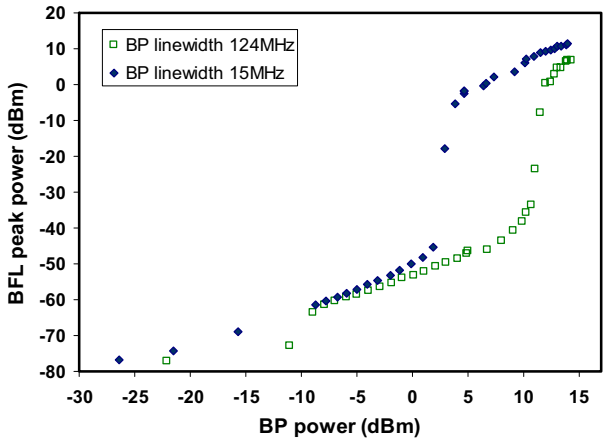

Fig. 6: BFL peak power as a function of BP power at different BP linewidths.

IV. Conclusion

The effect of the BP linewidth on the power, linewidth, and threshold of the BFL are demonstrated. At BP powers of 14.3 dBm, the BFL power of 8.5 dBm is obtained at the BP linewidth 15 MHz which is 9.7 dB higher as compared to the BFL power at a BP linewidth of 124 MHz. The measured ultra-narrow BFL linewidths revealed 24 Hz and 8 Hz as the BP linewidth is changed from 124 MHz to 15 MHz and the corresponding BFL threshold is decreased from approximately 11 dBm to 2 dBm. Thus, these results show ultra-narrow BFL linewidths and how the narrowing of the BP linewidth improves the performances of the BFL output.

References

[1] G. P. Agrawal, *Nonlinear Fiber Optics*, 3rd ed. San Diego, CA: Academic, Ch. 9, 2001.
[2] A. R. Chraplyvy, "Limitations in lightwave communications imposed by optical-fiber nonlinearities," *J. Lightwave Technol.*, vol. 10, pp. 1548–1557, 1990.
[3] Hill, K.O., Kawasaki, B.S., and Johnson, D.C.: 'CW Brillouin laser', *Appl. Phys. Lett.*, 28, pp. 608–609, 1976.
[4] S. P. Smith, F. Zarinetchi, and S. Ezekiel, "Narrow-linewidth stimulated Brillouin fiber laser and applications," *Opt. Lett.*, vol. 16, pp. 393–395, 1991.
[5] W. V. Sorin, *Fiber Optic Test and Measurement*, D. Derickson, Ed. Upper Saddle River, NJ: Prentice Hall, 1998, ch. 10.
[6] G.P. Agrawal, *Fiber Optic Communication System,* 3rd ed., New York, Wiley Interscience, John Wiley & Sons INC, pg.369, 2001.
[7] A. Debut, S. Randoux and J. Zemmouri, "Linewidth narrowing in Brillouin lasers: Theoretical analysis," *Phys. Rev.*, vol. A62, no. 2, pp. 023803-1 - 023803-4, 2000.

M.R. Shirazi (Mohammadreza Rezazadeh Shirazi) was born in Shiraz, Iran in 1970.This author received B.Sc. in applied physics and M.Sc. in physics (atomic & molecular branch) from Shahid Bahonar University of Kerman, Iran in 1993 and 1999, respectively.
From 2000 to 2006, he worked as a full-time academic member in physics department at the Islamic Azad University (Kerman branch). Now, as a student in PhD, he works in nonlinear fiber optics with Professor Dr. Harith Ahmad and Dr. Sulaiman Wadi Harun as supervisors and Mozhgun Biglary and Kelvin Thambiratnam as physics students in M.Sc at the University of Malaya, Malaysia.

Effects of different Raman pumping schemes on stimulated Brillouin scattering in a linear cavity

M. R. Shirazi,[1,*] M. Biglary,[1] S. W. Harun,[2] K. Thambiratnam,[1] and H. Ahmad[1]

[1]Photonics Research Center, Department of Physics, University of Malaya, 50603 Kuala Lumpur, Malaysia

[2]Department of Electrical Engineering, Faculty of Engineering, University of Malaya, 50603 Kuala Lumpur, Malaysia

*Corresponding author: behshirazi@yahoo.com

Received 23 January 2008; revised 25 March 2008; accepted 7 May 2008;
posted 9 May 2008 (Doc. ID 91934); published 2 June 2008

The effects of backward, forward, and bidirectional Raman pumping schemes on stimulated Brillouin scattering (SBS) is investigated in this study. By using a linear cavity, we utilize residual Brillouin pump (BP) and Raman pump (RP) power after each transmission through a 25 km single-mode fiber (SMF) used as a gain medium. The SBS threshold power is reduced in the forward, backward, and bidirectional Raman pumping schemes by 2.5, 1.75, and 2.75 dB, respectively when the 1480 nm RP power is fixed at 150 mW and the BP wavelength is 1580 nm. Surprisingly, it is revealed that the SBS threshold reduction depends strongly and solely on Raman gain and it is independent of the Raman pumping schemes. In addition, the effect of Raman amplification on SBS is more effective at the SBS threshold, especially in the bidirectional and forward schemes.

OCIS codes: 290.5900, 290.5860, 060.2320.

Raman and Brillouin scattering are inelastic processes in which part of the optical wave power is absorbed by the transmission medium while the remaining energy is reemitted as a wave (Stokes wave) with a down-shifted frequency called a Stokes shift. The growth of Brillouin and Raman Stokes waves is governed by the Brillouin-gain g_B and the Raman-gain g_R. For silica fibers, the peak values of g_B and g_R are about $g_B = 6 \times 10^{-11}$m/W and $g_R = 7 \times 10^{-14}$m/W and occur for the Brillouin and Raman Stokes shifts by about 13 THz and 10 GHz, respectively. In addition, stimulated Brillouin scattering (SBS) and stimulated Raman scattering (SRS) have threshold pump powers above which pump power transfer to the Stokes wave increases rapidly [1]. For signal transmission in optical fibers, SBS limits the launched power to a few milliwatts because of its low threshold in comparison to SRS [2]. However, SBS has been advantageously utilized in the past few years for some applications, such as Brillouin fiber lasers [3,4].

The effect of SBS on the properties of Raman amplifiers has been studied in previous works [5]. These studies show that SBS causes saturation of Raman gain with forward or copropagating Raman pumping, where the Raman pump (RP) light is injected in the same direction as the signal under amplification. Although forward pumping is used in some Raman amplification schemes, the most common type of Raman amplifiers currently in use for relative-intensity noise relies on backward or counterpropagating Raman pumping in which the RP travels in the opposite direction of the signal [6]. It has been indicated that by means of multiwavelength Raman pumping, it is possible to achieve flattening of Raman gain and broadening of Raman amplification bandwidth even with backward pumping. However, it has also been reported that without the use of forward Raman amplification, flattening of noise figure cannot be realized. This results in what is known as bidirectional Raman amplification where the forward and backward Raman pumping operates simultaneously [7]. For further explanation of RP schemes

0003-6935/08/173088-04$15.00/0

and details of definitions, the reader may also refer to Ref. [8]. There are still some debates on the advantages of either forward or backward Raman pumping schemes [9]. Since SRS and SBS are third order nonlinear optical effects, factors that increase Raman gain also facilitate in the generation of SBS [10]. Therefore, when using optical fibers such as dispersion compensating fibers (DCFs) where the effective area of the fiber core is small and the Raman gain is high in comparison with the standard SMFs, SBS readily occurs. To suppress SBS generation, we have to keep the light intensity below the SBS threshold power, or broaden the Brillouin pump linewidth [10,11]. The effect of Raman amplification on SBS threshold power has only been studied in backward or forward Raman pumping using different fibers [12,13].

In this work, the effects of the backward, forward, and bidirectional Raman pumping on SBS performance in a linear cavity are studied. We use a linear cavity to utilize residual Brillouin pump (BP) and RP power after each transmission through a 25 km SMF (gain medium). The results show that the reduction in SBS threshold power is interestingly related linearly to Raman gain, and this relationship is independent of Raman pumping schemes. In addition, Raman gain effect on the SBS is highly increased around the threshold especially in forward and bidirectional Raman pumping.

Figure 1 shows the experimental setup, where a 25 km SMF used as a gain medium located between Ports 2 of the two optical circulators (OC1 and OC2) to form a linear cavity. A (2 × 2) 1/99 coupler located between Port 3 and Port 1 of OC1 helps to inject BP into the cavity, to send a feedback signal, and at the same time, to extract part of the output. The BP signal is performed using an external cavity tunable laser source (TLS) amplified by an erbium-doped fiber amplifier (EDFA) to obtain the maximum power of 12 dBm at 1580 nm wavelength with a 15 MHz linewidth. The generated backward-propagating Brillouin Stokes and the transmitted BP signal reflected by OC2 are coupled from Port 2 to 3 in the circulator OC1 and 99% of that signal is reinjected back into the system by the coupler. Wavelength-division multiplexing couplers WDM1 and WDM2 are used simultaneously to inject Raman pump light into the system in bidirectional Raman amplification. However, to decrease loss in the cavity for forward Raman pumping, we remove WDM2 in the setup and connect Port 3 to the Port 1 of OC2. Similarly, WDM1 is removed for backward Raman pumping and BP is injected directly into the cavity through the 1/99 coupler. The SMF has a cutoff wavelength of 1161 nm with a zero dispersion wavelength of 1315 nm, a mode field diameter of 9.36 μm, and an attenuation coefficient of 0.19 dB/km at 1580 nm. The backward-propagating SBS is coupled out via the coupler and is characterized using an optical spectrum analyzer (OSA) with a resolution of 0.015 nm. WDM3 is incorporated in front of the OSA to suppress the residual Raman pump light in the output. In addition, an OSA is used in the setup instead of a power meter to avoid additional noises during measurement. Errors can originate from the measuring instruments, i.e., TLS, OSA in the setup, and the power meter used to measure the power at 1480 nm, each with, respectively, 0.05, 0,05, and 0.01 dB of optical power measurement error. The total error is calculated using the following equation [14]:

$$\text{Total error} = 2\sqrt{\sum \frac{U^2}{3}},$$

where U is the error or uncertainty of each individual instrument. For the current setup, the total error in our measurement is about 0.08 dBm.

Figure 2 shows the output Brillouin Stokes peak power and the transmitted BP peak power against the input signal BP power, with and without 1480 nm RPs, in various pumping schemes. Figures 2(a)–2(c) represent backward, forward, and bidirectional Raman pumping, respectively. Before the transmitted BP power starts to saturate quickly around −5 dBm in the schemes, the output power of the SBS increases in accordance with the increase of the BP power. The SBS threshold power, P_{SBS}, is defined as an input BP power at which the transmitted BP peak power equals the output peak power of the SBS [15]. To decrease loss, we remove WDM2 and

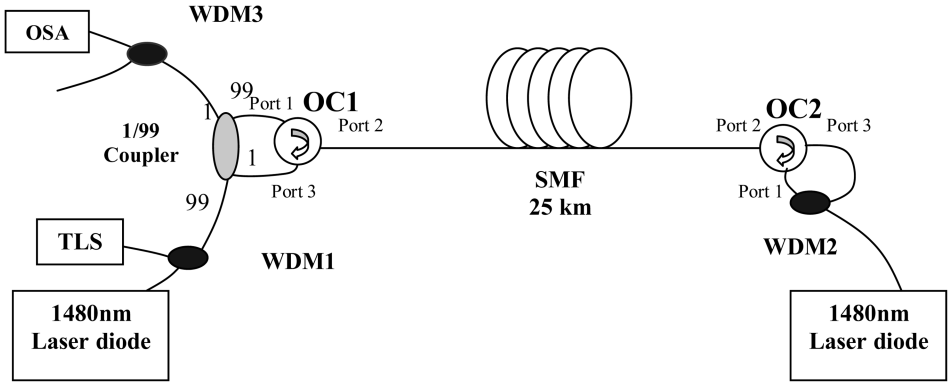

Fig. 1. Experimental setup for bidirectional Raman pumping. To decrease loss, WDM2 and WDM1 are removed from the configuration for forward and backward Raman pumping, respectively.

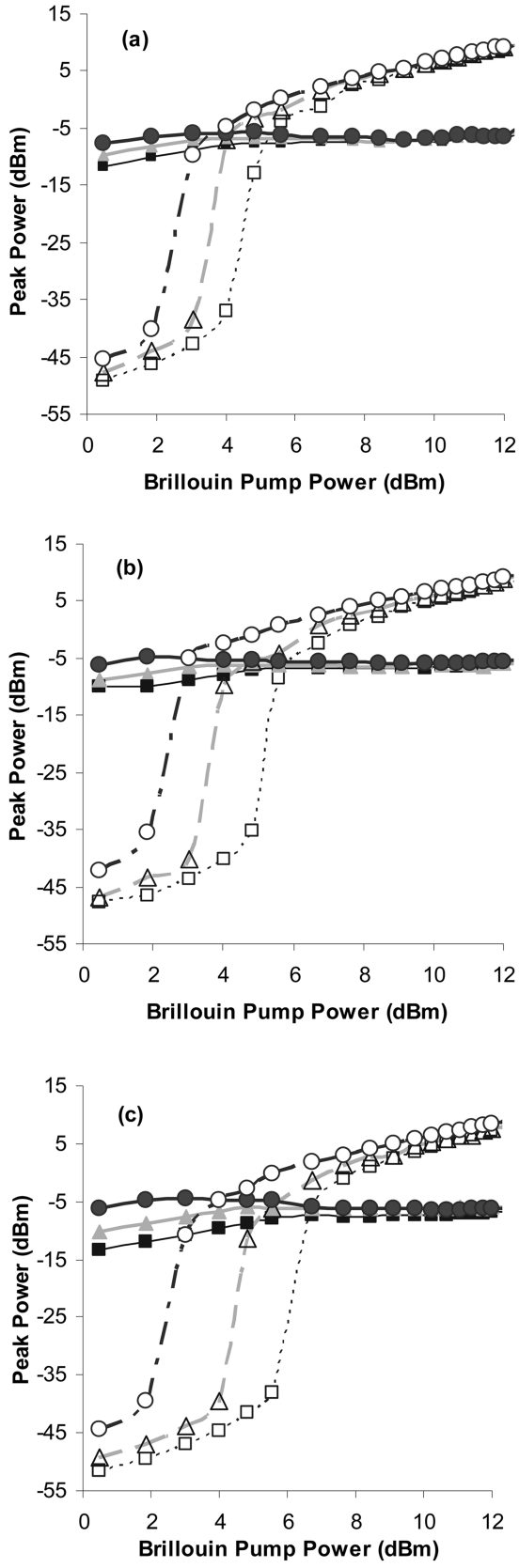

Fig. 2. Output transmitted BP power, solid lines, and Brillouin Stokes power, dashed lines, as a function of the input BP power in the case of (a) backward, (b) forward, and (c) bidirectional Raman pumping. The squares, triangles, and circles represent the cases where RP power is 0, 75, and 150 mW, respectively.

WDM1 from the configuration for forward and backward Raman pumping, respectively. Therefore, when the RP power is off, we have different SBS threshold powers, i.e., 5.25, 5.6, and 6.75 dBm, due to different losses for backward, forward, and bidirectional schemes, respectively. In the experiment, the RP power is varied from 0 to 150 mW. It should also be noted that the SBS threshold power decreases as the RP power is increased.

The SBS threshold reduction, Δ_{SBS} induced by Raman pumping, is examined and compared for different pumping schemes. It is at a maximum with the bidirectional Raman pumping scheme and at a minimum with the backward. It is also proportional to the RP power, as shown in Fig. 2. The SBS threshold power is reduced by 1.75, 2.5, and 2.75 dB in backward, forward, and bidirectional schemes, respectively, by the same 150 mW RP power at 1480 nm and a BP wavelength of 1580 nm. To further investigate the effect of Raman pumping on SBS, we define the Raman on–off gain (gain on–off) on the peak power of Brillouin Stokes as the increase in Brillouin Stokes peak power when Raman pumping operates. From Fig. 2, the gain can be measured easily for a given Brillouin pump power with RP power, $I = 75$ mW and $I = 150$ mW relative to $I = 0$ mW in the different Raman pumping schemes [Fig. 3(a)]. As expected, a decrease in P_{SBS} is observed with an increase in the RP power, especially in the case of the forward and bidirectional Raman pumping schemes. Because both SBS and SRS are related to the third order nonlinear susceptibility, the reduction of SBS threshold with an increase of the Raman pump means SBS dominates over SRS in a competition between them. In other words, SRS can effectively amplify Brillouin Stokes only around the Brillouin threshold power, as already shown in Fig. 2. Therefore, the Raman on–off gain must have a maximum around the SBS threshold. The gain starts to show saturation with the appearance of the SBS and is eliminated completely beyond the SBS threshold power. The gain on the SBS peak is also higher with a wider region for both the forward and the bidirectional pumping schemes in comparison to the backward pumping scheme.

Finally, from Figs. 2 and 3(a), the relationship between the SBS threshold reduction and the Raman peak gain on–off effect on the SBS threshold can be deduced as shown in Fig. 3(b). It is interesting that the relationship is almost linear and simple independent of the Raman pumping schemes.

In conclusion, the reduction in the SBS threshold power under different Raman pumping schemes is investigated experimentally in a linear cavity with 25 km SMF. The results show that SBS threshold decreases with the increase of Raman-gain effect on SBS and this decrease is much faster for bidirectional and forward pumping than for backward pumping due to a lower Raman gain on the SBS threshold. It is revealed that the amount of SBS threshold reduction depends strongly and solely on the gain effect on it, independent of Raman pumping scheme.

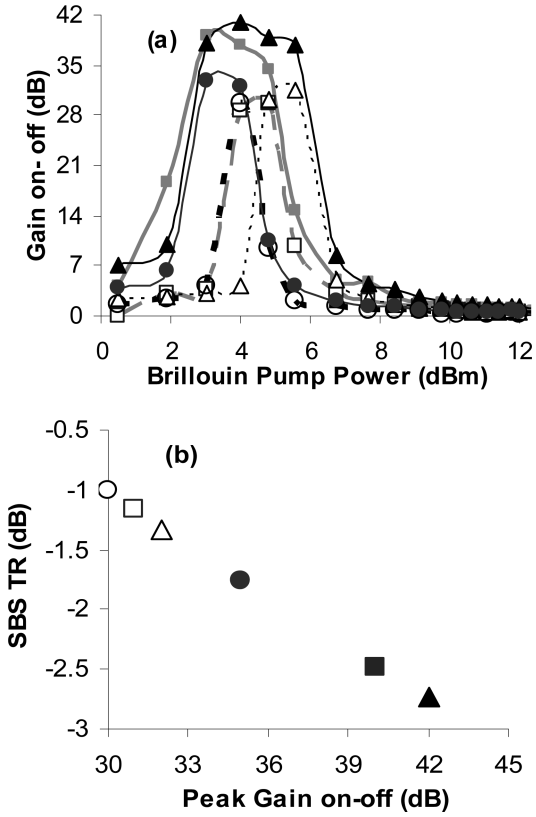

Fig. 3. (a) shows effect of Raman on–off gain on the peak power of Brillouin Stokes against various signal input BP and RP powers. From Figs. 2 and 3(a), we can immediately deduce the SBS threshold reduction (SBS TR) against peak Raman on–off gain effect on the Brillouin threshold, as shown in (b). Different Raman pumping schemes are indicated by markers, i.e., backward (circle), bidirectional (triangle), and forward (square). Solid lines and solid markers represent RP power at 150 mW, whereas dashed lines and hollow markers represent RP power at 75 mW.

References

1. G. P. Agrawal, *Nonlinear Fiber Optics*, 3rd ed. (Academic, 2001).
2. F. Forghieri, R. W. Tkach, and A. R. Chraplyvy, "Fiber nonlinearities and their impact on transmission systems," in *Optical Fiber Telecommunication IIIA*, I. P. Kaminow and T. L. Koch, eds. (Academic, 1997), pp. 196–264.
3. J. Geng, S. Staines, Z. Wang, J. Zong, M. Blake, and S. Jiang, "Highly stable low-noise Brillouin fiber laser with ultra narrow spectral line width," IEEE Photonics Technol. Lett. **18**, 1813–1815 (2006).
4. M. R. Shirazi, S. W. Harun, K. Thambiratnam, M. Biglary, and H. Ahmad, "New Brillouin fiber laser configuration with high output power," Microw. Opt. Technol. Lett. **50**, 265–266 (2008).
5. S. Hamidi, D. Simeonidou, A. S. Siddiqui, and T. Chaleon, "Effect of pump laser mode structure on the gain of forward pumped Raman fiber amplifier in the presence of stimulated Brillouin scattering," Electron. Lett. **28**, 1768–1770 (1992).
6. A. K. Zamzuri, M. A. Mahdi, A. Ahmad, M. I. Md Ali, and M. H. Al-Mansoori, "Flat amplitude multiwavelength Brillouin–Raman comb fiber laser in Rayleigh-scattering enhanced linear cavity," Opt. Express **15**, 3000–3005 (2007).
7. Y. Emori, S. Kado, and S. Namiki, "Independent control of the gain and noise figure spectra of Raman amplifiers using bidirectional pumping," Furukawa Rev. **23**, 11–15 (2003).
8. C. Headley and G. P. Agrawal, *Raman Amplification in Fiber Optical Communication Systems*, 1st ed. (Academic, 2005).
9. X. Liu and Y. Li, "Efficient algorithm and optimization for broadband Raman amplifiers," Opt. Express **12**, 564–573 (2004).
10. A. Kobyakov, M. Mehendale, M. Vasilyev, S. Tsuda, and A. F. Evans, "Stimulated Brillouin scattering in Raman-pumped fibers: a theoretical approach," J. Lightwave Technol. **20**, 1635–1643 (2002).
11. M. R. Shirazi, S. W. Harun, M. Biglary, K. Thambiratnam, and H. Ahmad, "Effect of Brillouin pump linewidth on the performance of Brillouin fiber laser," ISAST Transaction on electronics and signal processing **1**, 30–32 (2007).
12. T. Okuno and M. Nishimura, "Effects of stimulated Raman amplification in optical fiber on stimulated Brillouin scattering threshold power," Electron. Lett. **38**, 14–16 (2002).
13. M. Mehendale, A. Kobyakov, M. Vasilyev, S. Tsuda, and A. F. Evans, "Effect of Raman amplification on stimulated Brillouin scattering threshold in dispersion compensating fiber," Electron. Lett. **38**, 268–269 (2002).
14. D. Baney, C. Hentschel, and J. Dupre, "Optical fiber amplifiers-measurement of gain and noise figure," Hewlett-Packard Company, Lightwave Symposium, 1993.
15. T. Shimizu, K Nakajima, K. Shiraki, K. Ieda, and I. Sankawa, "Evaluation methods and requirements for stimulated Brillouin scattering threshold in a single-mode fiber," Opt. Fiber Technol. **14**, 10–15 (2008).

LASER PHYSICS LETTERS

www.lphys.org

Abstract: A multiple wavelength Brillouin fiber laser (BFL) is demonstrated using an injection of intense light at 1480 nm. The light generates Raman gain at around 1560 nm to amplify the Brillouin-Rayleigh backscattered light in the medium and allows the generation of multiple lines by self-feedback-seeding effects. Three Stokes are obtained in the BFL with the maximum power of the first Stokes at approximately −6 dBm from the injection of 1480 nm light at 150 mW. The line spacing is measured to be approximately 0.08 nm. There is no significant change in the power of the first Stokes with the injection of 1480 nm light; however the powers of additional Stokes are highest at Brillouin pump of 1560 nm.

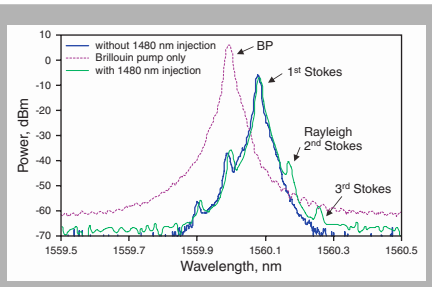

Comparison of BFL output spectrum with and without the 1480 nm light injection

Multiple wavelength Brillouin fiber laser from injection of intense signal light

S.W. Harun, [1] *M.R. Shirazi,* [2] *and H. Ahmad* [2]

[1] Department of Electrical Engineering, Faculty of Engineering, University of Malaya, Kuala Lumpur 50603, Malaysia
[2] Photonics Laboratory, Department of Physics, University of Malaya, Kuala Lumpur 50603, Malaysia

Received: 6 April 2007, Revised: 11 April 2007, Accepted: 14 April 2007
Published online: 27 April 2007

Laser Phys. Lett. **4**, No. 9, 678–680 (2007) / **DOI** 10.1002/lapl.200710039

WILEY-VCH

Laser Phys. Lett. **4**, No. 9, 678–680 (2007) / **DOI** 10.1002/lapl.200710039

Abstract: A multiple wavelength Brillouin fiber laser (BFL) is demonstrated using an injection of intense light at 1480 nm. The light generates Raman gain at around 1560 nm to amplify the Brillouin-Rayleigh backscattered light in the medium and allows the generation of multiple lines by self-feedback-seeding effects. Three Stokes are obtained in the BFL with the maximum power of the first Stokes at approximately −6 dBm from the injection of 1480 nm light at 150 mW. The line spacing is measured to be approximately 0.08 nm. There is no significant change in the power of the first Stokes with the injection of 1480 nm light; however the powers of additional Stokes are highest at Brillouin pump of 1560 nm.

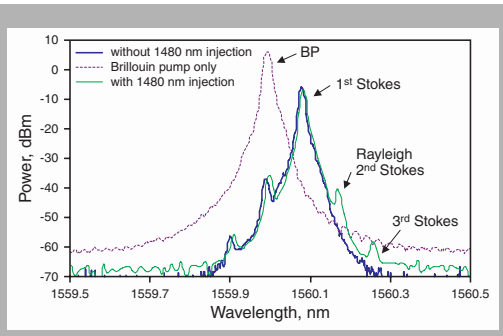

Comparison of BFL output spectrum with and without the 1480 nm light injection

Multiple wavelength Brillouin fiber laser from injection of intense signal light

S.W. Harun, [1,*] *M.R. Shirazi,* [2] *and H. Ahmad* [2]

[1] Department of Electrical Engineering, Faculty of Engineering, University of Malaya, Kuala Lumpur 50603, Malaysia
[2] Photonics Laboratory, Department of Physics, University of Malaya, Kuala Lumpur 50603, Malaysia

Received: 6 April 2007, Revised: 11 April 2007, Accepted: 14 April 2007
Published online: 27 April 2007

Key words: multi-wavelength light source; Brillouin fiber laser; stimulated Brillouin scattering

PACS: 42.60.Da, 42.81.-i, 42.81.Wg, 42.81.Uv

1. Introduction

Stimulated Brillouin Scattering (SBS) is a nonlinear effect resulting from the interaction between intense pump light and acoustic waves in a medium, giving rise to backward propagating frequency-shifted light [1]. The thermally excited acoustic waves generate an index grating that co-propagates with the pump at the acoustic velocity in the SMF. This moving grating reflects the pump light and causes the backscattered light to experience a downshift in the frequency through the Doppler Effect. The frequency shift with respect to the pump is given by $\Delta\nu_{BS} = (2V_A/c)\nu_P$, where V_A is the acoustic velocity in fiber and ν_P is the optical frequency of the pump beam. The frequency shift in the 1550 nm region is approximately 10 GHz, in the frequency domain or 0.08 nm in the wavelength domain. Although SBS generation can be detrimental in coherent optical communication systems [2], it can also be used to produce Brillouin fiber lasers [3–5]. BFLs have generated interest for a number of applications such as gyroscopes and sensors owing to their extremely narrow linewidth. Linewidths of only a few kHz are required for some of fiber optic sensors such as strain or temperature sensors. Narrow linewidth BFLs can be used to build distributed fiber optic sensor systems to detect, locate and classify disturbances over lengths greater than 10 km using a frequency modulated continuous wave technique, thus providing a cost effective security system for nuclear power plants and military bases as well as oil and gas pipeline integrity monitoring systems, and national border intrusion detection systems [6].

Multi-wavelength fiber lasers have been a topic of extensive study over the past decade with their potential application in optical communications, sensors and tera-

* Corresponding author: e-mail: swharun@um.edu.my

hertz frequency generation. They can be obtained through a number of approaches such as ASE slicing [7] and Brillouin/Erbium fiber lasers (BEFL) [8–10]. The BEFLs use erbium ion amplification in conjunction with a feedback loop to assist a cascading process for multi-wavelength operation. In this letter, a multi-wavelength Brillouin fiber laser (BFL) is demonstrated without any kind of re-injection port or ring structure and erbium-doped fiber. The BFL utilizes Raman gain from the injection of intense light at 1480 nm to assist in the generation of multi Stokes lines without the need for complex structures.

2. Experimental setup

The experimental setup for the multiple wavelength BFL is shown in Fig. 1. The resonator consists of a 3 dB coupler and a 25 km long single mode fiber (SMF) as the gain medium. The SMF has a cut-off wavelength of 1161 nm, zero dispersion wavelength of 1315 nm and a mode field diameter of 9.36 μm. The BFL is pumped by an external cavity tunable laser source (TLS) with a linewidth of approximately 20 MHz and a maximum power of approximately 5.5 dBm. A 1480/1550 nm wavelength division multiplexing (WDM) coupler is used to inject the 1480 nm intense light from laser diode into the system to assist the cascading process. The power of the 1480 nm laser diode is fixed at 150 mW.

The Brillouin pump (BP) is sent through the WDM coupler (which is also used to inject the 1480 nm intense light) and the optical circulator to generate backward-propagating Stimulated Brillouin Scattering (SBS). The backward-propagating SBS oscillates inside the loop of the 3 dB coupler to generate the Brillouin Stokes. The Stokes power is amplified by Raman gain through the injection of 1480 nm intense light to assists in the cascading process to generate a multiple line BFL. The laser output is characterized using an optical spectrum analyzer (OSA) which is located at port 3 of the optical circulator.

3. Results and discussion

Fig. 2 compares the output spectrum with and without the injection of intense light at 1480 nm. Without 1480 nm injection, a 5.5 dBm BP produces one Brillouin Stokes with -6 dBm peak power. In spite of the fact that the threshold of first-order SBS in a SMF is very low, the generation of second order SBS is not usually achieved. There are two factors that make the cascading process in SMF is ineffective. Firstly, as the pump power increases above the first-order threshold, the SBS power distribution inside the fiber becomes increasingly concentrated near the input of the fiber, subsequently decreasing the fiber length available for the SBS interaction. Secondly, in contrast to the first-order SBS process which is initiated using a monochromatic pump, the second-order SBS

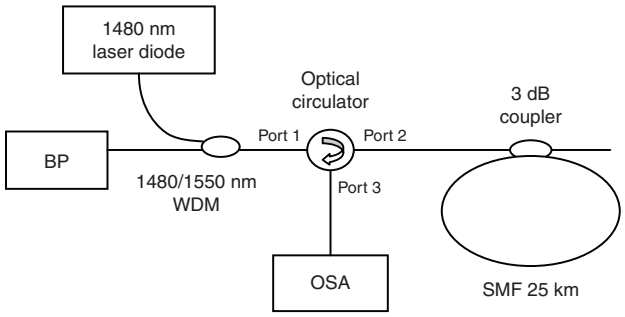

Figure 1 Experimental setup

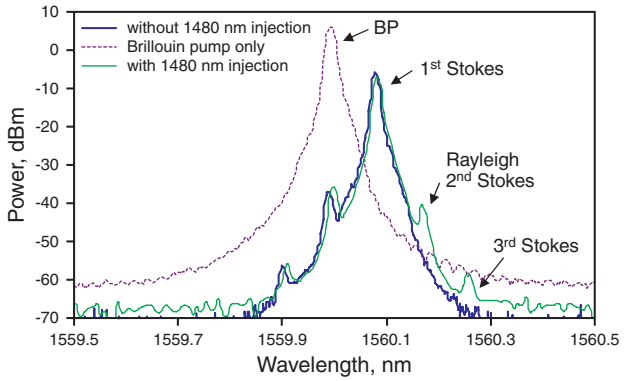

Figure 2 (online color at www.lphys.org) Comparison of BFL output spectrum with and without the 1480 nm light injection

is pumped by first-order Stokes radiation that is essentially non-monochromatic: its spectrum is only about 4 times narrower than the SBS gain spectrum in the fiber [11]. The situation however becomes very different in the presence of feedback to the SBS process as the feedback can cause considerable narrowing in the first-order SBS spectrum. Therefore, second-order SBS generation is commonly observed with the feedback [12].

As the 1480 nm power is injected, second and third Stokes lines are generated with no significant changes in the output power of the first Stokes as shown in Fig. 2. The first Stokes generates the second Stokes of Brillouin laser in the opposite direction, which is amplified by the Raman gain with the 1480 nm light injection. The second line from the peak in Fig. 2 is the amplified Rayleigh backscattered light from the second Stokes. The second Stokes also generates a third Brillouin Stokes in a direction similar to the first Stokes as shown in Fig. 2. The amplified Brillouin-Rayleigh backscattered light in the medium provides self feedback-seeding effects for generation of the multiple lines BFL. This feedback provides very effective linewidth narrowing of the laser radiation creating the conditions required for SBS.

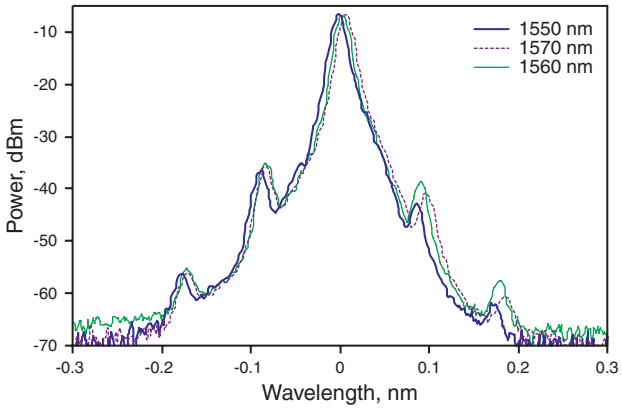

Figure 3 (online color at www.lphys.org) BFL output comb at different center wavelength of Brillouin pump

Fig. 3 shows the BFL output spectrum at different BP wavelengths. The BP and 1480 nm laser powers are fixed at 5.5 dBm and 150 mW respectively. There are no significant changes in power of the first Stokes as shown in Fig. 3. However, the powers of higher-order Stokes are seen to be highest at a wavelength of 1560 nm. This is attributed to the cavity loss which is lowest at this wavelength, making the Rayleigh scattering and Raman gain more pronounced at this wavelength. The number of Stokes is expected to be higher if the 1480 nm pump power is higher. The spacing between the lines is approximately 0.08 nm, as measured by an optical spectrum analyzer with a 0.015 nm resolution. Anti-Stokes lines are also generated through four-wave mixing between the Brillouin pump and Stokes line as shown in Fig. 2 and Fig. 3.

4. Conclusion

We demonstrate that the generation of multiple Stokes in the BFL can arise through an injection of 1480 nm intense light. The light amplifies Brillouin-Rayleigh backscattering Stokes in the medium to provide self-feedback seeding effects. Three Stokes were obtained in the BFL with the injection of 1480 nm intense light at 150 mW. The line spacing is measured to be approximately 0.08 nm. The first Stokes power obtained is approximately −6 dBm and does not change with the injection of 1480 nm light. However, the powers of additional Stokes are highest at a Brillouin pump of 1560 nm.

References

[1] G.P. Agrawal, Nonlinear Fiber Optics, 2nd ed. (Academic, San Diego, 1995), pp. 370–403.
[2] A.R. Chraplyvy, J. Lightwave Technol. **10**, 1548–1557 (1990).
[3] S.P. Smith, F. Zarinetchi, and S. Ezekiel, Opt. Lett. **16**, 393–395 (1991).
[4] K.O. Hill, B.S. Kawasaki, and D.C. Johnson, Appl. Phys. Lett. **28**, 608–609 (1976).
[5] C. Ye, P. Yan, L. Huang, Q. Liu, and M. Gong, Laser Phys. Lett. **4**, 376–381 (2007).
[6] B. Wu, Y. Liu, and Z. Dai, in: Proc. Int. Conf. Commun., Circuits, and Syst. **3**, 1971–1974 (2006).
[7] S.W. Harun, F.A. Rahman, K. Dimyati, and H. Ahmad, Laser Phys. Lett. **3**, 495–497 (2006).
[8] G.J. Cowle and D.Y. Stepanov, IEEE Photon. Technol. Lett. **8**, 1465–1467 (1996).
[9] M.H. Al-Mansoori, A.W. Naji, S.J. Iqbal, M.K. Abdullah, and M.A. Mahdi, Laser Phys. Lett. **4**, 371–375 (2007).
[10] S.W. Harun, M.Z. Zulkifli, and H. Ahmad, Laser Phys. Lett. **3**, 369–371 (2006).
[11] A.A. Fotiadi, R. Kiyan, O. Deparis, P. Megret, and M. Blondel, Opt. Lett. **27**, 83–85 (2002).
[12] S. Randoux, V. Lecoeuche, B. Segard, and J. Zemmouri, Phys. Rev. A **52**, 2327–2334 (1995).

ofs

Leading Optical Innovations

THE FURUKAWA ELECTRIC CO.,LTD.
Mie plant : 20-16,Nobono-cho,
Kameyama-shi, Mie 519-0292, Japan
Telephone : +81-595-85-2056
Facsimile : +81-595-85-2433
Head Office : 6-1,Marunouchi 2-chome,Chiyoda-ku,Tokyo 100-8322,Japan

Report No.: QSO 06246

Date : JUN. 22, 2006

TEST REPORT

Commodity	:	SINGLE MODE OPTICAL FIBER
Product No.	:	89-F6285
Type	:	G.652.D
Quantity	:	50,400m

Signed : for Naoto Oyama
TAKAAKI AOYAMA

MANAGER OF MIE OPTICAL FIBERS GROUP
QUALITY ASSURANCE DEPARTMENT
TELECOMMUNICATIONS COMPANY
THE FURUKAWA ELECTRIC CO.,LTD.

COMMODITY: Single Mode Optical Fiber
TYPE: G.652.D

ofs
Leading Optical Innovations
The Furukawa Electric Co.,Ltd.
Telecommunications Company

ITEM	CONTRACT LENGTH	ACTUAL LENGTH	CASE No.	BOX No.	ATTENUATION				MODE FIELD DIAMETER	ZERO DISPERSION WAVELENGTH	ZERO DISPERSION SLOPE	CABLE CUT-OFF WAVELENGTH	CORE CONCENTRICITY ERROR	CLADDING DIAMETER	CLADDING NONCIRCULARITY	COATING DIAMETER
					1310nm	1383nm	1550nm	1625nm	1310nm							
ID No.	(m)	(m)	(-)	(-)	(dB/km)				(um)	(nm)	(ps/nm2.km)	(nm)	(um)	(um)	(%)	(um)
F6285 A0001	25200	25290	1	BF6285001	0.326	0.277	0.187	0.199	9.36	1315.0	0.085	1165	0.15	125.1	0.1	244
F6285 A0002	25200	25290	1	BF6285001	0.327	0.277	0.196	0.216	9.36	1314.9	0.085	1161	0.22	125.1	0.2	244